

Pertanika Journal of
**SCIENCE &
TECHNOLOGY**

JST

VOL. 27 (S1) 2019

*A special issue devoted to
Adapting to Challenges*

Guest Editors

**Rosnah Shamsudin, Norhashila Hashim
& Intan Syafinaz Mohamed Amin Tawakkal**



PERTANIKA
JOURNALS

A scientific journal published by Universiti Putra Malaysia Press

Journal of Science & Technology

About the Journal

Overview

Pertanika Journal of Science & Technology (JST) is the official journal of Universiti Putra Malaysia published by UPM Press. It is an open-access online scientific journal which is free of charge. It publishes the scientific outputs. It neither accepts nor commissions third party content.

Recognized internationally as the leading peer-reviewed interdisciplinary journal devoted to the publication of original papers, it serves as a forum for practical approaches to improving quality in issues pertaining to science and engineering and its related fields.

JST is a **quarterly** (January, April, July and October) periodical that considers for publication original articles as per its scope. The journal publishes in **English** and it is open to authors around the world regardless of the nationality.

The Journal is available world-wide.

Aims and scope

Pertanika Journal of Science and Technology aims to provide a forum for high quality research related to science and engineering research. Areas relevant to the scope of the journal include: bioinformatics, bioscience, biotechnology and bio-molecular sciences, chemistry, computer science, ecology, engineering, engineering design, environmental control and management, mathematics and statistics, medicine and health sciences, nanotechnology, physics, safety and emergency management, and related fields of study.

History

Pertanika was founded in 1978. A decision was made in 1992 to streamline Pertanika into three journals as Journal of Tropical Agricultural Science, Journal of Science & Technology, and Journal of Social Sciences & Humanities to meet the need for specialised journals in areas of study aligned with the interdisciplinary strengths of the university.

After almost 25 years, as an interdisciplinary Journal of Science & Technology, the revamped journal now focuses on research in science and engineering and its related fields.

Goal of *Pertanika*

Our goal is to bring the highest quality research to the widest possible audience.

Quality

We aim for excellence, sustained by a responsible and professional approach to journal publishing. Submissions are guaranteed to receive a decision within 14 weeks. The elapsed time from submission to publication for the articles averages 5-6 months.

Abstracting and indexing of *Pertanika*

Pertanika is 40 years old; this accumulated knowledge has resulted in Pertanika JST being abstracted and indexed in SCOPUS (Elsevier), Clarivate - Emerging Sources Citation Index (ESCI), BIOSIS, National Agricultural Science (NAL), Google Scholar, MyCite, ISC.

Future vision

We are continuously improving access to our journal archives, content, and research services. We have the drive to realise exciting new horizons that will benefit not only the academic community, but society itself.

Citing journal articles

The abbreviation for Pertanika Journal of Science & Technology is *Pertanika J. Sci. Technol.*

Publication policy

Pertanika policy prohibits an author from submitting the same manuscript for concurrent consideration by two or more publications. It prohibits as well publication of any manuscript that has already been published either in whole or substantial part elsewhere. It also does not permit publication of manuscript that has been published in full in Proceedings.

Code of Ethics

The Pertanika Journals and Universiti Putra Malaysia takes seriously the responsibility of all of its journal publications to reflect the highest in publication ethics. Thus all journals and journal editors are expected to abide by the Journal's codes of ethics. Refer to Pertanika's **Code of Ethics** for full details, or visit the Journal's web link at http://www.pertanika.upm.edu.my/code_of_ethics.php

International Standard Serial Number (ISSN)

An ISSN is an 8-digit code used to identify periodicals such as journals of all kinds and on all media—print and electronic. All Pertanika journals have ISSN as well as an e-ISSN.

Journal of Science & Technology: ISSN 0128-7680 (*Print*); ISSN 2231-8526 (*Online*).

Lag time

A decision on acceptance or rejection of a manuscript is reached in 3 to 4 months (average 14 weeks). The elapsed time from submission to publication for the articles averages 5-6 months.

Authorship

Authors are not permitted to add or remove any names from the authorship provided at the time of initial submission without the consent of the Journal's Chief Executive Editor.

Manuscript preparation

Refer to Pertanika's **INSTRUCTIONS TO AUTHORS** at the back of this journal.

Most scientific papers are prepared according to a format called IMRAD. The term represents the first letters of the words **I**ntroduction, **M**aterials and **M**ethods, **R**esults, **A**nd, **D**iscussion. IMRAD is simply a more 'defined' version of the "IBC" [Introduction, Body, Conclusion] format used for all academic writing. IMRAD indicates a pattern or format rather than a complete list of headings or components of research papers; the missing parts of a paper are: *Title, Authors, Keywords, Abstract, Conclusions, and References*. Additionally, some papers include Acknowledgments and Appendices.

The *Introduction* explains the scope and objective of the study in the light of current knowledge on the subject; the *Materials and Methods* describes how the study was conducted; the *Results* section reports what was found in the study; and the *Discussion* section explains meaning and significance of the results and provides suggestions for future directions of research. The manuscript must be prepared according to the Journal's **INSTRUCTIONS TO AUTHORS**.

Editorial process

Authors are notified with an acknowledgement containing a *Manuscript ID* on receipt of a manuscript, and upon the editorial decision regarding publication.

Pertanika follows a **double-blind peer-review** process. Manuscripts deemed suitable for publication are usually sent to reviewers. Authors are encouraged to suggest names of at least three potential reviewers at the time of submission of their manuscript to Pertanika, but the editors will make the final choice. The editors are not, however, bound by these suggestions.

Notification of the editorial decision is usually provided within ten to fourteen weeks from the receipt of manuscript. Publication of solicited manuscripts is not guaranteed. In most cases, manuscripts are accepted conditionally, pending an author's revision of the material.

As articles are double-blind reviewed, material that might identify authorship of the paper should be placed only on page 2 as described in the first-4 page format in Pertanika's **INSTRUCTIONS TO AUTHORS** given at the back of this journal.

The Journal's peer-review

In the peer-review process, three referees independently evaluate the scientific quality of the submitted manuscripts.

Peer reviewers are experts chosen by journal editors to provide written assessment of the **strengths** and **weaknesses** of written research, with the aim of improving the reporting of research and identifying the most appropriate and highest quality material for the journal.

Operating and review process

What happens to a manuscript once it is submitted to *Pertanika*? Typically, there are seven steps to the editorial review process:

1. The Journal's Chief Executive Editor (CEE) and the editorial board examine the paper to determine whether it is appropriate for the journal and should be reviewed. If not appropriate, the manuscript is rejected outright and the author is informed.
2. The CEE sends the article-identifying information having been removed, to three reviewers who are specialists in the subject matter represented by the article. The CEE asks them to complete the review in three weeks.

Comments to authors are about the appropriateness and adequacy of the theoretical or conceptual framework, literature review, method, results and discussion, and conclusions. Reviewers often include suggestions for strengthening of the manuscript. Comments to the editor are in the nature of the significance of the work and its potential contribution to the field.

3. The CEE, in consultation with the Editor in Chief (EIC), examines the reviews and decides whether to reject the manuscript, invites the author(s) to revise and resubmit the manuscript. The CEE may seek additional reviews. Final acceptance or rejection rests with the CEE and EIC who reserves the right to refuse any material for publication. In rare instances, the manuscript is accepted with almost no revision. Almost without exception, reviewers' comments (to the author) are forwarded to the author. If a revision is indicated, the editor provides guidelines for attending to the reviewers' suggestions and perhaps additional advice about revising the manuscript.
4. The authors decide whether and how to address the reviewers' comments and criticisms and the editor's concerns. The authors return a revised version of the paper to the chief executive editor along with specific information describing how they have answered the concerns of the reviewers and the editor, usually in a tabular form. The author(s) may also submit a rebuttal if there is a need especially when the author disagrees with certain comments provided by reviewer(s).

5. The CEE sends the revised paper out for re-review. Typically, at least one of the original reviewers will be asked to examine the article.
6. When the reviewers have completed their work, the CEE in consultation with the editorial board and the EIC examine their comments and decide whether the paper is ready to be published, or should be rejected.
7. If the decision is to accept, an acceptance letter is sent to all the author(s), the paper is sent to the Press. The article should appear in print in approximately three months.

The Publisher ensures that the paper adheres to the correct style (in-text citations, the reference list, and tables are typical areas of concern, clarity, and grammar). The authors are asked to respond to any minor queries by the Publisher. Following these corrections, page proofs are mailed to the corresponding authors for their final approval. At this point, **only essential changes are accepted**. Finally, the article appears in the pages of the Journal and is posted on-line.



Pertanika Journal of

SCIENCE & TECHNOLOGY

*A special issue devoted to
Adapting to Challenges*

VOL. 27 (S1) 2019
(Special Issue)

Guest Editors
**Rosnah Shamsudin, Norhashila Hashim &
Intan Syafinaz Mohamed**



A scientific journal published by Universiti Putra Malaysia Press



EDITOR-IN-CHIEF

Mohd Adzir Mahdi

Physics, Optical Communications

CHIEF EXECUTIVE EDITOR

Abu Bakar Salleh

Biotechnology and Biomolecular Science

UNIVERSITY PUBLICATIONS COMMITTEE

Zulkifli Idrus, Chair

EDITORIAL STAFF

Journal Officers:

Kanagamalar Silvarajoo, *ScholarOne*

Siti Zuhaila Abd Wahid, *ScholarOne*

Tee Syin Ying, *ScholarOne*

Ummi Fairuz Hanapi, *ScholarOne*

Editorial Assistants:

Rahimah Razali

Siti Juridah Mat Arip

Zulinaardawati Kamarudin

PRODUCTION STAFF

Pre-press Officers:

Nur Farrah Dila Ismail

Wong Lih Jiu

WEBMASTER

Muhammad Zamiruddin Sahar

PUBLICITY & PRESS RELEASE

Magdalene Pokar (*ResearchSEA*)

EDITORIAL OFFICE

JOURNAL DIVISION

Office of the Deputy Vice Chancellor (R&I)

1st Floor, IDEA Tower II

UPM-MTDC Technology Centre

Universiti Putra Malaysia

43400 Serdang, Selangor Malaysia.

Gen Enq.: +603 8947 1622 | 1616

E-mail: executive_editor.pertanika@upm.my

URL: www.journals-jd.upm.edu.my

PUBLISHER

UPM Press

Universiti Putra Malaysia

43400 UPM, Serdang, Selangor, Malaysia.

Tel: +603 8946 8855, 8946 8854

Fax: +603 8941 6172

E-mail: penerbit@putra.upm.edu.my

URL: <http://penerbit.upm.edu.my>

EDITORIAL BOARD

2018-2020

Adem Kilicman

Mathematical Sciences
Universiti Putra Malaysia, Malaysia.

Ali A. Moosavi-Movahedi

Biophysical Chemistry
University of Tehran, Tehran, Iran.

Amu Therwath

Oncology, Molecular Biology,
Université Paris, France.

Angelina Chin

Mathematics, Group Theory and
Generalisations, Ring Theory,
University of Malaya, Malaysia.

Bassim H. Hameed

Chemical Engineering: Reaction
Engineering, Environmental Catalysis
& Adsorption,
Universiti Sains Malaysia, Malaysia.

Biswa Mohan Biswal

Medical, Clinical Oncology,
Radiotherapy
Universiti Sains Malaysia, Malaysia.

Christopher G. Jesudason

Mathematical Chemistry, Molecular
Dynamics Simulations, Thermodynamics
and General Physical Theory,
University of Malaya, Malaysia.

Hari M. Srivastava

Mathematics and Statistics,
University of Victoria, Canada.

Ivan D. Rukhlenko

Nonlinear Optics, Silicon Photonics,
Plasmonics and Nanotechnology
Monash University, Australia.

Kaniraj R. Shenbaga

Geotechnical Engineering,
India.

Kanury Rao

Senior Scientist & Head, Immunology
Group, International Center for Genetic
Engineering and Biotechnology,
Immunology, Infectious Disease Biology
and System Biology
International Centre for Genetic
Engineering & Biotechnology, New
Delhi, India.

Ki-Hyung Kim

Computer and Wireless Sensor
Networks
AJOU University, Korea.

Kunnawee Kanitpong

Transportation Engineering-Road
Traffic Safety, Highway Materials and
Construction
Asian Institute of Technology, Thailand.

Megat Mohd Hamdan

Megat Ahmad
Mechanical and Manufacturing
Engineering
Universiti Pertahanan Nasional
Malaysia, Malaysia.

Mirnalini Kandiah

Public Health Nutrition, Nutritional
Epidemiology
UCSI University, Malaysia.

Mohamed Othman

Communication Technology and
Network, Scientific Computing
Universiti Putra Malaysia, Malaysia

Mohd. Ali Hassan

Bioprocess Engineering, Environmental
Biotechnology
Universiti Putra Malaysia, Malaysia.

Mohd Sapuan Salit

Concurrent Engineering and Composite
Materials
Universiti Putra Malaysia, Malaysia.

Narongrit Sombatsompop

Engineering & Technology: Materials
and Polymer Research
King Mongkut's University of
Technology Thonburi (KMUTT),
Thailand.

Prakash C. Sinha

Physical Oceanography, Mathematical
Modelling, Fluid Mechanics, Numerical
Techniques
Universiti Malaysia Terengganu,
Malaysia.

Rajinder Singh

Biotechnology, Biomolecular Sciences,
Molecular Markers/ Genetic Mapping
Malaysia Palm Oil Board, Kajang,
Malaysia.

Renuganth Varatharajoo

Engineering, Space System
Universiti Putra Malaysia, Malaysia.

Riyanto T. Bambang

Electrical Engineering, Control,
Intelligent Systems & Robotics
Bandung Institute of Technology,
Indonesia.

Roslani Abd-Shukur

Physics & Materials Physics,
Superconducting Materials
Universiti Kebangsaan Malaysia,
Malaysia.

Sabira Khatun

Engineering, Computer Systems
& Software Engineering, Applied
Mathematics
Universiti Malaysia Pahang, Malaysia.

Shiv Dutt Gupta

Director, IJHMR, Health Management,
Public Health, Epidemiology, Chronic
and Non-communicable Diseases
Indian Institute of Health Management
Research, India.

Suan-Choo Cheah

Biotechnology, Plant Molecular Biology
Asiatic Centre for Genome Technology
(ACGT), Kuala Lumpur, Malaysia.

Wagar Asrar

Engineering, Computational Fluid
Dynamics, Experimental Aerodynamics
International Islamic University,
Malaysia.

Wing Keong Ng

Aquaculture, Aquatic Animal Nutrition,
Aqua Feed Technology
Universiti Sains Malaysia, Malaysia.

Yudi Samudya

Chemical Engineering, Advanced
Process Engineering
Curtin University of Technology,
Malaysia.

INTERNATIONAL ADVISORY BOARD

2018-2021

Adarsh Sandhu

Editorial Consultant for Nature
Nanotechnology and Contributing
Writer for Nature Photonics, Physics,
Magneto-resistive Semiconducting
Magnetic Field Sensors, Nano-
Bio-Magnetism, Magnetic Particle
Colloids, Point of Care Diagnostics,
Medical Physics, Scanning Hall Probe
Microscopy, Synthesis and Application
of Graphene
Electronics-Inspired Interdisciplinary
Research Institute (EIIRIS), Toyohashi
University of Technology, Japan.

Graham Megson

Computer Science
The University of Westminster, U.K.

Kuan-Chong Ting

Agricultural and Biological Engineering
University of Illinois at Urbana-
Champaign, USA.

Malin Premaratne

Advanced Computing and Simulation
Monash University, Australia.

Mohammed Ismail Elnaggar

Electrical Engineering
Ohio State University, USA.

Peter J. Heggs

Chemical Engineering
University of Leeds, U.K.

Ravi Prakash

Vice Chancellor, JUIT, Mechanical
Engineering, Machine Design,
Biomedical and Materials Science
Jaypee University of Information
Technology, Indian.

Said S.E.H. Elnashaie

Environmental and Sustainable
Engineering
Penn. State University at Harrisburg,
USA.

Suhash Chandra Dutta Roy

Electrical Engineering
Indian Institute of Technology (IIT)
Delhi, India.

Vijay Arora

Quantum and Nano-Engineering
Processes
Wilkes University, USA.

Yi Li

Chemistry, Photochemical Studies,
Organic Compounds, Chemical
Engineering
Chinese Academy of Sciences, Beijing,
China.

ABSTRACTING AND INDEXING OF PERTANIKA JOURNALS

Pertanika is 40 years old; this accumulated knowledge has resulted in the journals being abstracted and indexed in **SCOPUS** (Elsevier), Clarivate - Emerging Sources Citation Index (**ESCI**), BIOSIS, National Agricultural Science (**NAL**), **Google Scholar**, **MyCite**, Islamic World Science Citation Center (**ISCI**).



The publisher of *Pertanika* will not be responsible for the statements made by the authors in any articles published in the journal. Under no circumstances will the publisher of this publication be liable for any loss or damage caused by your reliance on the advice, opinion or information obtained either explicitly or implied through the contents of this publication.

All rights of reproduction are reserved in respect of all papers, articles, illustrations, etc., published in *Pertanika*. *Pertanika* provides free access to the full text of research articles for anyone, worldwide. It does not charge either its authors or author-institution for refereeing/publishing outgoing articles or user-institution for accessing incoming articles.

No material published in *Pertanika* may be reproduced or stored on microfilm or in electronic, optical or magnetic form without the written authorization of the Publisher.

Copyright © 2019 Universiti Putra Malaysia Press. All Rights Reserved.



Pertanika Journal of Science & Technology
Vol. 27 (S1) 2019

Contents

Adapting to Challenges

Preface	i
<i>Rosnah Shamsudin</i>	
Characterization of Jackfruit Straw-based Films: Effect of Starch and Plasticizer Contents	1
<i>Muslimah Solehah Mohd Nazri, Intan Syafinaz Mohamed Amin Tawakkal, Nozieana Khairuddin, Rosnita A Talib and Siti Hajar Othman</i>	
Phytochemical Compositions and Antioxidant Activities of Malaysian Stingless Bee Honey	15
<i>Bernard Maringgal, Norhashila Hashim, Intan Syafinaz Mohamed Amin Tawakkal, Mahmud Tengku Muda Mohamed and Nur Indah Abdul Shukor</i>	
Impact of Gamma Irradiation on Physical Parameters, Microbial Safety and the Total Polyphenolic Content of Commercially Available Ceylon Black Tea (<i>Camellia sinensis</i> L.)	29
<i>Arosha Rashmi De Silva, Rathnayake Mudiyanseelage Nalaka Priyanga Rathnayake, Rampati Devage Roshani Ranasinghe and Chamila Vinodanee Liyanage Jayasinghe</i>	
Optimization of Enzymatic Hydrolysis for the Production of Antioxidative Peptide from <i>Nannochloropsis gaditana</i> using Response Surface Methodology	41
<i>Nur Izzati Md Saleh, Wan Azlina Wan Ab Karim Ghani, Mohd Razif Harun and Siti Mazlina Mustapa Kamal</i>	
Effect of Drying Temperature on Malaysia Pomelo (<i>Citrus grandis</i> (L.) Osbeck) Pomace Residue under Vacuum Condition	57
<i>Nur Farhana Abd Rahman, Amin Ismail, Nor Nadiah Abdul Karim Shah, Jaturapatr Varith and Rosnah Shamsudin</i>	
Assessment on Flux Reduction and Protein Rejection Behavior in Fractionating Tilapia By-Product Protein Hydrolysate by Ultrafiltration Membrane	67
<i>Jumardi Roslan, Siti Mazlina Mustapa Kamal, Khairul Faezah Md Yunos and Norhafizah Abdullah</i>	

Stochastic Models for Greenhouse Whitefly Flight Behavior based on Wireless Image Monitoring System Measurements <i>Dan Jeric Arcega Rustia and Ta-Te Lin</i>	81
Mechanical Properties of Tapioca Starch-Based Film Incorporated With Bulk Chitosan and Chitosan Nanoparticle: A Comparative Study <i>Ruzana Ahmad Shapi'i, Siti Hajar Othman, Mohd Nazli Naim and Roseliza Kadir Basha</i>	95
Optimization of Hydrothermal Conditioning Conditions for <i>Pennisetum purpureum x Pennisetum americanum</i> (Napier PakChong1 grass) to Produce the Press Fluid for Biogas Production <i>Pitchaya Suaisom, Patiroop Pholchan, Hasfalina Che Man and Pruk Aggarangsi</i>	109
Mapping the Distribution of Oil Palm using Landsat 8 Data by Comparing Machine Learning and Non-Machine Learning Algorithms <i>Nur Shafira Nisa Shaharum, Helmi Zulhaidi Mohd Shafri, Wan Azlina Wan Ab Karim Ghani, Sheila Samsatli and Badronnisa Yusuf</i>	123
Modification of Quality Index Method Scheme for Nile Tilapia Fillets and Application in Quality Assessment of the Product Stored at Low Temperatures <i>Mai Thi Tuyet Nga and Nguyen Thi Kieu Diem</i>	137
Physical and Mechanical Properties of Unripe <i>Nipah</i> Banana Fruit (<i>Musa Acuminata Balbisiana</i>) <i>Farahana Nabilah Zainal A'bidin, Rosnah Shamsudin, Mohd Salahuddin Mohd Basri and Zanariah Mohd Dom</i>	149
The Effect of Packaging Materials on the Quality of Freshness of Longan Fumigated with Medium Concentration-ozone Gas <i>Saranyapak Chamnan, Jaturapatr Varith, Somkiat Jaturonglumlert, Pisuthi Klinkajorn and Jakraphong Phimphimol</i>	159
Degradation Kinetics of Diazinon and Triazophos Pesticides in Dried Chili under Gaseous Ozone Fumigation <i>Panlop Sintuya, Kanjana Narkprasom, Jaturapatr Varith, Somkiat Jaturonglumlert, Niwooti Whangchai, Danuwat Peng-ont and Chanawat Nitatwichit</i>	169
Modeling River Flow using Artificial Neural Networks: A Case Study on Sumani Watershed <i>Nova Anika and Tasuku Kato</i>	179

The Potential of Fluorescence Technology for Quality Monitoring of Miyauchi Iyokan (<i>C. iyo</i> Hort. Ex Tanaka) during Post-harvest Treatment <i>Muharfiza, Dimas Firmanda Al Riza, Nie Sen, Yasushi Kohno, Tetsuhito Suzuki, Makoto Kuramoto and Naoshi Kondo</i>	189
Mechanical Analysis of a Wedge Device in Sawing Technology <i>Mohd Salahuddin Mohd Basri, Mohd Zuhair Mohd Nor and Rosnah Shamsudin</i>	197
Simulation Study for the Compressed BMC Materials of Kenaf/ Coir Reinforced Unsaturated Polyester: Flow Behaviour and the Effects of Charges Shapes Studies <i>Sameer Adnan Ibraheem, Khalina Abdan and Lee Ching Hao</i>	211
Evaluations of Soil Resistivity in Relation to Basal Stem Rot Incidences Using Soil Moisture Sensor <i>Mohd Hamim Abdul Aziz, Siti Khairunniza Bejo, Fazirulhisyam Hashim, Nur Hidayah Ramli and Desa Ahmad</i>	225



Preface

We are glad to present this Special Issue of the *Pertanika Journal of Science and Technology (JST)*. It is a compilation of 19 research articles from scholars who hail from Malaysia, Indonesia, Thailand, Japan, Sri Lanka and Vietnam. This Special Issue contains the 19 papers that were selected from a total of 128 papers presented at International Conference of Agricultural and Food Engineering 2018 (CAFE*i* 2018). The theme of the issue is “Adapting to Challenges”. The topics include but not limited to: Agriculture Engineering and Food Engineering. There are 13 papers focusing on Food Engineering in which 4 papers are on Process Modelling and Simulation, 3 papers on Packaging Engineering, 3 papers on Food Processing, 1 paper on Drying Technology, 1 paper on Food Agricultural Waste Management and 1 paper on Food Security and Safety. While, 6 papers on Agricultural Engineering topic includes 2 papers on Agricultural and Automation, 1 paper on Bio-information System, 1 paper on Soil and Water, 1 paper on Agricultural Processing and 1 paper on Postharvest Engineering. All the papers published in this issue underwent *Pertanika*’s stringent peer-review process involving a minimum of two reviewers comprising internal as well as external referees. It is a heavily-cited journal not only by authors and researchers in Malaysia but by worldwide. We would like to thank the contributors as well as the reviewers for their commitment and patience which made this edition a success. It is hoped this publication would encourage researchers from around the world to be more active in publishing their research papers to contribute to the scholarly world.

We are grateful to *Pertanika*’s Editor-in-chief and the Chief Executive Editor, and their dedicated publication team, for their tremendous efforts, leadership, courage and dedication to improving the quality of this issue. We would also like to thank all the reviewers who have contributed to this issue. This has certainly motivated us to do more and better in the future.

Guest Editors:

Rosnah Shamsudin (*Assoc. Prof. Dr.*)

Norhashila Hashim (*Assoc. Prof. Dr.*)

Intan Syafinaz Mohamed Amin Tawakkal (*Dr.*)



Characterization of Jackfruit Straw-based Films: Effect of Starch and Plasticizer Contents

Muslimah Solehah Mohd Nazri¹, Intan Syafinaz Mohamed Amin Tawakkal^{1*},
Nozieana Khairuddin², Rosnita A Talib¹ and Siti Hajar Othman¹

¹Department of Process and Food Engineering, Faculty of Engineering, Universiti Putra Malaysia, 43400 Serdang, Selangor, Malaysia

²Department of Basic Science and Engineering, Faculty of Agriculture and Food Science, Universiti Putra Malaysia, Bintulu Sarawak Campus, 97008 Bintulu, Sarawak, Malaysia

ABSTRACT

Jackfruit straws are normally disposed as waste by food industries and vendors which may lead to serious environmental issue. In order to reduce the wastage and negative effects to the environment, jackfruit straw waste generated by jackfruit (*Artocarpus heterophyllus*) shows potential as bio-based film incorporated with starch. This work describes the effect of different starch and plasticizer contents on mechanical and thermal properties of jackfruit straw powder (JSP)/starch films. Film-forming solutions were prepared and cast by mixing JSP with tapioca starch at different ratios and for the plasticized films, *ca.* 15 - 40% of plasticizers including sorbitol and glycerol were incorporated into the JSP/starch films respectively. The tensile strength and modulus of JSP/starch films pronouncedly increased with increasing starch content, accompanied with a slight decreasing in the elongation at break. The result demonstrated that starch interacted with JSP, resulting in the formation

of a new network to improve the properties of JSP films. FTIR spectrum analyses demonstrated the presence of hydrogen bonding in the JSP/starch film. The tensile strength of the plasticized JSP/starch films decreased with increasing sorbitol and glycerol content from 15% to 40%. However, the plasticizing effect of sorbitol became more significant than glycerol, particularly on the tensile properties and thermal stability. Thermal analysis by

ARTICLE INFO

Article history:

Received: 24 October 2018

Accepted: 15 February 2019

Published: 21 June 2019

E-mail addresses:

solehahmuslimah@yahoo.com (Muslimah Solehah Mohd Nazri)

intanamin@upm.edu.my (Intan Syafinaz Mohamed Amin

Tawakkal)

nozieana@upm.edu.my (Nozieana Khairuddin)

rosnita@upm.edu.my (Rosnita A Talib)

s.hajar@upm.edu.my (Siti Hajar Othman)

* Corresponding author

thermogravimetric showed an increment in the decomposition temperature with the addition of plasticizers into JSP/starch films. The results suggest that films containing JSP and starch have the potential for the development of edible food packaging materials.

Keywords: Edible films, jackfruit straw, tapioca starch, tensile properties, thermogravimetric analysis

INTRODUCTION

Growing environmental awareness among consumers and plastic manufacturers has driven research in the development of biodegradable packaging materials. The synthesis of bio-based polymers from naturally derived resources, including polysaccharides, proteins and lipids is one of the strategies to minimize the usage of petroleum-based polymers (Kuorwel et al., 2013; Nor et al., 2017). The main drawbacks of these petroleum-based polymers is that the high degree of stability, which has resulted in a low degradability in the environment. Natural biopolymers are the best alternative due to their renewability, biodegradability and commercial viability in order to reduce waste-related environmental problems and depletion of petroleum-based polymers (Debeaufort et al., 1998).

Generally, the biopolymers of natural origins are more environmental friendly than the synthetic biopolymers and among them, starch particularly is a favourable biopolymer due to its low cost, widely accessible, exhibiting thermoplastic and biodegradability properties (Almasi et al., 2010 and González et al., 2016). This biopolymer is edible, odorless, tasteless, colourless, and constitutes a good barrier against oxygen transfer, suitable for food packaging materials including films and coatings (Dufresne et al., 2013; Yan et al., 2012). Despite the advantages of starch-based films, however, the properties of films have been limited due to the relatively low mechanical and barrier properties. By considering these drawbacks, the addition of additives, particularly plasticizer into the biopolymer matrix in order to improve the properties of the films is necessary (González et al., 2016). The flexibility of the films can be enhanced by reducing the polymer intra-molecular forces by incorporating plasticizers into the matrix. Food grade plasticizers such as glycerol and sorbitol are stable and compatible with hydrophilic biopolymeric packaging film, particularly starch-based film (Fama et al., 2005).

Jackfruit straw can be extracted from crops of jackfruit (*Artocarpus heterophyllus L.*), which is obtainable in Southeast Asian countries such as Thailand, Indonesia and Malaysia. Jackfruit waste, including skin, straw, core and seed accounts for approximately *ca.* 60-70% of its total weight (Subburamu, 1992) which can result in a major disposal problem and negative impact on the environment. At present, the available information on edible films from jackfruit straw is still limited. As ripe jackfruit straw consists of low amount of starch (13%) with slightly higher sugar content of 16% (e.g. reducing and non-reducing sugar) (Datt et al., 2008; Subburamu, 1992). These compounds may however provide insufficient properties to form films. Thus, the incorporation of jackfruit straw with biopolymer such as starch can be potentially turned this fruit waste to a valuable packaging material.

The compatibility between the main elements in a film system comprised a JSP and incorporated with starch could potentially contribute to the biodegradability and sustainability of the system as a whole. The aim of the present study is to explore the physical, mechanical and thermal properties of the JSP/starch films as a function of starch and plasticizer contents.

MATERIALS AND METHODS

Materials

The tapioca starch with *the Kapal ABC* brand was imported from Thailand and supplied by Thye Huat Chan Sdn. Bhd. Jackfruit of *Mastura* (J35) species was obtained from Perladangan Nangka Pahang, Temerloh, Malaysia.

Preparation of JSP

Ripe jackfruit straw was separated from the jackfruit peel (see Figure 1) (by discarding the core, seed and skin) and washed with distilled water to remove impurities. After washing, the straw was dried in an oven (Memmert, UF110, Germany) at 60°C for 48 h. The dried jackfruit straw was grounded into powder at 1500 rpm rotor speed using a grinder (Retsch, Cutting Mill SM200, Germany) and passed through a 0.25 mm mesh sieve size.

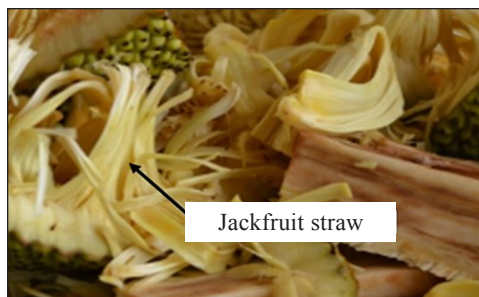


Figure 1. Jackfruit peel

Preparation of Films

For films preparation, the casting technique was employed as described by Shapi'i and Othman (2016) with slight modifications. Calculated amounts of JSP and tapioca starch were mixed in 200 mL of distilled water in a beaker by using a 1:20 ratio (solid to liquid). The ratio of JSP to starch (total solid of 10 g) was varied from 8:2, 7:3, 6:4, 5:5, and 4:6. The film forming solution was first mixed homogeneously in the beaker with constant stirring using a magnetic stirrer for 5 min and then heated on the hot plate until gelatinized completely at 75°C with constant stirring for *ca.* 15 min. For the preparation of plasticized films, the plasticizer such as glycerol and sorbitol at different concentrations (15, 25 and

40%) were added during the mixing of tapioca starch and JSP in a beaker with 200 mL of distilled water prior to heating. The gelatinized solution was cooled to room temperature before it was sonicated by using an ultrasonicator (QSonica LLC, Q500, USA) at 500 W, 20 Hz, 50% amplitude for 10 min by using probe with a diameter of 20 mm. Ultrasonic treatment of the film forming solution is crucial in order to remove insoluble granules in the starch matrix as suggested by Cheng, et al. (2010). This treatment can produce a good film with good transparency, improved moisture resistance and stronger structure. The sonicated film solution was then filtered by using filter paper and cast onto petri dish. The film thickness was measured with a hand-held digital micrometer (Mitutoyo 293-340-30, Japan) to the nearest 0.001 mm at four random locations on the film. No significant changes were observed for all thicknesses of JSP/starch films at different weight ratios, with an average thickness of 0.241 ± 0.007 mm.

Colour Test

The colour of JSP/starch films was measured using a Hunter Lab colourimeter (USP 1431 UltraScan Pro, USA) based on the CIE $L^*a^*b^*$ colour system, L^* , a^* and b^* . L^* describes the lightness ranging from black to white, a^* and b^* describe the chromatic coordinates ranging from $-a^*$: greenness to $+a^*$: redness and from $-b^*$: blueness to $+b^*$: yellowness. The films specimens were first placed on the surface of a white standard plate using value of $L^* = 97.39$, $a^* = 0.03$ and $b^* = 1.77$ in order to calibrate the equipment (Gutiérrez et al., 2015). The measurement was recorded at three different positions for each of the films.

Infrared Analyses

The infrared spectral analyses of the starch, JSP and JSP/starch films were measured using a Shimadzu IR Prestige Fourier transform infrared (FTIR) spectrophotometer with an attenuated total reflectance (ATR) attachment. All spectra were recorded in the range of $550 - 4000 \text{ cm}^{-1}$ with a resolution of 4 cm^{-1} and with 32 scans recorded at every point using Happ-Genzel apodization. A minimum of two random locations of the film was scanned per sample.

Tensile Properties

The tensile test was carried out based on ASTM D882 standard by using texture analyzer (Texture Analyzer Testing Machine 3365, USA) in order to determine tensile strength, Young's modulus and elongation at break. The films were cut into rectangular shape with dimension of 100×15 mm. The initial gauge clamp and the crosshead speed was set at 60 mm and 20 mm/min respectively. A minimum of three specimens was tested for these purposes. The tensile properties were calculated from the force-deformation curves as described by Chang et al. (2000).

Thermal Analysis

The degradation and/or decomposition temperature of the films was analyzed by using Thermogravimetric Analyzer (TGA) (STA6000 Pyris 1TGA, Perkin Elmer, USA) and measured by using Pyris Series TGA 7 software. The samples were weighed *ca.* 14 -16 g and heated from 25 to 550°C with 10°C/min heating rate. The degradation temperature (T_d) was determined by the slope change that was obtained from the thermal profile curve. A minimum of two replications per sample was tested.

Data Analysis

The Excel software (Microsoft Inc., USA) was used to analyze the data whereby the statistical analysis of the data was carried out by one-way analysis of the variance (ANOVA).

RESULTS AND DISCUSSION

Films Colour

Figure 2 shows the effect of starch content on the colour of JSP/starch films at different weight ratios. It was observed that the amount of starch could have a significant effect on the colour of JSP/starch films. The JSP/starch films became lighter as evidenced by

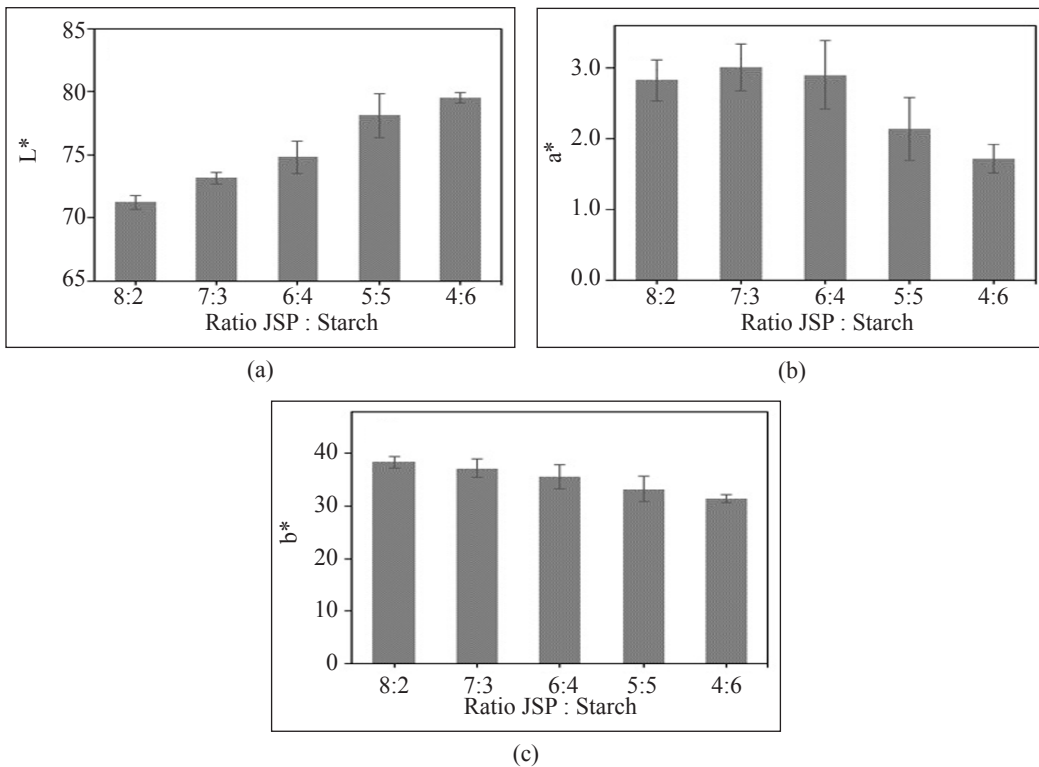


Figure 2. Colour analysis of JPS/starch films at different weight ratios: (a) value L*, (b) value a* and (c) value b*

the increase of L^* value (see Figure 2(a)), as the addition of starch content into the JSP/starch films increased. Tapioca starch is colourless and clear, hence the JPS/starch films with higher amount of starch demonstrated a higher lightness value. From Figure 2(b), no significant change of value a^* was observed for JSP to starch ratio of 8:2 and 6:4, respectively. However, the value a^* decreased at JSP to starch ratio of 5:5 and 4:6. The value b^* as shown in Figure 2(c), slightly decreased with increasing starch content which caused films to appear less yellowish. It is important to note that the natural colour of jackfruit straw itself is yellow in colour, thus it may lead to the overall colour of the films (Sayuti et al., 2015). Moreover, the colour of the JSP/starch films was not affected by the presence of plasticizers particularly sorbitol and glycerol, regardless the concentrations (no data presented). This finding is in agreement with a study by Nur Hanani and Abdullah (2016) who investigated the effect of plasticizers such as glycerol, sorbitol and polyethylene glycol (PEG) incorporated into unripe banana films. The researchers reported that no significant changes were observed on the colour of banana films containing glycerol and sorbitol from 10 to 50% concentration.

FTIR

To confirm the interaction between the JSP and starch on the film, surface FTIR spectra of JSP, starch and JSP/starch films were obtained and are shown in Figure 3. Generally, it was found that the spectrum of JSP/starch film at JSP and starch ratio of 4:6 was similar to the spectrum of the JSP film. In the spectrum of all films, a broad band of $-OH$ group was observed at approximately $3400 - 3300 \text{ cm}^{-1}$ region. This peak corresponds to the stretching vibration of $-OH$ group of starch and/or pectin as in the JSP film. Peak at 2921 cm^{-1} is attributed to an asymmetrically stretching vibration of $-CH$ band (Deeyai et al., 2013). A sharp absorption peak at approximately 1631 cm^{-1} of starch film is observed which corresponds to the $-OH$ stretching vibration of absorbed water in the starch film. The existence of this peak has been ascribed to the vibration of water molecules absorbed into the non-crystalline region of starch (Deeyai et al., 2013). As seen in Figure 3, there are major band changes associated with $-OH$ groups. For instance, the presence of new hydrogen bonding in the JSP/starch film could be interpreted from the peak of $-OH$ group (absorbed water) that shifts to 1587 cm^{-1} with a broader band than starch film (Liu et al., 2011). Interestingly, a new and prominent peak was observed from the JSP/starch and JSP film at 1741 cm^{-1} which indicates the stretching vibration of $-C=O$, attributes to the carbonyl group. According to Gnanasambandam and Proctor (2000), this band represents the ester carbonyl group of pectin at approximately $1760-1745 \text{ cm}^{-1}$. It was found that the existence of this peak was weak for JSP film and no peak was present in the starch film. Moreover, the $-COH$ banding of JSP/starch film was shifted to 1016 cm^{-1} with a narrow peak. Several others adsorption bands between $873-1471 \text{ cm}^{-1}$ of tapioca starch film are

attributed to the contribution of various functional group such as -COC at 1143 cm^{-1} and 933 cm^{-1} which indicate the asymmetric stretching glycosidic bond and skeletal mode of α -glycosidic linkage. This result is in agreement with the study by Deeyai et al. (2013) who investigated the effect of unmodified and modified tapioca starch in atmospheric argon plasma by FTIR spectroscopy.

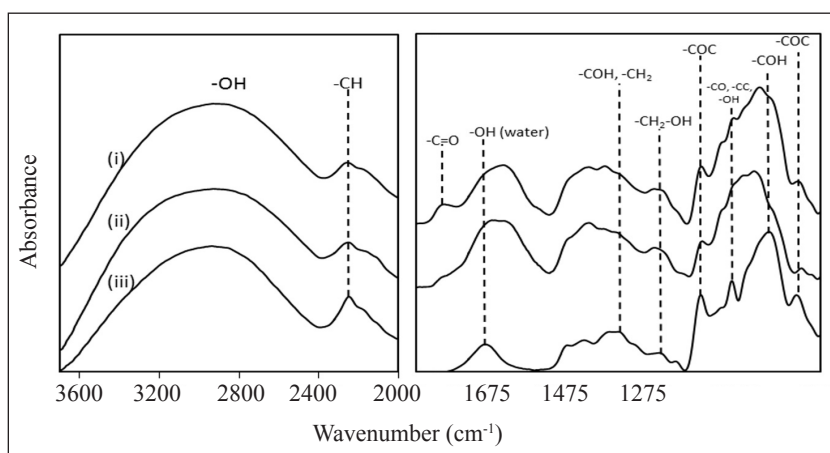


Figure 3. FTIR spectra of (i) JSP/starch film, (ii) JSP film and (iii) tapioca starch film

Tensile Properties of JSP/Starch Films

Figure 4(a) shows the tensile properties of the JSP/starch films as a function of the starch content. Generally, the tensile strength of the JSP/starch films was affected by the starch content. It was observed that the tensile strength of JSP/starch films increased with the addition of starch content and the maximum occurred at the JSP and starch ratio of 4:6 with approximately 8 MPa. This result indicates that the starch improves the tensile strength of the JSP/starch blends due to a good compatibility of JSP and starch in nature. The tensile strength of the JSP film containing more than 6g of starch content (e.g. JSP and starch ratio of 3:7) was dropped drastically and difficult to handle during testing due to the brittle characteristic of the starch (no data presented). From this finding, the starch increases the strength of the film when incorporated into JSP film at the JSP and starch ratio of 4:6. The tensile strength of the neat tapioca starch film without plasticizer was approximately 5 MPa as reported by Shapi'i and Othman (2016) which lowered than JSP/starch films at the ratio of 4:6. Starch may provide extra contacts of hydrogen bonding between the polymers chains, responsible for the film-forming property. Furthermore, the increasing tensile strength values of the JSP/starch films, with the increase of starch ratios from 8:2 to 4:6, may be attributed due to a good interfacial adhesion and/or high formation of intermolecular hydrogen bonding between JSP and a hydroxyl group (-OH) of the starch. The presence of linear amylose structure in the tapioca starch may provide stronger and

high rigidity films (Maran et al., 2013; Mali et al., 2006). Neswati et al. (2015) prepared jackfruit straw edible films with the incorporation of 5% glycerol and 1% carboxymethyl cellulose (CMC) to improve the JSP film properties. The weak mechanical properties of pure JSP films may be attributed due to the low amount of starch in the jackfruit straw (12%) with higher content of sugar (16%) as reported by Subburamu et al. (1992).

From Figure 4(b), the Young's modulus of the JSP film increases with the addition of higher starch content. It was found that the JSP and starch ratio of 8:2 had the lowest modulus value (4 MPa) while the film at a ratio of 4:6 demonstrated the highest value of Young's modulus (259 MPa). This trend was attributed to the stiffening effect of the starch. Moreover, the formation of chain-chain associations in the starch film matrix may be present. According to Mali et al. (2006), the presence of hydroxyl and carbonyl group in the JSP (see Figure 3) can interact with the hydroxyl group of tapioca starch to form hydrogen bonds, and as a result, amylose gels and films are becoming stiffer and stronger. The elongation at break of the JSP/starch films at different weight ratios is shown in Figure 4(c). As expected, the elongation at break was slightly affected by the starch content. It was found that the elongation at break of the JSP/starch films behaved inversely to the tensile strength and modulus, decreasing from 30% to a minimum of 21% when the JSP

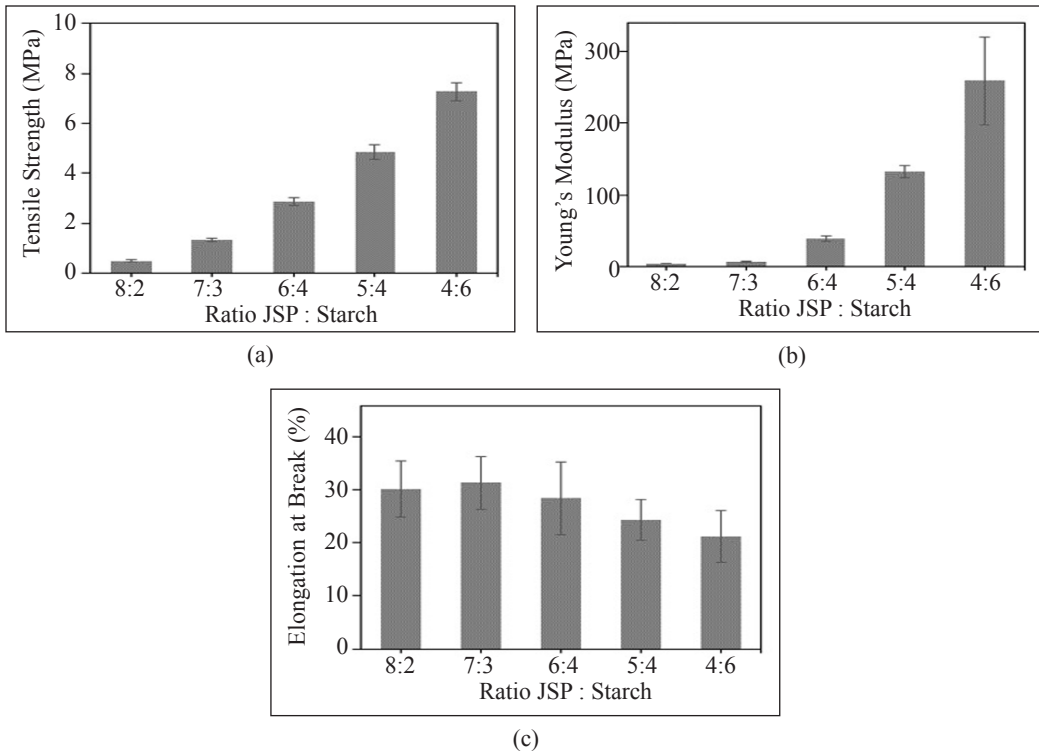


Figure 4. Tensile properties of JSP/starch films at different weight ratios: (a) tensile strength, (b) Young's modulus and (c) percentage elongation at break

and starch ratio was at 6:4. In general, the elongation at break of these films decreases with the addition of starch content. This indicates that the starch does not contribute to the elasticity of the films and this observation is likely attributed to the stiffness of the films as shown by the results in Figure 4(d). No significant change in the elongation at break of the JSP/starch films was observed with increased starch content.

Tensile Properties of Plasticized JSP/Starch Films

Figure 5 shows the tensile properties of plasticized JSP/starch films containing glycerol and sorbitol at different concentrations. In general, the presence of plasticizers influences the tensile properties of the JSP/starch films. It is interesting to note that the sorbitol-plasticized films exhibited higher tensile strength, Young's modulus and elongation at break than the plasticized films containing glycerol. This finding is in agreement with a study by Nur Hanani and Abdullah (2016) who investigated the effect of plasticizer on starch-based films. From Figure 5(a), the plasticized films with glycerol and sorbitol at 15% concentration demonstrate lower tensile strength which are 4.3 MPa and 1.4 MPa respectively, than the control JSP/starch film at JSP and starch ratio of 4:6 (without plasticizer) (see Figure 4(a)). The presence of plasticizers that lowers the tensile strength may be due to their ability to reduce intermolecular forces between the polymer chains and increase film flexibility in the JSP/starch films. The sorbitol-plasticized JSP/starch films demonstrated higher elongation at break than plasticized JSP/starch films containing glycerol as shown in Figure 5(a). This may be attributed due to the higher molecular weight and greater molecule size of sorbitol that result less effective in disturbing starch-starch interaction and thus, forming a stronger film than glycerol-plasticized film (Wittaya, 2013).

From Figure 5(b), as expected, the addition of plasticizers has significantly reduced the Young's modulus or stiffness of the JSP/starch films. It was found that the plasticized films containing glycerol at a concentration of 40% showed the lowest Young's modulus value (2.6 MPa). Generally, the presence of starch provides high rigidity to a film because of its high intermolecular forces. Hence, with the addition of plasticizers into the starch-based films, the rigidity of the films was reduced (Sothornvit & Krochta, 2001). From Figure 5(c), it was observed that the sorbitol-plasticized JSP/starch films demonstrated higher elongation at break than plasticized JSP/starch films containing glycerol. This may be due to the high stretch ability of sorbitol than the glycerol. Moreover, sorbitol has low water-attracting ability that limits its ability to reduce JSP/starch -chain hydrogen bonding. No significant changes on elongation at break were observed for films at different glycerol concentrations. However, the elongation at break of sorbitol-plasticized films show an increment from concentration 0% to 25%, but then slightly decreased to 46% at a concentration of 40%. According to Abdorreza et al. (2011), the flexibility of the starch-based film could be increased by increasing the sorbitol content, but this can lead to crystallization of sorbitol

in the film and thus, restricting the elasticity property. Based on these findings, plasticizer acts as film additive or lubricant able to increase the flexibility and elasticity of films (Mali et al., 2006).

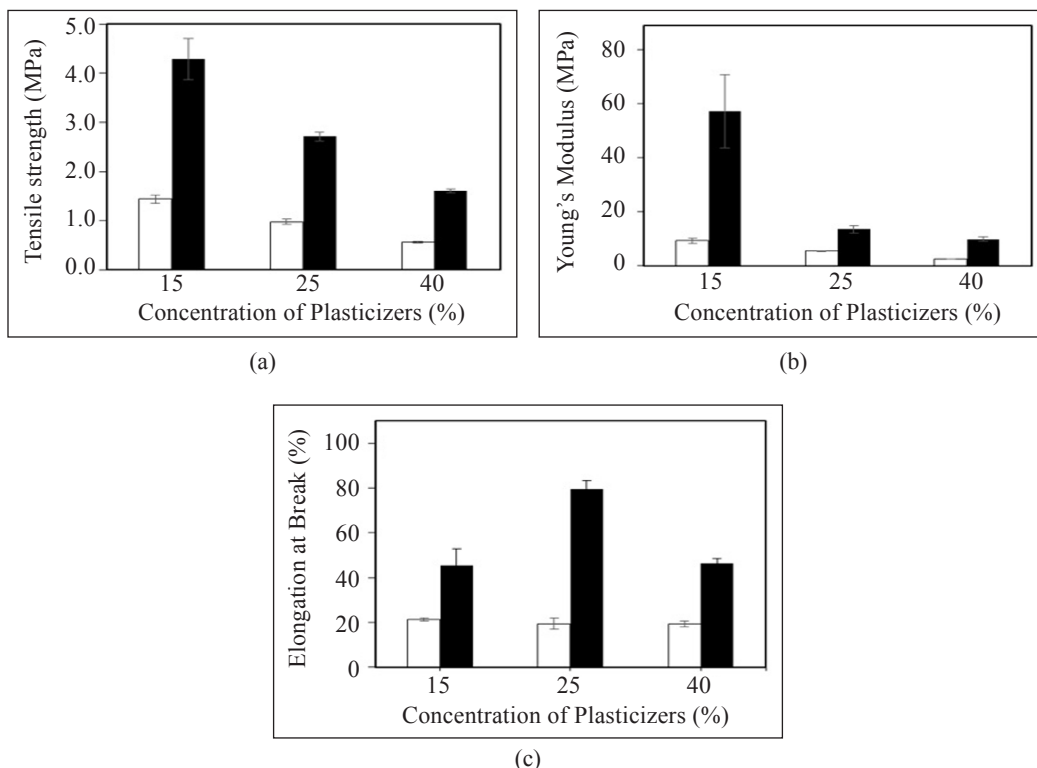


Figure 5. Tensile properties of plasticized JSP/starch films containing 15, 25 and 40% glycerol (□) or sorbitol (■); (a) tensile strength, (b) Young's modulus and (c) percentage elongation at break

Thermal Analysis of JSP/Starch Films

Thermal profiles of the JSP/starch films at different weight ratios are shown in Figure 6 and Table 1. In Figure 6, the thermal profile of the sorbitol-plasticized films at 15% and 40% loadings was compared with the control film (JSP and starch ratio of 4:6) and the results can also be observed from the derivative thermogravimetric (DTG) curves. The films have several degradation/decomposition step processes as seen in Figure 6. The thermal decomposition can occur in three main stages, which is in the first stage, an initial loss of weight was observed at temperatures between 100 and 130°C. This is due to a water loss or evaporation of water (Espitia et al., 2014; Gutiérrez et al., 2015). In the second stage, a decomposition step was observed at *ca.* 200 to 315 °C (T_{d1}), which is attributed to the decomposition of JSP and/or plasticizers (Espitia et al., 2014). The observed decomposition temperature, T_{d1} may be due to the presence of pectin and/or simple sugar from the JSP itself

that may be acting like a plasticizer. Next, the highest decomposition temperature occurred at the temperature range between 300 and 340°C (T_{d2}) with the maximum decomposition temperature of 336°C, which the onset decomposition temperature of starch that undergoes oxidation (Gutiérrez et al., 2015).

Table 1 represents the decomposition temperature of JSP/starch films at different weight ratios. The result shows no significant change of the decomposition temperature with increasing starch content of the JSP/starch films. This may be attributed due to the complex interaction between the JSP and the starch content. However, the decomposition temperature of plasticized films was found to be higher than the control JSP/starch films at 4:6 ratio. This finding is in agreement with a study by Gutiérrez et al. (2015), which reported that the onset decomposition temperature of plasticized starch films would occur at a higher temperature than the neat starch due to the good interaction between the plasticizer and the starch matrix. Moreover, sorbitol-plasticized films demonstrated slightly higher

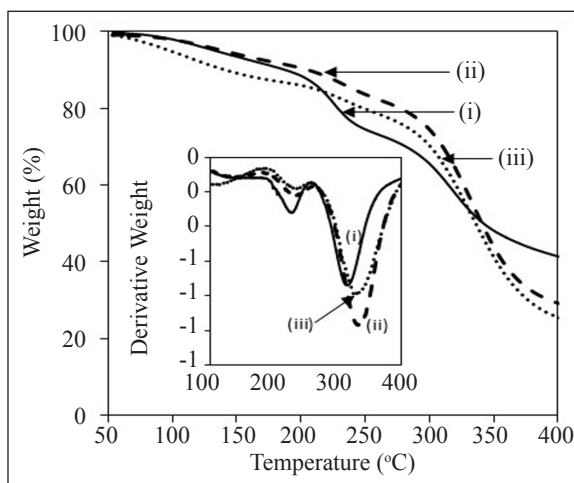


Figure 6. Thermogravimetric curves of JSP/starch films at 4:6 ratio including i) control film; ii) plasticized film at 15% sorbitol concentration and iii) plasticized film at 40% sorbitol concentration

Table 1
The decomposition temperature of JSP/starch films at different weight ratios

Blends JSP:starch	Decomposition temperature of JSP/starch films		Decomposition temperature of plasticized JSP/starch films		
	T_{d1} (°C)	T_{d2} (°C)	T_{d1} (°C)	T_{d2} (°C)	
8:2	226	321	JSP/S_Sor15	233	336
7:3	225	320	JSP/S_Sor25	237	335
6:4	226	323	JSP/S_Sor40	238	331
5:5	228	317	JSP/S_Gly15	232	330
4:6	228	318	JSP/S_Gly25	238	332
			JSP/S_Gly40	230	316

thermally stable films than plasticized films with glycerol as shown in Table 1. For example, the decomposition temperature of the sorbitol-plasticized and glycerol-plasticized films at 15% loading was 336°C and 330°C respectively, with approximately 2% reduction. This may be due to the good intermolecular interaction between the plasticizer and the JSP/starch films.

CONCLUSION

The results of this study indicate that the colour of films, FTIR spectra, tensile and thermal properties of JSP are affected by the addition of tapioca starch. The presence of the starch increases the tensile strength and modulus of JSP/starch film. It was noted that an increased loading of starch in the JSP/starch films resulted in a decrease of decomposition temperature indicating a reduced thermal stability of the films. Sorbitol-plasticized films demonstrated higher tensile properties and thermally stable than the plasticized films with glycerol in the TGA decomposition temperature. This JSP/starch film has the potential to be used as an edible bio-based packaging material. The results of this study provide some fundamental data related to physical, chemical, mechanical and thermal properties which can be used as reference for future research work.

ACKNOWLEDGEMENTS

The authors would like to thank the Ministry of Higher Education Malaysia for sponsoring this work under UPM Putra Grant: GP/2017/9548400.

REFERENCES

- Abdorreza, M. N., Cheng, L. H., & Karim, A. A. (2011). Effects of plasticizers on thermal properties and heat sealability of sago starch films. *Food Hydrocolloids*, 25(1), 56-60.
- Almasi, H., Ghanbarzadeh, B., & Entezami, A. A. (2010). Physicochemical properties of starch–CMC–nanoclay biodegradable films. *International Journal of Biological Macromolecules*, 46(1), 1-5.
- Chang, Y. P., Cheah, P. B., & Seow, C. C. (2000). Plasticizing - antiplasticizing effects of water on physical properties of tapioca starch films in the glassy state. *Journal of Food Science*, 65(3), 445-45.
- Cheng, W., Chen, J., Liu, D., Ye, X., & Ke, F. (2010). Impact of ultrasonic treatment on properties of starch film-forming dispersion and the resulting films. *Carbohydrate Polymers*, 81(3), 707-711.
- Datt C, Chhabra A, Singh N. P., & Bujarbaruah K. M. (2008). Nutritional characteristics of horticultural crop residues as ruminal feeds. *Indian Journal of Animal Sciences*, 78(3), 312–16.
- Debeaufort, F., Quezada-Gallo, J. A. & Voilley, A. (1998). Edible films and coatings: Tomorrow's packagings: A review. *Critical Review in Food Science and Nutrition*, 38(4), 299–313.

- Deeyai, P., Supphantharika, M., Wongsagonsup, R., & Dangtip, S. (2013). Characterization of modified tapioca starch in atmospheric argon plasma under diverse humidity by FTIR spectroscopy. *Chinese Physics Letters*, 30(1), 018103.
- Dufresne, A., Thomas, S., & Pothan, L. A. (2013). *Bionanocomposites: State of the art, challenges, and opportunities biopolymer nanocomposites*. New Jersey, USA; John Wiley and Sons, Inc.
- Espitia, P. J. P., Du, W. X., de Jesus Avena-Bustillos, R., Soares, N. D. F. F., & McHugh, T. H. (2014). Edible films from pectin: Physical-mechanical and antimicrobial properties-A review. *Food Hydrocolloids*, 35, 287-296.
- Fama, L., Rojas, A. M., Goyanes, S., & Gerschenson, L. (2005). Mechanical properties of tapioca-starch edible films containing sorbates. *LWT-Food Science and Technology*, 38(6), 631-639.
- Gnanasambandam, R., & Proctor, A. (2000). Determination of pectin degree of esterification by diffuse reflectance Fourier transform infrared spectroscopy. *Food Chemistry*, 68(3), 327-332.
- González, P., Medina, C., Famá, L., & Goyanes, S. (2016). Biodegradable and non-retrogradable eco-films based on starch – glycerol with citric acid as crosslinking agent. *Carbohydrate Polymers*, 138, 66–74.
- Gutiérrez, T. J., Tapia, M. S., Pérez, E., & Famá, L. (2015). Structural and mechanical properties of edible films made from native and modified cush-cush yam and cassava starch. *Food Hydrocolloids*, 45, 211-217.
- Kuorwel, K. K., Cran, M. J., Sonneveld, K., Miltz, J., & Bigger, S. W. (2013). Water sorption and physicomechanical properties of corn starch-based films. *Journal of Applied Polymer Science*, 128(1), 530-536.
- Liu, H., Chaudhary, D., Yusa, S. I., & Tadó, M. O. (2011). Glycerol/starch/Na⁺ montmorillonite nanocomposites: A XRD, FTIR, DSC and ¹H NMR study. *Carbohydrate Polymers*, 83(4), 1591–1597.
- Mali, S., Grossmann, M. V. E., García, M. A., Martino, M. N., & Zaritzky, N. E. (2006). Effects of controlled storage on thermal, mechanical and barrier properties of plasticized films from different starch sources. *Journal of Food Engineering*, 75(4), 453-460.
- Maran, J. P., Sivakumar, V., Sridhar, R., & Thirugnanasambandham, K. (2013). Development of model for barrier and optical properties of tapioca starch based edible films. *Carbohydrate Polymers*, 92(2), 1335-1347.
- Neswati, N., Murtius, W. S., & Prastica, A. (2015). Characteristics of jackfruit straw's edible film enriching by gingers red (*Zingiber officinale*, Rosc.). *International Journal on Advanced Science, Engineering and Information Technology*, 5(2), 144-148.
- Nor, M. H. M., Nazmi, N. N. M., & Sarbon, N. M. (2017). Effects of plasticizer concentrations on functional properties of chicken skin gelatin films. *International Food Research Journal*, 24(5), 1910-1918.
- Nur Hanani Z. A. & Abdullah S. (2016). Development of green banana (*Musa paradisiaca*) as potential food packaging films and coatings.” *International Journal on Advanced Science, Engineering and Information Technology*, 6(1), 88-91.
- Sayuti, K., Azima, F., & Marisa, M. (2015). The addition of “senduduk” fruit (*Melastoma malabathricum*, L.) extract as colorants and antioxidant on jackfruit straw (*Artocarpus heterophyllus*, L.) jam. *International Journal on Advanced Science Engineering Information Technology*, 5(6), 396-401.

- Shapi'i, R. A., & Othman, S. H. (2016). Effect of concentration of chitosan on the mechanical, morphological and optical properties of tapioca starch film. *International Food Research Journal*, 23, 187-193.
- Sothornvit, R., & Krochta, J. M. (2001). Plasticizer effect on mechanical properties of β -lactoglobulin films. *Journal of Food Engineering*, 50(3), 149-155.
- Subburamu, K., Singaravelu, M., Nazar, A., & Irulappan, I. (1992). A study on the utilization of jack fruit waste. *Bioresource Technology*, 40(1), 85-86.
- Wittaya, T. (2013). Influence of type and concentration of plasticizers on the properties of edible film from mung bean proteins. *Current Applied Science and Technology*, 13(1), 51-58.
- Yan, Q., Hou, H., Guo, P., & Dong, H. (2012). Effects of extrusion and glycerol content on properties of oxidized and acetylated corn starch-based films. *Carbohydrate Polymers*, 87(1), 707-712.

Phytochemical Compositions and Antioxidant Activities of Malaysian Stingless Bee Honey

Bernard Maringgal¹, Norhashila Hashim^{1,4*}, Intan Syafinaz Mohamed Amin Tawakkal², Mahmud Tengku Muda Mohamed³ and Nur Indah Abdul Shukor³

¹Department of Biological and Agricultural Engineering, Faculty of Engineering, Universiti Putra Malaysia, 43400 Serdang, Selangor, Malaysia

²Department of Process and Food Engineering, Faculty of Engineering, Universiti Putra Malaysia, 43400 Serdang, Selangor, Malaysia

³Department of Crop Science, Faculty of Agriculture, Universiti Putra Malaysia, 43400 Serdang, Selangor, Malaysia

⁴SMART Farming Technology Research Center, Faculty of Engineering, Universiti Putra Malaysia, 43400 Serdang, Selangor, Malaysia

ABSTRACT

The current study investigates the phytochemical composition of Malaysian stingless bee honey (Kelulut honey-KH), which consists of total phenolic (TPC) and total flavonoid content (TFC), and antioxidant activity. The honey was collected from five different regions in Malaysia i.e. south, central, eastern, northern and east coast regions. TPC and TFC were quantified by using Folin-Ciocalteu and the aluminum chloride colorimetric techniques, respectively. The antioxidant activity was investigated using two methods: 1) 1,1-diphenyl-2-picrylhydrazyl (DPPH) radical scavenging assay; 2) ferric reducing/antioxidant power assay (FRAP). The findings indicated that there were significant differences in phytochemical compositions and antioxidant activities of KH between different regions. This implies that geographical location, as well as cultivation and treatment processes, have significant effects on the KH quality.

Keywords: Kelulut honey, stingless bee honey, trigona spp, total phenolic content, total flavonoid content, antioxidant

ARTICLE INFO

Article history:

Received: 24 October 2018

Accepted: 15 February 2019

Published: 21 June 2019

E-mail addresses:

bernardmaringgal@yahoo.com (Bernard Maringgal)

norhashila@upm.edu.my (Norhashila Hashim)

intanamini@upm.edu.my (Intan Syafinaz Mohamed Amin Tawakkal)

mtmm@upm.edu.my (Mahmud Tengku Muda Mohamed)

indahshukor@yahoo.com (Nur Indah Abdul Shukor)

* Corresponding author

INTRODUCTION

Stingless bee honey, like many other types of honey is a sugary liquid which has a superb taste and odor (Chuttong et al., 2016a). It is produced by a stingless bee,

commonly known as “Kelulut” in Malaysia (Kek et al., 2014; Zainol et al., 2013). Stingless bee honey belongs to the order *Hymenoptera* under the family *Apidae* and sub-family tribe *Meliponini* (Chuttong et al., 2016b). Kelulut is naturally active all the time except during cold and cloudy weather. They are highly sociable, with one queen living together with thousands of workers (Chuttong et al., 2015). The bees normally inhabit in tropical and subtropical regions globally like Central and South America, Africa, Asia and northern Australia (Boorn et al., 2010). Shadan et al. (2018) reported that the selling price of kelulut honey (KH) could be as high as \$100/kg, which was almost double compared to the honey made by the regular honey (\$20–40/kg). This is mainly due to high contents of flavonoids and polyphenols.

In recent years, the kelulut industry has gained wide attention in Malaysia. Particularly, KH has been reported to be useful for medical and therapeutic purposes (Kek et al., 2014). KH has different phytochemical attributes as compared to regular honey bee in term of color, taste, viscosity, water and sugar contents (Biluca et al., 2014). Furthermore, KH has higher contents of flavonoids and polyphenols in contrast to honey produced by the *Apis* spp. (Biluca et al., 2016; Rodriguez-Malaver et al., 2013; Rodriguez-Malaver et al., 2009). Additionally, KH is more fluid in texture and undergoes slow crystallization. KH can be divided into various types according to the physical and chemical components. These components are linked to the physiology of making of the raw material, the territorial site of the floral source, the species of bee and the conditions of the ecosystem in which the bees live (Tuksitha et al., 2018). A previous study demonstrated that KH be made of mainly carbohydrates, water, amino acids, vitamins and minerals (Chuttong et al., 2016a). Another study reported that KH possesses distinctive and divergent phenolic and flavonoid composites that shown to have a vital function with regard to its antibacterial, anti-inflammatory and antioxidant activities of the Borneo (Sarawak) stingless bee honey (Tuksitha et al., 2018).

The topographical and botanical regions and the form of bees have essential function in forming the biological structure of honey plus the total antioxidant capacity (Erejuwa et al., 2012). A review by Nordin et al. (2018) reported that the phytochemical properties of honey varied significantly owing to the huge differences in bee species and geographic starting point. Recently, Kek et al. (2017) and Abu Bakar et al. (2017) analyzed the phytochemical of KH from various geographical and species from Malaysia. The authors demonstrated that KH had greater total phenolic content (TPC) with average amounts of 784.3 mg GAE/kg compared to the regular honey (Kek et al., 2014). The antioxidant activity of KH displayed superior antioxidant potential in comparison with another type of honey (Abu Bakar et al., 2017). Although, there have been few studies investigated on the phytochemical properties of KH from Malaysia, however, these studies only examined KH from peninsular Malaysia and some southern states. There are no studies

on the phytochemical and antioxidant properties of KH from other regions of Malaysia. Besides, there are no comparative studies on phytochemical properties and antioxidant activities of KH from different regions of Malaysia. Furthermore, because of limited data, there is a scarcity of characteristics and quality standards available for the KH. This is mainly due to variations in the standards established by the international honey standards (Codex Alimentarius Commission, 2001). Thus, this paper investigated the phytochemical properties and antioxidant activities of KH obtained from the southern, central, eastern, northern and east coast (Sarawak and Sabah) regions of Malaysia.

MATERIALS AND METHODS

Kelulut Honey Samples

One liter of KH samples produced by stingless bees from different regions i.e. south (Johore), central (Selangor), eastern (Kelantan), northern (Kedah) and east coast regions (Sabah and Sarawak) were purchased from respected local KH collectors between September to November 2017. It should be noted that all of the samples were cultivated by feeding with multifloral nectar source. The details of the samples region and time of collection are as tabulated in Table 1. All of the samples were kept in sterile airtight glass bottles at room temperature to prevent the absorption of moisture for the duration of sampling, storage and analytical test. In order to evaluate the pH values, color intensity, TPC, TFC and antioxidant capacity i.e. DPPH and FRAP activities, about two grams of KH were diluted with 20 mL of distilled water to produce 0.1 g/mL of concentration. Each analysis was repeated 3 times.

Table 1
KH samples region and time of samples collection

Sample Code	Time of collection	Region
Central	September 2017	Pusat Floral Cheras, Selangor
South	October 2017	Pusat Pertanian Parit Botak, Johore
East	October 2017	Kampung Rasal, Tok Uban, Pasir Mas, Kelantan
Sarawak	October 2017	Pusa District, Sarawak
North	November 2017	Pusat Pertanian Teluk Chengai, Kedah
Sabah	November 2017	Taman Pertanian Tenom, Sabah

Phytochemical Analysis

TPC and TFC of KH were analyzed by using Folin-Ciocalteu reagent (Berretta et al., 2005) and the aluminum chloride colorimetric technique (Ali, et al., 2015), respectively as shown in Figure 1. A total of 200 μ L of KH solution was added to 3 mL of 10% diluted Folin-Ciocalteu reagent. Later 90 minutes of placing the solution in the dark

at room temperature, the absorbance was quantified using a Multiskan GO microplate spectrophotometer (Thermo Scientific 1510) at 750 nm. The TPC value was stated as mg gallic acid equivalents per 100 g of honey.

For measuring TFC, 1 mL of the KH sample (0.1-0.4 g/mL) was mixed with 2% of aluminum chloride solution. Following the incubation for 10 minutes at 25°C, the absorbance of the mixture was quantified at 430 nm via a Multiskan GO microplate spectrophotometer (Thermo Scientific 1510). TFC was expressed in mg QUE/ 100 g FW by using the calibration curve according to quercetin standard.

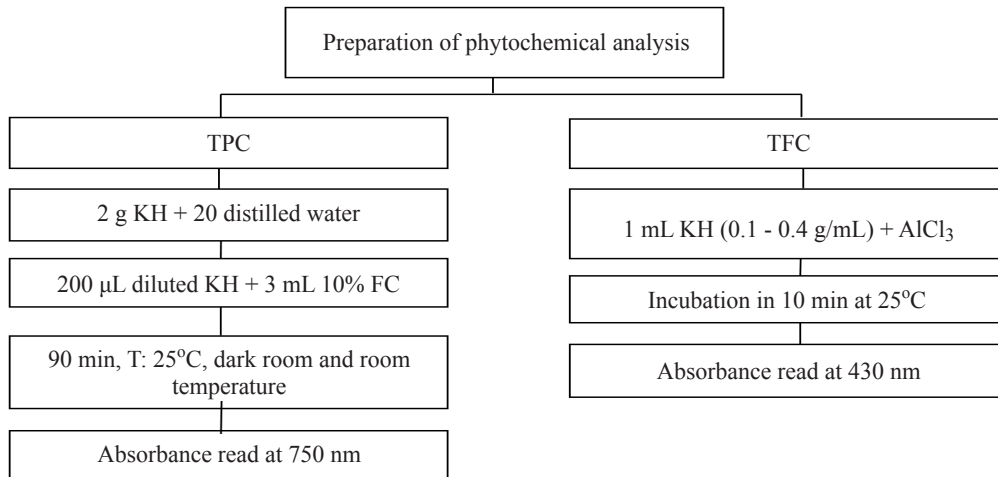


Figure 1. Flowchart representing steps in TPC and TFC determination

Antioxidant Activity

DPPH. The principle of DPPH method is based on the electron transfer, where it measures the scavenging activity of a particular sample (Garcia et al., 2012). The assay yields a concentrated violet solution that is constant at room temperature without the direct light exposure. In this study, radical scavenging activity of KH was determined using Multiskan GO microplate spectrophotometer at 517 nm against DPPH radical as described by Beretta et al. (2005). Following preparation of DPPH solution through dissolving 2 mg of DPPH in 100 mL of ethanol, 1 mL of ethanolic KH solution was mixed to 2 mL of DPPH solution (Figure 2). The reaction mixture was shaken vigorously using hands for yielding the good mixture and later stored without exposure to light for 30 minutes at a room temperature. Subsequently, the absorbance of the mixtures was recorded. The scavenging activity of KH via DPPH radical was quantified based on the equation given below:

$$\text{DPPH radical scavenging activity (\%)} = \frac{(\text{Abs control} - \text{Abs sample})}{\text{Abs control}} \times 100 \quad (1)$$

where Abs control denotes the absorbance of DPPH radical and ethanol, and Abs sample indicates the absorbance of DPPH radical and honey or ascorbic acid. The analysis was conducted three times.

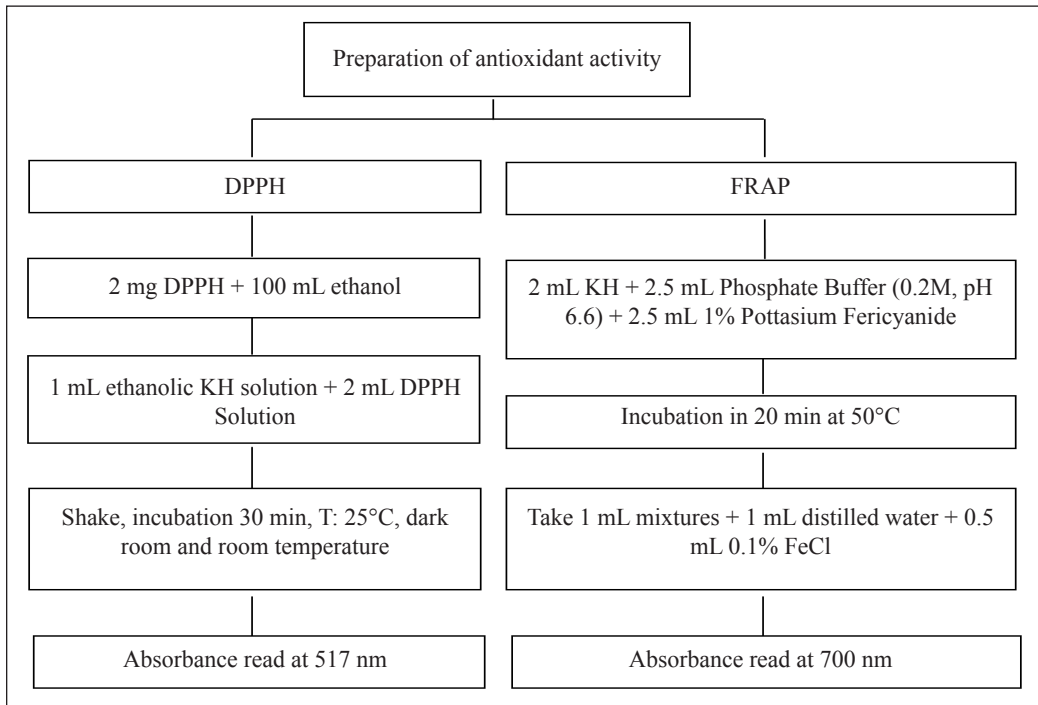


Figure 2. Flowchart representing steps in DPPH and FRAP analyses

Ferric Reducing Antioxidant Power (FRAP). FRAP is a parameter, which is used to measure the antioxidant or reductant activity in a sample. Total antioxidants were assessed by the reduction of Fe^{3+} to Fe^{2+} (Yen & Duh, 1993; Ahmad & Abdullah., 2013). In this study the FRAP analysis was conducted by combining a mixture of 0.5g KH and 100 mL distilled water with 2.5 mL of phosphate buffer (0.2M, pH 6.6) and 2.5 mL of 1% potassium ferricyanide (Figure 2). The mixtures were incubated for 20 min under 50°C . After incubation, a total of 2.5 mL of 10% trichloroacetic acid were combined to the mixture. The 1 mL mixture was added with 1 mL of distilled water and 0.5 mL of 0.1% ferric chloride. The absorbance of the solution was quantified at 700 nm via a Multiskan GO microplate spectrophotometer (Thermo Scientific 1510). The FRAP activity of KH was expressed in absorbance unit.

pH and Color Intensity

The color intensity that represents the darkness value of honey was determined by using the method described in a previous study (Beretta et al., 2005). A 50% (w/v) honey solution

was prepared with warm water at 45 to 50°C. The net absorbance was determined using the Multiskan GO microplate spectrophotometer at 450 nm. The pH was measured using a pH meter, model LAQUA twin pH (HORIVA, Japan).

Statistical Analysis

The significance between means were analyzed using one-way analysis of variance (ANOVA) as well as Tukey's multiple-comparisons analysis. The significant level was set at $P \leq 0.05$. The correlation between every measurement was examined via Pearson correlation coefficient.

RESULTS AND DISCUSSION

Total Phenolic Content and Total Flavonoid Content

Table 2 demonstrates the amount of TPC and TFC constituents in KH samples according to the standard curve of gallic acid and quercetin, correspondingly. The KH from the different geographical had different TPC and TFC values. The finding of this study is in agreement with a previous study that reported the significant differences between TPC and TFC of honey samples that were collected from Kedah and Johor (Ranneh et al., 2017). On that account, Silva et al. (2013) reported that flavonoids and polyphenols detected in honey resulted in superior antioxidant activity.

The findings indicated that the TPC varied significantly ($P \leq 0.05$) among the geographical locations in Malaysia. The TPC value was ranged from 3.045 to 9.370 mg GAE/100g FW. KH from south Malaysia demonstrated the highest TPC followed by the north, Sarawak, Sabah, east and central Malaysia. This significant differences could be due to the variations in the source of pollen surrounding the cultivated area. A research

Table 2
The phytochemical contents, antioxidant activities, color intensity and pH in KH from various regions in Malaysia

Regions	TPC (mg GAE/100g FW)	TFC (mg QUE/100 FW)	DPPH (%)	FRAP (abs)	Color Intensity (abs, mAU)	pH
South	9.37 ^a ± 0.23	14.44 ^a ± 0.18	2.77 ^c ± 1.02	0.22 ^a ± 0.002	0.30 ^a ± 0.02	5.13 ^{ab} ± 0.09
North	6.15 ^b ± 0.5	9.45 ^b ± 0.18	18.65 ^b ± 2.10	0.22 ^b ± 0.002	0.23 ^b ± 0.01	5.20 ^{ab} ± 0.16
Sarawak	5.49 ^{bc} ± 0.50	8.72 ^c ± 0.12	19.25 ^b ± 7.11	0.22 ^b ± 0.003	0.21 ^c ± 0.01	4.25 ^d ± 0.19
Sabah	5.17 ^c ± 0.05	7.29 ^d ± 0.14	1.98 ^c ± 0.45	0.20 ^c ± 0.02	0.21 ^c ± 0.02	4.58 ^{dc} ± 0.17
East	3.79 ^d ± 0.50	5.24 ^c ± 0.18	30.36 ^b ± 2.28	0.19 ^c ± 0.02	0.13 ^d ± 0.003	5.50 ^a ± 0.36
Central	3.04 ^d ± 0.1	3.63 ^f ± 0.25	44.05 ^a ± 11.04	0.19 ^c ± 0.002	0.09 ^c ± 0.003	4.8 ^{bc} ± 0.22

*Means with the same letter are not significantly different at $P \leq 0.05$ by using Tukey test

study by Kroyer and Hegedus (2001) found that flavonoids were among the important forms of polyphenols, which existed in pollen composed by honeybees. Nijveldt et al. (2001) demonstrated that this category of bioactive compounds functioned as a superior antioxidant that facilitated scavenging activity of free radicals. Additionally, the authors concluded that flavonoids stabilized and neutralized reactive oxygen species to generate a reduced reactive radical.

The results also revealed that the TFC demonstrated a significant difference between different geographical locations with the values ranged from 3.63 to 14.44 mg QUE/100g FW. The highest TFC was exhibited by the south and the lowest was from the central. KH samples were belonging to dissimilar geographical and botanical origins, which could be the reason for the differences. These findings are in agreement with the past studies by Biluca et al. (2016), Silva et al. (2013), Da Silva et al. (2013), Silici et al. (2010), Lachman et al. (2010) and Al et al. (2009), which demonstrated that the values of TPC and TFC of honey were influenced by the geographical floral origins.

Antioxidant Activity

Table 2 demonstrates that there was a significant difference between DPPH and FRAP activities as affected by geographical locations. KH from central Malaysia possessed the highest ability to scavenge DPPH radicals with inhibition of DPPH by 44% ($P \leq 0.05$) followed by the east, Sarawak and north, whereas the KH originated from the south and Sabah demonstrated low in DPPH inhibition with values lower than 5%. The results obtained was contradicted with Chan et al., (2017) who found that KH originated from the east coast region had the highest scavenging activity against DPPH radicals with scavenging percentage of 44.12-79.99%. Similarly, Tuksitha et al. (2018) found that DPPH assay contents of the three different stingless bees species (*Geniotrigona thoracica*, *Heterotrigona itama* and *Heterotrigona erythrogastra*) were ranged from 17.0 ± 7.5 to 47.4 ± 3.2 (%). Meanwhile, Abu Bakar et al. (2017) revealed that *Heterotrigona itama* honey collected in Jasin, Melaka exhibited the highest levels of DPPH assay with the values of $97.30 \pm 0.84\%$.

In the present study, FRAP activity for KH from the south of Malaysia demonstrated the highest antioxidant potential while KH from the central region of Malaysia obtained the lowest values ($P \leq 0.05$). The coincidence of KH from the south of Malaysia having the highest TPC, TFC, FRAP highlighted the contributions of these bioactive compounds in antioxidant activity. The roles of TPC and TFC in antioxidant activity of stingless bee honey have been studied extensively (Silva et al., 2013; Ibrahim et al., 2016; Kek et al., 2017). Therefore, evidence has confirmed that TPC and TFC play crucial role in the antioxidant activity of KH, with the effect of the geographical of the nectar source in determining the bioactive contents.

pH and Color

The differences with regard to pH and color among the honey varies according to the type of bee species, region, the season of collection and type of floral sources. The Malaysian Standard (2017) had established a standard pH range between 2.5 to 3.8 for stingless bee honey. Nonetheless, a review by Nordin et al. (2018) found the pH of stingless bee honey varied between 3.15 to 6.64. Furthermore, authors concluded the honey of *Melipona scutellaris* from Brazil had the lowest pH value of 3.15 (Marchini et al., 1998). Meanwhile, the honey of *Melipona quadrifasciata* from Brazil had the highest pH value (Carvalho et al., 2009).

Table 2 demonstrates that the KH from the north of Malaysia had the highest pH value in which the pH values of all the KH samples were ranged from 4.25 to 5.5. In a similar study, Syam et al. (2016) reported that pH of *Trigona* honey from Masamba, Indonesia was 3.34 while Chanchao (2009) revealed that pH honey of *Trigona Laviecep* from Thailand was 3.37. On the other hand, Boorn et al. (2010) found that pH of *Trigona carbonaria* honey from Queensland was 3.85. The aforementioned findings reveal that KH is acidic, which contributed to the sourness of KH. Thus, the antimicrobial capacity of KH may be derived from pH values.

Moniruzzaman et al. (2013) reported that color intensity of honey was a consistent parameter that specified the existence of pigments that had antioxidant activities including carotenoids and flavonoids. Solayman et al. (2016) stated that the color of honey could differ from straw yellow to nearly black as it was affected by the mineral, pollen and phenolic contents of the honey. This study has discovered that color intensity values of the honey from the south of Malaysia had the highest values followed by the north, Sarawak, Sabah, east and central of Malaysia (Table 2). The color intensity of each KH samples varied between 0.0925 mAU to 0.30125 mAU. Recently, Nordin et al. (2018) indicated that color varieties of stingless bee honey across the different countries were 26 Pfund to 150 Pfund, which were detected via a photometer. Furthermore, the authors reported the highest intensity of color, which was detected in *Tetragonisca angustula* honey from Brazil and the lowest intensity of color, which was detected in *Melipona ilota* from Peru.

A study by Bertonecelj et al. (2007) reported that color of honey was significantly affected by its geographical starting point. Kek, et al. (2014) demonstrated that KH had the highest color intensity compared to Tualang, Gelam, Pineapple, Borneo and commercial honey in Malaysia. Apart from geographical and species, the variations in the color intensity of the honey might be influenced by particular polluting pigments originating from handling, processing, and storage processes, or from biochemical reactions throughout honey maturation (Beretta et al., 2005). Nevertheless, there is a lack of standard available for honey with regard to pH and color.

Correlation Between Phytochemical Properties, Antioxidant Activity and Color

The correlation analysis revealed that there was a strong, negative and significant correlation between TPC and TFC with DPPH activity (Table 3). As such, this implies that the TPC and TFC increased inversely with DPPH activity. Furthermore, this indicates that the increase in TPC and TFC of KH resulted in the decrease in DPPH activity. The decrease in DPPH activity is correlated with the ability of the KH to neutralize the free radical of DPPH from being oxidized by reactive oxygen species (Nurdianah et al., 2016). The high content of TPC and TFC might not contribute to the strong antioxidant activity. These results are consistent with Chan et al. (2017), which demonstrated that KH had high TPC and TFC but low DPPH activity. Hence, this indicates that higher TPC and TFC may not lead to high DPPH activities.

Table 3

Correlation between phytochemical contents (TPC and TFC), antioxidant activities (DPPH and FRAP) and color intensity in KH collected from various regions in Malaysia

	TFC	TPC	DPPH	FRAP	Color Intensity
TFC	1				
TPC	0.97***	1			
DPPH	-0.80***	-0.73***	1		
FRAP	0.81***	0.81***	-0.79***	1	
Color Intensity	0.96***	0.94***	-0.83***	0.82***	1

*** Correlations are significant at $P \leq 0.001$

The findings also indicate that TPC and TFC correlated positively with FRAP activity. This implies that the TPC and TFC increased proportionally with the FRAP activity. These findings are consistent with Chan et al. (2017), which demonstrated that stingless bee honey had higher TPC and TFC contents, thus leading to high in FRAP activity. The strong FRAP activity possessed by KH is related to the potential of the KH in reducing Fe^{3+} to Fe^{2+} . A correlation between TPC and antioxidant activity in the KH was reported by other studies (Duarte et al., 2012; Sousa et al., 2016; Ranneh et al., 2017). Hence, polyphenols compounds could result in a greater antioxidant potential in KH. In addition, the correlation between KH and antioxidant was reported to be high due to the high content of ascorbic acid (Guerrini et al., 2009; Kek et al., 2014).

The color of KH was found to be positively correlated and significantly associated with TFC, TPC, and FRAP activities (Table 3). TPC and FRAP activity increased proportionately with the increase in the intensity of the darker colour of KH. The finding is in accordance to Saxena et al. (2010) who reported that color intensity has positive correlations (R values between 0.72 and 0.83) with antioxidant activities in honey samples. Higher absorbance value was associated with darker color in KH samples. The darker colour of KH could be

due to the higher content of TPC and TFC, which could increase the potential of KH as an antioxidant property. Nevertheless, the colour of KH demonstrated a negative correlation with DPPH activity.

The correlation between TPC and TFC with color intensity demonstrated that there were strong, positive and significant correlations with $R > 0.8$. The results of this study are in agreement with previous findings by Moniruzzaman et al. (2013) who reported that color intensity of KH was a consistent parameter that could indicate the existence of pigments. On that account, this finding indicates that the antioxidant activities like carotenoids and flavonoids. Kek et al. (2014) also reported a similar result and concluded that the TPC of honey increased with color intensity.

CONCLUSION

The current study indicated that TPC, TFC, antioxidant activity, color intensity and pH of KH could be elucidated by the natural disparities of floral nectar sources and geographical regions. Honey from the Southern region of Malaysia presented a good level of phytochemical composition and antioxidant activity as compared to the north, Sabah, Sarawak, east and central of Malaysia. The strong and positive correlations were observed between TPC, TFC, antioxidant property and color intensity of KH samples. Thus, the aforementioned findings suggest that honey with darker color had greater TPC, TFC, and antioxidant property. The findings could provide some fundamental data related to KH that can be used as a reference for future research.

ACKNOWLEDGMENTS

The authors are thankful to Universiti Putra Malaysia for providing financial support under the Geran Putra research funding (GP-IPS/9633300).

REFERENCES

- Abu Bakar, M. F., Sanusi, S. B., Abu Bakar, F. I., Cong, O. J., & Mian, Z. (2017). Physicochemical and antioxidant potential of raw unprocessed honey from Malaysian stingless bees. *Pakistan Journal of Nutrition*, 16(11), 888-894.
- Ali, F., Ranneh, Y., Ismail, A., & Esa, N. M. (2015). Identification of phenolic compounds in polyphenols rich extract of Malaysian cocoa powder using the HPLC-UV-ESI-MS/MS and probing their antioxidant properties. *Journal of Food Science and Technology*, 52(4), 2103-2111.
- Ahmad, R., & Abdullah, N. (2013). *Antioxidant Principles and In Vitro Evaluation Methods*. Shah Alam, Selangor: UiTM Press.
- Al, M. L., Daniel, D., Moise, A., Bobis, O., Laslo, L., & Bogdanov, S. (2009). Physicochemical and bioactive properties of different floral origin honeys from Romania. *Food Chemistry*, 112(4), 863-867.

- Biluca, F. C., Braghini, F., Gonzaga, L. V., Costa, A. C. O., & Fett, R. (2016). Physicochemical profiles, minerals and bioactive compounds of stingless bee honey (Meliponinae). *Journal of Food Composition and Analysis*, 50, 61-69.
- Biluca, F. C., Braghini, F., Gonzaga, L.V., Pereira, L. M., Costa, A.C.O., & Fett, R., (2014). 5-HMF and carbohydrates content in stingless bee honey by CE before and after thermal treatment. *Food Chemistry*, 159, 244-249.
- Boorn, K. L., Khor, Y. Y., Sweetman, E., Tan, F., Heard, T. A., & Hammer, K. A., (2010). Antimicrobial activity of honey from the stingless bee *Trigona carbonara* determined by agar diffusion, agar dilution, broth microdilution and time-kill methodology. *Journal of Applied Microbiology*, 108(5), 1534-1543.
- Bertoncelj, J., Dobersek, U., Jamnik, M., & Golob, T. (2007). Evaluation of the phenolic content, antioxidant activity and colour of Slovenian honey. *Food Chemistry*, 105(2), 822-828.
- Beretta, G., Granata, P., Ferrero, M., Orioli, M., & Facino, R. M. (2005). Standardization of antioxidant properties of honey by a combination of spectrophotometric/fluorimetric assays and chemometrics. *Analytica Chimica Acta* 533(2), 185-191.
- Chan, B. K., Haron, H., Talib, R. A., & Subramaniam, P. (2017). Physical properties, antioxidant content and antioxidative activities of Malaysian stingless kelulut (*Trigona spp.*) honey. *Journal of Agricultural Science*, 9(3), 32-40.
- Chuttong, B., Chanbang, Y., Sringarm, K., & Burgett, M. (2016a). Effects of long term storage on stingless bee (Hymenoptera: Apidae: Meliponini) honey. *Journal of Apicultural Research*, 54(5), 441-451.
- Chuttong, B., Chanbang, Y., Sringarm, K., & Burgett, M. (2016b). Physicochemical profiles of stingless bee (Apidae: Meliponini) honey from South East Asia (Thailand). *Food Chemistry*, 192, 149-155.
- Chuttong, B., Chanbang, Y., Sringarm, K., & Burgett, M. (2015). Physicochemical profiles of stingless bee (Apidae: Meliponini) honey from South East Asia (Thailand). *Food Chemistry*, 192, 149-155.
- Chanchao C., (2009). Antimicrobial activity by *Trigona laeviceps* (stingless bee) honey from Thailand. *Pakistan Journal of Medical Science*, 25(3), 364-369.
- Carvalho, C. A. L., Sodre, G. S., Fonseca, A. A. O., Alves, R. M. O., Souza, B. A., & Clarton, L. (2009). Physicochemical characteristics and sensory profile of honey samples from stingless bees (Apidae: Meliponinae) submitted to a dehumidification process. *Anais da Academia Brasileira de Ciências*, 81(1), 143-149.
- Codex Alimentarius Commission. (2001). Alinorm 41/10: revised standard for honey. *Alinorm 1*, 19-26.
- Sousa, J. M., de Souza, E. L., Marques, G., Meireles, B., de Magalhães Cordeiro, Â. T., Gullón, B., Pintado, M. M., & Magnani, M. (2016). Polyphenolic profile and antioxidant and antibacterial activities of monofloral honeys produced by Meliponini in the Brazilian semi-arid region. *Food Research International*, 84, 61-68.
- Da Silva, I. A. A., Da Silva, T. M. S., Camara, C. A., Queiroz, N., Magnane, M., & De Novais, J. S. (2013). Phenolic profile, antioxidant activity and palynological analysis of stingless bee honey from Amazonas, Northern Brazil. *Food Chemistry*, 141(4), 3552-3558.

- Duarte, A. W. F., Vasconcelos, M. R. D. S., de Menezes, A. P. D., da Silva, S. C., Oda-souza, M., & Lopez, A. M. Q. (2012). Composition and antioxidant activity of honey from Africanized and stingless bees in Alagoas (Brazil): a multivariate analysis. *Journal of Apicultural Research*, 51(1), 23-35.
- Erejuwa, O. O., Sulaiman, S. A., & Ab Wahab, M. S. (2012). Honey: A novel antioxidant. *Molecules*, 17(4), 4400-4423.
- Garcia, E. J., Oldoni, T. L. C., Alencar, S. M., Reis, A., Loguercio, A. D., & Grande, R. H. M. (2012). Antioxidant activity by DPPH assay of potential solutions to be applied on bleached teeth. *Brazil Dental Journal*, 23(1), 22-27.
- Guerrini, A., Bruni, R., Maietti, S., Poli, F., Rossi, D., Paganetto, G., & Sacchetti, G. (2009). Ecuadorian stingless bee (Meliponinae) honey: A chemical and functional profile of an ancient health product. *Food Chemistry*, 114(4), 1413-1420.
- Ibrahim, N., Zakaria, A.J., Ismail, Z., & Mohd, K.S., (2016). Antibacterial and phenolic content of propolis produced by two Malaysian stingless bees, *Heterotrigona itama* and *Geniotrigona thoracica*. *International Journal of Pharmacognosy and Phytochemical Research*, 8(1), 156-161.
- Kek, S. P., Chin, N. L., Yusof, Y. A., Tan, S. W., & Chua, L. S. (2017). Classification of entomological origin of honey based on its physicochemical and antioxidant properties. *International Journal of Food Properties*, 20(3), S2723-S2738.
- Kek, S. P., Chin, N. L., Yusof, Y. A., Tan, S. W., & Chua, L. S. (2014). Total phenolic contents and colour intensity of Malaysian honeys from the *Apis* spp. and *Trigona* spp. bees. *Agriculture and Agricultural Science Procedia*, 2, 150-155.
- Kroyer, G., & Hegedus, N. (2001). Evaluation of bioactive properties of pollen extracts as functional dietary food supplement. *Innovative Food Science and Emerging Technologies*, 2(3), 171-174.
- Lachman, J., Orsák, M., Hejtmánková, A., & Kovářová, E. (2010). Evaluation of antioxidant activity and total phenolics of selected Czech honeys. *LWT-Food Science and Technology*, 43(1), 52-58.
- Malaysian Standards. (2017). *Kelulut (Stingless Bee) honey-Specification*. Department of Standards Malaysia. MS, 2683.
- Moniruzzaman, M., Sulaiman, S. A., Khalil, M.I., & Gan, S. H. (2013). Evaluation of physicochemical and antioxidant properties of sourwood and other malaysian honeys: A comparison with manuka honey. *Chemistry Central Journal*, 7(1), 138.
- Marchini, L. C., Carvalho, C. A. L., Alves, R. M. O., Teixeira, G. M., & Rubia, V. R. (1998 October, 13-11). Características físico-químicas de amostras de méis da abelha Uruçu (*Melipona scutellaris*). In *XII Congresso Brasileiro de Apicultura 201* (pp. 270). Salvador, Brazil.
- Nordin, A., Sainik, N. Q. A. V., Chowdhury, S. R., Saim, A. B., & Idrus, R. B. H. (2018). Physicochemical properties of stingless bee honey from around the globe: A comprehensive review. *Journal of Food Composition and Analysis*, 73, 91-102.
- Nurdianah, H. F., Ahmad Firdaus, A. H., Eshaifol Azam, O., & Wan Adnan, W. O. (2016). Antioxidant activity of bee pollen ethanolic extracts from Malaysian stingless bee measured using DPPH-HPLC assay. *International Food Research Journal*, 23(1), 403-405.

- Nijveldt, R. J., Van Nood, E. L. S., Van Hoorn, D. E., Boelens, P. G., Van Norren, K., & Van Leeuwen, P. A. (2001). Flavonoids: A review of probable mechanisms of action and potential applications. *The American Journal of Clinical Nutrition*, 74(4), 418-425
- Ranneh, Y., Ali, F., Zarei, M., Akim, A. M., Hamid, H. A., & Khazaai, H. (2017). Malaysian stingless bee and Tualang honeys: A comparative characterization of total antioxidant capacity and phenolic profile using liquid chromatography-mass spectrometry. *Journal of Food Science and Technology*, 89, 1-9.
- Rodriguez-Malaver, Vit, P., Pedro, S. R. M., & Roubik, D. (2013). *Antioxidant activity of pot honey*. In *Pot-honey: A legacy of stingless bees*. New York, USA: Springer.
- Rodriguez-Malaver, A. J., Rasmussen, C., Gutierrez, M. G., Gil, F., Nieves, B., & Vit, P. (2009). Properties of honey from ten species of Peruvian stingless bees. *Natural Product Communications*, 4(9), 1221-1226.
- Shadan, A. F., Mahat, N. A., Wan Ibrahim, W. A., Ariffin, Z., & Ismail, D. (2018). Provenance establishment of stingless bee honey using multi element analysis in combination with chemometrics techniques. *Journal of Forensic Sciences*, 63(1), 80-85.
- Syam, Y., Usman, A. N., Natzir, R., Rahardjo, S. P, Hatta, M., Sjattar, E. L., Saleh, A., & Sa'na, M. (2016). Nutrition and pH of Trigona honey from Masamba, South Sulawesi, Indonesia. *International Journal of Sciences: Basic and Applied Research*, 27(1), 32-36.
- Solayman, M., Islam, M. A., Paul, S., Ali, Y., Khalil, M. I., Alam, N., & Gan, S. H. (2016). Physicochemical properties, minerals, trace elements, and heavy metals in honey of different origins: a comprehensive review. *Comprehensive Review in Food Science and Food Safety*, 15(1), 219-233.
- Silva, T. M. S., Dos Santos, F. P., Evangelista-Rodrigues, A., Da Silva, E. M. S., Da Silva, G. S., De Novais, J. S., Dos Santos, F. D. A. R., & Camara, C. A. (2013). Phenolic compounds, melissopalynological: physicochemical analysis and antioxidant activity of Jandaira (*Melipona subnitida*) honey. *Journal of Food Composition and Analysis*, 29(1), 10-18.
- Silici, S., Sagdic, O., & Ekici, L. (2010). Total phenolic content, antiradical, antioxidant and antimicrobial activities of *Rhododendron* honeys. *Food Chemistry*, 121(1), 238-243.
- Saxena, S., Gautam, S., & Sharma, A., (2010). Physical, biochemical and antioxidant properties of some Indian honeys. *Food Chemistry*, 118(2), 391- 397.
- Tuksitha, L., Chen, Y. L. S., Chen, Y. L., Wong, K. Y., & Peng, C. C. (2018). Antioxidant and antibacterial capacity of stingless bee honey from Borneo (Sarawak). *Journal of Asia Pacific and Entomology*, 21(2), 563-570.
- Yen, G.C., & Duh, P.D. (1993). Antioxidative properties of methanolic extracts from peanut hulls. *Journal of the American Oil Chemists Society*, 70(4), 383-386.
- Zainol, M.I., Yusoff, K.M., & Yusof, M.Y.M. (2013). Antibacterial activity of selected Malaysian honey. *International Society for Complementary Medicine Research*, 13(1), 1-10.



Impact of Gamma Irradiation on Physical Parameters, Microbial Safety and the Total Polyphenolic Content of Commercially Available Ceylon Black Tea (*Camellia sinensis* L.)

Arosha Rashmi De Silva^{1*}, Rathnayake Mudiyansele Nalaka Priyanga Rathnayake², Rampati Devage Roshani Ranasinghe² and Chamila Vinodanee Liyanage Jayasinghe¹

¹Department of Food Science and Technology, Faculty of Livestock, Fisheries and Nutrition, Wayamba University of Sri Lanka, Makandura (NWP), Gonawila, Sri Lanka

²Sri Lanka Gamma Center, Atomic Energy Board of Sri Lanka, Biyagama, Sri Lanka

ABSTRACT

The study was carried out to evaluate the impact of gamma irradiation on the physical parameters, microbial safety and the total polyphenolic content (TPPC) of Ceylon black tea (*Camellia sinensis* L.). Commercially available Broken Orange Pekoe Fannings (BOPF) black tea samples of 5 distinct brands (n=120) were irradiated at 0, 1, 2, 5, 10 and 30kGy doses using Co-60 gamma irradiator. Samples were analyzed for water activity (a_w), color of tea and tea infusion, microbial safety and TPPC. Water activities of samples were within the range of 0.32 to 0.58 and no effect had been observed due to the irradiation. The mean value of L, b and E hunter parameters of tea infusion was increased where the “a” value was decreased with the increment of irradiation dose when compared to the control sample. High irradiation doses resulted in darker color of the tea infusion. Irradiated samples showed a significant reduction of the total plate count. After 5kGy dose, irradiated samples were in sterilized condition. Yeast and mould counts were gradually decreased with the irradiation dose. TPPC of tea leaves of both irradiated and non-irradiated samples ranged from 9.17- 37.98 GAE/240 ml and TPPC values were increased with the irradiation dose.

Results conclude that 5kGy is the optimum dose for the effective microbial safety, preserving the physical parameters and TPPC of commercially available Ceylon black tea.

Keywords: Ceylon black tea, color of tea, irradiation, microbial safety, physical parameters, total polyphenolic content

ARTICLE INFO

Article history:

Received: 24 October 2018

Accepted: 15 February 2019

Published: 21 June 2019

E-mail addresses:

rashmi76831@gmail.com (Arosha Rashmi De Silva)

npbinara@gmail.com (Rathnayake Mudiyansele Nalaka

Priyanga Rathnayake)

roshani@aeb.gov.lk (Rampati Devage Roshani Ranasinghe)

cjayasinghe@wyb.ac.lk (Chamila Vinodanee Liyanage Jayasinghe)

* Corresponding author

INTRODUCTION

Tea is one of the major agricultural produces in Sri Lanka, approximately contributing 2% of the national GDP, 70% to the agricultural export earnings and nearly 15% of total export earnings (Herath & Weersink, 2009). The health benefits of tea include prevention of cancers and cardiovascular diseases, strengthening of immune systems and tea is a source of natural, -antioxidant (Fujita & Yamagami, 2008; Hamer, 2007).

Black tea is the most important one among all other teas consumed all over the world and made sometimes difficult to comprehend by the tea consumers as tea testers developed their own languages to describe various quality attributes of black tea infusion (Liang et al., 2005). There are two main categories of tea, which are orthodox black tea known as broken leaf grade and whole leaf grade. Broken leaf grade has three distinct types namely, Dust No.1, Broken Orange Pekoe (BOP) and Broken Orange Pekoe Fannings (BOPF). BOPF consists of particle size of 500 – 850 μm (Ratnasooriya & Muthunayake, 2014).

Black tea preparation mainly consists of harvesting, withering, rolling, fermentation and drying (Vargas & Vecchietti, 2016). Withering is the crucial step which facilitates the rolling process by disrupting cell structure and the beginning of the tea fermentation (Luczaj & Skrzydlewska, 2005). Contamination of microbes can easily occur during the withering stage due to high increment in the humidity level. Tea leaves and tea buds of plants are collected and taken for processing without cleaning and washing (Mishra et al., 2006). Kausar et al. (2013) indicated that microbes easily contaminated tea during harvest, drying, fermentation, and storage. When the tea is carrying microorganisms, it gives a potential health risk to consumers (Mishra et al., 2006).

Food Irradiation is a treatment, which uses ionizing radiations to improve the microbial safety and storability of food (Mali et al., 2011). Food irradiation causes some issues such as low microbial efficiency, color deviations, flavor changes and functional property losses compared to other preservation technologies that are applied for decontamination of dried foods. Mishra et al. (2006) showed that gamma irradiation could be used as a processing technique which would improve the microbial quality and safety of tea. However, tea manufacturers were concerned about the irradiation process which could result in chemical changes, vitamin depletion, transformation of xenobiotic and survival of bacterial toxins on tea. According to Kausar et al. (2013), instead of irradiation, chemical fumigation with Methyl Bromide (MeBr) and Phosphine (PH_3) is the conventional decontamination method of tea. However, it has been prohibited or been restricted gradually due to their safety or environmental concerns, necessitating the development of alternative methods. Only a limited number of researches conducted on the effect of irradiation on black tea (Mishra et al., 2006; Rashid et al., 2016; Fanaro et al., 2014). Further studies show that different doses of gamma irradiation influence on the chemical and physical structure differences in microorganisms (Farkas, 2006) and thereby reduction of microbial growth can happen.

The objective of this study was to determine the impact of gamma Irradiation on the physical parameters, microbial safety and total polyphenolic content (TPPC) of commercially available Ceylon black tea. Also, we expected to find out the effective irradiation dose for microbial decontamination of commercially available black tea in Sri Lanka.

MATERIALS AND METHODS

SAMPLE SELECTION

Five brands were selected considering the BOPF. Totally 120 packets, 24 from each brand, of 50 g were bought from the market. Tea samples were carefully selected to obtain the physical parameters, microbial safety and the TPPC. Proceeding with the test of each parameter, three replicates from each brand were selected per each irradiation dose level.

Irradiation

Tea samples were irradiated in a Co-60 irradiator (Sri Lanka Gamma Centre) with the targeted doses of 0, 1, 2, 5, 10 and 30kGy. Actual doses were 0, 1.06, 2.02, 4.97, 9.46 and 29.29kGy respectively. The targeted dose values are used in this context hereafter to represent the dose levels. The source strength was approximately 154 kCi with a dose rate of 4.2 Gy/min. Dosimetry was performed using Perspex dosimeters (Harwell-Type:3042, United Kingdom) and ceric-cerous dosimeters (BRIT, India). Samples were rotated during the irradiation process to achieve uniform doses.

Determination of Water Activity

The water activity was measured using a water activity meter (Novasina LabMASTER, Switzerland). A plastic chamber containing the test tea sample (2 g) was kept in the instrument to obtain the corresponding water activity at 25°C.

Moisture Content

The moisture content was determined on a dry weight basis using moisture balance (Mishra et al., 2006). The tea samples (2 g) were kept in the container of moisture balance (MRS 120-3, USA) and the percentage decrease in weight at $105 \pm 1^\circ\text{C}$ was conveyed as moisture content.

Determination of Color in Tea Powder

Color analysis on black tea powder was carried out using a chromameter (Chromameter-2 Reflectance, Minolta, Osaka, Japan) equipped with a CR-200 measuring head. Color was expressed in L, a, and b Hunter scale parameters on the digital screen of chromameter.

The Hunter scale color parameters ΔL , Δa and Δb represented the light–dark, red–green, yellow–blue in color.

$$\Delta E = \sqrt{(\Delta L^2 + \Delta a^2 + \Delta b^2)} \quad [1]$$

Determination of Color in Tea Infusion

Tea samples (5 g of each) were extracted into 240 ml of freshly boiled distilled water for 5 minutes. The infusion sample was cooled into room temperature before it was filtered using Double-ring No 102-filter paper (Xinhua Paper Industry Co Ltd, Hangzhou, China). The obtained filtrate was diluted using 10ml of distilled water up to 250 ml of total volume. Distilled water was used as the control to reduce the errors from different determination conditions of equipment and temperature differences. Color analysis on black tea infusion was carried out using a chromameter (Chromameter-2 Reflectance, Minolta, Osaka, Japan) equipped with a CR-200 measuring head.

Estimation of Total Polyphenolic Content (TPPC)

The TPPC in tea leaves were determined by colorimetric method using Folin-ciocalteu reagent according to the ISO standard 14502-1:2005(E) (International Organization for Standardization [ISO], 2005). The absorbance was read at 765 nm using UV-visible spectrophotometer (Optima, SP-300, Japan). Gallic acid was used as the standard solution and TPPC in 0.2g of black tea powder was expressed as milligram of Gallic acid equivalent (GAE) per 240ml.

Determination of Total Plate Count (TPC)

The TPC was determined according to the International Standard 4833-1:2013(E) (International Organization for Standardization [ISO], 2013). Plates were incubated in an inverted position for 72 hours at $30 \pm 1^\circ\text{C}$ in a culture incubator (ICP 600, Germany). Colonies were counted using colony-counting equipment (Rocker, Galaxy 330, India). The numbers of colony forming units (CFU) on plates (containing 25 to 250 colonies) were calculated per gram of sample.

Determination of Total Coliform

The total coliform count was determined according to the International Standard 4831-1:2006(E) (International Organization for Standardization [ISO], 2006). The prepared samples were placed in a water bath (GFL 1008, India) for 48 hours at $37 \pm 0.5^\circ\text{C}$. Tubes were noted which showed growth after 24 hours. When both total and fecal Coliforms were confirmed, a Brilliant Green Bile Broth (BGLB) and an *E. coli* medium tube were

inoculated from each presumptive positive. Then the tubes were carefully incubated for 48 hours at $37 \pm 0.5^\circ\text{C}$ for total *Coliforms* (BGLB broth) or for 24 hours at $44 \pm 0.5^\circ\text{C}$ for fecal coliforms (*E. coli* medium). After that tubes were noted which showed growth in the production of gas and recorded the number of positives for each sample dilution.

Determination of Yeast and Mould Count (YMC)

The YMC was determined according to the ISO 21527-2:2008(E) (International Organization for Standardization [ISO], 2008). Plates were incubated in upright position at $25 \pm 1^\circ\text{C}$ for 5 days to 7 days in a culture incubator (ICP 600, Germany). Then colonies were counted using colony-counting equipment (Rocker, Galaxy 330, India). The numbers of colony forming units (CFU) on plates (containing <150 colonies) were calculated per gram of sample.

Statistical analysis

Descriptive and inferential statistical analysis was done by using SPSS 16.0 software. The individual observations of tea samples in case of physical, microbial and TPPC activities were analyzed and expressed in terms of mean and standard deviation (SD). The mean values of control and irradiated samples were compared using one-way analysis of variance (ANOVA) to determine the significance of their difference ($P < 0.05$).

RESULTS AND DISCUSSION

Water Activity

The water activity of the control and irradiated tea were within the range of 0.32 to 0.58 and the differences were statistically insignificant ($P > 0.05$) (Table 1). Low water activity and low moisture content of foods act as significant barriers to the growth of microorganisms (Fanaro et al., 2014) and the minimum a_w required for the growth of microbes was 0.6

Table 1
Mean value of water activity and moisture content of commercially available Ceylon black tea samples with different irradiation doses

Dose (kGy)	Water activity	Moisture content (%)
0	0.46 ± 0.07	5.42 ± 0.94
1	0.49 ± 0.04	5.28 ± 1.02
2	0.44 ± 0.07	5.22 ± 0.93
5	0.49 ± 0.05	5.19 ± 0.89
10	0.51 ± 0.06	5.19 ± 1.02
30	0.51 ± 0.07	5.41 ± 1.18

The data represent the mean \pm SD of samples in each of five different tea brands. The mean values in a column are not significantly different ($P < 0.05$) as analyzed by one-way analysis of variance (ANOVA).

(Beuchat et al., 2013). Water is the major source of ions and radicals, as well as the greatest mass component in most foods. The irradiation process leads to the formation of radiolytic products such as e^- (aq), (H_2O^+) , (H_3O^+) , $(\cdot OH)$, $(H\cdot)$ and H_2O_2 (Breen & Murphy, 1995). The present study showed irradiation treatment did not affect the water activity level of tea.

Moisture Content

Table 1 shows the moisture content of the control and irradiated tea and they were within the range of 4.17 - 6.59%. Results reveal that the mean moisture content was not differed due to the higher doses of irradiation in each brand and the differences were statistically not significant ($P>0.05$). Tea approximately contains 6% of moisture during its proper storage, which reduces the microbial level in normal condition. Thomas et al. (2008) reported that the metabolic activities of microbes were accelerated by the moisture content of tea. The present study showed that irradiation treatment does not affect the moisture content of the tea samples.

Color of Tea and Tea Infusion

Compared with the control sample of tea infusion, hunter scale parameters of L and b increased with the irradiation dose level (Table 2). The present study, Hunter scale 'L' value depicted the enhancement of the lighter color in black tea infusion by irradiation. The 'b' value of infusion was increased with the higher dose levels that resulted in yellow color. When giving high irradiation doses, tea infusion remained darker in color and significant difference ($P<0.05$) was observed in the ' ΔE ' value after irradiation compared to the non-irradiated samples. Therefore, irradiation enhances the color of black tea infusion. According to Liang et al. (2005), darker color in tea infusion is considered as one of the main qualities in black tea.

Table 2
Mean value of L, a, and b in tea infusion and tea powder of commercially available Ceylon black tea samples with different irradiation doses

Dose (kGy)	Tea Infusion			Tea powder		
	L*	a	b*	L	a	b
0	44.56 ± 2.25	22.12 ± 1.11	37.14 ± 2.24	23.40 ± 0.38	4.03 ± 0.24	5.01 ± 0.59
1	50.41 ± 3.74	20.15 ± 1.78	45.04 ± 3.20	23.54 ± 0.27	4.02 ± 0.27	5.01 ± 0.48
2	48.39 ± 1.93	20.95 ± 1.01	41.83 ± 2.60	23.52 ± 0.27	4.04 ± 0.27	4.99 ± 0.53
5	50.26 ± 1.77	22.03 ± 1.95	45.20 ± 2.78	23.90 ± 0.47	3.85 ± 0.34	4.48 ± 0.69
10	52.14 ± 1.83	21.91 ± 1.49	47.30 ± 2.51	23.90 ± 0.47	3.97 ± 0.31	4.68 ± 0.49
30	53.71 ± 3.05	20.53 ± 2.69	48.03 ± 1.84	23.40 ± 0.39	3.85 ± 0.24	4.30 ± 0.58

The data represent the mean ± SD of samples in each of five different tea brands.

Positive values for L, a and b indicates lighter, redder and yellower accordingly.

*The values marked are significantly differed ($P<0.05$) with increasing irradiation doses when compared to the control sample. The analysis was performed by one-way analysis of variance (ANOVA).

Further, there was no significant difference ($P>0.05$) found in hunter scale L, a and b parameters before and after the irradiation of tea powder, hence not in ' ΔE ' value. Therefore, no effect was found on the color of tea powder due to irradiation.

Total Polyphenolic Content (TPPC)

The differences in the TPPC of 1, 2 and 5kGy irradiated tea samples were statistically insignificant ($P>0.05$) compared with the control (Figure 1). At higher doses of 10kGy and 30kGy, tea samples had an increment of TPPC when comparing with the control (Figure 1).

The differences in the TPPC of 1, 2 and 5kGy irradiated tea samples were statistically insignificant ($P>0.05$) compared with the control (Figure 1). At higher doses of 10kGy and 30kGy, tea samples had an increment of TPPC when comparing with the control (Figure 1).

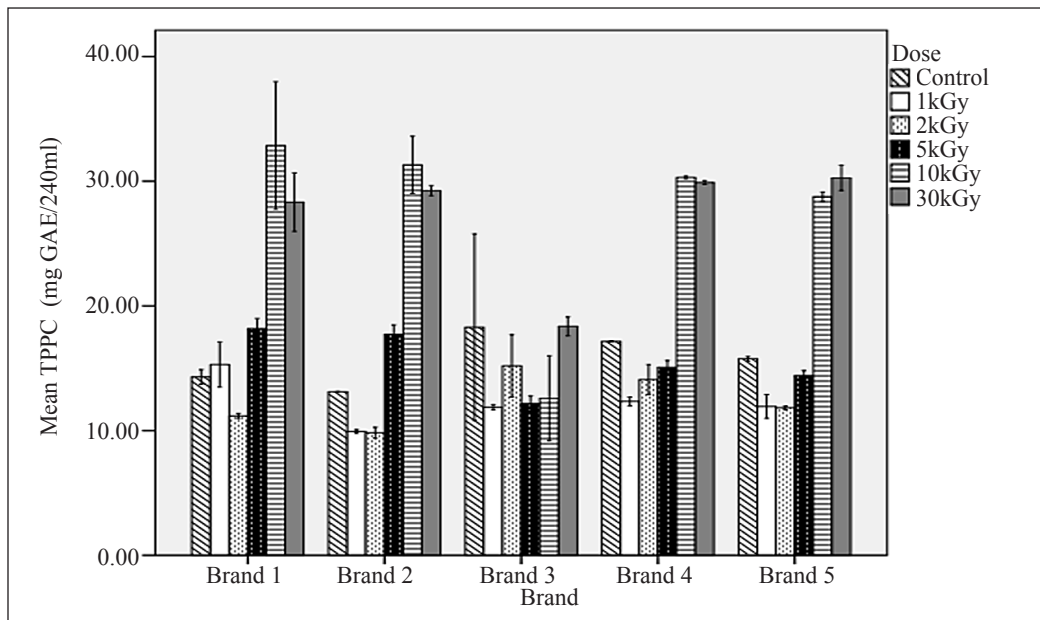


Figure 1. Variation of mean total polyphenolic content of each brand, according to different irradiation doses

Results of this study revealed that when increasing the irradiation dose level after 5kGy, the TPPC level was increased. Hirashima et al. (2013) indicated that the degradation or in solubilization of phenolic compounds occurred due to irradiation. It may be due to the breakdown of the aflavin fractions in tea. Wiseman et al. (1997) explained the breakdown of the aflavins, which resulted in the formation of the arubigins compound, which provided high TPPC levels. According to Mali et al. (2011), differences of the TPPC due to irradiation may be caused by plant type, geographical and environmental conditions, sample state and phenolic content of the sample. Hence the variation of TPPC in distinct brands of different magnitude might be due to the influence of those factors.

Microbial Safety of Tea

Total Plate Count (TPC). This study focused to assess the efficiency in removing bacterial contamination using gamma irradiation of commercially available Ceylon black tea. Hence, commercially available different tea brands were collected and analyzed for distinct types of microbial contaminations.

There was a significant difference ($P < 0.05$) between the values of TPC before and after irradiation in all samples (Figure 2). The TPC in all samples collected was within the range of 0.45×10^3 to 6.64×10^3 CFU/g. The presence of a high microbial load in the tea samples indicates that tea contamination has been occurred. This study showed that applying 1kGy of irradiation to the tea sample were eliminated approximately half of the viable bacteria count compared to the control sample. Beyond the 5kGy of irradiation dose, complete removal of bacteria can be seen (Figure 2). According to the Farkas, (2006) the mechanism behind ionizing radiation is mainly the inactivation of microbes' due to its nucleic acid damage, direct damage or indirect damage caused by the oxidative radicals originating from the radiolysis of water.

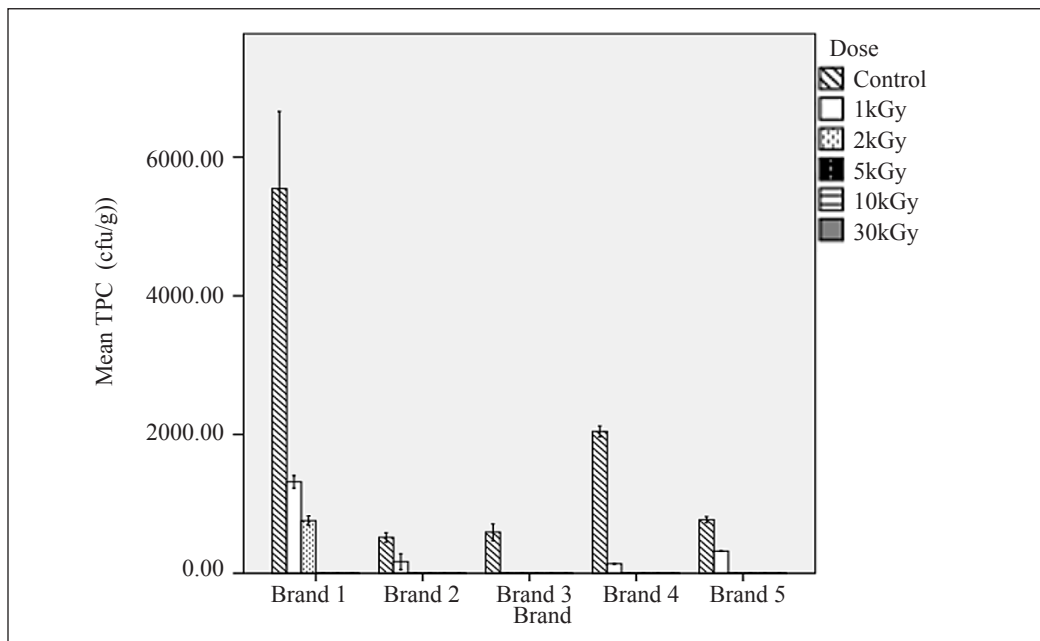


Figure 2. Variation of mean total plate count for each brand, according to the different irradiation doses

Coliform. Both Irradiated and non-irradiated Ceylon black tea samples were shown less than 01 coliform counts which confirmed that none of the tea samples were contaminated with coliform bacteria. According to Zhao et al. (1997), the presence of coliform may associate with the fecal contamination of food plant, including tea leaves. This may be the reason behind the low coliform counts, which have been observed in the present study.

Yeast and Mould Count (YMC). The yeast and mould contamination of commercially available Ceylon black tea were within the range of 0.45×10^2 to 6.81×10^2 CFU/g. Results revealed a significant reduction ($P < 0.05$) of the YMC with the increment of irradiation dose in all samples compared to the control (Figure 3). However, the study showed a high resistivity of yeast and mould when compared to the bacteria. Generally, yeast and mould are more resistant than bacteria for radiation (Rashid et al., 2016). According to the Mishra et al. (2006), 5kGy was the most effective dose for elimination of microbial contamination. According to Farkas (2006), the radiation energy amount needed to control microorganisms varies from the number of organisms present in the food and resistivity of the species. Results of the present study shows that, 5kGy irradiation dose ensures the microbial safety of black tea.

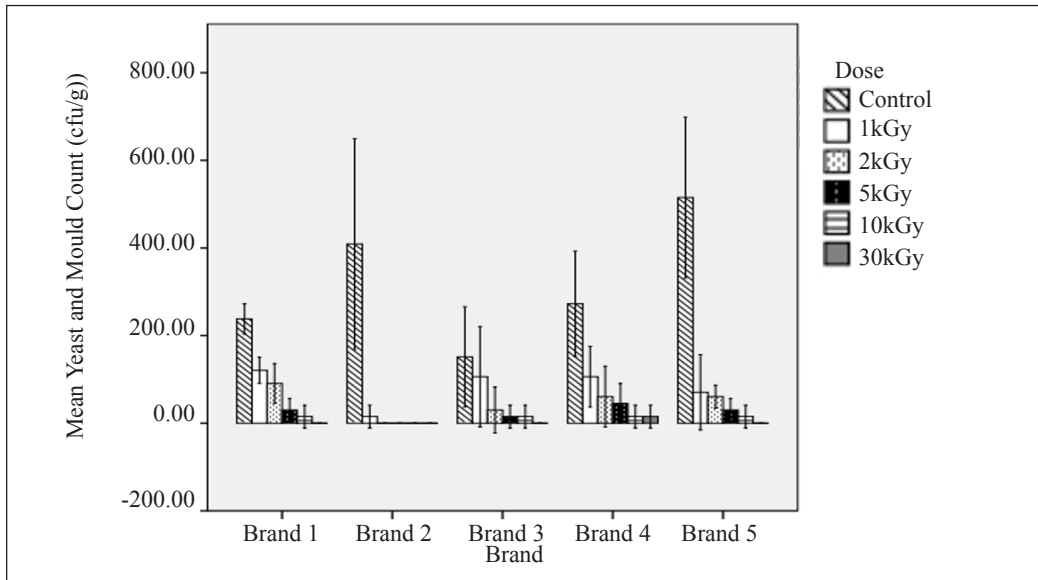


Figure 3. Variation of mean yeast and mould count of each brand, according to the different irradiation doses

Considering the quantity exported per year, the incidents of rejection of Sri Lankan teas from few ports of entry due to high microbial contamination was reported (Lei, 2017). Due to that the growing demand for irradiation as a substitute for chemical fumigation to quarantine the pests has been seen and tea is becoming an ideal large scale local candidate for irradiation (Kausar et al., 2013). Studies carried out on the effects of irradiation on quality of tea were limited in numbers and the studies carried out up to now was limited to green tea. Further, there were no studies conducted in Sri Lanka on irradiation of tea and impact on the chemical components naturally available in tea.

CONCLUSION

The present study carried out to measure the effectiveness of gamma irradiation on commercially available black tea. The research mainly focused on the behavior of certain attributes of tea. The 5kGy dose was the most effective dose for microbial control of commercially available Ceylon black tea, while preserving physical parameters, microbial safety and TPPC of tea. Therefore, irradiation can be used as a preservation technique in the tea industry with a much-regulated manner.

ACKNOWLEDGMENT

The authors would like to acknowledge for the financial support and facilities provided from the Department of Food Science and Technology, Wayamba University of Sri Lanka and Sri Lanka Gamma Centre of Sri Lanka Atomic Energy Board.

REFERENCES

- Breen, A. P., & Murphy, J. A. (1995). Reactions of oxyl radicals with DNA. *Free Radical Biology and Medicine*, 18(6), 1033-1077.
- Beuchat, L. R., Komitopoulou, E., Beckers, H., Betts, R. P., Bourdichon, F., Fanning, S., Joosten H.M. & Ter Kuile, B. H. (2013). Low-water activity foods: increased concern as vehicles of foodborne pathogens. *Journal of Food Protection*, 76(1), 150-172.
- Fanaro, G. B., Hassimotto, N. M. A., Bastos, D. H. M., & Villavicencio, A. L. C. H. (2014). Effects of γ -radiation on microbial load and antioxidant proprieties in black tea irradiated with different water activities. *Radiation Physics and Chemistry*, 97, 217-222.
- Farkas, J. (2006). Irradiation for better foods. *Trends in Food Science & Technology*, 17(4), 148-152.
- Fujita, H., & Yamagami, T. (2008). Antihypercholesterolemic effect of Chinese black tea extract in human subjects with borderline hypercholesterolemia. *Nutrition Research*, 28(7), 450-456.
- Hamer, M. (2007). The beneficial effects of tea on immune function and inflammation: a review of evidence from in vitro, animal, and human research. *Nutrition research*, 27(7), 373-379.
- Herath, D., & Weersink, A. (2009). From plantations to smallholder production: the role of policy in the reorganization of the Sri Lankan tea sector. *World Development*, 37(11), 1759-1772.
- Hirashima, F. K., Fabbri, A. D., Sagretti, J., Nunes, T. C., Sabato, S. F., Galvao, N. S., & Lanfer-Marquez, U. M. (2013). *Influence of gamma irradiation on phenolic compounds of minimally processed baby carrots*. International Nuclear Atlantic Conference, Brasilia, Brazil: ABEN
- International Organization for Standardization. (2006). *Microbiology of food and animal feeding stuffs -- Horizontal method for the detection and enumeration of coliforms -- Most probable number technique (ISO 4831:2006(E))*. Retrieved March 06, 2017 from <https://www.iso.org/standard/38280.html>

- International Organization for Standardization. (2013). *Microbiology of the food chain Horizontal method for the enumeration of microorganisms -- Part 1: Colony count at 30 degrees C by the pour plate technique* (ISO 4833-1:2013(E)). Retrieved March 16, 2017 from <https://www.iso.org/standard/53728.html>
- International Organization for Standardization. (2008). *Microbiology of food and animal feeding stuffs -- Horizontal method for the enumeration of yeasts and moulds Part 2: Colony count technique in products with water activity less than or equal to 0,95* (ISO 21527-2:2008(E)). Retrieved March 24, 2017 from <https://www.iso.org/standard/38276.html>
- International Organization for Standardization. (2005). *Determination of substances characteristic of green and black tea Part 1: Content of total polyphenols in tea -- Colorimetric method using Folin-Ciocalteu reagent.* (ISO 14502-1:2005(E)). Retrieved April 04, 2017 from <https://www.iso.org/standard/31356.html>
- Kausar, T., Akram, K., & Kwon, J. H. (2013). Comparative effects of irradiation, fumigation, and storage on the free amino acids and sugar contents of green, black and oolong teas. *Radiation Physics and Chemistry*, 86, 96-101.
- Lei, L. (2017). *Effects of standards on tea exports from developing countries: comparison of China and Sri Lanka* (No. 642). Institute of Developing Economies. Chiba, Japan: IDE-JETRO.
- Liang, Y., Lu, J., Zhang, L., Wu, S., & Wu, Y. (2005). Estimation of tea quality by infusion color difference analysis. *Journal of the Science of Food and Agriculture*, 85(2), 286-292.
- Luczaj, W., & Skrzydlewska, E. (2005). Antioxidative properties of black tea. *Preventive Medicine*, 40(6), 910-918.
- Mali, A. B., Khedkar, K., & Lele, S. S. (2011). Effect of Gamma Irradiation on Total Phenolic Content and in Vitro Antioxidant Activity of Pomegranate (*Punica granatum* L.) Peels. *Food and Nutrition*, 2(05), 428-433.
- Mishra, B. B., Gautam, S., & Sharma, A. (2006). Microbial decontamination of tea (*Camellia sinensis*) by gamma radiation. *Journal of Food Science*, 71(6), M151-M156.
- Rashid, M. H., Chowdhury, M. A. Z., Fardous, Z., Tanvir, E. M., Pramanik, M. K., Jahan, I. & Gan, S. H. (2016). Microbial decontamination of gamma irradiated black tea and determination of major minerals in black tea, fresh tea leaves and tea garden soil. *LWT-Food Science and Technology*, 73, 185-190.
- Ratnasooriya, W. D., & Muthunayake, T. B. S. (2014). Anticlotting properties of Sri Lankan low grown orthodox Orange Pekoe grade black tea (*Camellia sinensis* Linn). *World Journal of Pharmaceutical Science*, 2, 1-7.
- Thomas, J., Senthilkumar, R. S., Kumar, R. R., Mandal, A. K. A., & Muraleedharan, N. (2008). Induction of γ irradiation for decontamination and to increase the storage stability of black teas. *Food Chemistry*, 106(1), 180-184.
- Vargas, R., & Vecchiotti, A. (2016). Influence of raw material moisture on the synthesis of black tea production process. *Journal of Food Engineering*, 173, 76-84.
- Wiseman, S. A., Balentine, D. A., & Frei, B. (1997). Antioxidants in tea. *Critical Reviews in Food Science & Nutrition*, 37(8), 705-718.
- Zhao, T., Clavero, M. R. S., Doyle, M. P., & Beuchat, L. R. (1997). Health relevance of the presence of fecal coliforms in iced tea and leaf tea. *Journal of Food Protection*, 60(3), 215-218.



Optimization of Enzymatic Hydrolysis for the Production of Antioxidative Peptide from *Nannochloropsis gaditana* using Response Surface Methodology

Nur Izzati Md Saleh¹, Wan Azlina Wan Ab Karim Ghani^{1*}, Mohd Razif Harun¹ and Siti Mazlina Mustapa Kamal²

¹Department of Chemical and Environmental Engineering/ Sustainable Process Engineering Research Centre (SPERC), Faculty of Engineering, Universiti Putra Malaysia, 43400 UPM Serdang, Selangor, Malaysia

²Department of Process and Food Engineering, Faculty of Engineering, Universiti Putra Malaysia, 43400 UPM Serdang, Selangor, Malaysia

ABSTRACT

In the present research, microalgae protein hydrolysate of *Nannochloropsis gaditana* (MPH) was extracted via enzymatic hydrolysis using alcalase enzyme. Hydrolysis conditions like (pH, temperature, enzyme concentration and substrate concentration) were optimized by Response Surface Methodology (RSM) using Central Composite Design (CCD). Four range of independent variables namely; pH (7-9), temperature (45-55°C), substrate concentration (2-6 g/L) and enzyme concentration (0.2-0.4 g/L) were used to study the influence of these parameters on the degree of hydrolysis. The CCD consisted of twenty-four experimental points and six replicates of central points with the optimum conditions obtained from this experiment were at pH 8.14, a temperature 51.4°C, a substrate concentration 5.48 g/L and an enzyme concentration 0.26 g/L with maximum degree hydrolysis of 55.76%. All experiments were fixed at 24 hours reaction time. The degree of hydrolysis of MPH was analysed using O-phthaldehyde (OPA) method to quantify the cleavage of peptide bond. The optimized sample was evaluated for its antioxidant activity using 1,1-Diphenyl-2-picrylhydrazyl (DPPH) assay with 52.19% and 2, 2'- azino-bis (ethylbenzthiazoline-6-sulfonic acid (ABTS) assay with 14.13%. The bioactive peptides contained in *Nannochloropsis gaditana* have the ability to scavenge free radicals and act as good antioxidants

ARTICLE INFO

Article history:

Received: 24 October 2018

Accepted: 15 February 2019

Published: 21 June 2019

E-mail addresses:

nurizzatims@gmail.com (Nur Izzati Md Saleh)

wanazlina@upm.edu.my (Wan Azlina Wan Ab Karim Ghani)

mh_razif@upm.edu.my (Mohd Razif Harun)

smazlina@upm.edu.my (Siti Mazlina Mustapa Kamal)

* Corresponding author

Keywords: Antioxidant, bioactive peptide, degree hydrolysis, microalgae, optimization

INTRODUCTION

Microalgae are known as unicellular photosynthetic microorganisms and live in freshwater or saline environment. They utilize water, carbon dioxide, and sunlight to convert into algal biomass. For many years, microalgae have been considered as important potential feedstock in the biofuels and chemical area due to its valuable bioactive compounds (Markou & Nerantzis, 2013; Nobre et al., 2013). Lipids from microalgae have been utilized as biofuel feedstock and the sugars are extracted from microalgae as substrate for bioethanol production has been studied widely around the world (Chen et al., 2012; Chng, 2016; Chu, 2017; Geun Goo et al., 2013; Harun et al., 2010; Lee et al., 2013; Patnaik & Mallick, 2015; Shuping et al., 2010; Subhadra, 2010; Watanabe et al., 2014). However, the study on microalgae protein especially peptides is not as much as lipid and carbohydrate.

Peptides derived from protein can be found in all living beings of plant and animal origin and are classified as one of major food component. Peptides usually can be obtained through technological processes such as fermentation and enzyme hydrolysis (Martínez-maqueda et al., 2013). The process involving the breakage of protein molecules into various size of small peptides and eventually amino acids is called enzymatic protein hydrolysis (Sbroggio et al., 2016). These peptides typically have 3–20 amino acid residues, and their activities rely upon their sequences and amino acid composition (Pihlanto-leppä, 2001). Principally, the characteristics of an enzyme used must be at least a food grade and non-pathogenic if the enzyme is microbial origin (Bhaskar, 2008). However, enzymatic protein hydrolysis using commercial food grade enzymes is more desirable and consistent due to the better control in term of hydrolysates properties (Slizyte et al., 2005). The applications of protein peptide have been studied for antioxidant, anticoagulant, antimicrobial and antihypertensive which could be utilized as a component in food or pharmaceutical healthcare products (Kim et al., 2001; Mendis et al., 2005; Suetsuna et al., 2004).

The chemical composition of bioactive compounds in microalgae varies depending on species, cultivation, growth condition and type of extraction (Mirsiaghi & Reardon, 2015). One of microalgae species, *Nannochloropsis* is potentially known as source of lipids for production of biodiesel (Gouveia & Oliveira, 2009; Moazami et al., 2012). However, it is also considered as a source of protein, carbohydrates, carotenoid, and phenolic compounds (Lubián et al., 2000). The study on protein peptide from *Nannochloropsis gaditana* (*N.gaditana*) *sp* is very few and not much of literature can be found as most of researchers are focusing on the biofuel production. Research done by Sheih et al., (2009) reported that algae residual protein from *Chlorella vulgaris* *sp* possess antioxidative activity which had significant protective effects on DNA and could prevent cellular damage. Nevertheless, depth study on the algae protein in terms of optimization and selectivity of bioactive peptide still has not been explored so far. *N.gaditana* is well known among researchers as one of the best candidate for biofuel productions (Andrich et al., 2005; Gerde et al., 2013; Nobre et

al., 2013; Pan et al., 2010). However, the extraction of lipids for biofuel usually produces microalgal residual which consists of protein and carbohydrate. It is normally discarded as a waste. The microalga residues of *N.gaditana* is mainly consist of protein and carbohydrates which have value-added. Therefore, in this research, a microalga *N.gaditana* was chosen as a model to produce bioactive peptide for antioxidant activity. Antioxidant activity is mainly depending on the type of peptide produced during enzymatic hydrolysis process. Enzymatic hydrolysis is a crucial step in the bioactive peptide production. A suitable enzyme and parameter during the hydrolysis process should be chosen wisely. Ngo et al., (2013) reported that enzymes derived from microorganisms and animal digestive system was best to be used in obtaining bioactive peptide. Alcalase, neutrase, flavourzyme, protamex and kojizyme from microorganism and trypsin, papain and α -chymotrypsin from animals are commercial enzymes that could be found in the market. Among these enzymes, alcalase was used in this study because the alcalase hydrolysate exhibited good bioactivity (Wijesekara, Qian, Ryu, Ngo & Kim 2011), good functional properties (Amiza, Nurul Ashikin, & Faazaz, 2011) and most suitable for hydrolysis of protein especially in transpeptidation according to the manufacturer. Thus, a suitable approach in bioactive peptide production is needed for scaling up or commercialization in the future.

Optimization during enzymatic hydrolysis process and statistical analysis is required in maximizing protein peptide extraction and determine the independent and interaction effects of various process parameters on the extraction yields. Response Surface Methodology (RSM) is a known statistical method for planning an experiment, evaluating the impact factors, building a model, and optimizing the selected parameters (Kalil et al., 2000; Parimi et al., 2015). It is a statistically designed experimental protocol in which several factors are simultaneously varied (Rao et al., 2000) unlike the traditional method. The main objective of this research is to apply statistical method in optimizing the enzymatic hydrolysis parameters of protein peptide from microalgae *N.gaditana sp.* In this paper, four main parameters that influence the performance of enzymatic hydrolysis namely; pH, temperature, substrate concentration and enzyme concentration were optimized by RSM to determine the optimal condition for peptide production. The Central Composite Design (CCD) which required five levels of each factor was chosen to carry out experiments and estimate the coefficients of a quadratic model.

MATERIALS AND METHODS

Materials

Microalgae biomass of *Nannochloropsis gaditana* was purchased from Pure Bulk Inc. (USA), and delivered in a green powdered form. Liquid Alcalase® 2.4 L, (≥ 2.4 U/g) proteinase Subtilisin A from *Bacillus licheniformis* was purchased from Sigma-Aldrich.

All the chemicals used in different analysis were of analytical grade and purchased from Sigma-Aldrich and R&M Chemical.

Methods

Optimization of Enzymatic Hydrolysis Conditions of MPH by Response Surface Methodology (RSM). Optimization of enzymatic hydrolysis of *N.gaditana* was analysed using Response Surface Methodology (RSM) in Design Expert Software Version 10. RSM with randomized factorial design which is Central Composite Design (CCD) was employed to analyse the results. CCD is based on two-level factorial designs, augmented with center and axial points to fit quadratic models. A total number of 30 run with 24 non-center points and 6 center points was designed for the experiment. The center points were replicated to provide good predictive capabilities near the center of the factor space. Four different factors; pH(X_1), temperature (X_2), substrate concentration (X_3) and enzyme concentration (X_4) were employed over response variable; degree hydrolysis ,DH (Y). Enzymatic hydrolysis process value range for *N.gaditana* is shown in Table 1. Each run was performed with 100 mL of sodium phosphate buffer (PBS) containing microalgae biomass at specific pH, temperature, substrate concentration and enzyme concentration with a pre-determined reaction time. After 24 hours, enzymatic hydrolysis reaction was stopped by heating the hydrolysate in water bath at 95°C for 10 minutes. Then, the protein hydrolysate was centrifuged at 4000 × g using centrifuge model KUBOTA for 20 minutes followed by filtration to remove the solid residual (Agrawal et al., 2017). The supernatant was collected for the degree hydrolysis analysis.

Table 1
The variable levels of CCD for enzymatic hydrolysis of antioxidative peptide from *Nannochloropsis gaditana*

Factor level	pH, X_1	Temperature, X_2 (°C)	Substrate concentration, X_3 (g/L)	Enzyme concentration, X_4 (g/L)
-1	7	45	2	0.2
0	8	50	4	0.3
1	9	55	6	0.4

Determination of Degree Hydrolysis. Degree of hydrolysis (DH) plays an important role in protein peptide hydrolysis reaction. DH is defined as the percentage of cleaved peptide bond and can be calculated as per equation (1):

$$DH = \frac{h}{h_{tot}} \times 100 \tag{1}$$

where, h is the number of hydrolyzed bonds and h_{tot} is the total number of peptide bonds in the substrate. DH was measured by O-phthaldehyde (OPA) method according to (Nielsen et al., 2001) with slightly modification. Firstly, OPA reagent was prepared by dissolving 3.81 g sodium tetraborate decahydrate and 100 mg of sodium dodecyl sulphate with deionized water. 80 mg of O-Phthaldehyde 98% in 2 ml of ethanol 95% was mixed with the sodium solution. Then, 200 μl of β -mercaptoethanol was added and deionized water was top up to 100 ml.

Determination of Antioxidant Activity. The microalgae protein hydrolysate at optimum condition were analysed for antioxidant activity.

1,1-Diphenyl-2-picrylhydrazyl (DPPH) Assay. The DPPH assay was measured according to the method of (Huang & Mau, 2006). A 1 mL of protein hydrolysates was mixed with 1 mL of methanol solution containing 1 mM DPPH radicals. The mixture was allowed to stand for 40 min in the dark, and the absorbance was monitored at 517 nm using UV-Vis spectrophotometer model GENESYS. Distilled water was used instead of hydrolysates as a blank. Scavenging DPPH activity was calculated according to the equation (2):

$$\text{Antioxidant activity} = \frac{A_0 - A_1}{A_0} \times 100 \quad (2)$$

where A_1 is sample absorbance and A_0 is blank absorbance.

2, 2'- azino-bis (ethylbenzthiazoline-6-sulfonic acid (ABTS)) Assay. The radical cation was prepared by mixing 2.45 mM potassium persulfate with 7 mM ABTS stock solution with 1:1 ratio. The mixture was left for 4-16 h until the reaction was complete and the absorbance was stable. The ABTS⁺ solution was diluted with ethanol 95% to an absorbance of 0.700 ± 0.05 at 734 nm for measurements. The ABTS assay was measured by mixing 0.9 mL of ABTS⁺ solution with 0.1 mL of tested samples and mixed for 45 seconds. The mixture was measured immediately using UV-Vis spectrophotometer model GENESYS at 734 nm after 15 minutes. The antioxidant activity of microalgae protein hydrolysate was measured according to equation (2).

RESULTS AND DISCUSSION

Optimization of Hydrolysis Conditions by Response Surface Methodology (RSM)

The optimal enzymatic hydrolysis conditions was analysed using Central Composite Design (CCD) in RSM based on the degree of hydrolysis (DH) at four independent variables as

shown in Table 2. The DH value of *N.gaditana* was obtained from 18.12% to 73.03% with different hydrolysis conditions. This maximum DH value from *N.gaditana* was quite high if compared to algae source ;*Spirulina* sp.LEB-18, 60% (Pereira et al.,2016) and fish source; fish soluble concentrate, 68% (Nilsang et al., 2005); *Nemipterus japonicus*, 42.15% and *Exocoetus volitans*,43.21% (Naqash & Nazeer, 2012). The DH value of *N.gaditana* was higher compared to other source probably due to the different source of protein, different type of enzymes used and different range of parameters used.

Table 2
Enzymatic hydrolysis experimental design of independent variables along with the observed values for the response variable, degree of hydrolysis for N. gaditana (Y₁)

Run	pH (X ₁)	Temperature, °C (X ₂)	Substrate Concentration,g/L (X ₃)	Enzyme Concentration,g/L (X ₄)	Degree Hydrolysis,% (Y)
1	9	45	2	0.2	53.08
2	8	40	4	0.3	56.98
3	8	50	4	0.3	70.76
4	9	55	6	0.4	39.22
5	9	55	6	0.2	36.04
6	9	45	6	0.4	35.4
7	7	45	6	0.4	32.3
8	6	50	4	0.3	38.03
9	8	50	4	0.5	73.03
10	9	45	2	0.4	46.15
11	8	60	4	0.3	39.78
12	7	45	6	0.2	32.37
13	7	55	2	0.2	18.12
14	8	50	4	0.3	69.35
15	10	50	4	0.3	58.98
16	7	45	2	0.2	32.89
17	7	55	6	0.4	36.16
18	9	55	2	0.2	32.49
19	9	55	2	0.4	45.64
20	8	50	4	0.3	67.14
21	8	50	4	0.3	70.12
22	9	45	6	0.2	35.32
23	8	50	4	0.3	72.46
24	7	45	2	0.4	31.86
25	8	50	4	0.1	54.91
26	7	55	6	0.2	37.03
27	7	55	2	0.4	30.46
28	8	50	4	0.3	65.89
29	8	50	0	0.3	4.12
30	8	50	8	0.3	53.52

Data was analyzed for its analysis of variance (ANOVA), coefficient variation, diagnostic case statistics and response surface plots and effect of factors. The prediction model for the response variable could be fitted into linear, two-factor interaction (2FI), quadratic or cubic (Mat Amin et al., 2016). Table 3 shows the suggested model for the degree hydrolysis of *N.gaditana*. It can be seen that cubic model has the highest value of R-Squared but due to it was an aliased model, the model could not be appropriate and useful model. Thus, quadratic model was selected since the desirability value was close to 1 and the model fitted the experimental data with an acceptable determination coefficient $R^2 = 0.9708$ showing that the model had 97.08% of the total deviation of experimental data. While for the adjusted R-Squared, it is preferable to have the value close to 1. The adjusted R-squared that is closed to 1 and not aliased is quadratic model with 0.9394. In fact, the predicted R-Squared of 0.7976 is in reasonable agreement with the adjusted R-Squared which the difference is less than 0.2. Overall, quadratic model is suggested as the most suitable conditions to obtain the optimum DH with the predicted value is 55.76%.

Table 3
Model Summary statistics

Sources	Standard deviation	R-Squared	Adjusted R-Squared	Predicted R-Squared	
Linear	16.41	0.1169	-0.0367	-0.2025	
2FI	18.37	0.1815	-0.3000	-1.4064	
<u>Quadratic</u>	<u>3.97</u>	<u>0.9708</u>	<u>0.9394</u>	<u>0.7976</u>	<u>Suggested</u>
Cubic	2.22	0.9958	0.9810		Aliased

In Table 4 shows that pH, temperature and enzyme concentration had a linear effect, while pH, temperature and substrate concentration had a quadratic effect on DH value. Interaction for DH value could be seen from the interaction of pH and substrate concentration ($p < 0.01$), temperature and substrate concentration ($p < 0.01$), temperature and enzyme concentration ($p < 0.5$). The highest positive value of esteemed regression coefficient was observed for the pH ($X_1 = 4.75$) indicating that it was the most influential parameter of DH while the least influence was substrate concentration with highest negative value ($X_3^2 = -21.63$).

The regression equation for the degree of hydrolysis for *N.gaditana* with respect to four different independent variables; pH(X_1), temperature(X_2), substrate concentration(X_3) and enzyme concentration(X_4) were derived as follows:

$$Y = + 69.29 + 4.75 X_1 - 2.44X_2 - 0.43X_3 + 2.34X_4 - 0.56X_1X_2 - 3.49X_1X_3 - 0.056 X_1X_4 + 3.15X_2X_3 + 2.23X_2X_4 - 0.95X_3X_4 - 5.20X_1^2 - 5.23X_2^2 - 21.63X_3^2 - 1.33X_4^2$$

The results for analysis of variance (ANOVA) for degree of hydrolysis of *N.gaditana* by alcalase enzyme was observed that the model was highly significant at 99% confidence level ($p < 0.0001$) as shown in Table 4. The suggested optimum hydrolysis conditions for enzymatic hydrolysis of *N.gaditana* were pH 8.14, 51.4°C, 5.48 g/L substrate concentration and 0.26 g/L enzyme concentration.

Table 4
Results of ANOVA on degree of hydrolysis (DH) for *N. gaditana*

Factors	Sum of square	df	Mean square	F value	P value
Model	6804.53	14	486.04	30.87	< 0.0001
X₁-pH	541.98	1	541.98	34.43	< 0.0001
X₂-Temperature	143.13	1	143.13	9.09	0.0099
X₃-Substrate Concentration	2.93	1	2.93	0.19	0.6731
X₄-Enzyme Concentration	131.09	1	131.09	8.33	0.0128
X ₁ X ₂	4.96	1	4.96	0.32	0.5841
X ₁ X ₃	195.37	1	195.37	12.41	0.0037
X ₁ X ₄	0.050	1	0.050	3.145E-003	0.9561
X ₂ X ₃	158.32	1	158.32	10.06	0.0074
X ₂ X ₄	79.88	1	79.88	5.07	0.0422
X ₃ X ₄	14.46	1	14.46	0.92	0.3554
X ₁ ²	647.82	1	647.82	41.15	< 0.0001
X ₂ ²	655.63	1	655.63	41.64	< 0.0001
X ₃ ²	2806.44	1	2806.44	178.26	< 0.0001
X ₄ ²	42.40	1	42.40	2.69	0.1247
Residual	204.67	13	15.74		
Lack of Fit	175.58	8	21.95	3.77	0.0800
Pure Error	29.08	5	5.82		
Cor Total	7009.20	27			

P =level of significance

Response Surface Analysis. The effect of four main parameters in enzymatic hydrolysis of *N.gaditana* (pH, temperature, substrate concentration and enzyme concentration) was manifested in 3D response surface contour plot as shown in Figure 1.

As we can see from Figure 1(a), the DH value increased as the substrate concentration increased along the pH. The interaction between substrate concentration and pH had strong effect on the curvature of the response in according to high negative value of interaction coefficient ($X_1X_3 = -3.49$). This is because at pH 8 to 8.5, the enzyme is highly energetic and provide more active site to lock the substrate. While in Figure 1(b), the degree of hydrolysis of *N.gaditana* was indirectly proportional to the substrate and enzyme concentration. The degree of hydrolysis at high substrate concentration, 6 g/L was much lower if compared

to low substrate concentration. During the hydrolysis reaction, the enzyme activity of the enzyme can be inhibited by the product formed. Competition between original substrate and the peptide toward the active sites of enzymes was expected. After hydrolysis of a

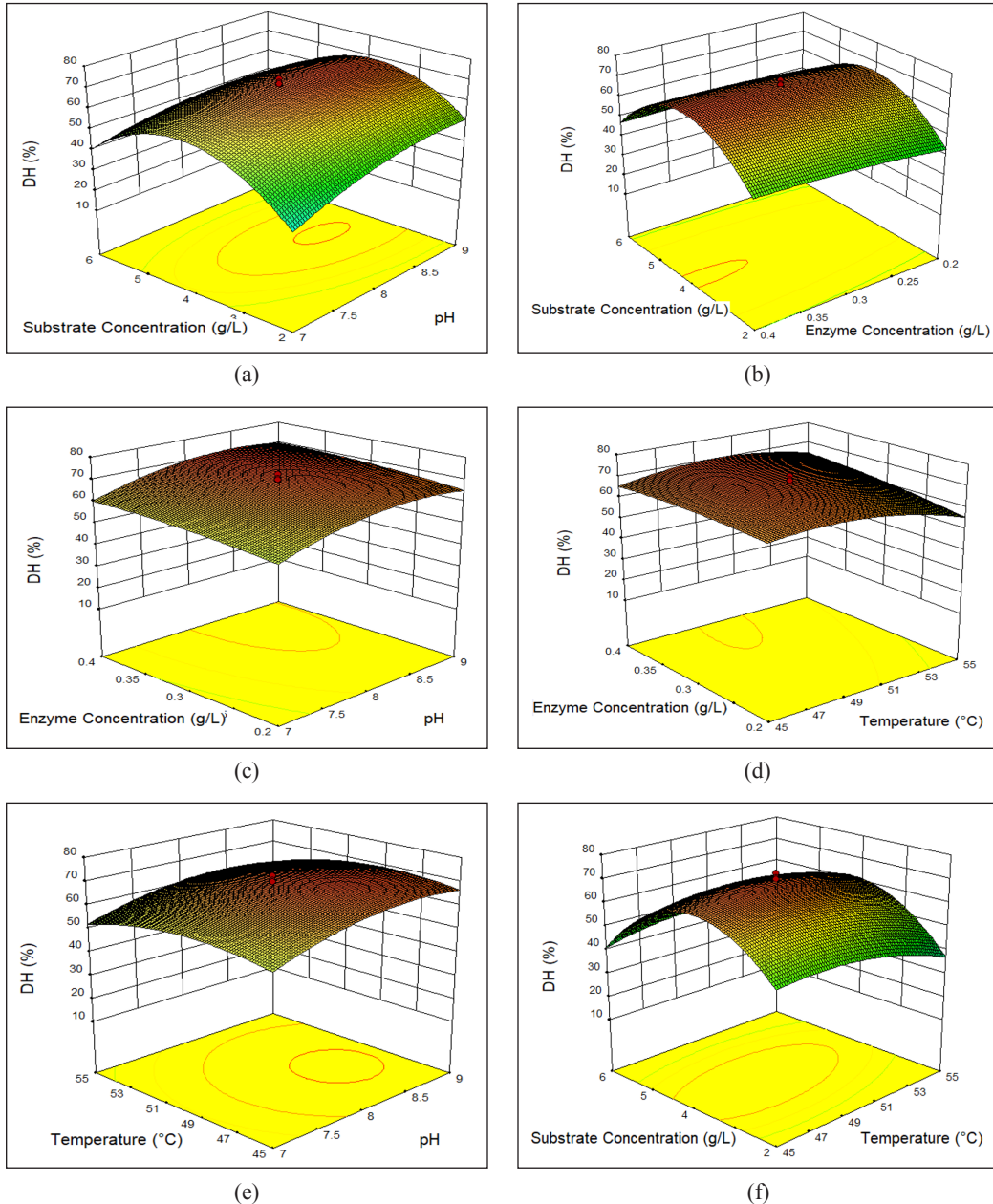


Figure 1. The three-dimensional response surface plot for the effect of (a) substrate concentration and pH (b) substrate concentration and enzyme concentration (c) enzyme concentration and pH (d) enzyme concentration and temperature (e) temperature and pH and (f) substrate concentration and temperature on DH of *N.gaditana*

peptide bond, terminal acyl is produced and could act as inhibitor, which can bind to the active site of the enzyme, forming an acyl-enzyme complex (Lisboa et al., 2014). Thus, at high substrate concentration, the enzyme has high chances to bind with other inactive protein region, thus preventing the formation of enzyme-substrate complex and reduce the formation of products (Pereira et al., 2016). At low substrate concentration, hydrolysis rate was decreased could be due to low concentration of peptides available to be bonded with enzyme. By having moderate substrate concentration at low usage of enzyme as obtained in this study is preferable and economic for scaling up.

In Figure 1(c), we can see that the DH increased as the pH value increased. The same finding was reported by (Montilha et al., 2017). This was because the pH was strongly influenced the stability of enzyme, which could cause irreversible denaturation of its conformational structure and loss of enzyme activity (Whitaker, 1994). The optimum pH in this study was found to be at pH 8 which was in the range of pH 7 to 9 as recommended by manufacturer. Other studies found that alcalase worked best at pH 7.7 for Angel Wing Clam (*Pholas orientalis*) meat (Mat Amin et al., 2016), pH 7 for soybean (Nguyen, 2015), pH 8.5 for shrimp waste (Dey & Dora, 2014), pH 8.0 for goat milk casein (Shu et al., 2016) and pH 8 for Viscera of Tuna (*Euthynnus affinis*) (Salwanee et al., 2013). It showed that the optimal pH might vary according to the system used in such reaction (i.e: substrate, enzyme concentration) (Salwanee et al., 2013). In Figure 1 (d) the three-dimensional response surface graph demonstrated that the interaction between temperature and enzyme concentration greatly influenced the DH value with low effect on the response surface curvature according to interaction coefficient ($X_2X_4 = 2.23$). This is because; any changes in temperature might change the shape of the enzyme and make it less complement to lock the substrate (Salwanee et al., 2013). In fact, the optimum temperature range of alcalase enzyme is between 45 to 60°C as per stated by the manufacturer.

Validation of Model

Based on the statistical results, the optimum conditions for the production of bioactive peptide from *N.gaditana* are as follows: pH of 8.14, temperature of 51.4°C, substrate concentration of 5.48 g/L and an enzyme concentration of 0.26 g/L with maximum predicted degree hydrolysis of 55.76%. The conditions are modified to make it easy for controlling and measure the parameters. Thus, a new experiment with modified optimal conditions of pH 8, temperature 51°C, substrate concentration 5 g/L and enzyme concentration 0.3 g/L were performed for verification the optimization. The degree hydrolysis at modified at optimal conditions is 57.59% which is 3.28% more than the predicted value. The value is slightly different might be due to the modification in the parameters of enzymatic hydrolysis. These results showed and confirmed the model is appropriate and robust to estimate the value of experiments.

Antioxidant Evaluation Assay

The best condition of enzymatic hydrolysis was further analysed for its antioxidant properties. Table 5 shows the antioxidant activity of the same sample but was evaluated with different free radical scavenging activity. DPPH assay with 52.19% gave high antioxidant activity compared to ABTS assay. This showed that microalgae protein hydrolysate had high ability to inhibit DPPH free radical at the same conditions. Similar result was found by Shalaby and Shanab (2013) where the protein using water extraction exhibit high antioxidant activity with DPPH instead of ABTS. It could be due to the increasing number of electron and hydrogen donating properties of the active peptides (Sbroggio et al., 2016). These active peptides have high possibility to react with free radicals in producing more stable products, and hence the radical chain reaction could be terminated (Pazinatto et al., 2013). DPPH is a stable free radical with a maximum absorbance at 517 nm in ethanol. When DPPH encounters a proton-donating substance, the radical is scavenged and the absorbance is reduced (Cian et al., 2013).

Table 5
Antioxidant assay of microalgae protein hydrolysate

Antioxidant Assay	DPPH	ABTS
Microalgae Protein Hydrolysate at optimum conditions	52.19%	14.13%

CONCLUSION

In this study, we found that the optimum conditions for enzymatic hydrolysis of *N.gaditana* is at pH 8.14, 51.4°C, 5.48 g/L substrate concentration and 0.26 g/L enzyme concentration with predicted degree hydrolysis of 55.76%. Antioxidant activity of microalgae protein hydrolysate varied depending on the free radical scavenger used. In this evaluation, DPPH assay revealed high antioxidant activity compared to ABTS assay. In conclusion, bioactive peptide derived from *N.gaditana* can be a valuable source for antioxidant. However, further characterization and purification of microalgae protein hydrolysate are needed to determine the properties of protein peptide.

ACKNOWLEDGEMENT

The authors would like to acknowledge Engineering and Physical Sciences Research Council for partial funding of this research through the BEFEW project (Grant No. EP/P018165/1).

REFERENCES

- Agrawal, H., Joshi, R., & Gupta, M. (2017). Isolation and characterisation of enzymatic hydrolysed peptides of green tender sorghum and their antioxidant activities. *LWT - Food Science and Technology*, *84*, 608-616.
- Andrich, G., Nesti, U., Venturi, F., Zinnai, A., & Fiorentini, R. (2005). Supercritical fluid extraction of bioactive lipids from the microalga *Nannochloropsis* sp. *European Journal of Lipid Science and Technology*, *107*(6), 381-386.
- Bhaskar, N., Benila, T., Radha, C. & Lalitha R. G. (2008). Optimization of enzymatic hydrolysis of visceral waste proteins of Catla (*Catla catla*) for preparing protein hydrolysate using a commercial protease. *Bioresource Technology*, *99*(2), 335-343.
- Chen, R., Yue, Z., Deitz, L., Liu, Y., Mulbry, W., & Liao, W. (2012). Use of an algal hydrolysate to improve enzymatic hydrolysis of lignocellulose. *Bioresource Technology*, *108*, 149-154.
- Chng, L. M., Chan D. J. C. & Lee, K. T. (2016). Sustainable production of bioethanol using lipid-extracted microalgae from *Scenedesmus dimorphus*. *Journal of Cleaner Production*, *130*, 68-73
- Chu, W. L. (2017). Strategies to enhance production of microalgal biomass and lipids for biofuel feedstock. *European Journal of Phycology*, *52*(4), 419-437.
- Cian, R. E., Alaiz, M., Vioque, J., & Drago, S. R. (2013). Enzyme proteolysis enhanced extraction of ACE inhibitory and antioxidant compounds (peptides and polyphenols) from *Porphyra columbina* residual cake. *Journal Applied Phycology*, *25*(4), 1197-1206.
- Dey, S. S., & Dora, K. C. (2014). Antioxidative activity of protein hydrolysate produced by alcalase hydrolysis from shrimp waste (*Penaeus monodon* and *Penaeus indicus*). *Journal of Food Science and Technology*, *51*(3), 449-457.
- Gerde, J. A., Wang, T., Yao, L., Jung, S., Johnson, L. A., & Lamsal, B. (2013). Optimizing protein isolation from defatted and non-defatted *Nannochloropsis* microalgae biomass. *Algal Research*, *2*(2), 145-153.
- Geun Goo, B., Baek, G., Jin Choi, D., Il Park, Y., Synytsya, A., Bleha, R., Ho Seong, D., Gyun Lee, C., Kweon Park, J. (2013). Characterization of a renewable extracellular polysaccharide from defatted microalgae *Dunaliella tertiolecta*. *Bioresource Technology*, *129*, 343-350.
- Gouveia, L., & Oliveira, A. C. (2009). Microalgae as a raw material for biofuels production. *Journal of Industrial Microbiology & Biotechnology*, *36*(2), 269-274.
- Harun, R., Danquah, M. K., & Forde, G. M. (2010). Microalgal biomass as a fermentation feedstock for bioethanol production. *Journal of Chemical Technology and Biotechnology*, *85*(2), 199-203.
- Huang, S., & Mau, J. L. (2006). Antioxidant properties of methanolic extracts from *Agaricus blazei* with various doses of g -irradiation. *LWT - Food Science and Technology*, *39*(7), 707-716.
- Kalil, S. J., Mageri, F., & Rodrigues, M. I. (2000). Response surface analysis and simulation as a tool for bioprocess design and Optimization. *Process Biochemistry*, *35*(6), 539-550.
- Kim, S., Kim, Y.-T., Byun, H., Park, P., & Ito, H. (2001). Purification and characterization of antioxidative peptide from Bovine Skin. *Journal of Biochemistry and Molecular Biology*, *34*(3), 219-224.

- Lee, O. K., Kim, A. L., Seong, D. H., Lee, C. G., Jung, Y. T., Lee, J. W., & Lee, E. Y. (2013). Chemo-enzymatic saccharification and bioethanol fermentation of lipid-extracted residual biomass of the microalga, *Dunaliella tertiolecta*. *Bioresource Technology*, *132*, 197–201.
- Lisboa, C. R., Pereira, A. M., Ferreira, S. P., & Costa, J. A. (2014). Utilisation of *Spirulina* sp. and *Chlorella pyrenoidosa* biomass for the production of enzymatic protein hydrolysates. *Journal of Engineering Research and Applications*, *4*(5), 29–38.
- Lubián, L. M., Montero, O., Moreno-garrido, I., Huertas, E., Sobrino, C., González-del Valle, M., & Parés, G. (2000). *Nannochloropsis* (Eustigmatophyceae) as source of commercially valuable pigments. *Journal of Applied Phycology*, *12*(3-5), 249–255.
- Markou, G., & Nerantzis, E. (2013). Microalgae for high-value compounds and biofuels production: A review with focus on cultivation under stress conditions. *Biotechnology Advances*, *31*(8), 1532–1542.
- Martínez-maqueda, D., Hernández-ledesma, B., Amigo, L., Miralles, B., & Gómez-ruiz, J. Á. (2013). *Extraction / Fractionation Techniques for Proteins and Peptides and Protein Digestion*. Boston: Springer.
- Mat Amin, A., H.A, L., & H, Z. (2016). Madridge Journal of Food Technology Optimization of enzymatic protein hydrolysis conditions to obtain maximum angiotensin-i- converting enzyme (ACE) inhibitory activity from Angel Wing Clam (*Pholas orientalis*) meat. *Madridge Journal of Food Technology*, *2*(1), 65–73.
- Mendis, E., Rajapakse, N., & Kim, S. (2005). Antioxidant Properties of a Radical-Scavenging Peptide Purified from Enzymatically Prepared Fish Skin Gelatin Hydrolysate. *Journal of Agricultural and Food Chemistry*, *53*(3), 581–587.
- Mirsiaghi, M., & Reardon, K. F. (2015). Conversion of lipid-extracted *Nannochloropsis salina* biomass into fermentable sugars. *Algal Research*, *8*, 145–152.
- Moazami, N., Ashori, A., Ranjbar, R., Tangestani, M., Eghtesadi, R., & Nejad, A. S. (2012). Large-scale biodiesel production using microalgae biomass of *Nannochloropsis*. *Biomass and Bioenergy*, *39*, 449–453.
- Montilha, M. S., Sbroggio, M. F., Figueiredo, G. De, Ida, E. ., & Kurozawa, L. E. (2017). Optimization of enzymatic protein hydrolysis conditions of okara with endopeptidase Alcalase. *International Food Research Journal*, *24*(3), 1067–1074.
- Nguyen, P. M. (2015). Alcalase and Protamex Hydrolysis of Bioactive Peptides from Soybean. *Bulletin of Environment, Pharmacology and Life Sciences*, *4*(7), 132–143.
- Nielsen, P. ., Petersen, D., & Dambmann, C. (2001). Improved Method for Determining. *Food Chemistry and Toxicology*, *66*(5), 642–646.
- Nilsang, S., Lertsiri, S., Suphantharika, M., & Assavanig, A. (2005). Optimization of enzymatic hydrolysis of fish soluble concentrate by commercial proteases. *Journal of Food Engineering* *70*(4), 571–578.
- Nobre, B. P., Villalobos, F., Barragan, B. E., Oliveira, A. C., Batista, A. P., Marques, P. A. S. S., Mendes, R. L., Sovova, H., Palavra A. F. & Gouveia, L. (2013). A biorefinery from *Nannochloropsis* sp. microalga - Extraction of oils and pigments. Production of biohydrogen from the leftover biomass. *Bioresource Technology*, *135*, 128–136.

- Pan, P., Hu, C., Yang, W., Li, Y., Dong, L., Zhu, L., Tong, S., Qing, R. & Fan, Y. (2010). The direct pyrolysis and catalytic pyrolysis of *Nannochloropsis* sp. residue for renewable bio-oils. *Bioresource Technology*, *101*(12), 4593–4599.
- Parimi, N. S., Singh, M., Kastner, J. R., Das, K. C., Forsberg, L. S., & Azadi, P. (2015). Optimization of protein extraction from *Spirulina platensis* to generate a potential co-product and a biofuel feedstock with reduced nitrogen. *Frontiers in Energy Research*, *3*, 1–9.
- Patnaik, R., & Mallick, N. (2015). Utilization of *Scenedesmus obliquus* biomass as feedstock for biodiesel and other industrially important co-products: An integrated paradigm for microalgal biorefinery. *Algal Research*, *12*, 328–336.
- Pereira, A. M., Lisboa, C. R., Pereira, A. M., Alberto, J., & Costa, V. (2016). Biopeptides with antioxidant activity extracted from the biomass of *Spirulina* sp. LEB 18. *African Journal of Microbiology Research*, *10*(3), 79–86.
- Pihlanto-leppa, A. (2001). Bioactive peptides derived from bovine whey proteins : opioid and ace- inhibitory peptides. *Trends in Food Science & Technology*, *11*(9-10), 347–356.
- Rao, K. J., Kim, C. H., & Rhee, S. K. (2000). Statistical optimization of medium for the production of recombinant hirudin from *Saccharomyces cerevisiae* using response surface methodology. *Process Biochemistry*, *35*(7), 639–647.
- Salwanee, S., Aida, W. M. W., Mamot, S., Maskat, M. Y. & Ibrahim, S. (2013). Effects of Enzyme Concentration , Temperature , pH and Time on the Degree of Hydrolysis of Protein Extract from Viscera of Tuna (*Euthynnus affinis*) by Using Alcalase. *Sains Malaysiana*, *42*(3), 279–287.
- Sbroggio, M. F., Montilha, M. S., Ribeiro, V., Figueiredo, G. De, Georgetti, S. R., & Kurozawa, L. E. (2016). Influence of the degree of hydrolysis and type of enzyme on antioxidant activity of okara protein hydrolysates. *Food Science and Technology*, *36*(2), 375–381.
- Shalaby, E. A., & Shanab, S. M. M. (2013). Comparison of DPPH and ABTS assays for determining antioxidant potential of water and methanol extracts of *Spirulina platensis*. *Indian Journal of Geo-Marine Sciences*, *42*(5), 556–564.
- Sheih, I., Fang, T. J., & Wu, T. (2009). Isolation and characterisation of a novel angiotensin I-converting enzyme (ACE) inhibitory peptide from the algae protein waste. *Food Chemistry*, *115*(1), 279–284.
- Shu, G., Zhang, B., Zhang, Q., Wan, H., & Li, H. (2016). Effect of temperature, pH, enzyme to substrate ratio, substrate concentration and time on the antioxidative activity of hydrolysate from goat milk casein by alcalase. *Food Technology*, *20*(2), 29–38.
- Shuping, Z., Yulong, W., Mingde, Y., Kaleem, I., Chun, L., & Tong, J. (2010). Production and characterization of bio-oil from hydrothermal liquefaction of microalgae *Dunaliella tertiolecta* cake. *Energy*, *35*(12), 5406–5411.
- Slizyte, R., Falch, E., Rustad, T., Dauks, E., & Storro, I. (2005). Yield and composition of different fractions obtained after enzymatic hydrolysis of cod (*Gadus morhua*) by-products. *Process Biochemistry*, *40*(3-4), 1415–1424.

- Subhadra, B. G. (2010). Sustainability of algal biofuel production using integrated renewable energy park (IREP) and algal biorefinery approach. *Energy Policy*, 38(10), 5892–5901.
- Suetsuna, K., Maekawa, K., & Chen, J. R. (2004). Antihypertensive effects of *Undaria pinnatifida* (wakame) peptide on blood pressure in spontaneously hypertensive rats. *Journal of Nutritional Biochemistry*, 15(5), 267–272.
- Watanabe, H., Li, D., Nakagawa, Y., Tomishige, K., Kaya, K., & Watanabe, M. M. (2014). Characterization of oil-extracted residue biomass of *Botryococcus braunii* as a biofuel feedstock and its pyrolytic behavior. *Applied Energy*, 132, 475–484.
- Naqash, S. Y., & Nazeer, R. A. (2012). Optimization of enzymatic hydrolysis conditions for the production of antioxidant peptides from muscles of *Nemipterus japonicus* and *Exocoetus volitans* using response surface methodology. *Amino Acids*, 43(1), 337–345.



Effect of Drying Temperature on Malaysia Pomelo (*Citrus grandis* (L.) Osbeck) Pomace Residue under Vacuum Condition

Nur Farhana Abd Rahman^{1,4}, Amin Ismail^{2,3}, Nor Nadiah Abdul Karim Shah¹, Jaturapatr Varith⁴ and Rosnah Shamsudin^{1,2*}

¹Department of Process and Food Engineering, Faculty of Engineering, Universiti Putra Malaysia, 43400 UPM Serdang, Selangor, Malaysia

²Halal Science Research Laboratory, Halal Products Research Institutes, Universiti Putra Malaysia, 43400 UPM Serdang, Selangor, Malaysia

³Department of Nutrition and Dietician, Faculty of Medicine and Health Science, University Putra Malaysia, 43400 UPM Serdang, Selangor, Malaysia

⁴Division of Food Engineering, Faculty of Engineering and Agro-Industry, Maejo University, Chiang Mai, Thailand

ABSTRACT

Pomelo pomace (PP) from Malaysia Tambun White (PO52) variety, dried at different temperature under vacuum condition were evaluated. PP was obtained after extraction process and contained high moisture content (MC). Dried PP can be used as an alternative to livestock feed, hence, dried concentrated form was preferable. Nevertheless, drying process significantly affects the physico-chemical properties of a dried product. Therefore, the present study was carried out to discover the effects of drying temperature on the physico-chemical properties (MC, pH, vitamin C, browning index (BI) and total color change) of PP. The PP was dried at different drying temperature (50, 60, 70, 80 and 90°C) using a vacuum drying (VD) oven for 24 hr. The freeze drying (FD) process was used as a control. The result showed the MC gradually decreased with increasing drying temperature, of which similar trend was also observed for the water activity and total soluble solids (TSS). In contrast, pH showed increment in value with elevated drying temperature.

Interestingly, at 90°C, vitamin C of VD (30.38 mg / 100 g DW) was higher than FD pomelo pomace (21.10 mg / 100 g DW). BI significantly increased as temperature increased. However, no significant changes were observed for total color change after VD. In conclusion, VD at 90°C showed the most recommended temperature because the composition of quality properties at this

ARTICLE INFO

Article history:

Received: 24 October 2018

Accepted: 15 February 2019

Published: 21 June 2019

E-mail addresses:

nfar3388@gmail.com (Nur Farhana Abd Rahman)

rosnahs@upm.edu.my (Rosnah Shamsudin)

aminis@upm.edu.my (Amin Ismail)

nadiahkarim@upm.edu.my (Nor Nadiah Abdul Karim Shah)

varithj@yahoo.com (Jaturapatr Varith)

* Corresponding author

temperature was not significantly varied with control. These fundamentals information of pomelo pomace could be the guideline for postharvest technologist and food processing manufacturers for various applications.

Keywords: Malaysian tambun pomelo, pomelo pomace, quality, temperature, vacuum drying

INTRODUCTION

Pomelo (*Citrus grandis* (L.) Osbeck) also known in Malay as ‘Limau Bali, Limau Abung, Limau Tambun, Limau Besar and Limau Betawi’, a native citrus fruit from South East Asia (Morton, 1987).

A significant quantity of the pomelo residues is generated in both Thailand and Malaysia every year. This is because of high export demand and domestic consumption of the pomelo fruits. Juice production from citrus fruits including pomelo leads to a higher yield production of pomelo pomace (Bai et al., 2013).

Pomelo pomace is the pulpy residues obtained after the juice has being extracted. The yield of pomelo pomace (16%) was recorded and collected from the whole pomelo pulp. Interestingly, previous research had revealed that pomelo residues containing bioactive compounds (phenolic compounds) were capable to promote health benefits (Chang & Azrina, 2017; Shah et al., 2012; Toh et al., 2013) and it also could become a potential source of dietary fibre due to high recovery from pomelo albedo (Zain et al., 2014). Dried citrus pulps were discovered as potential alternative sources of cereal substitute in livestock feed which contained high net energy particularly for dairy cow (Wadhwa & Bakshi, 2013). In addition, Bhatnagar et al. (2015) reviewed the potential source of production on renewable, low cost and sustainable adsorbent for water treatment from pomelo waste.

Pomelo pomace (PP) was obtained during a post-extraction process, whereby it might retain the remaining juice that contributed to higher moisture content and total soluble solids. Microorganism reaction favors this condition and leads to spoilage of fresh pomelo residues. Therefore, drying process reduces the probability of spoilage occurrence due to the removal of free moisture available for microorganism reaction in the dried concentrated form of pomelo pomace. Therefore, selection of drying condition is essential to prolong the shelf-life while retaining the quality (water activity, pH, total soluble solids (TSS), vitamin C and color analysis) of dried pomelo pomace.

Vacuum drying is generally applied for preservation of the heat-sensitive composition by reducing the pressure that leads to evaporation of water molecules (Karam et al., 2016). As a result, it allows limited changes to physicochemical properties and preserving ascorbic acid (Oikonomopoulou & Krokida, 2013).

Recently, researchers have studied the quality of juice from pomelo and its peels. For instance, chemical composition and physical properties (length, width, thickness, surface area, projected areas and volumes) of the juice and the whole pomelo fruits were

discovered for Ledang (PO55) and Tambun (PO52) varieties (Buang et al., 2015; Shah et al., 2012). As drying process occurs, the physicochemical properties of citrus fruit would change substantially. According to Shamsudin et al. (2015a), conventional drying method shows an effect on the color of pomelo pulp waste after being dried at 50, 60 and 70°C. Nevertheless, limited studies providing detailed of vacuum drying on physicochemical properties of pomelo fruits (pomelo pomace) have been conducted. Therefore, the aim of this research is to determine the effects of different drying temperature on physicochemical properties of Malaysia's pomelo pomace.

MATERIALS AND METHODS

Plant Materials

The pomelo (*Citrus grandis* (L.) Osbeck) was obtained from P052 Tambun White variety, Perak in Malaysia. Then, the flesh was inserted into a fruit press juicer (CL-003AP, Interglobal International, LTD, Taiwan) and manually operated. The juice and pomelo pomace (waste) were separated and pomelo pomace was used as raw material for the drying process.

Drying Process

Freeze drying process was conducted by weighing pomelo pomace (~100 g) and frozen in an ultra-low freezer (MDF-U2086S; Sanyo, Japan,) at -85°C overnight and lyophilized using freeze dryer at $4.5 \times 10^{-2} \sim 9.9 \times 10^{-3}$ mmHg (VirTis Benchtop K, PA, USA) for 96 hr. During vacuum drying (VD), the pomelo pomace was weighed (~60g) and was spread as a thin layer with a 0.2cm thickness on an aluminum foil (21 cm x 21 cm) and dried in vacuum oven (VD23, Binder GmbH, Germany) with pressure 90 – 110 mbar at 50, 60, 70, 80 and 90°C. The samples were dried for 24 hr, and stored at -20°C until the physicochemical analysis was conducted.

Physicochemical Properties

Determination of Moisture Content. The moisture content of pomelo pomace was conducted according to AOAC method 925.10 (AOAC, 2000). The initial moisture content of the fresh pomelo pomace was 82.46% fresh weight.

Determination of Water Activity. Water activity (a_w) was determined using Aqualab series 3TE (Decagon Devices Inc., Pullman, WA, US). The water activity was measured with an Aqualab water activity meter (Aqualab series 3TE, Decagon Devices Inc., Pullman, WA, USA) with a dew point hygrometer at 25°C.

Determination of Total Soluble Solids (TSS). The total soluble solids (TSS) content was expressed in °Brix, performing the measurement in a pomelo pomace using refractometer (Atago CO Ltda, Itabashi-Ku, Tokyo, Japan). Distilled water was used as a blank prior to analysis of the sample.

Determination of pH. The pH was recorded using pH meter (Fisher Scientific Accumet, AP 72 Waterproof Hand-held Meters, Hampton, New Hampshire, United States) at room temperature.

Determination of Ascorbic Acid. Ascorbic acid (Vitamin C) content of pomelo pomace was determined based on 2, 6-dichloroindophenol titrimetric method (AOAC, 2000) as it is a simple and rapid method to determine Vitamin C content.

Determination of Color. Furthermore, color analysis (L, a, b, hue, and chroma) including browning index (BI) and total color change (ΔE) were performed using a color reader (CR-10, Konica Minolta, Japan.) following Rahman et al. (2016) method. The lightness (L^*), redness/greenness (a^*) and yellowness/blueness (b^*) was evaluated. These parameters were used to calculate the hue angle, chroma, BI and total color changes. The hue angle (h), chroma (C^*), BI and total color changes (ΔE) was calculated using Equation 1, 2, 3, and 4 respectively. As total color changes involve the differences between dried product color with the fresh product, the parameter of fresh color of pomelo pomace involved are L (53.01), a (3.54) and b (24.87).

$$h^\circ = \arctan\left(\frac{b^*}{a^*}\right) \quad (1)$$

$$\text{Chroma} = \sqrt{a^{*2} + b^{*2}} \quad (2)$$

$$BI = \frac{[100(x - 0.31)]}{0.17} \quad (3)$$

$$\text{where } x = \frac{(a+1.75L)}{5.645L+a-3.012b}$$

$$\Delta E = \sqrt{(L^* - L_o)^2 + (a^* - a_o)^2 + (b^* - b_o)^2} \quad (4)$$

Statistical Analysis

A Duncan's test was performed using IBM SPSS Statistics 21.0 to differentiate and evaluate the significance between the mean values. The confidence limits was considered as 95% ($p < 0.05$). The values were stated as the mean \pm standard deviation.

RESULTS AND DISCUSSIONS

Table 1 shows the physicochemical properties consisting of moisture content, water activity, and TSS of dried pomelo pomace at different drying temperatures. FD pomelo pomace showed higher MC than a recommendable level of moisture content (Table 1). Despite the samples being completely frozen, the ice crystals formed (Rahman et al., 2016; Singh & Heldman, 2001) during frozen state might not completely be removed that leading to higher levels of moisture content. After that, sublimation process (evaporation of solid to vapor phase) occurs in a vacuum operation (Dzung, 2012). As can be seen, the moisture content of vacuum dried (VD) pomelo pomace was gradually decreased as temperature increased. This highlights the condition of the reduction of water vapor concentration at the product surface due to vapor pressure gradient between the product and the environment (partial vacuum in the drying chamber) (Dev & Raghavan, 2012; Karam et al., 2016). As suggested by Geankoplis (2003) moisture content (MC) less than 10% is preferable to make microorganism inactive in a dormant state preventing the undesired changes from occurring. Therefore, vacuum drying at 70, 80, and 90°C of pomelo pomace was less than 10% MC (8.67, 7.31 and 6.46 respectively).

Table 1
Physicochemical properties of dried pomelo pomace at a different drying temperature

Treatment	Temperature (°C)	Moisture content (%)	Water activity (a_w)	TSS (°Brix)
FD (control)		13.95±1.03c*	0.36±0.002c	2.97±0.06a
	50	22.31±0.23a	0.43±0.005a	2.33±0.06b
	60	14.93±0.09b	0.39±0.01b	2.33±0.06b
VD	70	8.67±0.24d	0.38±0.01b	2.17±0.06c
	80	7.31±0.26e	0.38±0.01b	2.03±0.12d
	90	6.46±0.07f	0.38±0.01b	2.23±0.06bc

*Source: Rahman et al. (2016)

Different letters in the same column showed significant difference at ($p<0.05$). FD: Freeze drying; VD: Vacuum drying.

Note: The value was measured in dry based weight (moisture content g /100 g of dried weight based).

Water activity (a_w) of VD at 50°C showed slightly higher value than FD. It could be due to the presence of bound moisture in the dried pomelo pomace as the pomace is considered a hygroscopic type. However, it was considered lower than recommended water activity level (<0.7) (Geankoplis, 2003) which is safe for the final dried product. Nevertheless, there is no significant ($p>0.05$) value observed when temperature increased. In contrast, the water activity of the fresh pomelo peels reported by Looyrach et al. (2015) was higher (~ 0.98) than the present study. Higher a_w value liable to all microbial growth and thus reducing the shelf stability of the fresh material which is not recommended.

Total soluble solids of the VD pomelo pomace (2.33-2.03°Brix) showed a significant reduction ($p<0.05$) with FD pomelo pomace (2.97°Brix). The reducing value could be due to exposure to heat treatment eventually leading to an oxidative breakdown of the complex material such as organic acid, starch, and sugars to simple molecules such as carbon dioxide and water (Yau et al., 2010).

The pH of VD pomelo pomace (4.65-4.95) was lower than FD (6.07) pomelo pomace (Figure 1). Low value of pH in VD indicates a higher concentration of acidity (H^+ ion) in comparison with FD. It could be due to dissociation of carboxylic acid during heat treatment from the vacuum drying process. The lower pH value might be due to the dissociation of carboxyl group in amino acids from protein in pomelo pomace (Shamsudin et al., 2015b).

As for vitamin C in Figure 1, during elevated temperature, vitamin C of VD pomelo pomace increased simultaneously (11.54-30.83 mg AA/100 g DW), particularly for VD90 which was higher than freeze dried (FD) (21.10 mg AA/ 100 g DW). It could be due to the reduction of moisture content leading to increment of the aqueous phase viscosity and reactants precipitation affecting the diffusion and retaining the vitamin C (Santos & Silva, 2008). In addition, this effect could be attributed to the oxygen-free environment, which promoted a protective atmosphere and reduced the aerobic degradation of ascorbic acid preventing the oxidation process (Kongsoontornkijkul et al., 2007; Wang et al., 2018). Thomkapanich et al. (2007) observed similar phenomenon during low-pressure superheated steam drying (LPSSD) of Indian gooseberry at 75°C.

Color is an essential quality index of foods and agricultural products. The unstable color changes lead to the low marketing value and reduce the quality. The color, browning index and total color change of dried pomelo pomace at different drying temperature are

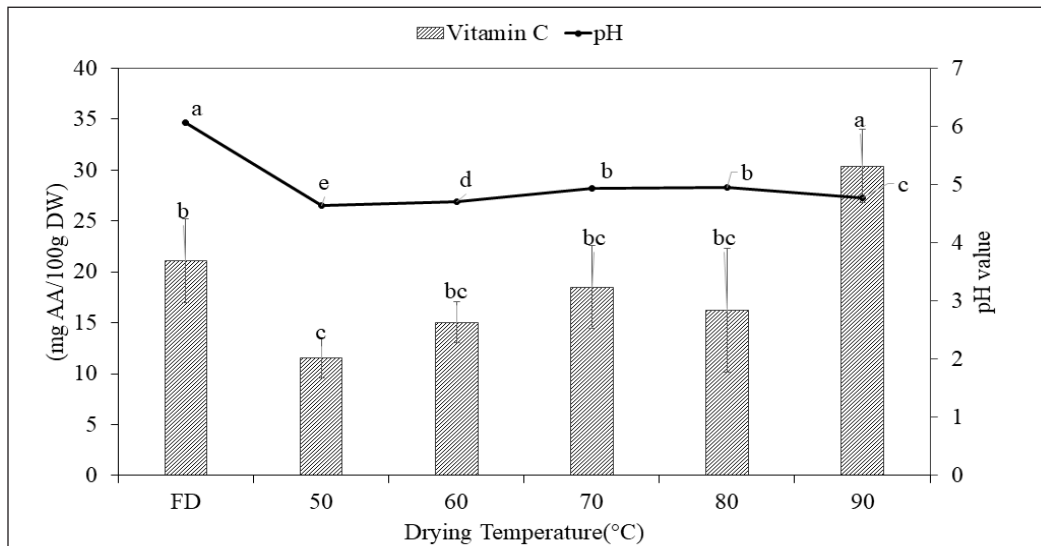


Figure 1. Effect of different drying temperature on pH and vitamin C of pomelo pomace (PP)

shown in Table 2 and Figure 2 respectively. Color denoted by CIE lightness (L, a, b) and browning index (BI) of vacuum drying process were changed significantly ($p < 0.05$). Similar changes were observed in hue angle and chroma parameter. During elevated temperature, the hue angle reduced significantly ($p < 0.05$). It might indicate the hue angle was in the range < 90 that corresponds to yellow-orange-red (brown) color. The lower the hue angle value indicates the darker color of the material. Meanwhile, chroma represents the intensity of the color. Table 2 shows that the chroma level increases significantly ($p < 0.05$) during elevated drying temperature. It could be due to the instability and degradation of the color

Table 2
Color of dried pomelo pomace (PP) at different drying temperature

Treatment	Temperature (°C)	L	a	b	hue	Chroma
FD (control)*		66.50±0.17a	6.87±0.61d	28.00±0.35b	86.55±0.53a	28.83±0.47c
	50	43.60±0.70c	6.63±0.20d	28.26±0.91b	86.84±0.21a	29.03±0.90c
	60	45.37±0.42b	7.63±0.10c	30.83±0.10a	86.50±0.07a	31.76±0.12b
VD	70	44.87±0.25b	8.36±0.06b	31.43±0.36a	85.95±0.07b	32.52±0.36ab
	80	45.20±0.20b	8.56±0.15ab	31.76±0.50a	85.84±0.15b	32.90±0.50a
	90	43.50±0.66c	9.03±0.26a	30.56±0.15a	85.01±0.34c	31.87±0.09b

*Source: Rahman et al. (2016)

Different letters in the same column showed significant different at ($p < 0.05$). FD: Freeze drying; VD: Vacuum drying

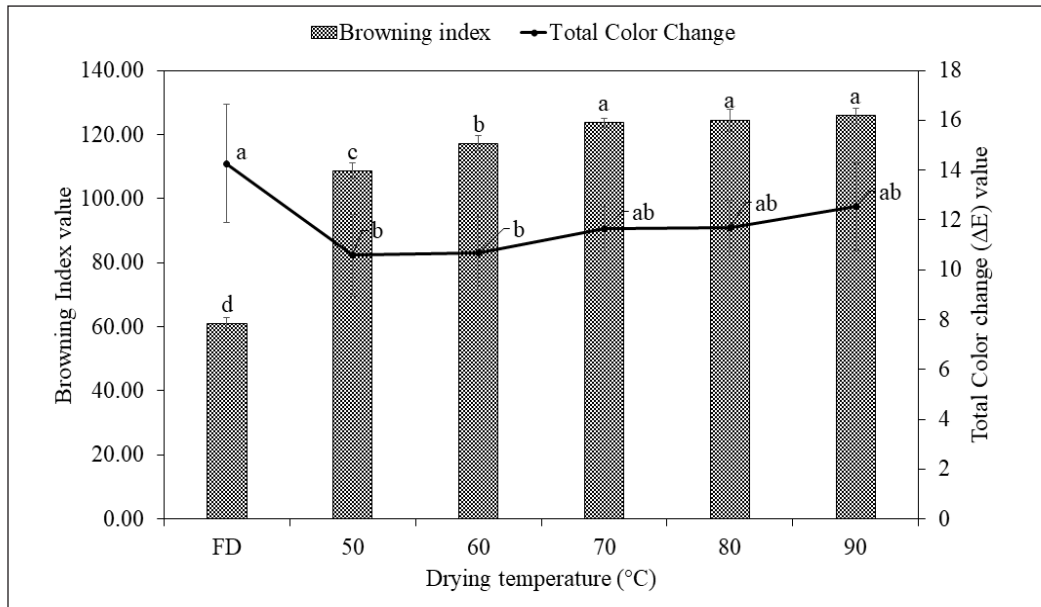


Figure 2. Effect of different drying temperature on the browning index and total color change of pomelo pomace (PP)

pigment when dried at a higher temperature (Chong et al., 2008; Lee et al., 2012). In addition, acceleration of Maillard and enzymatic reactions could be the reason of brown pigment formation (Adam et al., 2000; Kiranoudis et al., 1993) or caramelization process occurred during the increment of drying temperature (Díaz et al., 2003; Ghanem et al., 2012). A similar trend has been discovered by dried lemon slices using pulsed vacuum drying process during elevated different drying temperature (60, 65, 70 and 75°C) (Wang et al., 2018). Nevertheless, in general, no significant changes were observed for total color change particularly VD pomelo pomace at 70, 80 and 90°C compared to FD pomelo pomace.

CONCLUSION

In brief, vacuum drying at 90°C showed the most recommended drying temperature in vacuum condition. Vitamin C is the essential micro vitamin which can be an indicator of the product. By taking these compound into consideration, VD 90 is selected as the best condition as it comprises a higher value of retention. The composition of physico-chemicals and color properties at this temperature were equivalent or better than that of freeze drying process. Identification of the best drying operation applied for preservation method is highly recommended. Minimum changes of physico-chemical of the final product after drying process is highly preferable. Therefore, different drying operation is suggested to achieve the requirement of final product (natural supplement for vitamin C).

ACKNOWLEDGEMENT

The authors would like to thank the Ministry of Higher Education of Malaysia, for providing financial support under the Fundamental Research Grants Scheme (FRGS) (Project Number: 03-01-14-1412FR), and Department of Agriculture Kinta District, Ipoh, Perak for the pomelo fruits of this study.

REFERENCES

- Adam, E., Muhlbauer, W., Esper, A., Wolf, W., & Spiess, W. (2000). Quality changes of onion (*Allium cepa* L.) as affected by the drying process. *Nahrung/Food*, 44(1), 32-37.
- AOAC. (2000). *Official methods of analysis* (17th ed.). Association of Official Analytical Chemists, Gaithersberg, USA.
- Bai, H., Balevre O., Liao Y., Sun Z., & Zhao, Q. (2013). *Patent Application No. PCT/EP2012/064145*. Dried pulp preparation from unprocessed raw materials. WO 2013/014053 A1.
- Bhatnagar, A., Sillanpää, M., & Witek-Krowiak, A. (2015). Agricultural waste peels as versatile biomass for water purification – A review. *Chemical Engineering Journal*, 270, 244-271.

- Buang, N. S., Shamsudin, R., & Aziz, N. A. (2015). Mass modeling of Malaysian varieties Pomelo fruit (*Citrus grandis* L. Osbeck) with some physical characteristics. *International Food Research Journal*, 22(2), 488-493.
- Chang, S. Q., & Azrina, A. (2017). Antioxidant content and activity in different parts of pomelo (*Citrus grandis* (L.) Osbeck) by-products. *Acta Horticulturae 1152*, 27-34.
- Chong, C. H., Law, C. L., Cloke, M., Hii, C. L., Abdullah, L. C., & Daud, W. R. W. (2008). Drying kinetics and product quality of dried Chempedak. *Journal of Food Engineering*, 88(4), 522-527.
- Dev, S. R. S., & Raghavan, V. G. S. (2012). Advancements in drying techniques for food, fiber, and fuel. *Drying Technology*, 30(11-12), 1147-1159.
- Díaz, G. R. z., Martínez-Monzó, J., Fito, P., & Chiralt, A. (2003). Modelling of dehydration-rehydration of orange slices in combined microwave/air drying. *Innovative Food Science & Emerging Technologies*, 4(2), 203-209.
- Dzung, N. T. (2012). Optimization the freeze drying process of penaeus monodon to determine the technological mode. *International Journal of Chemical Engineering and Applications*, 3(3), 187-194.
- Geankoplis, C. J. (2003). *Transport Processes and Separation Process Principles: Includes Unit Operations*: New Jersey, USA: Prentice Hall PTR.
- Ghanem, N., Mihoubi, D., Kechaou, N., & Mihoubi, N. B. (2012). Microwave dehydration of three citrus peel cultivars: Effect on water and oil retention capacities, color, shrinkage and total phenols content. *Industrial Crops and Products*, 40, 167-177.
- Karam, M. C., Petit, J., Zimmer, D., Baudelaire Djantou, E. B., & Scher, J. (2016). Effects of drying and grinding in production of fruit and vegetable powders: A review. *Journal of Food Engineering*, 188, 32-49.
- Kiranoudis, C. T., Maroulis, Z. B., Tsami, E., & Marinos-Kouris, D. (1993). Equilibrium moisture-content and heat of desorption of some vegetables. *Journal of Food Engineering*, 20(1), 55-74.
- Kongsoontornkijkul, P., Ekwongsupasarn, P., Chiewchan, N., & Devahastin, S. (2007). Effects of drying methods and tea preparation temperature on the amount of vitamin C in indian gooseberry tea. *Drying Technology*, 24(11), 1509-1513.
- Lee, C. W., Oh, H. J., Han, S. H., & Lim, S. B. (2012). Effects of hot air and freeze drying methods on physicochemical properties of citrus 'hallabong' powders. *Food Science and Biotechnology*, 21(6), 1633-1639.
- Looyrach, J., Methacanon, P., Gamonpilas, C., Lekpittaya, P., & Lertworasirikul, A. (2015). Pomelo (*Citrus maxima*) peel-inspired property for development of eco-friendly loose-fill foam. *Key Engineering Materials*, 659, 279-283.
- Morton, J. F. (1987). *Fruits of Warm Climates*. Miami, FL: J.F. Morton.
- Oikonomopoulou, V. P., & Krokida, M. K. (2013). Novel aspects of formation of food structure during drying. *Drying Technology*, 31(9), 990-1007.
- Rahman, N. F. A., Shamsudin, R., Ismail, A., & Karim Shah, N. N. A. (2016). Effects of post-drying methods on pomelo fruit peels. *Food Science and Biotechnology*, 25(S1), 85-90.

- Santos, P. H. S., & Silva, M. A. (2008). Retention of vitamin c in drying processes of fruits and vegetables—A Review. *Drying Technology*, 26(12), 1421-1437.
- Shah, N. N. A. K., Rahman, R. A., Shamsudin, R., & Adzahan, N. M. (2012, November, 26-28). Effect of enzymatic clarification treatment on phenolic compounds of Pummelo (*Citrus grandis* L. Osbeck) fruit juices. In *International Conference on Agricultural and Food Engineering for Life* (pp. 122-130). Putrajaya, Malaysia.
- Shamsudin, R., Abd Rahman, N. F., Ismail, A., & Ahmad, N. S. N. W. (2015a August 10-12). Effect of oven-drying on the colour of pomelo fruit waste. In *8th Asia-Pacific Drying Conference*. Kuala Lumpur, Malaysia.
- Shamsudin, R., Abd Rahman, N. F., Ismail, A., & Shah, N. N. A. K. (2015b August 25-27). Proximate analysis of dried pomelo waste (*Citrus grandis* (L.) Osbeck). In *7th International Conference on Sustainable Agriculture for Food, Energy and Industry in Regional and Global Context*. Serdang, Malaysia.
- Singh, R. P., & Heldman, D. R. (2001). *Introduction to Food Engineering*. Cambridge, USA: Elsevier Science.
- Thomkapanich, O., Suvarnakuta, P., & Devahastin, S. (2007). Study of intermittent low-pressure superheated steam and vacuum drying of a heat-sensitive material. *Drying Technology*, 25(1), 205-223.
- Toh, J. J., Khoo, H. E., & Azrina, A. (2013). Comparison of antioxidant properties of pomelo (*Citrus grandis* (L.) Osbeck) varieties. *International Food Research Journal*, 20(4), 1661-1668.
- Wadhwa, M., & Bakshi, M. P. S. (2013). *Utilization of fruit and vegetable wastes as livestock feed and as substrates for generation of other value*. Rome, Italy: RAP Publication FAO.
- Wang, J., Law, C. L., Nema, P. K., Zhao, J. H., Liu, Z. L., Deng, L. Z., Gao, Z. J. & Xiao, H. W. (2018). Pulsed vacuum drying enhances drying kinetics and quality of lemon slices. *Journal of Food Engineering*, 224, 129-138.
- Yau, E. W., Rosnah, S., Noraziah, M., Ching, N. L., & Osman, H. (2010). Physico-chemical compositions of the red seedless watermelons (*Citrullus Lanatus*). *International Food Research Journal*, 17(2), 327-334.
- Zain, N. F. M., Yusop, S. M., & Ahmad, I. (2014). Preparation and characterization of cellulose and nanocellulose from pomelo (*Citrus grandis*) albedo. *Journal of Nutrition & Food Sciences*, 05(1), 334.

Assessment on Flux Reduction and Protein Rejection Behavior in Fractionating Tilapia By-Product Protein Hydrolysate by Ultrafiltration Membrane

Jumardi Roslan¹, Siti Mazlina Mustapa Kamal^{2*}, Khairul Faezah Md Yunos² and Norhafizah Abdullah³

¹Faculty of Food Science and Nutrition, Universiti Malaysia Sabah, Jalan UMS, 88400 Kota Kinabalu, Sabah, Malaysia

²Department of Process and Food Engineering, Faculty of Engineering, Universiti Putra Malaysia, 43400 UPM Serdang, Selangor, Malaysia

³Department of Chemical and Environmental Engineering, Faculty of Engineering, Universiti Putra Malaysia, 43400 UPM Serdang, Selangor, Malaysia

ABSTRACT

Modification of tilapia by-products (TB) into fish protein hydrolysate (FPH) using enzymatic treatment is a favorable approach for enhancing their values and applications in the food industry. The TB protein hydrolysate has a wide range of sizes, which is possible to be fractionated using ultrafiltration (UF) membrane for obtaining small sized peptides. Thus, the present study aims to assess the flux reduction behavior of ultrafiltration membrane by varying transmembrane pressure, stirring speed and solution pH. Regenerated cellulose membrane of 10 kDa molecular weight cut-off (MWCO) was used throughout of the study. It was found that the trends for flux behavior of all parameters were reaching steady state within 60 – 70 minutes. At completion of filtration (at 70 minutes), the highest permeate flux for each operating and physicochemical parameters were at 3 bar (13.6 L/m²h), 600 rpm (42.8 L/m²h) and pH 8 (53.4 L/m²h). In term of protein rejections, significant effects were attained for stirring speeds with reduction of 57% from 0 to 600 rpm and lowest protein

rejection (9.6%) was obtained at pH 8. Thus, controlling the operating parameters of the UF process could reduce membrane fouling.

Keywords: Fish protein hydrolysate, flux reduction, protein hydrolysate, protein rejection, tilapia by-product, ultrafiltration

ARTICLE INFO

Article history:

Received: 24 October 2018

Accepted: 15 February 2019

Published: 21 June 2019

E-mail addresses:

jumardi@ums.edu.my (Jumardi Roslan)

smazlina@upm.edu.my (Siti Mazlina Mustapa Kamal)

kfaezah@upm.edu.my (Khairul Faezah Md Yunos)

nhafizah@upm.edu.my (Norhafizah Abdullah)

* Corresponding author

INTRODUCTION

Processing of tilapia fish for the production of tilapia fillet would eventually generates a huge amount of by-products such as bones, frames, heads, and skin. Disposal of these by-products to the land fill may result in serious environmental problem (Arvanitoyannis & Kassaveti, 2008). Alternatively, such by-products can be converted into valuable products such as bioactive peptides for applications in food, healthcare and pharmaceutical products. Enzymatic hydrolysis is the most preferred method used for converting fish by-products into fish protein hydrolysate which composed of peptide mixtures with different sizes and biological functions (Kristinsson & Rasco, 2000). Several studies have reported that small-sized peptides have great biological activities such as antioxidant (Suwal et al., 2018; Sabeena Farvin et al., 2016; Zhong et al., 2011; Picot et al., 2010), antihypertensive (Roslan et al., 2017; Raghavan & Kristinsson, 2009; Bougatef et al., 2008; Theodore & Kristinsson, 2007) and antimicrobial (Najafian & Babji, 2012). Production of peptides with small-sized (<10 kDa) through enzymatic hydrolysis is a challenging process which cannot be achieved by merely controlling the degree of hydrolysis (DH). Therefore, it requires downstream processes such as fractionation and purification approaches to ensure that the production of peptides on a large scale and the desired molecular sizes is successful. Purification of bioactive peptides from protein hydrolysates can be achieved through chromatographic methods due to its high selectivity, but the process required high cost especially for scale-up applications (Agyei et al., 2016).

In this regard, ultrafiltration (UF) process is the most promising technology that offers several advantages including high throughput, ability to separate protein hydrolysate effectively, easily controlled and scale-up and could maintain the peptide with high biological activity (Abejon et al., 2018; Raghavan & Kristinsson, 2009; Je et al., 2005). Ultrafiltration process has been widely used as a tool for obtaining peptides with sizes less than 10 kDa (Raghavan & Kristinsson, 2009; Kim et al., 2007; Ranathunga et al., 2006; Jeon et al., 1999). Production of these specific peptide sizes in greater amounts using ultrafiltration membranes still continues as a major constraint. In UF processes, the occurrence of membrane fouling cannot be avoided, eventually decreasing the separation of the FPH and consequently reducing the yield of peptide (Prata-Vidal et al., 2001). This is because the effectiveness of peptides fractionation is not merely influenced by membrane properties (pore size), but also affected by the hydrodynamic conditions and feed solution characteristics (She et al., 2009). Protein aggregation may also occur as a result of protein-protein and protein-membrane interactions in the feed solution. Such interactions could lead to extensive accumulation of protein near the membrane surface, thus causing detrimental effect to the final product throughput. An efficient UF process for improving the yields is highly desirable. Several studies have demonstrated that proteins

and peptides can be effectively separated by manipulating the operating conditions such as solution pH and salt concentration which greatly influence the electrostatic interaction between the proteins and membrane (Saidi et al., 2013; Das et al., 2009; Ghosh & Cui, 1998). The effectiveness of proteins and peptides separation using ultrafiltration membrane could be monitored through the flux reduction (decline) and protein rejection behaviour which are the most important indicator of fouling and selectivity (Almecija et al., 2007; Das et al., 2009; Datta et al., 2009; Saidi et al., 2013). In order to minimize membrane fouling during fractionation, controlling the operating parameters, particularly the transmembrane pressure, system hydrodynamics, and pH of feed solution are necessary in order to achieve high throughput of the desired product. Fractionation of tilapia protein hydrolysate using UF membranes has been conducted by several researchers (Raghavan & Kristinsson, 2009; Dekkers et al. 2011). However, in their studies, the UF membrane was merely used as a tool for separation of small-sized peptides and lacked discussion on the effect of operating parameters on the fractionation process. Hence, the objective of this study is to investigate the effectiveness of UF membrane in fractionating tilapia by-product (TB) protein hydrolysate by manipulating the operating parameters such as pressure, stirring speed, and pH to obtain high yield of peptide.

MATERIALS AND METHODS

Tilapia By-product Mince Preparation

Tilapia (*Oreochromis niloticus*) (500-600 g) was bought from a local fish farm in Rawang, Selangor, Malaysia. The sample was kept cool using ice and afterward cleaned, washed and filleted to get the tilapia by-products (TB) (frames, head, and tail). A high-speed grinder was used to mince the TB, kept in polyethylene plastic bags and frozen it at -20°C . Prior to enzymatic hydrolysis, the frozen minced TB was defrosted in a refrigerator ($4 \pm 1^{\circ}\text{C}$).

Tilapia By-product Protein Hydrolysate Preparation

Hydrolysis of the TB was conducted by mixing 7.5 g of the minced TB with 50 mL (15% w/v, 0.05 M) phosphate buffer solution (pH 7.5) and 60 AU/kg of alcalase enzyme (a bacterial endoproteinase from a strain of *Bacillus licheniformis*, Novo Nordisk, Denmark) followed by 60 min incubation at 60°C . After that, the mixture was heated in a water bath (temperature at 90°C) for 15 min with intermittent agitation to terminate the hydrolysis reaction. Ice was used to cool the mixture, then a refrigerated high-speed centrifuge (Eppendorf, Model 5804 R) at 10,000 rpm ($14,136 \times g$) for 20 min was used to separate the particle (sedimentation) and solution, which the supernatant (top solution) was saved (Roslan et al., 2015) for further processes. Analytical grade with $> 95\%$ purity of chemical reagents were used in this experiment.

Membrane Module and Type

Dead-end ultrafiltration membrane (Amicon Model 8200 stirred ultrafiltration cell, Amicon Corp., Danvers, MA) with 10 kDa MWCO flat sheet regenerated cellulose (RC) membrane (Ultracell PLGC; 28.7 cm² filtration area) was used to fractionate the TB protein hydrolysate. Setup of the UF process is shown in Figure 1. The UF stirring system consisted of suspended bar impeller that magnetically driven stirring hot plate (Favorit). A digital photo tachometer (HYELEC Model MS6208B) was used to monitor the stirring speed.

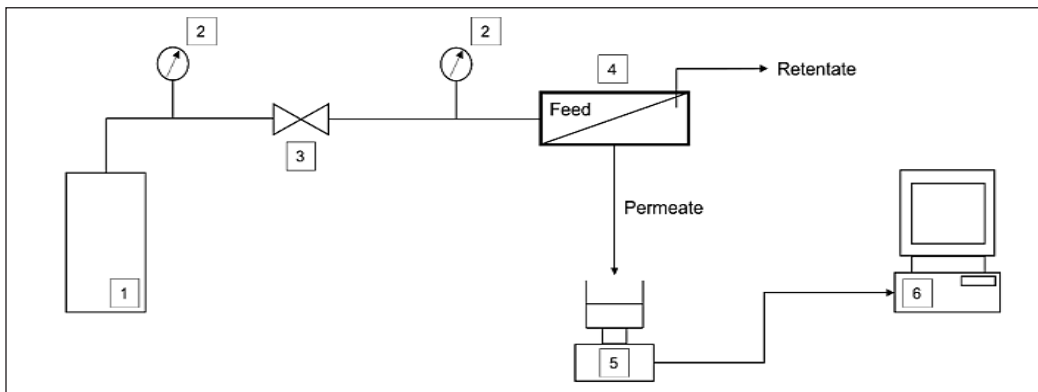


Figure 1. Schematic of experimental set-up (1. Oxygen gas tank; 2. Pressure gauge; 3. Valve; 4. Stirred cell module; 5. Balance; 6. Computer).

Membranes Preparation

The 10 kDa MWCO flat sheet regenerated cellulose (RC) membrane was soaked in deionized water (DI) overnight. To prevent any alterations in membrane hydraulic resistance throughout the process, the membrane had undergone compaction at 3.5 bar until the water flux value became steady (Das et al., 2009). The water flux was determined at different pressure from 0.5, 1, 1.5, 2, to 2.5 bar, that was used as a reference for cleaning process.

Cleaning Procedure

The RC membrane was first rinsed with deionized water, followed by soaking in 0.1% of NaOH solution and sonicated for 15 minutes. The membrane was then moved into a beaker containing deionized water and once more sonicated for 15 minutes. Finally, rinsed the membrane using deionized water up to neutral condition and then measured the water flux. If water flux obtained did not reach the initial value, the cleaning procedure needed to be repeated. The cleaned membrane was stored in a chiller at 4°C until further use.

Evaluation of the Membrane Performance

The membrane performance was assessed based on permeate flux and protein rejection factor.

Permeate Flux. In a membrane separation process, the permeate flux is used as indicator of productivity of the process. The flux value is influenced by several factors such as properties of the membrane, the system hydrodynamics, the transmembrane pressure, the concentration of protein in the feed, and the protein and solvent properties. the permeate flux was measure using equation (1) (Ghosh, 2003):

$$\text{Flux} = \frac{\text{Total quantity passed through membrane}}{\text{Membrane area} \times \text{time}} \text{ L}/(\text{m}^2\text{h}) \quad (1)$$

Protein Rejection Factor. Another factor used to describe the membrane system performance is the rejection factor. Protein rejection factor is expressed by the following equation (Lin et al. 2008):

$$\text{Protein rejection factor, } R_f (\%) = 1 - \frac{C_p}{C_f} \times 100 \quad (2)$$

where C_f is the concentration of solute in the feed solution and C_p is the concentration of solute in the permeate.

Membrane Filtration Experiments at Different Trans-Membrane Pressure, Stirring Speed and Solution pH. *The Effect of Trans-Membrane Pressure (Tmp) on Permeate Flux Reduction and Protein Rejection.* TB protein hydrolysate was fractionated using RC membrane (pore size 10 kDa) at TMP of 1, 2 and 3 bars while the other parameters such as stirring speed and pH were fixed at 0 rpm, pH 6.8 (original pH solution), respectively. Permeate was collected at 5 minutes interval until 70 minutes and permeate flux was measured. The protein rejection was calculated based on the permeate at 70 minutes. All experiments were carried out in duplicate. The highest TMP value is used for the next experiment. The same procedure was repeated for the effect of stirring speed and pH.

Statistical Analysis

Statistical analysis was performed using the Statistical Analysis System (1989) with ANOVA and Duncan's multiple range test for multiple comparisons. The same software was used to calculate the standard deviation.

RESULTS AND DISCUSSION

Effects of Transmembrane Pressure (TMP) on Flux Reduction and Protein Rejection

The fractionation was conducted under different transmembrane pressure (TMP; 1 to 3 bar) with the feed solution was kept at original pH (pH 6.8) and without stirring. The flux reduction behaviour was shown in Figure 2. Generally, the percentages of flux reduction

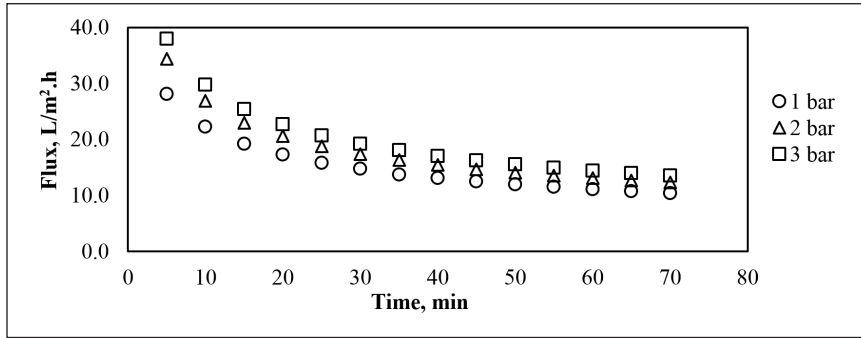


Figure 2. Flux reduction with different transmembrane pressure

up to 70 minutes of operating time were different for each pressure, which 64.3% for 1 bar, 64.7% for 2 bar and 63.2% for 3 bar. As the TMP increased from 1 to 3 bar, the permeate flux also increased significantly ($p < 0.05$) and the highest flux value was found at 3 bar.

As expected, the highest initial flux was achieved at 3 bar with 38 L/m²h followed by 2 bar (34.4 L/m²h) and 1 bar (28.1 L/m²h). The rate of flux reduction is higher in the first 20 min of the fractionation for all pressures studied. This result is consistent with the previous studies by Wang & Tang (2011) who found that higher initial flux tended to stimulate severe fouling due to increase in permeate drag force and concentration polarization. A moderate flux reduction was observed for subsequent period (30 to 55 min), and stable permeate flux was achieved within 60 to 70 min. All pressures studied have shown a different stable flux (at 70 minutes) with the value of 13.6, 12.3 and 10.4 L/m² h at 3, 2 and 1 bar, respectively.

As for the protein rejection, it was observed (Figure 3) that with the increase of TMP from 1 to 3 bar would reduce the protein rejection significantly ($p < 0.05$) with the values of 81.73%, 78.88% and 77.93%, respectively. The lower protein rejection at the higher TMP could be explained by the sufficient driving force provided under high pressure, thus allowing more solute to be transported pass through the membrane (Sarkar et al. 2009; Das et al., 2009; Datta et al., 2009). In addition, the tendency for the formation of layer cake on membrane surface is high at lower TMP making a resistance for solute to pass through the

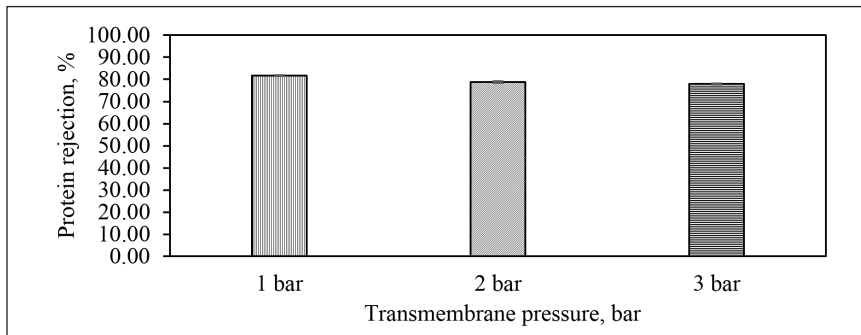


Figure 3. Protein rejection with different transmembrane pressure

membrane, thus resulting in higher protein rejection (Datta et al. 2009). This observation is in agreement with study reported by Das et al. (2009), who found the fall in protein rejection with increase in TMP. The TMP of 3 bars was selected for further experiments as it provided highest permeate flux and reasonably protein rejection.

Effects of Stirring Speed on Flux Reduction and Protein Rejection

Stirring speed is one of the major operating parameters in membrane separation process particularly for dead-end UF membrane. Figure 4 shows the effect of stirring speeds (0, 300 and 600 rpm) on flux reduction over time with other conditions were fixed at TMP of 3 bar and pH 6.8. The flux reduction percentages up to 70 minutes of operating time for each stirring speed were 63.2% for 0 rpm, 51.6% for 300 rpm and 43.4% for 600 rpm which indicated that the flux reduction decreased as the stirring speed increased. The cumulative values of permeate flux increases significantly ($p < 0.05$) with the increase in stirring speed due to the high shear field at the membrane surface. At the initial stage, the permeate flux was observed to be decreasing rapidly and eventually as the fractionation progress, the flux value became stable within 60 to 70 min. Changing the stirring speed to 300 and 600 rpm, the steady state permeate fluxes increased by 114% and 207%, respectively as compared to 13.6 L/m²h without stirring. This is possibly due to the high shear field near the membrane that could remove the solutes accumulated on the membrane surface, which reduces the effect of concentration polarization and ultimately resulting in high permeation rate (Datta et al., 2009; Sarkar et al., 2010).

Figure 5 shows the effect of stirring speed on protein rejection at three different stirring speeds (0, 300 and 600 rpm). Similar trend of peptide rejection were observed for stirring speeds and TMP, where protein rejection decreases significantly ($p < 0.05$) with the increase in stirring speed. The lowest protein rejection was found at 33.7% (600 rpm) followed by 51.3% (300 rpm) and 77.9% (without stirring). Low protein rejection observed at a high stirring speed is mainly due to the reduction of membrane fouling effect on the membrane surface, as discussed in the previous section (Datta et al., 2009). The results obtained

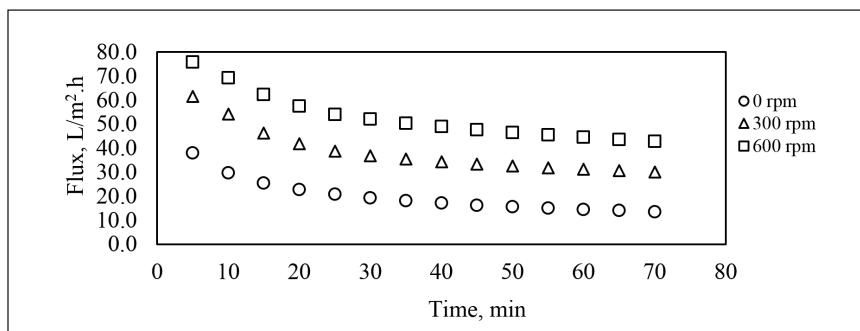


Figure 4. Flux reduction with different stirring speed

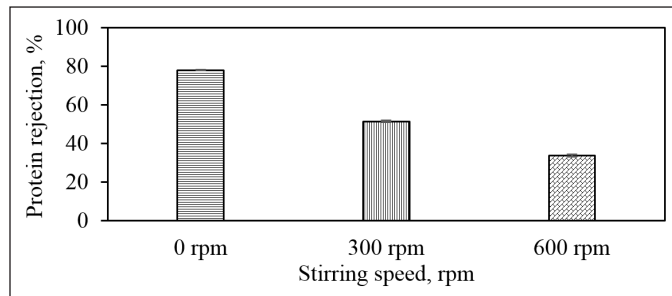


Figure 5. Protein rejection with different stirring speed

here suggested the strong correlation between stirring speed and flux value as well as the protein rejection. Therefore, for the next section, stirring speed of 600 rpm was selected with respect to the highest permeate flux and protein rejection obtained.

Effects of Solution pH on Flux Reduction and Protein Rejection

The effect of solution pH (pH 3, 5, 7, 8 and 9) over time on permeate flux is shown in Figure 6 with other conditions were fixed at 3 bar (TMP) and 600 rpm (stirring speed). It was found that the flux reduction for all pH range were 31.9% (pH 3), 48.7% (pH 5), 27.8% (pH 7), 29.3% (pH 8) and 49.4% (pH 9). The lowest flux was achieved at pH 5 with the initial flux of 78 L/m²h. After this point, permeate flux decreased dramatically between 10 to 45 min of fractionation and then reached a steady value (40 L/m²h) within 50 to 70 min. It seems that the effect of fouling is more pronounced at this pH, which is most likely to be at the isoelectric point. Generally, fouling is more apparent when the protein in the feed solution is uncharged, which is known as the isoelectric point (IEP). At this point, protein adsorption and aggregation are more likely to occur due to the less repulsive forces between the protein molecules (McDonogh et al., 1990, Kelly & Zydney, 1995). Accumulation of the aggregated protein on the membrane surface causes a low permeate flux (Das et al., 2009).

The highest and stable permeate flux was achieved at pH 8 with an initial permeate flux of 75.1 L/m²h. A slight flux reduction occurred in the first 10 min with the value of 72.6 L/m²h and then gradually decreased from 15 to 70 min (71.1 to 53.4 L/m²h) which seemed to have reached the steady-state permeation flux. This might be explained by a reduced tendency to aggregate at higher pH value (basic condition) as the membrane and the peptides are repulsed by their negative charge (Groleau et al., 2003). When the pH was changed to pH 9, the initial permeate flux was obtained at the value of 87.0 L/m²h. A rapid permeate flux reduction occurred from the 87.0 L/m²h (initial flux) to 55.1 L/m²h in 30 min of fractionation. Then, a steady permeate flux (46.4-44.4 L/m²h) was obtained within 60 to 70 min. However, this result is inconsistent with the previous studies where the permeate flux is expected to be higher at pH 9 as a result of the electrostatic repulsion between

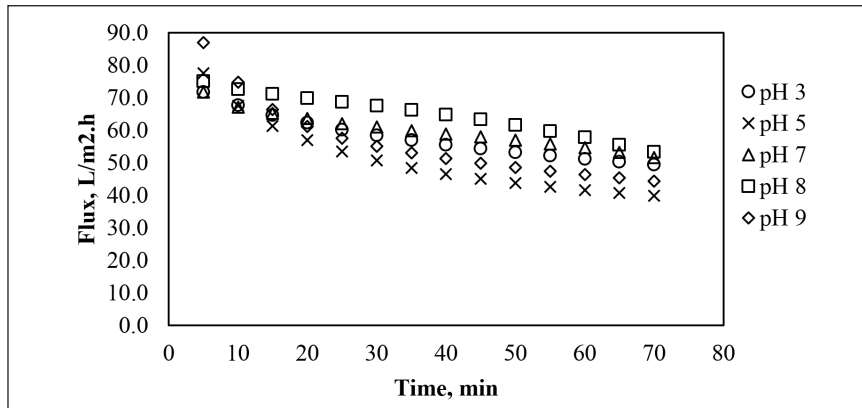


Figure 6. Flux reduction with pH effects

similar charge (negatively charged) owing by the membrane and the peptides (Lapointe et al., 2005; Groleau et al., 2004; Pouliout et al., 1999). This contradicted result possibly is due to the interaction between hydrophobic peptides that leads to peptide aggregation and eventually resulted in a significant flux reduction ($p < 0.05$) (Groleau et al., 2004).

When the fractionation was conducted at pH 7 (neutral condition), a slightly lower permeate flux was obtained as compared to pH 8 with an initial flux of 71.8 L/m²h. Permeate flux decreased gradually from 67.2 to 59.9 L/m²h from 10 to 35 min, and then flux declined slowly from 58.9-51.7 L/m²h within 40 to 70 min. At pH 3 (acidic condition), the permeate flux reduction behaviour was exactly similar with pH 7 where the initial permeate flux was obtained at 71.8 L/m²h and then decreased steadily from 67.7 to 57.0 L/m²h in 10 to 35 min. Further flux reduction was much milder and attaining a steady permeate flux value within 60 to 70 min with values ranging from 51.3-49.5 L/m²h. There was a significant difference ($p < 0.05$) in the stable permeate flux values for all pH studied, which indicated that pH of the solutions significantly affected the permeate flux performance.

The minimum permeate flux was found at the isoelectric point (IEP) (pH 5). Apparently, the permeate flux increased as the pH is shifted away from the isoelectric point. The membrane permeability becomes more pronounced when the fractionation was performed in alkaline condition (above the isoelectric point), where the permeate flux shows the maximum value. This is possibly due to the strong electrostatic repulsive force between the membrane and peptide that promotes permeate flux increment. Several studies have reported a similar behavior where the better flux performance was observed under alkaline condition (Saidi et al., 2013; Wang & Tang, 2011; She et al., 2009). Low permeate flux observed at pH 3 might be the result of strong interaction between the oppositely charged peptides (positive) and membrane surface (negative) which caused the peptide to accumulate on the surface of the membrane thus lowering the permeate flux (Saidi et al., 2013). The difference in flux values obtained for fractionation conducted in acidic and basic conditions probably

due to the greater electrostatic repulsion at the alkaline condition as stated by Lapointe et al. (2005) and Pouliot et al. (1999).

Figure 7 shows the effect of various pH on protein rejection of TB protein hydrolysate. The protein rejection results have shown a significant difference ($p < 0.05$) at all pH studied. It can be seen that the highest protein rejection was achieved at pH 5 (36.2%), followed by pH 9 (26.7%), pH 3 (20.7%), pH 7 (15.5%) and the lowest rejection was at pH 8 (9.6%). These results suggest that effect of pH on protein rejection is not certain as other pH dependent phenomena might take place during the process such as pH-electrostatic double layer interaction, pH-protein-membrane repulsion, and the pH-dependent conformation of protein as reported elsewhere (Ghosh & Cui, 1998; Das et al., 2009; Wan et al., 2006; Sarkar et al., 2010; Groleau et al., 2003).

Based on the lowest permeate flux and highest protein rejection obtained previously, pH 5 is considered as the IEP of the TB protein hydrolysate. This finding was also observed by Sarkar et al. (2009) and Das et al. (2009) who found that the protein rejection was highest at the isoelectric point. The possible explanation for this result is the high tendency of protein aggregation and adsorption to occur on dead-end ultrafiltration membrane (Das et al., 2009). Furthermore, at or closer to the isoelectric point, the protein molecules are more likely entangled/elongated which resulted in higher rejection or lower transmission (Sarkar et al. 2009).

When the solution's pH changed to pH 3 (acidic condition), the protein rejection was significantly decreased which could be due to the enhanced electrostatic repulsion and low tendency of peptide to accumulate on the membrane surface, allowing more peptides to pass through the membrane (Ghosh & Cui, 1998; She et al., 2009). The convective transport of solute as a result of high permeate flux at pH 3 can also contribute to the lower protein rejection (Almecija et al., 2007). However, the protein rejection in pH 3 is considered high as compared to protein rejection obtained at pH 7 and 8. The strong electrostatic repulsion between the negatively charged peptides and membrane in neutral and basic condition may limit the peptide aggregation and accumulation, therefore further peptide can permit through

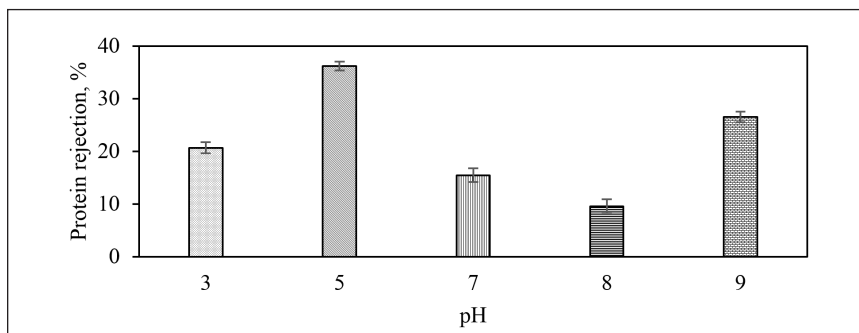


Figure 7. Protein rejection with the effect of pH

the membrane (Almecija et al., 2007). Less electrostatic repulsion may be responsible for the high protein rejection at pH 3 that can lead to the interaction between positively charged peptides on the oppositely charged surface of membrane. A slightly higher protein rejection was observed at pH 9 possibly due to the presence of hydrophobic peptides (positively charged) that had a tendency to adsorb or accumulates on the membrane surface (Groleau et al., 2004). This results clearly indicated that solution pH had a great influence on the fractionation of tilapia by-product protein hydrolysate. The best pH condition (pH 8) was obtained at the lowest protein rejection.

CONCLUSION

The flux reductions for all parameters reached steady state within 60 – 70 minutes. It seems that the trends of flux reduction behavior for TB protein hydrolysate were quite similar for each operating parameters, i.e transmembrane pressure (TMP), stirring speed and pH. The highest permeate flux at final filtration time (70 minutes) for each operating parameters were at 3 bar (13.6 L/m²h), 600 rpm (42.8 L/m²h) and pH 8 (53.4 L/m²h). In term of protein rejections, less significant effects were observed at various range of pressure, but significant effects were attained for both range of stirring speeds and pH. Controlling the stirring speed and pH could minimize the effect of concentration polarization and fouling, which is preferable due to higher permeate flux and less protein loss. The findings from this study provide an essential information on the effective separation conditions for obtaining a high yield of peptides from TB protein hydrolysate.

ACKNOWLEDGEMENTS

The authors are grateful for the financial support from Universiti Putra Malaysia through the RUG Scheme (05-01-12-1646RU) and Ministry of Science, Technology, and Innovation (MOSTI), Malaysia through Science Fund Research Grant (06-01-04-SF1602).

REFERENCES

- Abejon, R., Belleville, M. P., Sanchez-Mercano, J., Garea, A., & Irabien, A. (2018). Optimal design of industrial scale continuous process for fractionation by membrane technologies of protein hydrolysate derived from fish waste. *Separation and Purification Technology*, 197, 137-146.
- Agyei, D., Ongkudon, C. M., Wei, C. Y., Chan, A. S., & Danquah, M. K. (2016). Bioprocess challenges to the isolation and purification of bioactive peptides. *Food and Bioproducts Processing*, 98, 244-256.
- Almecija, M. C., Ibanez, R., Guadix, A., & Guadix, E. M. (2007). Effect of pH on the fractionation of whey proteins with a ceramic ultrafiltration membrane. *Journal of Membrane Science*, 288(1-2), 28-35
- Arvanitoyannis, I. S., & Kassaveti, A. (2008). Fish industry waste: treatments, environmental impacts, current and potential uses. International. *Journal of Food Science & Technology*, 43(4), 726-745.

- Bougatef, A., Nedjar-Arroume, N., Ravallec-Plé, R., Leroy, Y., Guillochon, D., Barkia, A., & Nasri, M. (2008). Angiotensin I-converting enzyme (ACE) inhibitory activities of sardinelle (*Sardinella aurita*) by-products protein hydrolysates obtained by treatment with microbial and visceral fish serine proteases. *Food Chemistry*, *111*(2), 350–356.
- Das, R., Bhattacharjee, C., & Ghosh, S. (2009). Effects of operating parameters and nature of fouling behavior in ultrafiltration of sesame protein hydrolysate. *Desalination*, *237*(1-3), 268–276.
- Datta, D., Bhattacharjee, S., Nath, A., Das, R., Bhattacharjee, C., & Datta, S. (2009). Separation of ovalbumin from chicken egg white using two-stage ultrafiltration technique. *Separation and Purification Technology*, *66*(2), 353-361.
- Dekkers, E., Raghavan, S., Kristinsson, H. G., & Marshall, M. R. (2011). Oxidative stability of mahi mahi red muscle dipped in tilapia protein hydrolysates. *Food Chemistry*, *124*(2), 640-645.
- Ghosh, R. (2003). *Protein Bioseparation using ultrafiltration*. London, UK: Imperial College Press.
- Ghosh, R., & Cui, Z. F. (1998). Fractionation of BSA and lysozyme using ultrafiltration: Effect of pH and membrane pretreatment. *Journal of Membrane Science*, *139*(1), 17-28.
- Groleau, P. E., Morin, P., Gauthier, S. F., & Pouliot, Y. (2003). Effect of physicochemical conditions on peptide-peptide interactions in a tryptic hydrolysate of β -lactoglobulin and identification of aggregating peptides. *Journal of Agricultural and Food Chemistry*, *51*(15), 4370-4375.
- Groleau, P. E., Lapointe, J. F., Gauthier, S. F., & Pouliot, Y. (2004). Effect of aggregating peptides on the fractionation of β -LG tryptic hydrolysate by nanofiltration membrane. *Journal of Membrane Science*, *234*(1-2), 121–129
- Je, J. Y., Park, P. J., & Kim, S. K. (2005). Antioxidant activity of a peptide isolated from Alaska pollack (*Theragra chalcogramma*) frame protein hydrolysate. *Food Research International*, *38*(1), 45–50.
- Jeon, Y. J., Byun, H. G., & Kim, S. K. (1999). Improvement of functional properties of cod frame protein hydrolysates using ultrafiltration membranes. *Process Biochemistry*, *35*(5), 471–478.
- Kelly, S.T., & Zydney, A. L. (1995). Mechanism of BSA fouling during microfiltration. *Journal of Membrane Science*, *107*(1-2), 115–124.
- Kim, S., Je, J. Y., & Kim, S. K. (2007). Purification and characterization of antioxidant peptide from hoki (*Johnius belengerii*) frame protein by gastrointestinal digestion. *Journal of Nutritional Biochemistry*, *18*(1), 31–38.
- Kristinsson, H. G., & Rasco, B. A. (2000a). Fish protein hydrolysates: Production, biochemical, and functional properties. *Critical Reviews in Food Science and Nutrition*, *40*(1), 43–81.
- Kristinsson, H. G., & Rasco, B. A. (2000b). Biochemical and functional properties of atlantic salmon (*Salmo Salar*) muscle proteins hydrolyzed with various alkaline proteases. *Journal of Agricultural and Food Chemistry*, *48*(3), 657–666.
- Lapointe, J. F., Gauthier, S. F., Pouliot, Y., & Bouchard, C. (2005). Characterization of interactions between β -lactoglobulin tryptic peptides and a nanofiltration membrane: Impact on the surface membrane properties as determined by contact angle measurements. *Journal of Membrane Science*, *261*(1-2), 36–48.

- Lapointe, J. F., Gauthier, S. F., Pouliot, Y., & Bouchard, C. (2003). Effect of hydrodynamic conditions on fractionation of β -lactoglobulin tryptic peptides using nanofiltration membranes. *Journal of Membrane Science*, 212(1-2), 55–67.
- Lin, S. H., Hung, C. L., & Juang, R. S. (2008). Effect of operating parameters on the separation of proteins in aqueous solutions by dead-end ultrafiltration. *Desalination*, 234(1-3), 116-125.
- McDonogh, R. M., Bauser, R. M., Stroh, N., & Chmiel, H. (1990). Concentration polarisation and adsorption effect in cross flow UF of proteins. *Desalination*, 79(2-3), 217–231.
- Najafian, L., & Babji, A. S. (2012). A review of fish-derived antioxidant and antimicrobial peptides: Their production, assessment, and applications. *Peptides*, 33(1), 178-185.
- Picot, L., Ravallec, R., Fouchereau-Peron, M., Vandanjon, L., Jaouen, P., Chaplain-Derouiniot, M., Guerard, F., Chabeaud, A., LeGal, Y., Alvarez, O. M. Berge, J.P., Piot, J.M., Batista, I., Pires, C., Thorkelsson, G., Delannoy, C., Jakobsen, G., Johansson, I., & Bourseau, P. (2010). Impact of ultrafiltration and nanofiltration of an industrial fish protein hydrolysate on its bioactive properties. *Journal of the Science and Food Agriculture*, 90(11), 1819–1826.
- Pouliot, Y., Wijers, M. C., Gauthier, S. F., & Nadeau, L. (1999). Fractionation of whey protein hydrolysates using charged UF/ NF membranes. *Journal of Membrane Science*, 158(1-2), 105-114.
- Prata-Vidal, M., Bouhallab, S., Henry, G., & Aimar, P. (2001). An experimental study of caseinomacropptide hydrolysis by trypsin in a continuous membrane reactor. *Biochemical Engineering Journal*, 8(3), 195–202.
- Raghavan, S., & Kristinsson, H. G. (2009). ACE-inhibitory activity of tilapia protein hydrolysates. *Food Chemistry*, 117(4), 582–588.
- Ranathunga, S., Rajapakse, N., & Kim, S. K. (2006). Purification and characterization of antioxidative peptide derived from muscle of conger eel (*Conger myriaster*). *European Food Research Technology*, 222(3-4), 310–315.
- Roslan, J. Mustapa Kamal, S. M., Md. Yunos, K. F., & Abdullah, N. (2015). Optimization of enzymatic hydrolysis of tilapia (*Oreochromis niloticus*) by-product using response surface methodology. *International Food Research Journal*, 22(3), 1117-1123.
- Roslan, J., Mustapa Kamal, S. M. Md. Yunos, K. F., & Abdullah, N. (2017). Assessment on multilayer ultrafiltration membrane for fractionation of tilapia by-product protein hydrolysate with angiotensin I-converting enzyme (ACE) inhibitory activity. *Separation and Purification Technology*, 173, 250-257.
- Sabeena Farvin, K. H., Andersen, L. L., Otte, J., Nielsen, H. H., Jessen, F., & Jacobsen, C. (2016). Antioxidant activity of cod (*Gadus morhua*) protein hydrolysate: Fractionation and characterization of peptide fraction. *Food Chemistry*, 204, 409-419.
- Saidi, S., Deratani, A, Amar, R. B., & Belleville, M. P. (2013). Fractionation of a tuna dark muscle hydrolysate by a two-step membrane process. *Separation and Purification Technology*, 108, 28–36.
- Sarkar, P., Ghosh, S., Dutta, S., Sen, D., & Bhattacharjee, C. (2009). Effect of different operating parameters on the recovery of proteins from casein whey using a rotating disc membrane ultrafiltration cell. *Desalination*, 249(1), 5-11.

- Sarkar, D., Bhattacharya, A., & Bhattacharjee, C. (2010). Modelling the performances of a standard single stirred ultrafiltration cell using variable velocity back transport flux. *Desalination*, 261(1-2), 89-98.
- She, Q. Tang, C. Y. Wang, Y. N., & Zhang, Z. (2009). The role of hydrodynamic conditions and solution chemistry on fouling during ultrafiltration. *Desalination*, 249(3), 1079-1087.
- Statistical Analysis System (1989). NC, USA: SAS Institute, Inc.
- Suwal, S., Ketnawa, S., Liceaga, A. M., & Huang, J. Y. (2018). Electro-membrane fractionation of antioxidant peptides from protein hydrolysates of rainbow trout (*Oncorhynchus mykiss*) byproducts. *Innovative Food Science & Emerging Technologies*, 45, 122-131.
- Theodore, A. E., & Kristinsson, H. G. (2007). Angiotensin converting enzyme inhibition of fish protein hydrolysates prepared from alkaline-aided channel catfish protein isolate. *Journal of the Science of Food and Agriculture*, 87(12), 2353–2357.
- Wang, Y. N., & Tang, C. Y. (2011). Protein fouling of nanofiltration, reverse osmosis, and ultrafiltration membranes-The role of hydrodynamic conditions, solution chemistry, and membrane properties. *Journal of Membrane Science*, 376(1-2), 275–282.
- Wan, Y., Lu, J., & Cui, Z. (2006). Separation of lysozyme from chicken egg white using ultrafiltration. *Separation and Purification Technology*, 48(2), 133-142.
- Zhong, S. Ma, C. Lin, Y. C., & Luo, Y. (2011). Antioxidant properties of peptide fractions from silver carp (*Hypophthalmichthys molitrix*) processing by-product protein hydrolysates evaluated by electron spin resonance spectrometry. *Food Chemistry*, 126(4), 1636-1642.

Stochastic Models for Greenhouse Whitefly Flight Behavior based on Wireless Image Monitoring System Measurements

Dan Jeric Arcega Rustia and Ta-Te Lin*

Department of Bio-Industrial Mechatronics Engineering, National Taiwan University, Taipei City 10617, Taiwan

ABSTRACT

One of the most harmful greenhouse insect pests is the *Trialeurodes vaporariorum* or most commonly known as the greenhouse whitefly. The easiest way to monitor the population of greenhouse whiteflies is by the use of yellow sticky paper traps. The insect count information from the traps can be used for analyzing insect behavior by constructing biological models. In this work, stochastic models describing the effects of temperature and the time of day on the flight behavior of greenhouse whiteflies were developed. Sticky paper images and temperature data were collected from an organic tomato seedling greenhouse by using integrated wireless imaging and environmental sensors. The greenhouse whitefly counts were determined by processing the images using an insect counting algorithm. From the results obtained, differences between the flight rates of the greenhouse whiteflies for different ranges of temperature were observed. The relationship was shown to be best fit using a double Weibull distribution function with an r^2 of 0.988 and mean squared error of prediction (MSEP) of 0.001. Using the model, it was found that the optimal temperature for flight of greenhouse whiteflies was around 20-26°C. From the real-time counting data, different daily peak flight times were discovered. The peak flight rates were modeled using multi-peak probability distribution functions where it shows that the multi-

peak Gaussian distribution has the best fit with an r^2 of 0.961 and MSEP of 0.006. The developed models can be used for developing insect pest control methods such as fuzzy temperature control and pesticide application scheduling.

Keywords: Biological model, insect population, insect flight, integrated pest management, yellow sticky paper

ARTICLE INFO

Article history:

Received: 24 October 2018

Accepted: 15 February 2019

Published: 21 June 2019

E-mail addresses:

d05631006@ntu.edu.tw (Dan Jeric Arcega Rustia)

m456@ntu.edu.tw (Ta-Te Lin)

* Corresponding author

INTRODUCTION

One of the most tackled issues in agriculture is the need for a drastic increase in world food production to meet with rapid population growth. As a result, there is a more urgent need to assist farmers in making decisions for insect pest management in order to protect their crops. The primary method to prevent insect pests is the use of pesticides. However, with careless application of pesticides, insect pests tend to develop immunity and it becomes more difficult to eliminate them. In addition, reduction of pesticide usage is also necessary for environmental protection. The only way to determine the optimal dosage and timing of spraying pesticides is through prior insect population monitoring (Lamichhane et al., 2016; Potamitis et al., 2017). The greenhouse whitefly, *Trialeurodes vaporariorum*, is one of the main transmitters of plant diseases. In general, the weakness of all whitefly species is their attraction to yellow color and light (Bonsignore, 2015). The three basic methods to monitor whitefly population include the use of sticky paper traps, pheromone traps, and light traps. Among the three methods, the use of sticky paper traps is the most efficient trapping method due to its availability and simplicity (Pinto-Zevallos & Vänninen, 2013). The number of whiteflies trapped on the yellow sticky traps can be counted by manual inspection to obtain their population density. However, this is very cumbersome and time-consuming. In order to simplify the process, automatic detection and counting of whiteflies through wireless cameras was achieved in our previous work (Rustia & Lin, 2017). In spite of this, the raw information gathered cannot be simply given to the farmers as they should be interpreted. With the use of mathematical models, the phenomena related to whitefly behavior can be quantified. The models can be used to obtain measures or indices that can guide them in taking actions for whitefly prevention and control (Wang & Song, 2009; Watt, 1961).

Furthermore, whiteflies are ectothermic or cold-blooded insects. This means that their activity and reproduction rate is greatly affected by warm ambient temperature (Nava-Camberos et al., 2001; Bonsignore, 2015). In fact, it was proven by Bonsignore (2015) through a controlled experiment that the best temperature for the reproduction of greenhouse whiteflies on tomatoes was around 25°C. On the other hand, the development rate of whiteflies declines at temperature ranges below 20°C and above 30°C (Nava-Camberos, Riley, & Harri., 2001). However, from recent studies, most mathematical models for whitefly population were derived from controlled environments. Obtaining inconsistent interpretations is highly possible due to the unpredictable climate change (Lamichhane et al., 2016). The only solution is to continuously develop models that are derived from new data.

The goal of this paper is to establish stochastic models based on collected data from wireless image and environmental monitoring system that can describe the flight behavior of greenhouse whiteflies. Using the modeling methods developed herein, combined with the monitoring system, a decision-making system could be designed for the use of farmers in integrated pest management.

MATERIALS AND METHODS

Data Collection

The greenhouse whitefly population count and temperature data were obtained from a wireless imaging and sensor network with 7 nodes installed in a 528.8 m² seedling greenhouse in Chiayi County, Taiwan. Each wireless node held a yellow sticky paper trap using an acrylic board installed 8-10 cm above the crops. The greenhouse grew lettuce, cabbage, and tomato seedlings which were some of the most common host plants for whiteflies. Spraying of pesticides, installation of pheromone traps, and other preventive measures were not applied to remove biases and effects to the experimental results.

Throughout this text, the number of whitefly detections is defined as the number of whiteflies trapped on the yellow sticky paper traps. It was automatically counted from yellow sticky paper RGB images processed using an image processing and deep neural network algorithm that has 97% accuracy for whitefly identification (Rustia et al., 2018). The temperature readings were collected using AM2301 temperature and humidity sensors (Aosong Electronics Co. Ltd., China) with resolution of 0.1°C and accuracy of $\pm 0.5^\circ\text{C}$. The images were collected every 10 minutes from 7am to 7pm while the temperature data were read every 5 minutes all day. The selected image collection time was determined from previous experiments using the wireless imaging and sensor network in which it was observed that virtually no insects are detected during the night and early morning when light is not yet present (Rustia & Lin, 2017). The observations were conducted from July 2017 to March 2018 in which each observation period lasted for 2 weeks to enable replacement of the yellow sticky paper traps and avoid overcrowded sticky papers that would reduce the accuracy of the counting algorithm.

Biological Modeling and Data Analysis

In this work, non-linear stochastic models were proposed that can possibly best describe the effects of temperature and time of day in relation to the flight behavior of whiteflies. All plotting and data analysis were done using R version 3.4.3, coded in RStudio version 1.0.153, with the assistance of Table Curve 2D version 5.01.02 for automated equation fitting. R was used since it is a programming language purposely optimized for fast statistical analysis and scientific plotting, while Table Curve 2D was used to find different available equations that can be used for fitting the data sets.

Flight Rate and Temperature Model

Our previous experimental observations showed that temperature has a significant effect on the number of whiteflies detected on the sticky paper per day (Rustia & Lin, 2017). This proves that temperature can largely affect the reproductive rate and flight behavior

of whiteflies. However, collecting more data further proved that the number of whiteflies trapped on the sticky papers followed a certain distribution that could best describe when the reproduction or flight of whiteflies might stop. Using the data obtained, Table Curve 2D was used to search for the best equations that can represent the distribution. Based on model simplicity and goodness of fit parameters, four-parameter log-normal, four-parameter Weibull, and double Weibull functions were selected. Other than that, the first two equations were already used several times for describing insect flight and reproduction behavior (Damos & Savopoulou-Soultani, 2012; Régnière et al., 2012) and have been proven to be suitable for most ectothermic insect species. Both functions can describe why at certain extreme low and high temperatures, insects cannot reproduce effectively. On the other hand, the double Weibull function, the product of a two parameter Weibull function and its complement, is a flexible function that is widely used for modeling biological phenomena (Haefner, 2005). Equations 1, 2 and 3 show the respective functions used for four-parameter log-normal, four-parameter Weibull, and five-parameter double Weibull function and their corresponding parameters.

Four-parameter log-normal function:

$$F = k_1 \exp \left[-\frac{\ln(2)}{\ln(k_4)^2} \ln \left(\frac{(T-k_2)(k_4^2-1)}{k_3 k_4} + 1 \right)^2 \right] \tag{1}$$

Four-parameter Weibull function:

$$F = k_1 \left(\frac{k_4-1}{k_4} \right)^{\frac{1-k_4}{k_4}} \left[\frac{T-k_2}{k_3} + \left(\frac{k_4-1}{k_4} \right)^{\frac{1}{k_4}} \right]^{k_4-1} e^{\left[-\left(\frac{T-k_2}{k_3} + \left(\frac{k_4-1}{k_4} \right)^{\frac{1}{k_4}} \right)^{k_4} + \frac{k_4-1}{k_4} \right]} \tag{2}$$

where:

F = flight rate (time⁻¹)

T = temperature (°C)

k_1 = amplitude (max. of F)

k_2 = center (T value at max of F)

k_3 = width

k_4 = shape

Five-parameter double Weibull function (Haefner, 2005):

$$F = k_1 \left(1 - e^{-\left(\frac{T}{k_2}\right)^{k_4}} \right) e^{-\left(\frac{T}{k_3}\right)^{k_5}} \tag{3}$$

where:

F = flight rate (time⁻¹)

T = temperature (°C)

k_1 = amplitude (max. of F)

k_2 = center (T value at max of F)

k_3 = width

k_4 = shape (1) (coefficient of variation of Weibull)

k_5 = shape (2) (coefficient of variation of Complemented Weibull)

In this work, the flight rate F is defined as the derivative of the whitefly count on the yellow sticky papers determined from the automatic image monitoring system described above. Specifically, it is computed from the difference of whitefly detection count at time t and $t-1$. The flight rate can partially describe the reproduction rate and growth rate of the whiteflies (Bonsignore, 2015). Additionally, the flight rate was normalized from 0 to 1 in order to generalize the model. Therefore, the k_1 values for all functions are always equal to 1 and k_2 is the peak temperature level at which there is the highest probability of whitefly flight. The width parameter k_3 and shape parameter k_4 of all the functions affect the area under the curve of the models, which reflects the actual number of flights on the specified temperature level. Moreover, the width parameter is used to control the skewness and kurtosis of the curve while the shape parameter affects the slope of the curve. Differently, the double Weibull function has two shape parameters which are used for its ordinary Weibull function and a complementary Weibull function with parameters named k_4 and k_5 , respectively. The Levenberg–Marquardt method for nonlinear least square curve-fitting problems, more commonly known as the LM method, was used as a parameter estimation method to iteratively obtain the most optimal parameters for both functions (Press et al., 1992). However, due to the limitation in the range of the measured temperature data, extrapolated points were added by obtaining the flight rate at selected minimum temperature values as specified for temperatures at 9°C, 10°C, and 11°C. The collected flight rates and mean temperature values per day, fitted with all the functions, are shown in Figure 1.

The model presented in Figure 1 is based on the mean flight rates, with a unit time^{-1} , at each temperature T . The mean flight rates represent how fast flight can occur for each temperature point. The observed data shows that there are certain points at which whiteflies begin and stop emerging. After obtaining the median of the flight rate probability points, a threshold line was drawn to specify high and low probability. Specifically, at temperature levels between 15°C and 27°C, the probability of flight was high; outside this range, the probability was low. This observed phenomenon was also found to be true for other whitefly subspecies. As mentioned, Bonsignore (2015) found through a controlled experiment that the ideal temperature for the development of greenhouse whiteflies was around 25°C which is very close to the data collected in this work. Similarly, their work also showed that below 15°C, the developmental rates were close to 0. Additionally, visual inspection showed that the double Weibull function had the best fit compared to the other functions

used, as can be seen from the low and high temperature ranges in which the very low probabilities of flight dropped to zero, unlike the two other functions that failed to show the low probabilities when the temperature range was extended to 5°C.

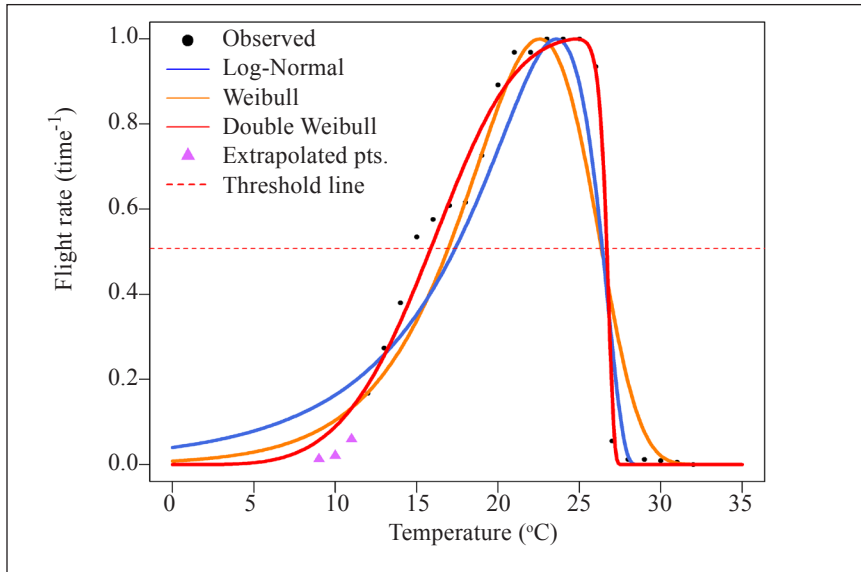


Figure 1. Observed normalized flight rates at each mean temperature level and fitted non-linear function curves. A dotted threshold line indicates the separation between low and high probability of flight based on the median of the flight rate.

Flight Rate and Temperature Model Validation

Furthermore, the models were tested based on several model validation parameters. Model validation was done in order to test the correctness and sensitivity of the models. Statistical validation was done through F-test for variance comparison and Welch two sample t-test for mean comparison with significance confidence level (α) of 0.05 for both tests. For goodness of fit testing, the traditional coefficient of determination, r^2 , was used and adjusted r^2 . The susceptibility of the models to error was tested using mean square error of predictions (MSEP) and Theil's U (Haefner, 2005), a statistic that measures the accuracy of the model by significantly increasing the errors. Table 1 shows a summary of the validation tests.

The statistical validation results in Table 1 show that the null hypotheses of the model, having different mean and variance from the observed values, are not rejected based on F-tests and T-tests. Therefore, it means that the three models were not significantly different according to the data derived from the experiments. Additionally, the coefficient of determination values show that the models are suitable for showing the trend of the observed values and are robust enough to accept new observations without losing the

Table 1
Evaluation summary of flight rate and temperature relationship models

Parameter	Weibull	Log-Normal	Double Weibull
F-test F value ($\alpha > 0.05$, $df = 20$)	0.018	0.017	0.016
Paired T-test T value ($\alpha > 0.05$, $df = 20$)	-5.162	-4.845	-4.822
Coefficient of determination, r^2	0.891	0.925	0.988
Adjusted r^2	0.777	0.847	0.976
Theil's U	0.102	0.086	0.032
MSEP	0.016	0.011	0.001

trend information. However, the three models differ greatly in terms of adjusted r^2 values, signifying that the double Weibull model can successfully predict the observed values, and better in comparison to the other two; even the number of predictors was decreased. Theil's U and MSEP values of double Weibull show that it is more robust and resistant to error compared to the other two models.

The model validation results prove that the models can also be used as a reference at which temperature levels whitefly flight or reproduction can possibly be prevented. It also proved that integrating environmental sensors into the imaging system can successfully collect data that can accurately describe the whitefly flight behavior as affected by temperature; the results match other controlled experiments.

Flight Pattern Model

Another bit of valuable information that can be obtained from the whitefly count collected is the probability of flight in correspondence to the time of day. From our previous observation results, the change in insect pest count has some possible correlation to the time of day, most especially in relation to light intensity (Rustia & Lin, 2017). It appears that insects, similar to human beings, have a similar daily activity pattern in which they are more active during the day, especially at noon, and before the evening. During these peak times, our data showed that light intensity had its highest change in values during those times. This was similarly observed in a research by Jha et al. (2009) which showed that chilli thrips were most active several times of the day. This was also proven from a research which showed that insects had a tendency to exhibit poikilothermic behavior, which meant they would need light to provide heat and prepare their muscles before flying (Ribak et al., 2016; Liang et al., 2010). Therefore, this work also aims to develop a model that can approximate the time of day when the whiteflies will take flight.

One of the ways to discover the time of day the whiteflies might begin to fly is to investigate the number of whiteflies detected per hour on the yellow sticky paper traps. The derivative of the insect pest counts per hour were computed to obtain the peaks that can

indicate the times of day the flight rate of the whiteflies are at its highest. At first glance, the raw data show that the hourly flight rate of the whiteflies can possibly be described by using logistic curves. However, it can also be noticed that during some days there are multiple normalized flight rate peaks. The results obtained match previous researches that discovered multiple peaks during different times of day (Jha et al., 2009). Therefore, it shows that there are instances that the logistic curve function might not be an appropriate model to accurately describe the whitefly flight behavior. To solve this problem, multi-peak distribution models were used in this work.

Two multi-peak distribution model functions were compared: Gaussian probability density function and logistic probability density function. The formula and corresponding parameters of the said functions are shown in Equation 4 and 5:

Multi-peak logistic probability density function:

$$F = \frac{e^{-\frac{(t-\mu_1)}{\sigma_1}}}{\sigma_1(1+e^{-\frac{(t-\mu_1)}{\sigma_1}})^2} + \frac{e^{-\frac{(t-\mu_2)}{\sigma_2}}}{\sigma_2(1+e^{-\frac{(t-\mu_2)}{\sigma_2}})^2} + \dots + \frac{e^{-\frac{(t-\mu_i)}{\sigma_i}}}{\sigma_i(1+e^{-\frac{(t-\mu_i)}{\sigma_i}})^2} \quad (4)$$

where:

F = flight rate (time⁻¹)

t = time

μ = mean

σ = standard deviation

i = logistic function number

Multi-peak Gaussian probability density function:

$$F = \frac{1}{\sigma\sqrt{2\pi}} e^{-\frac{(t-\mu_1)^2}{2\sigma_1^2}} + \frac{1}{\sigma\sqrt{2\pi}} e^{-\frac{(t-\mu_2)^2}{2\sigma_2^2}} + \dots + \frac{1}{\sigma\sqrt{2\pi}} e^{-\frac{(t-\mu_{i_1})^2}{2\sigma_i^2}} \quad (5)$$

where:

F = flight rate (time⁻¹)

t = time

μ = mean

σ = standard deviation

i = Gaussian function number

Equation 4 and 5 expresses the sum of multiple logistic and Gaussian probability density functions, respectively. The number of functions for each model may be tuned depending on how the system should be described and it corresponds to the number of peaks in the model. The mean of both model functions are used for determining the location

of the peaks and the standard deviation controls the amplitude of each peak. The multiple logistic function model is very useful for analyzing systems that have more than one phase of logistic growth, which is also appropriate to describe the data gathered, rather than a single logistic growth curve (Meyer, 1994). On the other hand, the multiple Gaussian function model or often called as Gaussian Mixture Model (GMM) is one of the best general models notably used for biometric systems, speech recognition, and applications that make use of multiple peak detection (Reynolds, 2015). To generalize both models, the mean observed hourly flight rates of all the experiments were computed. The averaged data were fitted using Equations 4 and 5 and parameters were optimized using the LM method. Model fits comparing the two multi-peak models are shown in Figure 2.

A visual inspection of Figures 2a and 2b shows that the fitted three-peak Gaussian model can better describe the hourly flight rate pattern of the whiteflies compared to the fitted three-peak logistic model. It can also be seen in Figure 2a that the sources of fitting error in using three-peak logistic model is that the troughs at around 10:00 and 15:00 were exaggerated and some under-fitting occurred during the afternoon and evening periods. While on the other hand, the three-peak Gaussian model was able to define the troughs properly and there were less prediction errors on the troughs. Using the two multi-peak fitting methods, the most possible times of day, specifically at around 8:00, 12:00, and 16:00, were predicted and proves that the whiteflies do follow a certain optimal flight schedule. One possible reason for the three-peak activity phenomenon is that the changes in environmental conditions may possibly be highest at the peaks. This is because the change in environmental condition causes the whiteflies to fly and search for a more ideal place to stay (Nava-Camberos et al., 2001). The model can be used as a reference to further understand the flight behavior of the whiteflies. This also proves that the imaging system

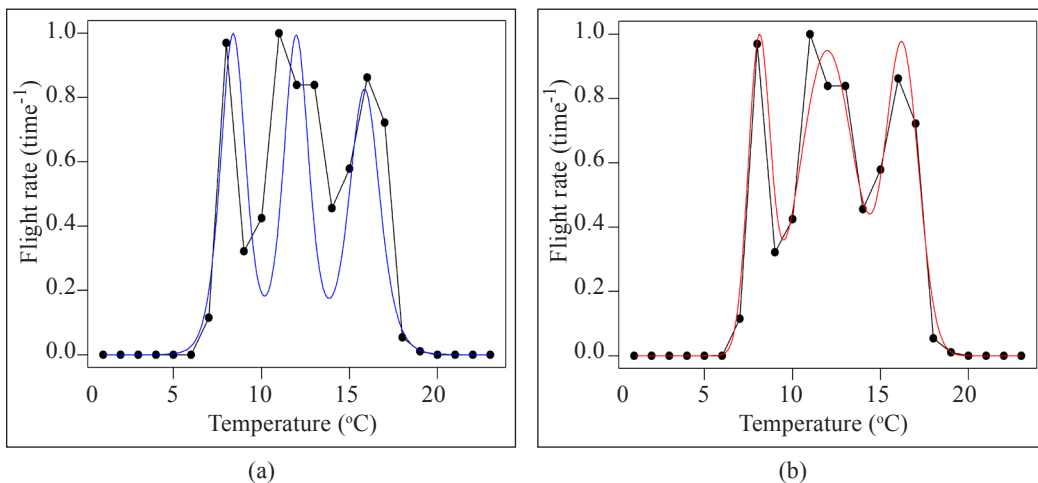


Figure 2. Mean hourly flight rates for all experiments and the corresponding fitted models using (a) summed logistic functions and (b) Gaussian Mixture Model

can be used to discover more about the flight behavior not only of whiteflies, but also of other insects, in a more systematic way. However, it is highly recommended to correlate the flight rate pattern to the environmental conditions to know the exact reasons for the phenomena observed.

Flight Pattern Model Validation

The flight pattern models were validated using similar validation methods to those applied in Table 1. The validation methods were done individually for each model as shown in Table 2.

Table 2 shows that the three-peak Gaussian model has better model predictions compared to the three-peak logistic model based on F-test. The T-test T value results show that the prediction results of the three-peak Gaussian model are more significant. From the statistical tests, high correlation and low prediction errors, it clearly shows that the three-peak Gaussian function model outperformed the three-peak logistic model. The validation results obtained showed that the three-peak probability density function models are proven to be generalized models that can be used for understanding the flight behavior of the whiteflies in relation to the time of day. As future work, multivariate analysis can be done to make the prediction method more holistic by including the effects of the environmental conditions.

Table 2

Evaluation summary of hourly flight rate models using the three-peak logistic function model and the three-peak Gaussian Mixture Model

Parameter	Three-peak logistic	Three-peak Gaussian
F-test F value ($\alpha > 0.05$, $df = 20$)	1.356	1.035
Paired T-test T value ($\alpha > 0.05$, $df = 20$)	0.537	-0.124
Coefficient of determination, r^2	0.719	0.961
Adjusted r^2	0.424	0.919
Theil's U	0.221	0.076
MSEP	0.039	0.006

RESULTS AND DISCUSSION

Model Testing and Application

Using the model in Figure 1, a threshold line can be used as a reference to simply determine the temperature ranges at which there is a high or low probability of whitefly flight. From the raw observations, it can be seen that there were least detections for temperature levels higher than 27°C and below 17°C, as shown in Figure 3.

Figure 3 is based on the total daily whitefly detections per experimental period (every 2 weeks) and the mean temperature on the specified period. The red marked experimental periods indicate that the mean temperature in that period is higher than 27°C. On the other

hand, experiments with mean temperatures of 15°C to 26°C are marked with blue. It can be proven in Figure 3 that the model developed in Figure 1 can be used to determine thresholds in which whitefly flight is low or high at specific mean temperature points. Additionally, it can be seen in Figure 3 that for a 15-day experiment, the increase in whitefly counts are quite constant, depending on the mean temperature in that period. Otherwise, if the mean temperature is inside the optimal flight temperature range, sudden increases in whitefly counts were observed. This shows that temperature changes also have a lot of potential effect on the whitefly flight; however, this effect should be analyzed deeper by developing more models that can describe the effects of temperature change to the whitefly flight, and can be used for future improvement of this work.

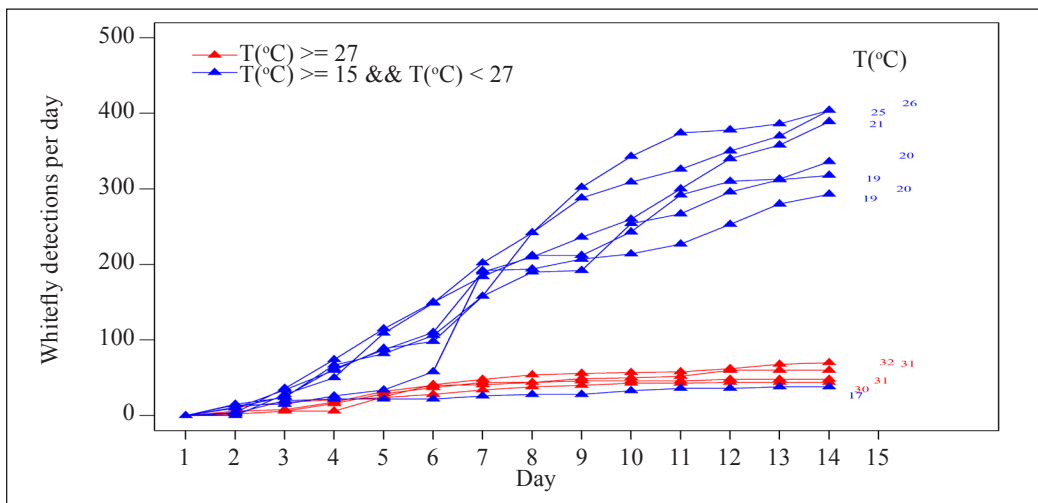


Figure 3. Number of whitefly detections detected per day in each experiment in relation to mean ambient temperature. The mean temperature for each experimental period are shown at the end of each line

CONCLUSION

In this work, different models were developed to further understand the flight behavior of greenhouse whiteflies using information obtained from a wireless image monitoring system. Two models were presented based on: flight rate in relation to temperature and hourly flight rate. The flight rate vs. temperature model was able to describe the phenomenon with an r^2 of 0.976. Using the model, it was found that the optimal flight temperature range for the whiteflies is around 20-26°C. The hourly flight rate model, using a multi-peak Gaussian model, was able to accurately show the possible peak rates for flight of the whiteflies with an r^2 of 0.961. However, it is recommended to include the effects of other environmental parameters, such as light intensity and humidity, to the models to further understand whitefly flight behavior. The models developed herein may be used as references for possible

pesticide application scheduling and environmental control. In conclusion, this work can be used for real-time entomological behavior analysis and integrated insect pest management.

ACKNOWLEDGEMENT

The authors would like to acknowledge the support provided by the staff members of Yu Jia farm in Chiayi County, Taiwan, for providing the experimental site. This work was supported by a grant (Grant No. 106AS-18.2.1-ST-a1) from the Council of Agriculture, Taiwan, ROC.

REFERENCES

- Bonsignore, C. P. (2015). Effect of environmental factors on the flight activity of *Trialeurodes vaporariorum* (Westwood) under greenhouse conditions. *Entomological Science*, 18(2) 207-216.
- Damos, P., & Savopoulou-Soultani, M. (2012). Temperature-driven models for insect development and vital thermal requirements. *Psyche*, 2012, 1-13.
- Haefner, J. W. (2005). *Modeling Biological Systems Principles and Applications (2nd ed.)*. New York, USA: Springer.
- Jha, V. K., Seal, D. R., Schuster, D. J., & Kakkar, G. (2009). Diel flight pattern and periodicity of chilli thrips (Thysanoptera: Thripidae) on selected hosts in South Florida. *Proceedings of the Florida State Horticultural Society* 122, 267-271.
- Lamichhane, J. R., Aubertot, J.-N., Begg, G., Birch, A. N. E., Boonekamp, P., Dachbrodt-Saaydeh, S., Hansen, J. G., Hovmøller, M. S., Jensen, J. E., Jørgensen, L. N., Kiss, J., Kudsk, P., Moonen, A.-C., Rasplus, J.-Y., Sattin, M., Streito, J.-C., & Messéan, A. (2016). Networking of integrated pest management: A powerful approach to address common challenges in agriculture. *Crop Protection* 89, 139-151.
- Liang, X.-H., Lei, Z. R., Wen, J.-Z., & Zhu, M.-L. (2010). The diurnal flight activity and influential factors of *Frankliniella occidentalis* in the greenhouse. *Insect Science*, 17(6), 535-541.
- Meyer, P. (1994). Bi-logistic growth. *Technological Forecasting and Social Change*, 47, 89-102.
- Nava-Camberos, U., Riley, D. G., & Harris, M. K. (2001). Temperature and host plant effects on development, survival, and fecundity of *Bemisia argentifolii* (Homoptera: Aleyrodidae). *Environmental Entomology*, 30(1), 55-63.
- Pinto-Zevallos, D. M., & Vänninen, I. (2013). Yellow sticky traps for decision-making in whitefly management: What has been achieved?. *Crop Protection*, 47, 74-84.
- Potamitis, I., Eliopoulos, P., & Rigakis, I. (2017). Automated remote insect surveillance at a global scale and the internet of things. *Robotics* 6(3), 19.
- Press, W. H., Teukosky, S. A., Vetterling, W. T., & Flannery, B. P. (1992). *Numerical Recipes in C (2nd ed.)*. Cambridge, UK: Cambridge University Press.

- Régnière, J., Powell, J., Bentz, B., & Nealis, V. (2012). Effects of temperature on development, survival and reproduction of insects: Experimental design, data analysis and modeling. *Journal of Insect Physiology* 58(5), 634-647.
- Reynolds, D. (2015). *Gaussian Mixture Models*. In Li S.Z., Jain A.K. (eds) *Encyclopedia of Biometrics*. Bostom, USA: Springer.
- Ribak, G., Dafni, E., & Gerling, D. (2016). Whiteflies stabilize their take-off with closed wings. *Journal of Experimental Biology*, 219(11), 1639-1648.
- Rustia, D. J. A., & Lin, T.T. (2017). An lot-based wireless imaging and sensor node system for remote greenhouse pest monitoring. *Chemical Engineering Transactions* 58, 601-606.
- Rustia, D. J. A., Lin, C. E., Chung, J.-Y., & Lin, T.-T. (2018, May 28-30). A real-time multi-class insect pest identification method using cascaded convolutional neural networks. In *9th International Symposium on Machinery and Mechatronics for Agricultural and Biosystems Engineering (ISMAB)* (p. 67). Jeju, Korea.
- Wang, X., Tao, Y., & Song, X. (2009). Mathematical model for the control of a pest population with impulsive perturbations on diseased pest. *Applied Mathematical Modelling* 33(7), 3099-3106
- Watt, K. E. F. (1961). Mathematical models for use in insect pest control. *Memoirs of the Entomological Society of Canada* 93(S19), 5-62.



Mechanical Properties of Tapioca Starch-Based Film Incorporated With Bulk Chitosan and Chitosan Nanoparticle: A Comparative Study

Ruzana Ahmad Shapi'i¹, Siti Hajar Othman^{1,2*}, Mohd Nazli Naim¹ and Roseliza Kadir Basha¹

¹Department of Process and Food Engineering, Faculty of Engineering, Universiti Putra Malaysia, 43400, UPM Serdang, Selangor, Malaysia

²Materials Processing and Technology Laboratory, Institute of Advanced Technology, Universiti Putra Malaysia, 43400 UPM Serdang, Selangor, Malaysia

ABSTRACT

Tapioca starch-based film exhibits poor mechanical properties, thus limiting the application of the film as food packaging material. The present study aims to improve the mechanical properties of tapioca starch-based film by varying the concentration of glycerol (0, 5, 10, 15, 20, 25% w/w). Then, the starch-based films were incorporated with bulk chitosan (CH) and chitosan nanoparticle (CNP) to produce the starch/CH film and starch/CNP film, respectively. The mechanical properties of all the films which are tensile strength (TS), elongation at break (EAB), and Young's modulus (YM) were characterised using texture analyser. The morphological properties of both CH and CNP were observed under scanning electron microscopy (SEM) and transmission electron microscopy (TEM). The results revealed that 25% w/w of glycerol was sufficient to overcome the brittleness of film and improve the flexibility of the film. The addition of CH and CNP led to the increment in TS and EAB values of the films, thus confirming the role of the reinforcing agent of both CH and CNP in the films. A comparison study between CH and CNP demonstrated that CNP was more effective to improve the mechanical properties of the starch films compared to CH.

Keywords: Bulk chitosan, chitosan nanoparticles, food packaging, glycerol, ionic gelation, mechanical properties, tapioca starch.

ARTICLE INFO

Article history:

Received: 24 October 2018

Accepted: 15 February 2019

Published: 21 June 2019

E-mail addresses:

ruzannashapii91@gmail.com (Ruzana Ahmad Shapi'i)

s.hajar@upm.edu.my (Siti Hajar Othman)

mohdnazli@upm.edu.my (Mohd Nazli Naim)

roseliza@upm.edu.my (Roseliza Kadir Basha)

* Corresponding author

INTRODUCTION

Food packaging plays an important role in food industry to protect food products during processing, storage, and distribution,

thus maintaining the quality of the food products. The majority of food products use plastic as the packaging material due to its lightweight, low cost, convenient, and good barrier properties towards foreign contaminants. However, conventional plastic is usually made from petroleum-based sources which is non-degradable, leading to the dumping of municipal solid waste on the landfill (Othman et al., 2017). Biopolymer materials such as starch, cellulose, chitosan, and fish gelatin exhibit good film-forming properties and are easy to decompose, and thus are promising alternatives to replace conventional plastics (Rhim et al., 2015).

One of the most abundant biopolymers in tropical countries such as Malaysia, Thailand, Indonesia, Brazil, and some regions in Africa is tapioca starch or also known as cassava starch (*Manihot esculenta* Crantz) (Lagos et al., 2015; Versino & García, 2014). Tapioca starch is a promising biopolymer matrix film due to its good film-forming property, availability, and inexpensiveness (Jiménez, Fabra, Talens, & Chiralt, 2012; Kowalczyk et al., 2015). Another advantage of tapioca over other crops is its high tolerance to poor climate conditions, and therefore is a promising supply of starch for production of food packaging materials (Hanif et al., 2016; Piyachomkwan, 2011). In Malaysia, tapioca plant is cultivated for the starch production while other starches such as corn and rice are cultivated as the main food supplies for humans and animals (Hanif et al., 2016).

However, starch-based film usually exhibits poor mechanical properties which limit the application of the produced film for food packaging purposes. It is very important to produce a tough and flexible film so that the film is able to wrap the food properly. Addition of plasticiser such as glycerol, sorbitol, xylitol, and glucose into the biopolymer matrix can enhance the elasticity of the film (Vieira et al., 2011). Among various plasticisers mentioned, glycerol is widely used as a plasticiser in starch-based films due to its stability and compatibility with the structure of starch (Chillo et al., 2008b; Mali et al., 2005). However, high concentration of glycerol in the starch film reduces the strength of the film. This is due to the increase of free volume in starch matrix created by the interruption of glycerol molecules between the starch chain. Thus, it is very important to determine the optimum concentration of glycerol to produce efficient food packaging film.

Nevertheless, starch-based film can be blended with other biopolymers such as chitosan to improve the strength of the film (Chillo et al., 2008a; Shapi'i et al., 2016; Xu et al., 2005). Chitosan ($C_6H_{11}NO_4$) is a linear polysaccharide and the second most abundant polysaccharide found in nature after cellulose (Dutta et al., 2009). Chitosan is derived from chitin which is naturally found in the waste of crustacean shells such as crabs, shrimps, and lobsters (Goy et al., 2009). Chitosan is non-toxic, biodegradable, biofunctional, biocompatible, and exhibit good antimicrobial properties (Byun et al., 2013), and is a promising biopolymer to be incorporated in food packaging material. Several studies have revealed that the addition of chitosan into starch-based film increases the intermolecular

interaction between both biopolymers due to the different ionic charges (Shapi'i & Othman, 2016). The combination of hydrogen bonding and opposite charge attraction between OH^- of starch molecules and NH_3^+ of chitosan provides strong adherence between starch and chitosan molecules, thus ensuring the stability of the two different compounds in the film (Bangyekan et al., 2006).

Advancement of nanotechnology reveals that bulk chitosan (CH) can be synthesised into nanoparticles, also known as chitosan nanoparticles (CNP), in which the size ranges from 1 to 100 nm (Othman, 2014). CNP can be produced via many methods such as ionic gelation (Calvo et al., 1997), reverse emulsion (Brunel et al., 2008), precipitation, and polyelectrolyte complexation (Nishimura et al., 2004). Among those methods, ionic gelation is the most popular method used to produce CNP because the process is relatively simple and non-toxic (Al-Qadi et al., 2012; Rampino et al., 2013). Addition of CNP into the matrix of biopolymer is more effective to improve the properties of the biopolymer compared to CH (Hannon et al., 2015). CNP acts as the reinforcing agent and tends to form good interfacial interaction with the biopolymer matrix, thus improving the structure and mechanical properties of the film compared to CH (Chang et al., 2010a; Hosseini et al., 2015; Moura et al., 2011; Shapi'i et al., 2017).

To the best of our knowledge, only Chang et al. (2010b) had investigated the effect of CNP in starch-based film, particularly potato starch. Moreover, no work has been published on the comparison of mechanical properties of starch/CH film and starch/CNP film. It is also crucial to find the suitable concentration of glycerol for tapioca starch-based film due to the difference in various sources and composition of tapioca starch used in this work compared to other previous works. Therefore, the objective of this study was to find the suitable concentration of glycerol to produce tapioca starch-based film and to compare the mechanical properties (TS, EAB, YM) of starch/CH film and starch/CNP film.

MATERIALS AND METHODS

Materials

Chitosan (low molecular weight) and sodium tripolyphosphate (TPP) were purchased from Sigma-Aldrich, USA. Tapioca starch was obtained from Thye Huat Chan Sdn Bhd (Brand Kapal ABC, Thailand). Acetic acid and glycerol were purchased from R&M Marketing, UK.

Preparation of Starch Film-Forming Solution

An amount of 3 g tapioca starch was dispersed in 100 mL distilled water-glycerol solutions to obtain 3% w/v (weight of starch per volume of distilled water) of starch suspensions. The composition of glycerol added into the starch solution was varied from 0, 5, 10, 15, 20, and 25% w/w (weight of glycerol per weight of starch) as shown in Table 1. Then, the

solution was heated with continuous stirring until it completely gelatinised at 75°C. The starch solution was then subjected to film casting.

Table 1
Formulation of starch-film forming solutions

Film samples	Amount of tapioca starch (g)	Volume of distilled water (mL)	Concentration of glycerol (%)
1	3	100	0
2	3	100	5
3	3	100	10
4	3	100	15
5	3	100	20
6	3	100	25

Preparation of Starch/CH Film

CH solution (15% w/w of solid starch) was prepared by dispersing 0.45 g of chitosan flakes into 50 mL aqueous acetic acid solution (concentration of acetic acid: 1% v/v [volume of acetic acid per volume of distilled water]) for 30 min using a magnetic stirrer (FAVORIT HS0707V2, Indonesia). Then, the pH of the solution was adjusted to 4.6 using NaOH. The CH solution was mixed with gelatinised starch film-forming solution using a magnetic stirrer for 30 min and then subjected to film casting.

Preparation of Starch/CNP Film

The parameters to synthesise CNP were fixed based on the optimum parameters that produced the most stable and smallest size of CNP (3–12 nm) as reported by Gokce et al. (2014)) with some modifications. First, CH solution (15% w/w of solid starch) was prepared by dispersing 0.45 g chitosan flakes into 50 mL aqueous acetic acid solution (1% v/v) for 30 min using a magnetic stirrer. Then, the pH of the solution was adjusted to 4.6 using NaOH. TPP solution was prepared according to the ratio of chitosan to TPP (5:1) by dissolving 0.09 g of TPP powder in 50 mL distilled water.

CNP was spontaneously obtained upon the addition of 50 mL of TPP solution drop by drop to the 50 mL CH solution under vigorous magnetic stirring at room temperature (25°C) for 30 min. Then, an ultrasonic probe (QSonica Q500, USA) was used to disperse the CNP in the suspension for 15 min with a sequence of 1 min sonication and 10 s rest at an amplitude of 50%. The beaker containing CNP was placed in an ice bath during ultrasonication to ensure that the temperature of CNP suspension was in the favourable range (30 to 35°C). The starch/CNP film solution was prepared by mixing 100 mL CNP suspension with 100 mL gelatinised starch film-forming solution and stirred for 30 min using the magnetic stirrer.

Film Casting

An amount of 50 mL of the solution was poured into an acrylic petri dish (diameter: 14 cm) and left in an air-conditioned room (20°C) for 48 h on a flat table. Then, the petri dish containing starch/CNP film was dried at 40°C for 5 h in a ventilated oven to constant weight. A neat starch film without the addition of CNP was also prepared as control. After drying, the film was peeled off from the petri dish and conditioned in a desiccator containing saturated magnesium nitrate solution (R&M Marketing, UK) with a relative humidity of 51% and temperature of 30°C (Xu et al., 2005).

Mechanical Properties

Tensile strength, elongation at break, and Young's modulus were determined using a texture analyser (TA.XT2 Stable Micro Systems, UK) according to ASTM D882-09. Film strips (100 × 15 × 0.06 mm) were cut from each preconditioned sample and placed between the grips. Initial grip separation and test speed were set at 60 mm and 0.5 mm·s⁻¹, respectively. Force and distance were recorded during extension of the strips to break. TS, EAB, and YM were calculated according to Equations 1, 2, and 3, respectively. A minimum of five replications for each test sample were run.

TS was calculated according to the following equation:

$$TS = F/A \quad (1)$$

here F is the maximum force and A is the cross-sectional area of the film.

EAB was calculated according to the following equation:

$$EAB = \frac{l_f - l_o}{l_o} \times 100 \quad (2)$$

where l_f is the final length at specimen break and l_o is the initial length of the film.

YM was calculated according to the following equation:

$$YM = \frac{\text{Stress}}{\text{strain}} \quad (3)$$

Morphological Properties

Morphological properties of the CH and CNP were observed under SEM (LEO 1455 VP) and TEM (FE-TEM HF-3300). A drop of CH solution was deposited and left to dry on a specimen holder, and examined using SEM. For TEM analysis sample preparation, CNP was dispersed in deionised water using an ultrasonic bath for 10 min. The CNP solution was then dropped on a formvar grid and allowed to dry before being examined using the TEM.

RESULTS AND DISCUSSION

Effect of Glycerol Concentration on the Mechanical Properties of the Starch Film

The results for mechanical properties were obtained only for 10% to 25% w/w of glycerol. Mechanical properties of films containing 0% and 5% w/w of glycerol could not be measured because the films were very brittle, difficult to peel off from the petri dish, and easily broken into pieces as can be seen in Figure 1.



Figure 1. Neat tapioca starch film without the addition of glycerol

Figure 2(a) shows the effect of glycerol concentration (10% to 25% w/w) on the TS of the starch films. Increase in glycerol concentration from 10% to 25% has reduced the TS of the starch films from 7.12 to 1.12 MPa ($p < 0.05$). This finding is consistent with the study reported by Souza et al. (2012). The authors investigated the effect of glycerol concentration on tapioca starch film containing sucrose and inverted sugar. They revealed that the TS values of the films were around 6.06 to 2.72 MPa when glycerol concentrations were varied from 0% to 15% w/w. The trend of this finding is also consistent to the study done by Tang et al. (2008), who reported that addition of 20% w/w of glycerol into corn starch/montmorillonite films reduced the TS of the film from 20 to 6 MPa. This was due to the interruption of glycerol molecules that caused an increase of empty spaces within the starch matrix (Souza et al., 2012). Formation of empty spaces in the starch matrix reduced the intermolecular attraction force in amylose and amylopectin, thus producing starch films that were less dense and less compact. When the film was less dense and compact, it was easy to deform when stress was applied which was indicated by the low TS of the starch films.

Figure 2(b) shows the effect of glycerol concentration on the EAB of the starch films. The addition of glycerol into starch film improved the EAB of the films. The EAB increased from 1.89% to 67% with the increase in glycerol concentration from 10% to 25% w/w, respectively, which was a 34-fold improvement. This finding revealed that the EAB of the starch films was highly dependent on the concentration of glycerol ($p < 0.05$). The result is similar to the work done by Alves et al. (2007), where they found that an increment in the concentration of glycerol from 20% to 45% w/w increased the EAB of tapioca starch films enriched with different amylose contents from 5.2% to 153.2%. In comparison, the trend of TS values (Figure 2(a)) was reciprocal to the trend of EAB values (Figure 2(b)). As the concentration of glycerol increased, the EAB increased but the TS decreased. This finding is consistent with the work reported by Tang et al. (2008), who studied the effect of glycerol concentration on the mechanical properties of corn starch film incorporated

with MMT. They found that an increment in glycerol concentration up to 20% w/w led to the increase in EAB but reduced the TS. The increase in the EAB of starch films when the glycerol concentration was increased was due to the formation of free volume created by glycerol molecules that interrupted the starch chain. The presence of empty spaces in the starch matrix facilitated the movement of starch chain when external stress was applied, thus improving the EAB of the films (Lim & Hoag, 2013). This phenomenon contributed to the increase in elasticity but reduced the strength of the film.

Figure 2(c) shows the effect of glycerol concentration on the YM of the starch films. It can be seen that the addition of glycerol into the starch film reduced the YM of the film. These findings revealed that the addition of glycerol reduced the rigidity of starch films, thus increasing the elasticity of the film. Starch films containing 10% w/w of glycerol exhibited the highest YM which was 378.09 MPa, followed by starch films containing 15% w/w of glycerol which was 178.87 MPa. Further increase in the concentration of glycerol to 25% w/w resulted in further reduction of YM to 5.96 MPa (62-fold reduction compared to 10% glycerol), which indicated that the film was flexible and less stiff. Suzana Mali et

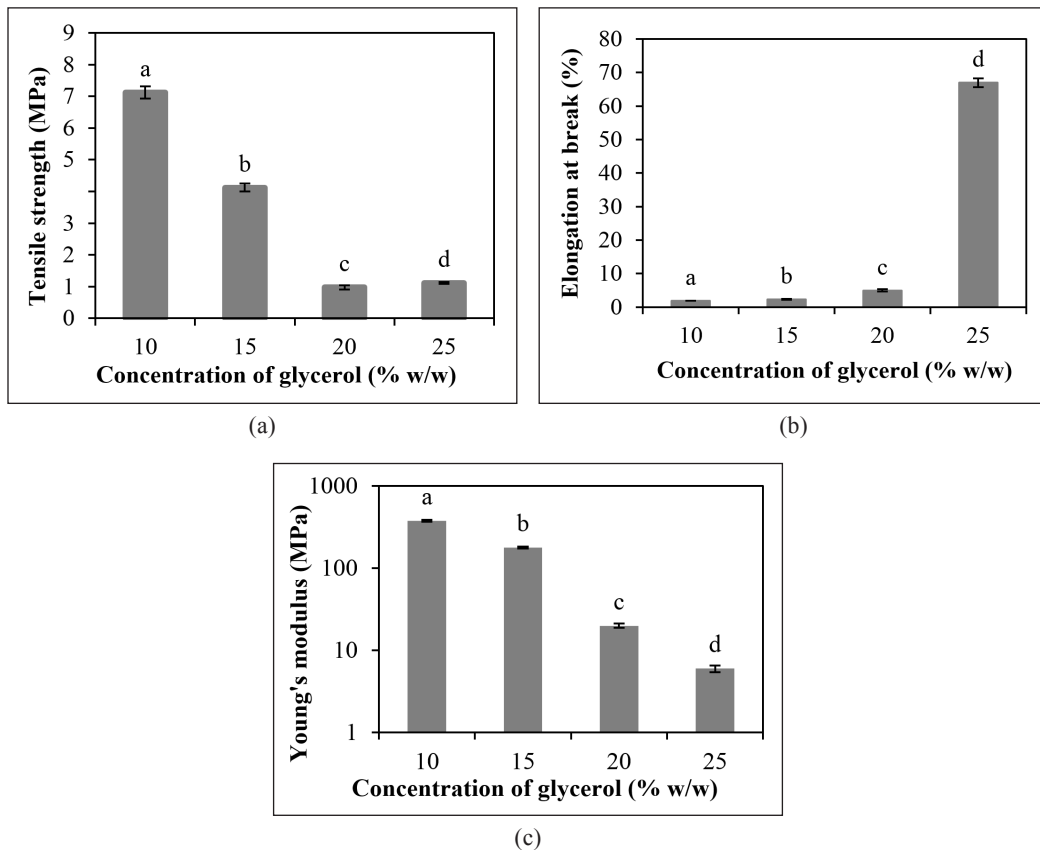


Figure 2. Effect of glycerol concentration on mechanical properties of tapioca starch film: (a) TS, (b) EAB, (c) YM

al. (2006) also reported that tapioca starch film containing 40% w/w glycerol exhibited a low YM of 9 MPa. They explained that addition of glycerol increased the hydrophilic behaviour of starch films, thus increasing the tendency of films to hold water molecules from the surrounding. As the moisture content of starch films increased, the structure of the film became less stiff, compact, and rigid, thus increasing the flexibility of the films.

It was found that 25% w/w glycerol was sufficient to be used for producing starch film. The EAB of starch films produced using 25% w/w glycerol was 67%, which was comparable with the EAB of commercial LDPE film (69%) (Cirillo et al., 2015). Although further increment of glycerol concentration could further increase the EAB of the films, the TS of starch film is expected to further decrease with further increase in glycerol concentration. Starch films containing 25% w/w glycerol exhibited low TS which was not comparable with the TS of commercial LDPE film (16 MPa) (Cirillo et al., 2015). Too high concentration of glycerol in the starch films weakened the attraction forces in the starch chains and created a higher number of glycerol–glycerol bonds than glycerol–starch bonds (Müller, Yamashita, & Laurindo, 2008). Formation of the glycerol–glycerol bonds in starch matrix led to the phase separation of glycerol zones and starch–glycerol zones, thus producing non-homogenous film which was sticky, soggy, and wrinkly (Kim et al., 2015). Therefore, CNP was utilised as the reinforcing agent to further improve the mechanical properties of the starch films.

Effect of CH and CNP on the Mechanical Properties of Starch Film

Previous studies have proven the ability of CH to improve the properties of starch films, especially mechanical properties (Chillo et al., 2008b; Shapi'i & Othman, 2016; Xu et al., 2005). However, there is a study done to compare the mechanical properties of films incorporated with CH and CNP. A comparison study between CH and CNP is very important to find out the efficiency of CNP in improving the properties of films compared to CH. To the best of our knowledge, only one study has been done to compare the effect of CH and CNP on tara gum (TG) films in terms of thermomechanical, physicochemical, morphological, and barrier properties (Antoniou et al., 2015). Therefore, a comparative study was done to determine the efficiency of CNP as a filler compared to CH. The concentrations of both CH and CNP in starch films were fixed to 15% w/w. All the films produced in this part of work were added with 25% w/w of glycerol. Table 2 shows the mechanical properties of neat starch films with the addition of CH and CNP.

From Table 2, neat starch film exhibited poor mechanical properties where the values of TS, EAB, and YM were 1.12 MPa, 67%, and 5.96 MPa, respectively. The addition of CH and CNP into neat starch films increased the TS and EAB of the films, thus confirming the potential of chitosan to improve the mechanical properties of the neat starch film. This result is consistent with the studies by Shapi'i and Othman, (2016), and Xu et al., (2005),

Table 2
Comparison of CH and CNP as filler

Film	TS (MPa)	EAB (%)	YM (MPa)
Neat starch	1.12 ± 0.03 ^a	67.00 ± 1.32 ^a	5.96 ± 0.58 ^c
Starch/CH	3.16 ± 0.07 ^b	76.90 ± 1.23 ^b	4.43 ± 0.16 ^a
Starch/CNP	4.95 ± 0.01 ^c	90.77 ± 1.40 ^c	5.70 ± 0.15 ^b

The data are reported as mean ± SD with n=3 and p<0.05

who reported that incorporation of suitable amount of chitosan into tapioca starch films improved the mechanical properties of the films.

From Table 2, the starch/CNP film exhibited higher improvement of TS (4-fold increment) compared to starch/CH film (2.9-fold increment), where the TS of both films were 4.95 and 3.16 MPa, respectively. The EAB of starch/CNP film (1.36-fold increment) also exhibited a slightly higher improvement than the EAB of starch/CH film (1.15-fold increment), where the EAB of both films were 90.77% and 76.90%, respectively. Addition of both CNP and CH into starch films slightly reduced the YM of the film where the decrement were 0.04-fold and 0.26-fold, respectively. These findings revealed that CNP was more efficient to increase the strength, elasticity, and flexibility of the film compared to CH. The difference in the performance of CH and CNP to improve the mechanical properties of starch films was due to the difference in the morphological properties of CH and CNP. Figure 3 shows the morphology of CH and CNP viewed under SEM and TEM, respectively. As shown in Figure 3(a), CH is in a continuous phase and not in a regular shape compared to CNP. From Figure 3(b), CNP has a regular spherical shape and is tiny in size due to the crosslinking of chitosan and TPP during ionic gelation process.

Different morphological properties of both CH and CNP resulted in the difference in matrix–filler interaction mechanism between chitosan and starch. In order to produce

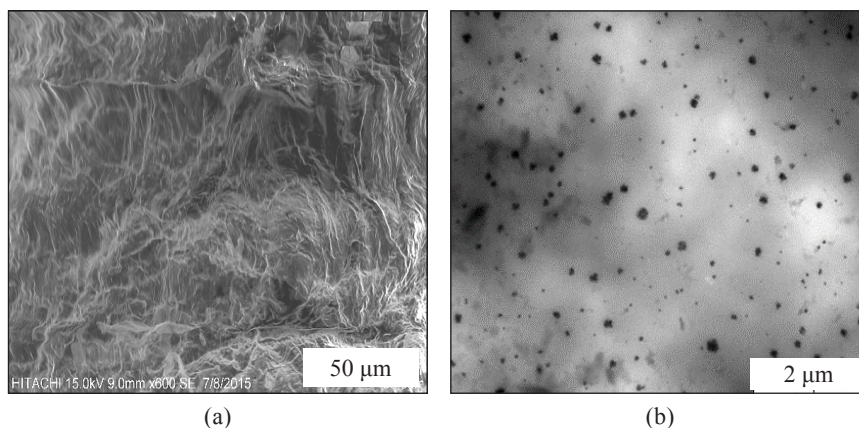


Figure 3. Morphology of (a) bulk chitosan and (b) chitosan nanoparticle

starch/CH film, starch and CH were blended together immediately when CH was added into the starch solution due to the similar continuous phases (Silva-Weiss et al., 2013). The blending of starch and CH changed the physical and rheological properties of the film-forming solution. This was different when CNP was incorporated into the starch matrix as a filler where CNP did not change the physical and rheological properties of the film-forming solution. The tiny size and regular shape of CNP facilitated the CNP to fill in the empty spaces between the matrix of the starch film (Lorevice et al., 2015).

Furthermore, the tiny size of CNP provided a large surface area of CNP to be exposed to the starch, thus increasing the intermolecular interaction between the starch and CNP. Good molecular interaction that occurred between CNP and starch chain increased the intermolecular attraction forces which brought the distances of adjacent starch chain closer (Ma et al., 2009). This phenomenon increased the density of the starch film to become more compact, strong, and higher resistant towards physical stress. Meanwhile, improvement of film elasticity was also attributed to the good intermolecular interaction between both CH and CNP to the starch matrix (Ghani et al., 2016). Good interaction between starch and chitosan led to the strong intermolecular forces that were able to resist the applied tensile stress. When the intermolecular forces in the starch/CNP films were sufficient to resist the applied forces, the films were difficult to deform and break and thus increased the film elasticity and flexibility.

CONCLUSION

The optimum concentration of glycerol in the starch film was successfully determined, where 25% w/w glycerol was sufficient to overcome the brittle property of tapioca starch films. Incorporation of CH and CNP into the starch films improved the mechanical properties of the films, where the TS and EAB of the films increased significantly, thus proving the role of both CH and CNP as reinforcing agents in the films. The comparison study of CH and CNP revealed that CNP was more effective to improve the mechanical properties of starch film compared to CH due to the stronger intermolecular interaction between CNP and starch compared to CH and starch. This finding indicates that it is worth to explore the potential of CNP as a filler in the biopolymer materials to improve the properties of the material. Other properties of the starch/CH film and the starch/CNP film such as thermal, water vapor permeability, and oxygen permeability properties should be characterised to better understand the application of the film.

ACKNOWLEDGEMENT

The authors would like to acknowledge the financial support provided by Fundamental Research Grant Scheme (Vote number: 5524980) of the Ministry of Higher Education, Malaysia.

REFERENCES

- Al-Qadi, S., Grenha, A., Carrion-Recio, D., Seijo, B., & Remunan-Lopez, C. (2012). Microencapsulated chitosan nanoparticles for pulmonary protein delivery: in vivo evaluation of insulin-loaded formulations. *Journal of Controlled Release*, *157*(3), 383–390.
- Alves, V. D., Mali, S., Beleia, A., & Grossmann, M. V. E. (2007). Effect of glycerol and amylose enrichment on cassava starch film properties. *Journal of Food Engineering*, *78*(3), 941–946.
- Antoniou, J., Liu, F., Majeed, H., & Zhong, F. (2015). Characterization of tara gum edible films incorporated with bulk chitosan and chitosan nanoparticles: A comparative study. *Food Hydrocolloids*, *44*, 309–319.
- Bangyekan, C., Aht-Ong, D., & Srikulkit, K. (2006). Preparation and properties evaluation of chitosan-coated cassava starch films. *Carbohydrate Polymers*, *63*(1), 61–71.
- Brunel, F., Veron, L., David, L., Domard, A., & Delair, T. (2008). A novel synthesis of chitosan nanoparticles in reverse emulsion. *Langmuir: The ACS Journal of Surfaces and Colloids*, *24*(20), 11370–7.
- Byun, S. M., No, H. K., Hong, J. H., Lee, S. Il, & Prinyawiwatkul, W. (2013). Comparison of physicochemical, binding, antioxidant and antibacterial properties of chitosans prepared from ground and entire crab leg shells. *International Journal of Food Science and Technology*, *48*(1), 136–142.
- Calvo, P., Remunan-Lopez, C., Vila-Jato, J. L., & Alonso, M. J. (1997). Novel Hydrophilic Chitosan – Polyethylene Oxide Nanoparticles as Protein Carriers. *Journal of Applied Polymer Science*, *63*(1), 125–132.
- Chang, P. R., Jian, R., Yu, J., & Ma, X. (2010). Fabrication and characterisation of chitosan nanoparticles/plasticised-starch composites. *Food Chemistry*, *120*(3), 736–740.
- Chillo, S., Flores, S., Mastromatteo, M., Conte, A., Gerschenson, L., & Del Nobile, M. A. (2008). Influence of glycerol and chitosan on tapioca starch-based edible film properties. *Journal of Food Engineering*, *88*(2), 159–168.
- Cirillo, G., Spizzirri, U. G., & Iemma, F. (2015). *Functional Polymers in Food Science: From Technology to Biology*. Beverly, MA: Scrivener Publishing.
- Dutta, P. K., Tripathi, S., Mehrotra, G. K., & Dutta, J. (2009). Perspectives for chitosan based antimicrobial films in food applications. *Food Chemistry*, *114*(4), 1173–1182.
- Ghani, S. W. A., & Bakar, A. A., Samsudin, S. A. (2016). Mechanical and physical properties of tapioca starch nanocomposite films. *Journal of Plastic Film and Sheeting*, *32*(2), 1–23.
- Gokce, Y., Cengiz, B., Yildiz, N., Calimli, A., & Aktas, Z. (2014). Ultrasonication of chitosan nanoparticle suspension: Influence on particle size. *Colloids and Surfaces A: Physicochemical and Engineering Aspects*, *462*, 75–81.
- Goy, R. C., Britto, D. de, & Assis, O. B. G. (2009). A review of the antimicrobial activity of chitosan. *Polimeros*, *19*(3), 241–247.
- Hanif, M., Mahlia, T. M. I., Aditiya, H. B., & Chong, W. T. (2016). Techno-economic and environmental assessment of bioethanol production from high starch and root yield Sri Kanji 1 cassava in Malaysia. *Energy Reports*, *2*, 246–253.

- Hannon, J. C., Cummins, E., Kerry, J., Cruz-Romero, M., & Morris, M. (2015). Advances and challenges for the use of engineered nanoparticles in food contact materials. *Trends in Food Science and Technology*, 43(1), 43–62.
- Hosseini, S. F., Rezaei, M., Zandi, M., & Farahmandghavi, F. (2015). Fabrication of bio-nanocomposite films based on fish gelatin reinforced with chitosan nanoparticles. *Food Hydrocolloids*, 44, 172–182.
- Kim, S. R. B., Choi, Y. G., Kim, J. Y., & Lim, S. T. (2015). Improvement of water solubility and humidity stability of tapioca starch film by incorporating various gums. *LWT - Food Science and Technology*, 64(1), 475–482.
- Kowalczyk, D., Kordowska-Wiater, M., Nowak, J., & Baraniak, B. (2015). Characterization of films based on chitosan lactate and its blends with oxidized starch and gelatin. *International Journal of Biological Macromolecules*, 77, 350–9.
- Lagos, J. B., Vicentini, N. M., Santos, R. M. C. Dos, Bittante, A. M. Q. B., & Sobral, P. J. A. (2015). Mechanical properties of cassava starch films as affected by different plasticizers and different relative humidity conditions Jeannine. *International Journal of Food Studies*, 4(1), 116–125.
- Lim, H., & Hoag, S. W. (2013). Plasticizer effects on physical-mechanical properties of solvent cast Soluplus® films. *AAPS PharmSciTech*, 14(3), 903–910.
- Lorevice, M. V., Otoni, C. G., Moura, M. R. de, & Mattoso, L. H. C. (2015). Chitosan nanoparticles on the improvement of thermal, barrier, and mechanical properties of high- and low-methyl pectin films. *Food Hydrocolloids*, 52, 732–740.
- Ma, X., Chang, P. R., Yang, J., & Yu, J. (2009). Preparation and properties of glycerol plasticized-pea starch/zinc oxide-starch bionanocomposites. *Carbohydrate Polymers*, 75(3), 472–478.
- Mali, S., Grossmann, M. V. E., Garcia, M. A., Martino, M. N., & Zaritzky, N. E. (2006). Effects of controlled storage on thermal, mechanical and barrier properties of plasticized films from different starch sources. *Journal of Food Engineering*, 75(4), 453–460.
- Mali, S., Sakanaka, L. S., Yamashita, F., & Grossmann, M. V. E. (2005). Water sorption and mechanical properties of cassava starch films and their relation to plasticizing effect. *Carbohydrate Polymers*, 60(3), 283–289.
- Moura, M. R., Lorevice, M. V., Mattoso, L. H. C., & Zucolotto, V. (2011). Highly Stable, Edible Cellulose Films Incorporating Chitosan Nanoparticles. *Journal of Food Science*, 76(2), 25–29.
- Nishimura, K., Nishimura, S. I., Seo, H., Nishi, N., Tokura, S., & Azuma, I. (2004). Macrophage activation with multi-porous beads prepared from partially deacetylated chitin. *Journal of Biomedical Materials Research*, 20(9), 1359–72.
- Othman, S. H. (2014). Bio-nanocomposite Materials for Food Packaging Applications: Types of Biopolymer and Nano-sized Filler. *Agriculture and Agricultural Science Procedia*, 2, 296–303.
- Othman, S. H., Hassan, N., Talib, R. A., Kadir Basha, R., & Risyon, N. P. (2017). Mechanical and thermal properties of PLA/halloysite bio-nanocomposite films: Effect of halloysite nanoclay concentration and addition of glycerol. *Journal of Polymer Engineering*, 37(4), 381–389.

- Piyachomkwan, K. (2011). Cassava Bioethanol Production. In *South-South Technology Transfer: Ethanol Production from Cassava*. Bangkok, Thailand. Retrieved October 1, 2018 from <https://www.nstda.or.th>.
- Rampino, A., Borgogna, M., Blasi, P., Bellich, B., & Cesàro, A. (2013). Chitosan nanoparticles: Preparation, size evolution and stability. *International Journal of Pharmaceutics*, 455(1-2), 219–228.
- Rhim, J. W. & Ng, P. K. W. W. (2007). Natural biopolymer-based nanocomposite films for packaging applications. *Critical Reviews in Food Science and Nutrition*, 47(4), 411–33.
- Shapi'i, R. A. & Othman, S. H. (2015). Edible Nanofiller for Development of Edible Bio- Nanocomposite Film: A Review. *Journal of Polymer Science and Technology*, 1(1), 37–45.
- Shapi'i, R. A. & Othman, S. H. (2016). Effect of concentration of chitosan on the mechanical, morphological and optical properties of tapioca starch film. *International Food Research Journal*, 23, 187–193.
- Shapi'i, R. A., Othman, S. H., Nazli Naim, M., & Kadir Basha, R. (2017). Effect of ball milling and ultrasonication time on particle size of chitosan for potential nanofiller in food packaging film. *Acta Horticulturae*, 1152, 125–130.
- Silva-Weiss, A., Bifani, V., Ihl, M., Sobral, P. J. A., & Gomez-Guillen, M. C. (2013). Structural properties of films and rheology of film-forming solutions based on chitosan and chitosan-starch blend enriched with murta leaf extract. *Food Hydrocolloids*, 31(2), 458–466.
- Souza, A. C., Benze, R., Ferrao, E. S., Ditchfield, C., Coelho, A. C. V., & Tadini, C. C. (2012). Cassava starch biodegradable films: Influence of glycerol and clay nanoparticles content on tensile and barrier properties and glass transition temperature. *LWT - Food Science and Technology*, 46(1), 110–117.
- Tang, X., Alavi, S., & Herald, T. J. (2008). Effects of plasticizers on the structure and properties of starch-clay nanocomposite films. *Carbohydrate Polymers*, 74(3), 552–558.
- Versino, F. & García, M. A. (2014). Cassava (*Manihot esculenta*) starch films reinforced with natural fibrous filler. *Industrial Crops and Products*, 58, 305–314.
- Vieira, M. G. A., Da Silva, M. A., Dos Santos, L. O., & Beppu, M. M. (2011). Natural-based plasticizers and biopolymer films: A review. *European Polymer Journal*, 47(3), 254–263.
- Xu, Y. X. X., Kim, K. M. M., Hanna, M. A., & Nag, D. (2005). Chitosan–starch composite film: preparation and characterization. *Industrial Crops and Products*, 21(2), 185–192.



Optimization of Hydrothermal Conditioning Conditions for *Pennisetum purpureum x Pennisetum americanum* (Napier PakChong1 grass) to Produce the Press Fluid for Biogas Production

Pitchaya Suaisom^{1,3}, Patiroop Pholchan^{1*}, Hasfalina Che Man² and Pruk Aggarangsi³

¹Department of Environmental Engineering, Faculty of Engineering, Chiang Mai University, Suthep road, Chiang Mai, 50200, Thailand.

²Department of Biological and Agricultural Engineering, Faculty of Engineering, University Putra Malaysia, 43400, UPM Serdang, Selangor, Malaysia.

³Energy Research and Development Institute-Nakornping, Chiang Mai University, Chiang Mai, 50200, Thailand.

ABSTRACT

This study focused on the optimization of hydrothermal conditioning conditions for Napier PakChong1 grass to produce press fluid for biogas production. The integrated generation of solid fuel and biogas from biomass (IFBB) process was adopted to separate press fluid from the biomass. Napier PakChong1 grass was hydrothermally pretreated and then mechanically pressed. The press fluid was used for biochemical methane potential (BMP) test while the press cake could be utilized as the solid fuel. The full factorial design of experiment with center points and the Central Composite Design (CCD) were developed to obtain the best possible combination of harvesting time, grass to water ratio, temperature and soaking time for the maximum organic substance (as COD) in press fluid. It was found that the obtained model could satisfactorily predict the mass of COD in press fluid used as the model response. The optimum hydrothermal conditioning conditions were as follows; harvesting time 75 d, ratio of grass to water of 1:6 (by weight), ambient temperature (about 25°C) of the water and the soaking time of 355 min. The mass of COD obtained

ARTICLE INFO

Article history:

Received: 24 October 2018

Accepted: 15 February 2019

Published: 21 June 2019

E-mail addresses:

monphitchaya@gmail.com (Pitchaya Suaisom)

patirop@eng.cmu.ac.th (Patiroop Pholchan)

hasfalina@upm.edu.my (Hasfalina Che Man)

kunpruk@gmail.com (Pruk Aggarangsi)

* Corresponding author

in these conditions was 226.42 g equating to 71.5% of the value predicted by the model (316.68 g). The microbial kinetic coefficients and biogas yield potential of press fluid at these optimum conditions were properly fitted with the modified Gompertz equation (adjusted $R_2 = 0.995$). The methane yield potential (P), the maximum methane production rate (R_m) and lag phase time (λ) were 412.18 mlCH₄/gVS_{added}, 51.47 mlCH₄/gVS_{added}/d and 4.36 days, respectively.

Keywords: BMP, Grass liquor, hydrothermal conditioning, modified gompertz equation, *pennisetum purpureum* x *pennisetum americanum* (napier PakChong1 grass).

INTRODUCTION

Energy consumption in Thailand has been increased continuously since the year 2011 due to the expansion of domestic demands. Thailand's Alternative Energy Development Plan: AEDP 2015 has been launched with the target of using renewable and alternative energy to replace up to 30 percent of final energy consumption (in form of electricity, heat and bio-fuel) by 2036. This plan partly focuses on the utilization of energy crop, in which 680 MW of electricity is expected to be produced from biogas production using energy crop as the raw material (Energy Policy and Planning Office, 2017). Grass is one of the most important energy crops for Thailand because it is a perennial plant and can grow in every region of the country. Compared to other grass species, Napier PakChong1 grass has a higher production yield (up to 75 ton/ha-yr and carbohydrate content 36-38% as dry basis (Negawo et al., 2017; Rengsirikul et al., 2013). These characteristics make Napier PakChong1 grass to be suitable as a feedstock for biogas production and combustion. However, as grasses are lignocellulosic biomass, they are rather recalcitrant to anaerobic fermentation (Bruni et al., 2010). Low methane yields at long retention time have been observed from anaerobic biodegradation of grasses (Richter et al., 2011; Richter et al., 2009). In addition, long term of mono-digestion of grass may result in the decrease of biogas production due to the effect of trace element deficiency (Thamsiriroj et al., 2012). Moreover, system failure due to the floating of grasses could cause the blockage in the gas pipe (Thamsiriroj & Murphy, 2010). Most of biogas plants using grasses as the feedstock in Germany are co-digestion of grass silage with manure to stabilize the process and maintain biogas production. As the source for renewable energy production, grass can also be used as a substrate for combustion. However, there are many problems due to its high element concentrations which would cause ash slagging (K, Mg), corrosion (Cl, S) and emissions (Cl, S, N) (Jenkins et al., 1998; Obernberger et al., 2006).

The better method of utilizing Napier PakChong1 grass could be the integrated generation of solid fuel and biogas from biomass (IFBB) (Wachendorf et al., 2009),

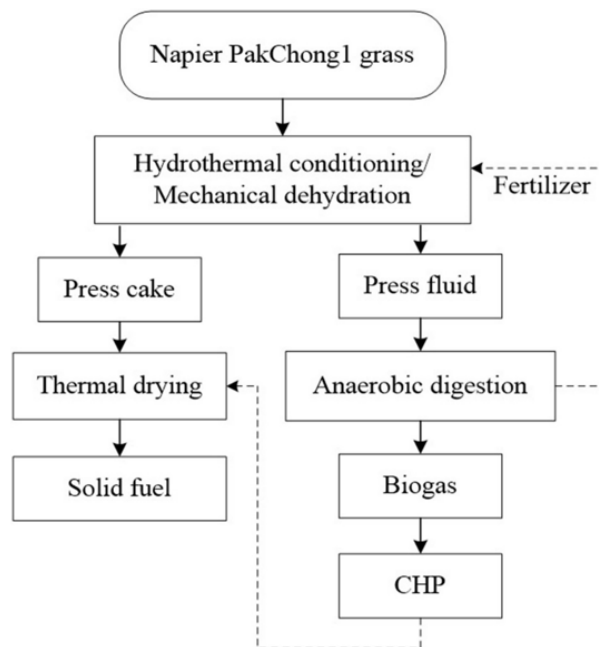


Figure 1. Process diagram of the IFBB (Wachendorf et al., 2008)

which has been developed for increasing efficiency of conversion and methane production yield. In IFBB method, grass is separated into two parts, i.e. press fluid and press cake (Figure 1). Hydrothermal conditioning, which is the process of grass soaking and heated under continuous stirring for cell wall maceration, and mechanical dehydration process are done in order to transfer the elements and organic compounds into the press fluid for efficient anaerobic digestion. Several works have been conducted using this hydrothermal conditioning and mechanical dehydration process with semi-natural grassland (Wachendorf et al., 2009); green cut material from landscape (Hensgen et al., 2011) and sward maturity (Richter et al., 2011). The process was reported to be able to efficiently transfer minerals and organic compounds required for biogas production to the press fluid. The press fluid of semi-natural grassland was found to contain high crude protein and had the methane yield (397-426 NL/kgVS after 13 day) two times higher than the whole crop grassland silage (218 NL/kgVS after 27 day) (Richter et al., 2009). Similarly, Reulein et al. (2007) observed the high value of methane yields 500 LCH₄/kgVS from the press fluids of whole crop silages of maize and wheat. The press cake obtained after the mechanical dehydration process was a high solid fibrous fraction (cellulose, hemicellulose and lignin). This solid is a high quality fuel as it contains low element concentrations, e.g. potassium, magnesium and chloride (Bühle et al., 2012) which would produce less amounts of air pollution after combustion.

Efficiency of the dehydration process of a biomass depends on several factors, e.g. solid: liquid ratio, temperature, incubation time, mechanical pressing, detergent and harvesting time (Jia et al., 2013; King et al., 2012; Kuila et al., 2011; Wachendorf et al., 2009). This study aimed to utilise Napier PakChong1 grass to produce renewable energies using IFBB process. Therefore, the objective of this work was to (1) optimize the hydrothermal conditioning, i.e. harvesting time (day), ratio of solid to water (by weight), soaking time (min) and temperature (°C) and (2) determine the methane yield of the obtained press fluid.

MATERIALS AND METHODS

Napier PakChong1 grass

Napier Pak Chong1 grass was collected from Chiang Mai Fresh Milk farm, Lamphun, Thailand. After harvested and delivered to the laboratory, the grass was chopped by a hammer mill to the average size of 2 cm. Grass sample were stored at 4°C before each use.

Optimization of Hydrothermal Conditioning Conditions for Napier PakChong1 Grass

The 2-level full factorial design of experiment with center points and the Central Composite Design (CCD) were employed to obtain the optimum Napier PakChong1 grass pressing condition. For the full factorial experiments, the chopped Napier PakChong1 grass samples (harvesting time 30 and 60 d) were hydrothermally conditioned by mixing with water (solid: water = 1:3 and 1:5 by weight) at different temperatures (37 and 80°C) and different soaking times (10 and 240 minutes). Then the conditioned Napier PakChong1 samples were gravitationally separated from water. Subsequent mechanical dehydration of the Napier PakChong1 samples were conducted using screw press. Axial points used in the CCD for constructing the response surface to estimate the coefficients of quadratic terms are as follows; harvesting time (15 and 75 d), ratio of grass to water (1:2 and 1:6 by weight), soaking time (0 and 355 minutes) and soaking temperature (15.5 and 90°C). All experiments were developed and the results were analyzed using MINITAB version 16. Organic substance in form of mass of total COD (COD_t) was used as the response for optimization as it was the most pertinent parameter relating to biogas production potential. Mass of COD_t was calculated from the sum of mass of COD_t in press fluid and in drained water generated after the hydrothermal process.

Biochemical Methane Potential (BMP) Test

The press fluid obtained from the optimum condition for pressing conditioning was investigated for biogas production potential using the BMP test. The BMP test was conducted according to the German Standard Procedure VDI 4630 (Ingenieure, 2006) using

Table 1

Medium solution

Chemical	Concentration	Unit
KH_2PO_4	0.27	g/L
$\text{Na}_2\text{HPO}_4 \cdot 12\text{H}_2\text{O}$	1.12	g/L
NH_4Cl	0.53	g/L
$\text{CaCl}_2 \cdot 2\text{H}_2\text{O}$	0.075	g/L
$\text{MgCl}_2 \cdot 6\text{H}_2\text{O}$	0.10	g/L
$\text{FeCl}_2 \cdot 4\text{H}_2\text{O}$	0.02	g/L
$\text{Na}_2\text{S} \cdot 9\text{H}_2\text{O}$	0.10	g/L
$\text{MnCl}_2 \cdot 4\text{H}_2\text{O}$	0.50	mg/L
H_3BO_3	0.05	mg/L
ZnCl_2	0.05	mg/L
CuCl_2	0.03	mg/L
$\text{Na}_2\text{MoO}_4 \cdot 2\text{H}_2\text{O}$	0.01	mg/L
$\text{CoCl}_2 \cdot 6\text{H}_2\text{O}$	1.00	mg/L
$\text{NiCl}_2 \cdot 6\text{H}_2\text{O}$	0.10	mg/L
Na_2SeO_3	0.05	mg/L

1000 ml glass bottle GL 45 (Schott Duran, Germany) with a working volume of 400 ml. Inoculum was collected from the final part of an anaerobic channel digester treating cow dung of Chiang Mai Fresh Milk farm in Lamphun province, Thailand. The inoculum was diluted to 20 gVS/L with medium solution (Table 1).

Press fluid and inoculum added in each bottle were 164 and 236 ml, respectively, equivalent to a ratio of press fluid to inoculum of 0.5 (by VS). Also, a bottle with only inoculum and distilled water was prepared and used as the control. All the experiments were done in triplicate including the control experiment. Microcrystalline cellulose was also used as a reference sample for checking the activity of inoculum. The gas production of this reference sample should be at least 80% of 740-750 mL_N/gVS_{added}. Nitrogen gas was used in flushing the headspace for 3 minutes to ensure the anaerobic condition. Each bottle was sealed with PTFE/silicone septa with PP screw cap and then kept in the temperature controlled room at 35°C. The gas volume was measured indirectly by pressure equipment (Kimo, model MP112) and then converted to that at STP condition (0°C and 1 atm). Complete anaerobic digestion was obtained when daily biogas production rate was less than 1% of total volume biogas production.

Analytical Method

Total solid, volatile solid and COD were analysed according to standard methods (Rice et

al., 2012). The methane composition was measured using a gas chromatograph (Agilent 7890A) with a thermal conductivity detector (TCD). The temperature of the injector and detector were 120°C and 150°C, respectively. The carrier gas was He with the flow rate of 10 ml/min. Methane potential was calculated as $L_N\text{CH}_4/\text{kgVS}_{\text{added}}$. The modified Gompertz model (Eq.1) was used to predict the maximum methane yield (Ho & Shihwu, 2010).

$$M = P \times \exp \left\{ -\exp \left[\frac{R_m \times e}{P} (\lambda - t) + 1 \right] \right\} \quad [1]$$

Where, M is the cumulative methane yield (mL/gVS_{added}), P the maximum methane yield (mL/gVS_{added}), R_m the maximum methane production rate (mL/gVS_{added}/d), λ the lag phase (days), t the digestion time (days), e the exp(1)=2.718. All parameters (P, R_m, and λ) were estimated by the least square method using Solver function in Microsoft®Office Excel 2013. The sum of the squared errors (SSE) was set to minimize. The error value was the difference between the experimental value and predicted value.

RESULTS AND DISCUSSION

Characteristic of Napier PakChong1 grass

Characteristics of Napier PakChong1 grass are shown in Table 2. The TS of Napier PakChong1 grass was in the range of 14.30-16.44%. This result was similar with those of Lounglawan et al. (2014) who found that the dry matter of King Napier grass was 13.37-18.39%. However, Ansah et al. (2010) reported TS values of four varieties of Napier grass in Ghana in the higher range (48-51%) at harvesting time 60-120 day. Lower TS values of Napier PakChong1 grass found in this current study could be attributed to the variety of Napier grass species, planting location and climate and, in particular, the shorter harvesting time. As founded in this current study, the 60 d-grass had higher lignin compared to those at shorter harvesting times, which could affect volumes and characteristics of the obtained grass juice.

Table 2
Characteristics of Napier PakChong1 Grass

Composition	Harvesting time (day)		
	30 (n=1)	45 (n=6)	60 (n=6)
Total solid (%)	14.42	16.44	14.30
VS (%)	12.56	14.27	12.60
Ether extract (% as dry matter)	3.63	3.72	3.40
Crude fiber (% as dry matter)	33.18	31.95	33.35
Crude protein (% as dry matter)	9.07	13.13	12.65
Ash (% as dry matter)	12.04	13.12	12.57

Table 2 (Continued)

Composition	Harvesting time (day)		
	30 (n=1)	45 (n=6)	60 (n=6)
Nitrogen-free extract, NFE (% as dry matter)	42.08	38.08	38.03
Cellulose (% as dry matter)	40.44	36.35	37.25
Hemicellulose (% as dry matter)	20.09	22.41	23.99
Lignin (% as dry matter)	4.04	4.74	4.92
Potassium (% as dry matter)	1.32	0.38	0.47

Optimization of Press Fluid

Normally, grasses have high water content up to 80-85%. The preservation methods of grasses, such as silage or drying, for use as a raw material is essential (Xiu & Shahbazi, 2015). For the green biorefinery of biomass, mechanical dehydration with screw press is the primary method used to press grasses to press fluid. To increase maceration of the cell walls a pretreating method of biomass by adding water needs to be applied before press juice separation is conducted by screw press (Arlabosse et al., 2011). Effects of harvesting time (A), grass to water ratio (B), soaking time (C) and temperature (D) on the organic substance (as mass of COD_t) obtained in the press juice were investigated. The experimental data and the regression model of the mass of COD_t (at confidence level of 90%) are shown in table 3 and table 4, respectively. The mathematical equation for the relationship between mass of COD_t and values of studied factors (uncoded values) gained from regression analysis can be shown in equation 2. The experimental data showed quadratic correlation between studied factors and the responses. Moreover, interaction effects between experimental variables had also been found.

$$Y_{COD} = 172.364 - 3.037 (\text{Harvested time}) + 17.536 (\text{Grass: water ratio}) + 0.176 (\text{Time}) - 2.213 (\text{Temp}) + 0.04 (\text{Harvested time})^2 + 0.0004(\text{Time})^2 + 0.021(\text{Temp})^2 - 0.003 (\text{Time} \times \text{Temp}) \quad [2]$$

As the press fluid from Napier PakChong1 grass was intended to be used for biogas production, COD_t was chosen as the response for optimization as it was the most pertinent characteristics for the bioreactor feedstock. The result showed that harvesting time, the ratio of grass to water and soaking time had significant effects on the total mass of COD_t (P<0.1). Optimum conditions obtained from the optimization were harvesting time 75 d, grass: water ratio 1: 6 (kg: L), soaking time 355 min and temperature 15.5°C. Under these conditions, the predicted maximum mass of COD_t was 85.06 g/kg wet weight Napier PakChong1

Table 3

Experimental data of design of experiment for the mass of COD_t of the press fluid, in term of coded factor

Run order	Harvesting time (d)	Grass to water ratio (w/w)	Soaking time (min)	Temperature (°C)	Mass of COD _t (g)	
					Experimental	Predicted
1	-1 (30)	-1 (1:3)	-1 (10)	-1 (37)	122.88	110.24
2	+1 (60)	-1 (1:3)	-1 (10)	-1 (37)	142.33	128.25
3	-1 (30)	+1 (1:5)	-1 (10)	-1 (37)	139.81	145.32
4	+1 (60)	+1 (1:5)	-1 (10)	-1 (37)	160.54	163.32
5	-1 (30)	-1 (1:3)	+1 (240)	-1 (37)	144.42	148.05
6	+1 (60)	-1 (1:3)	+1 (240)	-1 (37)	185.55	166.06
7	-1 (30)	+1 (1:5)	+1 (240)	-1 (37)	173.03	183.13
8	+1 (60)	+1 (1:5)	+1 (240)	-1 (37)	200.41	201.14
9	-1 (30)	-1 (1:3)	-1 (10)	+1 (80)	121.21	121.71
10	+1 (60)	-1 (1:3)	-1 (10)	+1 (80)	141.28	139.72
11	-1 (30)	+1 (1:5)	-1 (10)	+1 (80)	153.06	156.79
12	+1 (60)	+1 (1:5)	-1 (10)	+1 (80)	178.11	174.80
13	-1 (30)	-1 (1:3)	+1 (240)	+1 (80)	129.61	127.90
14	+1 (60)	-1 (1:3)	+1 (240)	+1 (80)	139.45	145.91
15	-1 (30)	+1 (1:5)	+1 (240)	+1 (80)	164.29	162.97
16	+1 (60)	+1 (1:5)	+1 (240)	+1 (80)	171.66	180.98
17	0 (45)	0 (1:4)	0 (125)	0 (58.5)	130.71	134.59
18	0 (45)	0 (1:4)	0 (125)	0 (58.5)	135.63	134.59
19	0 (45)	0 (1:4)	0 (125)	0 (58.5)	126.67	134.59
20	0 (45)	0 (1:4)	0 (125)	0 (58.5)	133.99	134.59
21	- α (15)	0 (1:4)	0 (125)	0 (58.5)	167.29	161.97
22	α (75)	0 (1:4)	0 (125)	0 (58.5)	189.84	197.99
23	0 (45)	- α (1:2)	0 (125)	0 (58.5)	92.26	109.04
24	0 (45)	α (1:6)	0 (125)	0 (58.5)	195.61	179.18
25	0 (45)	0 (1:4)	- α (0)	0 (58.5)	136.60	132.15
26	0 (45)	0 (1:4)	α (355)	0 (58.5)	181.92	166.11
27	0 (45)	0 (1:4)	0 (125)	- α (15.5)	179.14	188.30
28	0 (45)	0 (1:4)	0 (125)	α (90.0)	174.09	162.31
29	0 (45)	0 (1:4)	0 (125)	0 (58.5)	142.60	144.11
30	0 (45)	0 (1:4)	0 (125)	0 (58.5)	125.93	144.11

Table 4

Results of regression analysis of the mass of COD_i from the press fluid

Model term	Regression coefficient	Standard error coefficient	t-statistic	P-value
Constant	136.07	3.585	37.954	0.000
Block	-5.523	2.089	-2.644	0.016
A	9.004	2.143	4.201	0.000
B	17.536	2.143	8.182	0.000
C	9.530	2.415	3.946	0.001
D	-2.242	2.286	-0.981	0.338
A ²	9.093	1.964	4.631	0.000
C ²	4.977	2.622	1.898	0.072
D ²	9.911	2.409	4.114	0.001
CD	-7.907	2.625	-3.012	0.007
R ² = 88.98%	R ² (adj) = 70.65%			

grass. Hensgen et al. (2011) and Wachendorf et al. (2009) found that increase of water temperature in the range of 40-60°C did not increase of mass flow of minerals into the press fluid. Likewise, King et al. (2012) studied the effect of water temperature of hydrothermal conditioning process at 20, 40 and 60°C and reported that concentrations of elements in the press fluid from grass silage obtained at these temperatures were not significantly different. However, Richter et al. (2011) found that higher temperature of hydrothermal conditioning increased mass flows of elements into press fluids and decreased concentrations of elements in press cake when the soaking time and silage grass: water ratio were maintained at 10 min and 1:4 (w/w), respectively. Reasons for different effects of temperature on the quality of press fluid found in these studies are not clear. However, grass species (and structure), characteristics of soaking water and level of grass pretreatment might play some parts on the difference found. In this current study, it was found that the optimum temperature was lower than the normal ambient temperature in Thailand, which was not suitable for actual use. Therefore, the temperature was adjusted to the ambient temperature which was about 25°C. The mass of COD obtained in these adjusted conditions was 56.60 g/kg wet weight Napier PakChong1 grass equating to 71.5% of the value predicted by the model (79.17 g/kg wet weight Napier PakChong1 grass). Therefore, this is suitable conditions for producing press fluid from Napier PakChong1 grass to press fluid. Kuila et al. (2011) reported that increasing soaking time also increased the reducing sugar production from cashew apple bagasse. The maximum yield of 56.89 g reducing sugar/100 g dry substrate was obtained at liquid: solid of 3.26 (mL/g), pH 6.42, incubation time 6.30 h and temperature 52.27°C. Similarly, in this current study, increasing of solid: liquid ratio also resulted in the mass of COD_i and reducing sugar being increased (data not shown).

Biochemical Methane Potential (BMP) Test

The press fluid from the optimum hydrothermally conditioned grass (harvesting time 75 d, grass: water ratio 1: 6 (kg: L), soaking time 355 min and temperature about 25°C) was investigated for biogas production potential using the BMP test. The average methane yield of press fluid was 396.32 ± 5.39 LCH₄/kgVS. The average methane content was 68.6%. Relatively, high methane yield could be attributed to the fact that press fluid contained mainly the biodegradable and soluble organic substances. The obtained methane yield is in the same range as those found in the studies of Hensgen et al. (2014), Hensgen et al. (2011), Nayono et al. (2010) and Richter et al. (2009) though different grass species and conditioning conditions before fluid pressing were used. Hensgen et al. (2014) found that methane yields of press fluid from IFBB for twelve European semi-natural grassland varied between 312-405 LCH₄/kgVS. In this work, the ensile samples were sprinkled with 25°C warm tap water and the ratio of biomass to mash water was 1:8. The previous study of Hensgen et al. (2011) reported that different water temperature in hydrothermal conditioning (40 and 60°C) did not affect the methane yields of the press fluid, in which 396-415 LCH₄/kgVS were obtained. Richter et al. (2009) also found that methane yields of press fluid from different types of semi-natural grassland conditioned under hydrothermal conditions were ranged 304-522 LCH₄/kgVS. This means that the optimum conditioning conditions achieved in this current study is as effective as those reported in previous works. Compared with the whole crop, methane yields of press fluid gained in this current study was significantly higher than that reported from the whole crop silage (218 LCH₄/kgVS) (Richter et al., 2009). Even though, Thamsiriroj and Murphy (2010) reported relatively high methane yield (455 LCH₄/kgVS) from the Irish silage, the organic loading rate used was only 1 kgVS/m³.d and hydraulic retention time was more than 70 days. As the required digestion time of press fluid was only 15 d (time duration required to reach the maximum biogas production during the BMP test and the pipe clogging problem, normally found when the fibrous whole grass was used as the substrate) (Hensgen et al., 2014), is not the issue for press fluid, renewable energy production according to IFBB process is clearly more advantageous.

The cumulative methane data was used to fit with the modified Gompertz model (equation 1) to estimate the microbial kinetic parameters, with an assumption that biogas production is a function of the methanogens growth in batch digester. The best fit to modified Gompertz equation is compared with the experiment data as illustrated in Figure 2. The regression coefficient (R^2) was 0.995 demonstrating the suitability of the model for accurate estimation of the anaerobic digestion of press fluid. The methane yield potential (P), the maximum methane production rate (R_m) and lag phase time (λ) were 412.18 mLCH₄/gVS_{added}, 51.47 mLCH₄/gVS_{added}/d and 4.36 days, respectively. Kacprzak et al. (2012) studied the kinetics of anaerobic digestion of canary grass by using modified Gompertz

model. They found that the yield of biogas production and the lag phase were 648.44 L/kg VS and 14.67 d. In addition, Xie et al. (2011) reported specific methane yield and lag phase of co-digestion of pig manure and grass silage ratio at 1:0, 3:1, 1:1 and 1:3 which were equal to 279.8, 304.2, 302.8 and 267.3 mLCH₄/gVS and 29.5, 28.1, 24.6 and 21.3 d, respectively. Furthermore, Prapinagson et al. (2017) found that the ratio of grass with cow dung and silage with cow dung at 3:1 by VS gave the maximum methane yield of 179.59 and 208.11 mLCH₄/gVS_{added}, respectively. The lag phase of these conditions were 11.9 and 5.9 day, respectively. Compared to microbial kinetic values obtained when grasses were used as either the sole substrate or codigested with animal manures, it is obvious that the grass press juice used in this current study rendered much higher maximum methane yield and shorter lag phase time. This means that, to produce the same amount of biogas, a reactor needed for biogas production from the grass press juice could be less complicated (as the mixing system is not necessary); smaller in size (as it is very likely to accepted higher organic loading rate); easier to start-up (as it needs shorter time for microbial acclimatization) and cheaper to operate (as elements required for microbial degradation are transferred into the press juice in soluble form).

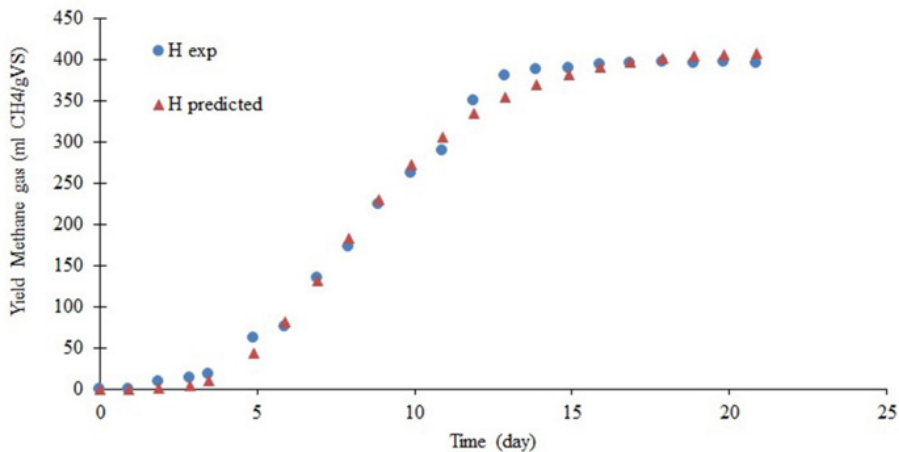


Figure 2. Comparison between the experimental data and modified Gompertz equation data

CONCLUSION

The study revealed that the optimum hydrothermal conditioning conditions for Napier PakChong1 grass were as follows; harvesting time 75 d, ratio of grass to water of 1:6 (by weight), ambient temperature (about 25°C) of the water and the soaking time of 355 min. The mass of COD in the press juice obtained in these conditions was 226.42 g equating

to 71.5% of the value predicted by the model (316.68 g). Results from the BMP test showed that methane yield of press fluid was 396.32 L_NCH₄/kgVS with methane content of 68.6%. The microbial kinetic coefficients and biogas yield potential of press fluid were properly fitted with the modified Gompertz equation (adjusted R² = 0.995). The methane yield potential (P), the maximum methane production rate (R_m) and lag phase time (λ) were 412.18 mLCH₄/gVS_{added}, 51.47 mLCH₄/gVS_{added}/d and 4.36 days, respectively. Producing biogas from the press fluid was clearly superior to that from the whole grass in a commercial scale.

ACKNOWLEDGEMENT

This study was financially supported by the Chiang Mai University and the Energy Research and Development Institute-Nakornping Chiang Mai University, Chiang Mai, Thailand. Authors wish to thank the Chiang Mai Fresh Milk farm for samples of grasses and inoculum provided.

REFERENCES

- AEDP. (2015). *Energy policy and planning office, Ministry of Energy*. Alternative Energy Development Plan. Retrieved March 7, 2017, from <http://www.eppo.go.th/images/POLICY/ENG/AEDP2015ENG.pdf>
- Arlabosse, P., Blanc, M., Kerfai, S. & Fernandez, A. (2011). Production of green juice with an intensive thermo-mechanical fractionation process. Part I: Effects of processing conditions on the dewatering kinetics. *Chemical Engineering Journal*, 168(2), 586-592.
- Bruni, E., Jensen, A. P., & Angelidaki, I. (2010). Comparative study of mechanical, hydrothermal, chemical and enzymatic treatments of digested biofibers to improve biogas production. *Bioresource Technology*, 101(22), 8713-8717.
- Bühle, L., Reulein, J., Stülpnagel, R., Zerr, W., & Wachendorf, M. (2012). Methane yields and digestion dynamics of press fluids from mechanically dehydrated maize silages using different types of digesters. *Bioenergy Research*, 5(2), 294-305.
- Hensgen, F., Bühle, L., Donnison, I., Heinsoo, K., & Wachendorf, M. (2014). Energetic conversion of European semi-natural grassland silages through the integrated generation of solid fuel and biogas from biomass: Energy yields and the fate of organic compounds. *Bioresource Technology*, 154, 192-200.
- Hensgen, F., Richter, F., & Wachendorf, M. (2011). Integrated generation of solid fuel and biogas from green cut material from landscape conservation and private households. *Bioresource Technology*, 102(22), 10441-10450.
- Ho, J., & Shihwu, S. (2010). Methanogenic activities in anaerobic membrane bioreactors (AnMBR) treating synthetic municipal wastewater. *Bioresource Technology*, 101(7), 2191-2196.
- Ingenieure, V. D. (2006). VDI 4630: Fermentation of organic materials-Characterisation of the substrate, sampling, collection of material data, fermentation tests. In V. D. Ingenieure (Ed.), *VDI Handbuch Energietechnik* (pp. 44-59). Berlin: Beuth Verlag GmbH.

- Jenkins, B. M., Baxter, L. L., Miles, Jr., T. R., & Miles, T. R. (1998). Combustion properties of biomass. *Fuel Processing Technology*, 54(1-3), 17-46.
- Jia, F., Chawhuaymak, J., Riley, M. R., Zimmit, W., & Ogden, K. L. (2013). Efficient extraction method to collect sugar from sweet sorghum. *Journal of Biology Engineering*, 7(1), 1-8.
- Kacprzak, A., Krzystek, L., Paździor, K., & Ledakowicz, S. (2012). Investigation of kinetics of anaerobic digestion of canary grass. *Chemical Papers*, 66(6), 550-555.
- King, C., McEniry, J., O'Kiely, P., & Richardson, M. (2012). The effects of hydrothermal conditioning, detergent and mechanical pressing on the isolation of the fibre-rich press-cake fraction from a range of grass silages. *Biomass and Bioenergy*, 42, 179-188.
- Kuila, A., Singh, A., Mukhopadhyay, M., & Banerjee, R. (2011). Process optimization for aqueous of reducing sugar from cashew apple bagasse: A potential, low cost substrate. *LWT-Food Science and Technology*, 44(1), 62-66.
- Lounglawan, P., Lounglawan, W., & Suksombat, W. (2014). Effect of cutting interval and cutting height on yield and chemical composition of King Napier grass (*Pennisetum purpureum* x *Pennisetum americanum*). *APCBEE Procedia*, 8, 27-31.
- Nayono, S.E., Winter, J., & Gallert, C. (2010). Anaerobic digestion of pressed off leachate from the organic fraction of municipal solid waste. *Waste Management*, 30(10), 1828-1833.
- Negawo, A.T., Teshome, A., Kumar, A., Hanson J., & Jones, C. S. (2017). Opportunities for napier grass (*Pennisetum purpureum*) improvement using molecular genetics. *Agronom*, 7(2), 28.
- Obernberger, I., Brunner, T., & Bärnthaler, G. (2006). Chemical properties of solid biofuels-significance and impact. *Biomass and Bioenergy*, 30(11), 973-982.
- Prapinagson, W., Sittijunda, S., & Reungsang, A. (2017). Co-digestion of napier grass and its silage with cow dung for methane production. *Energies*, 10(10), 1654-1673.
- Rengsirikul, K., Ishii, Y., Kanfvansaichol, K., Sripichitt, P., Punsuvon, V., Vaithanomsat, P., Nakamane, G., & Tudsri, S. (2013). Biomass yield, chemical composition and potential ethanol yields of 8 cultivars of napiergrass (*Pennisetum purpureum* schumach.) harvested 3-monthly in central Thailand. *Journal of Sustainable Bioenergy System*, 3(2), 107-112.
- Reulein, J., Scheffer, K., Stülpnagel, R., Bühle, L., Zerr, W., & Wachendorf, M. (2007). Efficient utilization of biomass through mechanical dehydration of silages. In *Proceedings of the 15th European Biomass Conference and Exhibition* (pp. 1770-1774). Berlin, Germany.
- Rice, E. W., Baird, R. B., Eaton, A. D., & Clesceri, L. S. (Eds.) (2012). *Standard Methods for the Examination of Water and Wastewater* (22nd edition). Washington, USA: American Public Health Association, American Water Works Association, Water Environment Federation.
- Richter, F., Fricke, T., & Wachendorf, M. (2011). Influence of sward maturity and pre-conditioning temperature on the energy production from grass silage through the integrated generation of solid fuel and biogas from biomass (IFBB): 2. Properties of energy carriers and energy yield. *Bioresource Technology*, 102(7), 4866-4875.

- Richter, F., Graß, R., Fricke, T., Zerr, W., & Wachendorf, M. (2009). Utilization of semi-natural grassland through integrated generation of solid fuel and biogas from biomass. II. Effects of hydrothermal conditioning and mechanical dehydration on anaerobic digestion of press fluids. *Grass and Forage Science*, 64(4), 354-63.
- Thamsiriroj, T., & Murphy, J. D. (2010). Difficulties associated with monodigestion of grass as exemplified by commissioning a pilot scale digester. *Energy and Fuels*, 24(8), 4459-4469.
- Thamsiriroj, T., Nizami, A. S., & Murphy, J. D. (2012). Why does mono-digestion of grass silage fail in long term operation? *Applied Energy*, 95, 64-76.
- Wachendorf, M., Richter, F., Fricke, T., Graß, R., & Neff, R. (2009). Utilization of semi-natural grassland through integrated generation of solid fuel and biogas from biomass. I. Effects of hydrothermal conditioning and mechanical dehydration on mass flows of organic and mineral plant compounds, and nutrient balances. *Grass and Forage Science*, 64(2), 132-143.
- Xie, S., Lawlor, P. G., Frost, J. P., Hu, Z., & Zhan, X. (2011). Effect of pig manure to grass silage ratio on methane production in batch anaerobic co-digestion of concentrated pig manure and grass silage. *Bioresource Technology*, 102(10), 5728-5733.
- Xiu, S., & Shahbazi, A. (2015). Development of green biorefinery for biomass utilization: A review. *Trends in Renewable Energy*, 1(1), 4-15.

Mapping the Distribution of Oil Palm using Landsat 8 Data by Comparing Machine Learning and Non-Machine Learning Algorithms

Nur Shafira Nisa Shaharum¹, Helmi Zulhaidi Mohd Shafri^{1*},
Wan Azlina Wan Ab Karim Ghani², Sheila Samsatli³ and Badronnisa Yusuf¹

¹Department of Civil Engineering /Geospatial Information Science Research Centre (GISRC), Faculty of Engineering, Universiti Putra Malaysia, 43400 UPM Serdang, Selangor, Malaysia.

²Department of Chemical and Environmental Engineering/Sustainable Process Engineering Research Centre (SPERC), Faculty of Engineering, Universiti Putra Malaysia, 43400, UPM Serdang, Selangor, Malaysia.

³Department of Chemical Engineering, University of Bath, Claverton Down, BA2 7AY, United Kingdom.

ABSTRACT

Oil palm is one of the major crops in Malaysia; it accounts for 47% of the global palm oil supply. Equatorial climate has provided Malaysia with the potential to produce oil palm biomass, which is one of the major contributors to the local economy. The utilisation of oil palm biomass as a source of renewable energy is one of the effective methods to promote green energy. Therefore, there is a need to have sufficient data related to oil palm biomass such as yield estimation, oil palm distributions, and locations. The aim of this study was to produce a land cover map on the distribution of oil palm plantations on

three districts located in Selangor. Landsat 8 images of resolutions 15 x 15 m were used and classified via machine learning and non-machine learning algorithms. In this study, three different classifier algorithms were compared using support vector machines, artificial neural networks, and maximum likelihood classifications in which the values obtained for overall accuracy were 98.96%, 99.39%, and 15.30% respectively. The output showed that machine learning algorithms, support vector machines and

ARTICLE INFO

Article history:

Received: 24 October 2018

Accepted: 15 February 2019

Published: 21 June 2019

E-mail addresses:

fieranisa94@gmail.com (Nur Shafira Nisa Shaharum)

helmi@upm.edu.my (Helmi Zulhaidi Mohd Shafri)

wanazlina@upm.edu.my (Wan Azlina Wan Ab Karim Ghani)

S.M.C.Samsatli@bath.ac.uk (Sheila Samsatli)

nisa@upm.edu.my (Badronnisa Yusuf)

* Corresponding author

artificial neural networks gave rise to high accuracies. Hence, the mapping of oil palm distributions via machine learning algorithm was better than that via non-machine learning algorithm.

Keywords: Landsat 8, machine learning, oil palm, remote sensing, support vector machine

INTRODUCTION

Malaysia is blessed with plenty of biomass crops such as paddy, rubber, and oil palm. In fact, Malaysia is currently one of the largest suppliers of palm oil in the world. As a tropical country that experiences both hot and humid weather, oil palm can be grown over a large area; this in turn brings forth benefits to the local economy in terms of increase in oil palm cultivation (Ng et al., 2012; Sumathi et al., 2008 ; Yusoff, 2006). In 2011, 4.98 Mha of oil palm was grown in Malaysia, and this figure rose to 5.64 Mha in 2016, an increment of 13.25% in 5 years (Malaysian Palm Oil Board, 2016). The aforementioned area is expected to increase over time, and this enhances the feasibility of oil palm as a renewable source of energy (Awalludin et al., 2015).

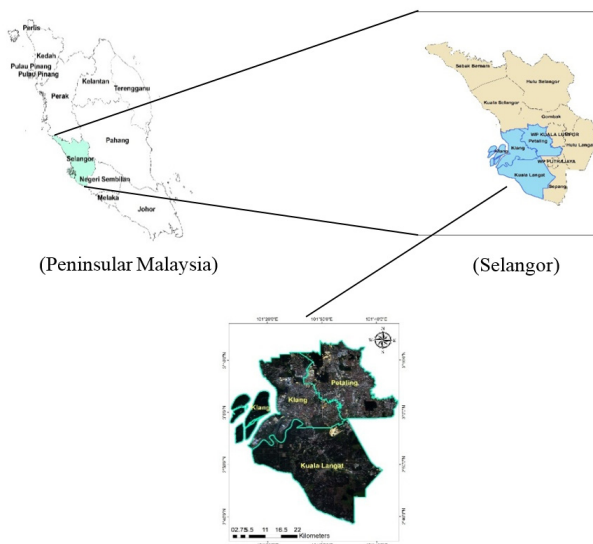
Globally, the demand for biomass is growing. The development of the oil palm biomass industry in Malaysia needs to be monitored while the role of oil palm biomass as a source of renewable energy requires evaluation (Ng et al., 2012). Biomass is an important alternative to fossil fuels in the production of electricity. Without proper adoption of biomass as a source of renewable energy, Malaysia is likely to contend with an energy crisis in the future (Chuah et al., 2006). In order to fully optimise the local usage of oil palm biomass, detailed information of the distribution of oil palm is vital.

Remote sensing can provide a large area's worth of information from a distance. Data is obtained from the energy that is reflected from the surface of the Earth. A few studies on oil palm mapping have employed various sensors and techniques (Chong et al., 2017; Koh et al., 2011; Nooni et al., 2014). For example, Landsat 7 has been used to map the distribution of oil palm in Selangor via the Nearest Neighbour (NNB) technique, for which the overall accuracy of the results was 98%. However, the image obtained from Landsat 7 was covered with clouds and the map produced was for 2002 (Wahid et al., 2005). Cheng et al. (2017) had utilised MODIS and ALOS Phased Array type L-band Synthetic Aperture Radar mosaiced data via different approaches to map the distribution of oil palm. According to Li et al. (2015), support vector machine is found to be the best classifier to map oil palm using PALSAR data with 50 m spatial resolution. The uses of support vector machines and artificial neural networks for crops classifications give good results (Peña et al., 2014). However, the algorithms need to be tested in order to produce an updated map of oil palm distributions. In this study, Landsat 8 data of spatial resolution 15 x 15 m was used to map the distributions of oil palm. Due to the richness of oil palm area in Selangor, Ahmed et al. (2010) had conducted a study on land cover mapping using Quick Bird and

Sentinel 1 data. Therefore, 3 districts within Selangor were chosen for this study, namely Klang, Petaling, and Kuala Langat. In order to identify the best algorithm for oil palm mapping, maximum likelihood classifier, support vector machines, and artificial neural networks were compared in this study.

MATERIALS AND METHODS

Data which was taken by Landsat 8 Operational Land Imager (OLI) on 29th March 2016 was used in this study. The image shown in Figure 1 has 5.63% of cloud cover and the image was acquired at <https://libra.developmentseed.org/>. It covered the entire area of Selangor, and was composed of many pixels, each of which was assigned a certain value called Digital Number (DN). The image comprised 11 bands (including Multispectral, Thermal Infrared, Panchromatic, and Cirrus) whose spatial resolutions ranged from 15 x 15 m to 100 x 100 m. In this study, only Multispectral and Panchromatic bands were used, while the areas of interest were the three aforementioned districts (Klang, Petaling, and Kuala Langat). Figure 2 shows the workflow of the study.



(Klang, Kuala Langat, and Petaling districts as captured by Landsat 8)

Figure 1. Study area covering the three districts

Image Processing

Pre-processing was applied and conducted in ENVI software version 5.3 (ITT Visual Information Solutions, Boulder, CO, USA). A Radiometric Calibration tool was used to correct the raw image of Landsat 8 by converting the DN to reflectance. Multispectral bands contain various number of bands including red, green, blue, and near-infrared with

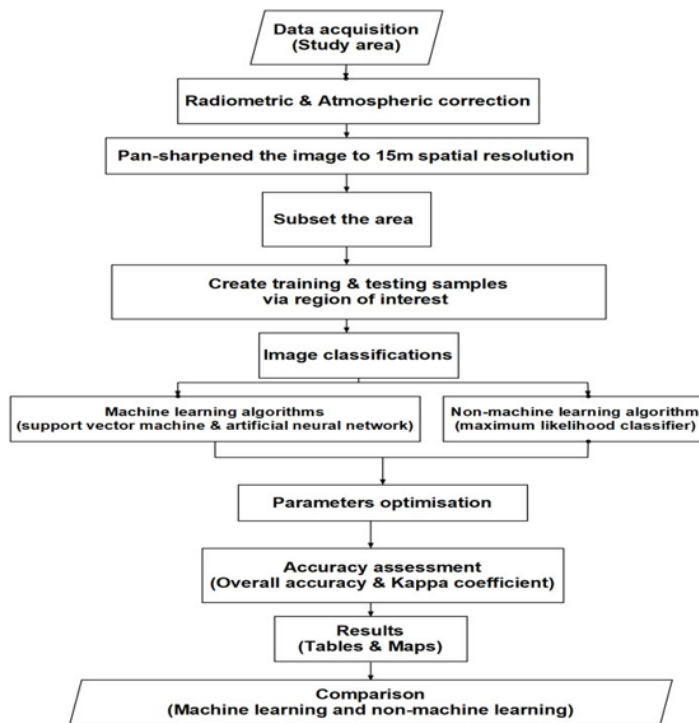


Figure 2. Work flow of the study

the spatial resolution of 30 x 30m. By combining three different bands, it can produce an image with colours. For Landsat 8, a combination of band 4 (Red), band 3 (Green), and band 2 (Blue) will produce an image with true colours shown in Figure 3. On the other hand, panchromatic band is based on higher spatial resolution with 15 x 15m. Following atmospheric correction of the image, an image pan-sharpening technique was employed to increase the spatial resolution from 30 x 30m to 15 x 15 m (Gilbertson et al., 2017; Shaharum et al.,2018). Subsequently, the image was cropped (subset) using the region of interest (ROI) tool in ENVI, leaving only the areas of interest. In addition, the training and testing samples were created using the same ROI tool, with high-resolution images from Google Earth as the reference. The samples were created and labelled according to their classes: oil palm, non-oil palm, bare soil, built-up areas, and water. After that, the image was classified by support vector machines, artificial neural networks, and maximum likelihood classifications. The study area and the placement of the training samples were shown in Figure 3 and Figure 4.

Support Vector Machines

A support vector machine (SVM) is an advanced classifier and one of the powerful machine



Figure 3. True colour of the study area



Figure 4. The samples are placed on the pixels according to the assigned classes

learning algorithms that has been widely used to classify remote sensing images (Shafri, 2016). SVM, which was introduced by Vapnik et al. (1995) is a technique which involves regressions and classifications (Shafri & Ramle, 2009). In light of its high-performance generalisations without the need for prior knowledge, SVM has the ability to produce outstanding results in various applications (Hermes et al., 1999; Kavzoglu & Colkesen, 2009; Shafri & Zeen, 2011; Shafri, 2016). In addition, SVM works by mapping or grouping the data in a high dimensional feature space; this allows the non-linear data points to be separated into the desired classes. Using a hyperplane, SVM separates the support vectors by maximising the distance between the support vectors of each class. In ENVI, four types of kernels are available for SVM: linear, polynomial, radial basis function (RBF), and sigmoid. RBF was chosen for in this study in view of its good performance in previous studies (Kuo et al., 2014; Feizizadeh et al., 2017).

Artificial Neural Networks

Apart from SVM, artificial neural networks (ANNs) are another type of non-parametric machine learning algorithm. The method by which ANN processes information is slightly different from those of other machine learning algorithms such as Decision Tree (DT) and Random Forest (RF). Unlike ANN, DT and RF use a tree-like form to perform classifications (Dibs et al., 2017; Pal, 2005). However, ANN imitates the way by which a human brain processes information (Braga et al., 2016). In the latter, billions of interconnected neurons allow humans to learn and recognise a variety of input pattern. A neuron is made up of a cell body, a longer thread axon, and many fine threads (dendrites), of all which enable the

neurons to send and receive impulses in a human brain. As a result, the brain is capable of learning, predicting, and recognising patterns with ease (Agatonovic-Kustrin & Beresford, 2000; Kumar et al., 2015; Wang et al., 2015).

To produce the structure of biological neurons in a computational design, ANN has been structured in terms of input, hidden, and output layers. Each layer can consist of one or several neurons called nodes. These nodes are connected, with each connection being assigned a certain weight that can be adjusted during the back-propagation method. From the input layer, information is fed onwards to the hidden layer and finally the output layer. An activation function occurs at the nodes when the value from previous node is added to the weight. Theoretically, back-propagation takes place when a signal is sent back to the input layer and again to the output layer. Throughout the process, the weights are adjusted using the provided training samples to minimise errors between the output and actual values. This adjustment process continues until a desired number of iterations is attained (Wang et al., 2015; Shi et al., 2017).

Maximum Likelihood Classifier

A maximum likelihood classifier (MLC) is a non-machine learning algorithm and is the most popular supervised parametric classifier in the field of remote sensing. It works by making assumptions of the probability that a pixel belongs to a certain class. Theoretically, MLC assumes that the probabilities are the same for all classes under the basis that the input bands are normally distributed (Gómez et al., 2016; Rawat & Kumar, 2015).

$$g_i(x) = \ln p(\omega_i) - \frac{1}{2} \ln |\Sigma_i| - \frac{1}{2} (x - m_i)^T \Sigma_i^{-1} (x - m_i) \quad (1)$$

Class, i ; n -dimensional data (where n is the number of bands), x ; Probability that class ω_i occurs in the image and is assumed the same for all classes, $p(\omega_i)$; Determinant of the covariance matrix of the data in class ω_i , $|\Sigma_i|$; Its inverse matrix, Σ_i^{-1} ; Mean vector, m_i

Furthermore, MLC assigns each pixel to the class that has the highest probability. If the highest probability is lower than the specified threshold, the pixel will not be classified. Unlike SVM and ANN, MLC needs prior knowledge. However, the usage decision boundaries by MLC can lead to poor quality results for land cover classifications of large areas (Hubert-Moy et al., 2001).

Parameters Optimisation

Owing to the flexibility of machine learning algorithms, parameters of the algorithms can be tuned to improve the accuracy (Li et al., 2015; Mountrakis et al., 2011). Since no studies had optimised the parameters for mapping oil palm distributions, the parameters in SVM, ANN, and MLC were optimised in this study to improve the classifications using automated approach via python programming language and non-auto parameter tuning in ENVI.

Accuracy Assessment

The accuracy assessment in this study was calculated using confusion matrix provided in ENVI. It produces an error matrix where an overall accuracy and kappa coefficient were given which allow the accuracy of the maps generated to be compared. The overall accuracy is calculated by adding the number of correctly classified values and divide it by the total number of values while kappa coefficient measures the agreement between classification and truth values. Kappa value is ranging from 1 to 0 where the value of 1 represents perfect agreement, while a value of 0 represents no agreement. Example for the calculation of overall accuracy and the kappa coefficient formula were computed as follows:

$$\text{Overall accuracy} = [(13098+296+80+504+1388)/15519] \times 100 = 99.01\%$$

$$K = \frac{N \sum_{i=1}^n m_{i,i} - \sum_{i=1}^n (G_i C_i)}{N^2 - \sum_{i=1}^n (G_i C_i)} \quad (2)$$

The class number, i ; The total number of classified values compared to truth values, N ; The number of values belonging to the truth class i that has also been classified as class i , $m_{i,i}$; The total number of predicted values belonging to class i , C_i ; The total number of truth values belonging to class i , G_i

In the example confusion matrix, the kappa coefficient is 0.9644

RESULTS AND DISCUSSIONS

Three classifiers were used to classify the image, and the resultant images of each are shown in Figure 5(a), Figure 5(b), and Figure 5(c).

The images in Figure 5 were classified using the same pixel-based technique. Each pixel was 15 m in length and width. With reference to these images, it can be inferred that machine learning algorithms, like SVM and ANN provided good quality classifications in which the parameters were tested and optimised. The best results from the optimised parameters were used to classify the maps. However, a non-machine learning algorithm, MLC gave rise to the worst classification as the overall accuracy of the same was a mere 15.30% (Table 2).

As per the confusion matrix table generated in ENVI, SVM produced an image with producer's and user's accuracies of 92.74% and 89.35% respectively for oil palm. Meanwhile, the said values for ANN were 99.67% and 100% respectively. ANN produced results of better accuracies than SVM. Though ANN produced higher overall accuracy than SVM, the visualisation of the classified map generated by SVM reflected the closest to the satellite image. On the other hand, owing to the misclassification of water as built-up, the map produced by MLC had an excess of built-up areas, which directly affected the overall accuracy. The example of confusion matrix is tabulated in Table 1.

With reference to Table 2, SVM and ANN classified images with high accuracy, this showing that machine learning algorithms performed better than non-machine learning. The overall accuracies of the images produced by SVM and ANN exceeded 98%. In light of the fact that non-parametric algorithms do not make any assumptions, they can easily learn the functional forms of the training data (Ruiz et al., 2014). Also, machine learning algorithms have been proven to be more intelligent than non-machine learning ones owing to their generality and flexibility in fitting many functional forms (Lary et al., 2016; Shafri, 2016).

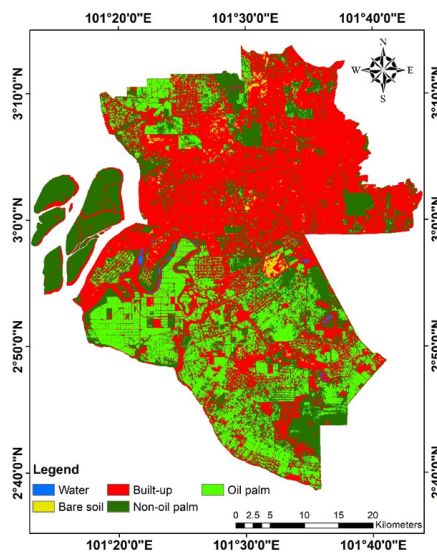


Figure 5(a). Result of maximum likelihood classifier

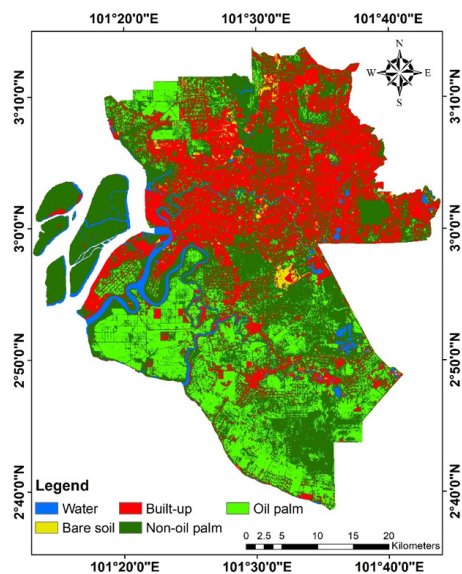


Figure 5(b). Result of support vector machine

Oil Palm Mapping Using Different Algorithms

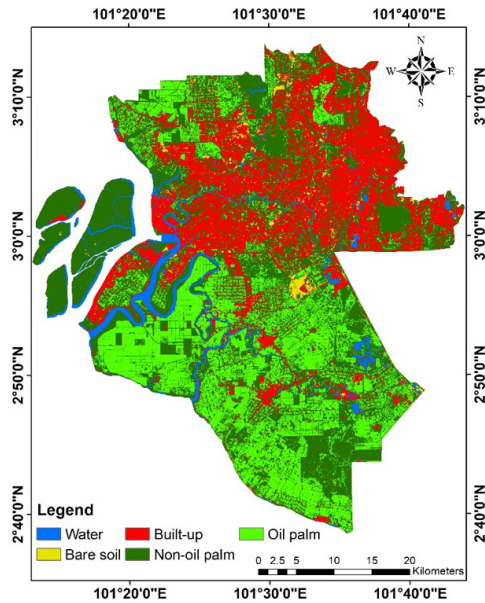


Figure 5(c). Result of artificial neural network

Table 1

Confusion matrix table for a classifier

		Truth					Total
		Class A	Class B	Class C	Class D	Class E	
Predicted	Class A	13098	0	0	0	5	13103
	Class B	0	296	0	0	0	296
	Class C	0	6	80	0	0	86
	Class D	0	0	0	504	39	543
	Class E	0	1	0	102	1388	1491
Total		13098	303	80	606	1432	15519

Table 2

Classification results for maximum likelihood classifier, support vector machine, and artificial neural network algorithms

Classifier	Overall accuracy (%)	Kappa coefficient
Maximum likelihood	15.30	0.1297
Support vector machine	98.96	0.9623
Artificial neural network	99.39	0.9779

McNemar's Test

McNemar's test is a statistical test which employs a 2 x 2 matrix to compare the significance of the difference between two methods. Usually, a significance level of 95% is used, for which a test is said to be statistically significant when $\rho \leq 0.05$. As per Table 2, the accuracies of the images produced by SVM and ANN were relatively close to each other. Subsequently, McNemar's test was done to compare the results between ANN and SVM. A p-value of 0.06 was obtained, while the chi-square (χ^2) was calculated as follows:

$$\chi^2 = \frac{(b-c)^2}{b+c} \quad (3)$$

Number of samples that were correctly identified by classifier 1 but wrongly classified by classifier 2, b ; Number of samples that were wrongly classified by classifier 1 but correctly classified by classifier 2, c

The value of χ^2 was 3.50 for 1 degree of freedom. Since the value was less than 3.84, the hypothesis that there was no association between the training samples and classifiers was accepted and as the model befitted the data. Also, the absence of a statistically significant association was also in light of the fact that the calculated p-value was greater than 0.05.

CONCLUSION

The main objective of this study is to measure the effectiveness of machine learning and non-machine learning algorithms on land cover mapping. With a slight difference of less than 0.5%, the results produced by SVM and ANN were considered to be comparable. Furthermore, these machine learning algorithms are capable of improving the accuracy of the map produced by optimising the desired parameters. In terms of overall accuracy, both aforementioned machine learning algorithms outperformed the non-machine learning parametric classifier, MLC by more than 83%. The effectiveness of machine learning algorithms in classifying the land cover – including the oil palm plantations – of the three districts was promising. The said gap has shown that machine learning was a powerful and an advanced algorithm that worked better than non-machine learning algorithms in the classification of images. The ability to produce highly accurate results with a limited number of training samples was an advantage of SVM. In addition, SVM is much easier to optimise the parameters. However, the ability of ANN to work like a human brain and learn from prior experience has led to its production of best overall accuracy result. Generally, areas of oil palm crops can be well-detected by machine learning algorithms. This method can later can be used for further analysis by quantifying information such as areas of biomass crops and estimations of yield for an optimisation and improvement. In conclusion, machine learning algorithms work better with limited training samples and produce better results than non-machine learning algorithms.

ACKNOWLEDGEMENT

The author would like to thank UPM for their facilities and funding of this research. Apart from that, our heartfelt gratitude also goes to Engineering and Physical Sciences Research Council for their financial support through the BEFEW project (Grant No. EP/P018165/1).

REFERENCES

- Agatonovic-Kustrin, S., & Beresford, R. (2000). Basic concepts of artificial neural network (ANN) modeling and its application in pharmaceutical research. *Journal of Pharmaceutical and Biomedical Analysis*, 22(5), 717-727.
- Ahmed, A. A., Pradhan, B., Sameen, M. I., & Makky, A. M. (2018). An optimized object-based analysis for vegetation mapping using integration of Quickbird and Sentinel-1 data. *Arabian Journal of Geosciences*, 11(11), 1-10.
- Awalludin, M. F., Sulaiman, O., Hashim, R., & Nadhari, W. N. A. W. (2015). An overview of the oil palm industry in Malaysia and its waste utilization through thermochemical conversion, specifically via liquefaction. *Renewable and Sustainable Energy Reviews*, 50, 1469-1484.
- Braga, J. R. G., Conte, G., Doherty, P., Velho, H. F. C., & Shiguemori, E. H. (2016). Use of artificial neural networks for automatic categorical change detection in satellite imagery. In *4th Conference of Computational Interdisciplinary Sciences* (pp. 1-13). São Paulo, Brazil.
- Cheng, Y., Yu, L., Xu, Y., Lu, H., Cracknell, A. P., Kanniah, K., & Gong, P. (2018). Mapping oil palm extent in Malaysia using ALOS-2 PALSAR-2 data. *International Journal of Remote Sensing*, 39(2), 432-452.
- Chong, K. L., Kanniah, K. D., Pohl, C. & Tan, K. P. (2017). A review of remote sensing applications for oil palm studies. *Geo-spatial Information Science*, 20(2), 184-200.
- Chuah, T. G., Ghani, W. A. W. A. K., Yunus, Robiah., & Omar, R. (2006). Biomass as the renewable energy sources in Malaysia: An overview. *International Journal of Green Energy*, 3(3), 323-346.
- Dibs, H., Idrees, M. O., & Alsalhin, G. B. A. (2017). Hierarchical classification approach for mapping rubber tree growth using per-pixel and object-oriented classifiers with SPOT-5 imagery. *The Egyptian Journal of Remote Sensing and Space Science*, 20(1), 21-30.
- Feizizadeh, B., Roodposhti, M. S., Blaschke, T., & Aryal, J. (2017). Comparing GIS-based support vector machine kernel functions for landslide susceptibility mapping. *Arabian Journal of Geosciences*, 10(5), 122.
- Gilbertson, J. K., Kemp, J., & Van Niekerk, A. (2017). Effect of pan-sharpening multi-temporal Landsat 8 imagery for crop type differentiation using different classification techniques. *Computers and Electronics in Agriculture*, 134, 151-159.
- Gómez, C., White, J. C., & Wulder, M. A. (2016). Optical remotely sensed time series data for land cover classification: A review. *ISPRS Journal of Photogrammetry and Remote Sensing*, 116, 55-72.
- Hermes, L., Friauff, D., Puzicha, J. & Buhmann, J. M. (1999). Support vector machines for land usage classification in Landsat TM imagery. In *Proceedings of International Geoscience and Remote Sensing Symposium* (Vol. 1, pp. 348-350). Hamburg, Germany.

- Hubert-Moy, L., Cotonnec, A., Le Du, L., Chardin, A., & Perez, P. (2001). A comparison of parametric classification procedures of remotely sensed data applied on different landscape units. *Remote Sensing of Environment*, 75(2), 174-187.
- Kavzoglu, T., & Colkesen, I. (2009). A kernel functions analysis for support vector machines for land cover classification. *International Journal of Applied Earth Observation and Geoinformation*, 11(5), 352-359.
- Koh, L. P., Miettinen, J., Liew, S. C., & Ghazoul, J. (2011). Remotely sensed evidence of tropical peatland conversion to oil palm. *Proceedings of the National Academy of Sciences*, 108(12), 5127-5132.
- Kumar, P., Gupta, D. K., Mishra, V. N., & Prasad, R. (2015). Comparison of support vector machine, artificial neural network, and spectral angle mapper algorithms for crop classification using LISS IV data. *International Journal of Remote Sensing*, 36(6), 1604-1617.
- Kuo, B. C., Ho, H. H., Li, C. H., Hung, C. C., & Taur, J. S. (2014). A kernel-based feature selection method for SVM with RBF kernel for hyperspectral image classification. *IEEE Journal of Selected Topics in Applied Earth Observations and Remote Sensing*, 7(1), 317-326.
- Lary, D. J., Alavi, A. H., Gandomi, A. H., & Walker, A. L. (2016). Machine learning in geosciences and remote sensing. *Geoscience Frontiers*, 7(1), 3-10.
- Li, L., Chen, Y., Xu, T., Liu, R., Shi, K., & Huang, C. (2015). Super-resolution mapping of wetland inundation from remote sensing imagery based on integration of back-propagation neural network and genetic algorithm. *Remote Sensing of Environment*, 164, 142-154.
- Li, L., Dong, J., Njeudeng Tenku, S., & Xiao, X. (2015). Mapping oil palm plantations in Cameroon using PALSAR 50-m Orthorectified Mosaic images. *Remote Sensing*, 7(2), 1206-1224.
- Mountrakis, G., Im, J., & Ogole, C. (2011). Support vector machines in remote sensing: A review. *ISPRS Journal of Photogrammetry and Remote Sensing*, 66(3), 247-259.
- Malaysian Palm Oil Board. (2016). *NKEA Biogas Working Group (BIOGAS WG). NKEA Biogas Working Group Report - Monthly update*. Bangi, Malaysia.
- Ng, W. P. Q., Lam, H. L., Ng, F. Y., Kamal, M., & Lim, J. H. E. (2012). Waste-to-wealth: Green potential from palm biomass in Malaysia. *Journal of Cleaner Production*, 34, 57-65.
- Nooni, I. K., Duker, A. A., Van Duren, I., Addae-Wireko, L., & Osei Jnr, E. M. (2014). Support vector machine to map oil palm in a heterogeneous environment. *International journal of Remote Sensing*, 35(13), 4778-4794.
- Pal, M. (2005). Random forest classifier for remote sensing classification. *International Journal of Remote Sensing*, 26(1), 217-222
- Peña, J. M., Gutiérrez, P. A., Hervás-Martínez, C., Six, J., Plant, R. E., & López-Granados, F. (2014). Object-based image classification of summer crops with machine learning methods. *Remote Sensing*, 6(6), 5019-5041.
- Rawat, J. S., & Kumar, M. (2015). Monitoring land use/cover change using remote sensing and GIS techniques: A case study of Hawalbagh block, district Almora, Uttarakhand, India. *The Egyptian Journal of Remote Sensing and Space Science*, 18(1), 77-84.

- Ruiz, P., Mateos, J., Camps-Valls, G., Molina, R., & Katsaggelos, A. K. (2014). Bayesian active remote sensing image classification. *IEEE Transactions on Geoscience and Remote Sensing*, 52(4), 2186-2196.
- Shaharum, N. S. N., Shafri, H. Z. M., Gambo, J., & Abidin, F. A. Z. (2018). Mapping of Krau Wildlife Reserve (KWR) protected area using landsat 8 and supervised classification algorithms. *Remote Sensing Applications: Society and Environment*, 10, 24-35.
- Shafri, H. Z. M., & Ramle, F. S. H. (2009). A comparison of support vector machine and decision tree classifications using satellite data of Langkawi Island. *Information Technology Journal*, 8(1), 64-70.
- Shafri, H. Z. M., & Zeen, R. M. (2011). Mapping Malaysian urban environment from airborne hyperspectral sensor system in the VIS-NIR (0.4-1.1 μm) Spectrum. *Research Journal of Environmental Sciences*, 5(6), 587.
- Shafri, H. Z. M. (2016). Machine learning in hyperspectral and multispectral remote sensing data analysis. In *Proceedings of the 2016 International Conference* (pp. 3-9). Shanghai, China.
- Shi, B., Bai, X., & Yao, C. (2017). An end-to-end trainable neural network for image-based sequence recognition and its application to scene text recognition. *IEEE Transactions on Pattern Analysis and Machine Intelligence*, 39(11), 2298-2304.
- Sumathi, S., Chai, S. P., & Mohamed, A. R. (2008). Utilization of oil palm as a source of renewable energy in Malaysia. *Renewable and Sustainable Energy Reviews*, 12(9), 2404-2421.
- Vapnik, V., Guyon, I., & Hastie, T. (1995). Support vector machines. *Mach Learn*, 20(3), 273-297.
- Wahid, B. O., Nordiana, A. A., & Tarmizi, A. M. (2005). Satellite mapping of oil palm land use. *MPOB Information Series, MPOB TT*, 255, 1511-7871.
- Wang, L., Zeng, Y., & Chen, T. (2015). Back propagation neural network with adaptive differential evolution algorithm for time series forecasting. *Expert Systems with Applications*, 42(2), 855-863.
- Yusoff, S. (2006). Renewable energy from palm oil—innovation on effective utilization of waste. *Journal of Cleaner Production*, 14(1), 87-93.



Modification of Quality Index Method Scheme for Nile Tilapia Fillets and Application in Quality Assessment of the Product Stored at Low Temperatures

Mai Thi Tuyet Nga^{1*} and Nguyen Thi Kieu Diem^{1,2}

¹Department of Food Technology, Faculty of Food Technology, Nha Trang University,
2 Nguyen Dinh Chieu Street, Nha Trang, Khanh Hoa, Vietnam.

²Faculty of Fisheries-Technology, Can Tho Technical Economic College,
9 Cach Mang Thang Tam Street, Ninh Kieu, Can Tho, Vietnam.

ABSTRACT

This work describes the modification of quality index method (QIM) scheme for de-skinned Nile tilapia (*Oreochromis niloticus*) fillets, firstly developed for the farmed product in Iceland, and its application in sensory evaluation of the product originated from Vietnam during low temperature storage. Three batches of tilapia fillets were used during modification of the QIM scheme. During the storage study, five stable storage temperature regimes were set at 1, 4, 9, 15 and $19 \pm 1^\circ\text{C}$, three batches of fish were assessed for every temperature. The modified QIM scheme consisted of 6 attributes, including Colour and Mucus of the skin side, Odour, Colour, Texture and Stickiness of the flesh (fillet side), with the total score or quality index (QI) of 13. Changes of some attributes and describing words from the previous scheme were made, due to the fish origin differences, to describe the sensory changes better. All the QI at different temperatures were in a well positive linear correlation with storage time. Furthermore, QI increased faster at higher storage temperatures. Parallel sensory evaluation by other methods like quantitative descriptive analysis (QDA) and Torry gave less clear sample differentiation throughout storage hours compared to QIM results. These supported the advantage of QIM over other methods and the application of QIM during cold chain management.

ARTICLE INFO

Article history:

Received: 24 October 2018

Accepted: 15 February 2019

Published: 21 June 2019

E-mail addresses:

ngamtt@ntu.edu.vn (Mai Thi Tuyet Nga)

ntkdiem@ctec.edu.vn (Nguyen Thi Kieu Diem)

* Corresponding author

Keywords: Chilled product, tilapia, quality index method, sensory.

INTRODUCTION

Sensory quality index method (QIM), originally developed by the Tasmanian Food Research Unit in Australia (Bremner, 1985) and further developed by European fisheries research institutions, was often used for freshness evaluation of raw fish materials. A QIM scheme consists of a number of attributes with demerit score range from 0 for very fresh fish to 1, 2, or 3 as the fish deteriorates (Martinsdóttir et al., 2001). The total score of all attributes called quality index (QI) is linearly correlated with time at a certain storage condition, thus useful for estimating the shelf life of the product. The method is considered unique and reliable as QIM scheme has been developed for each fish species and/or product.

Tilapia, one of the most popular aquaculture species (Cai, 2017), is widely promoted as a healthy protein source thanks to its high-quality protein and low-fat content. World production of tilapia was about 5.67 million tons from aquaculture and 0.7 tons from capture in 2015 (FAO, 2017); and reached over 6 million tons in 2016 with top producers including China, Indonesia, Egypt, Brazil, Bangladesh, the Philippines, Thailand, and Vietnam (VASEP, 2017). Nile tilapia production alone was more than 3.67 tons in 2014 (FAO FishStat, 2017), Tilapia fillets have gained popularity among consumers in the Europe, the United States, and elsewhere. The most popular form of this product is frozen, which may be thawed and purchased as chilled/fresh fish at retailers at later stage. Some significant part of tilapia fillets are also processed and purchased as fresh (Fitzsimmons, 2010).

Temperature and time of storage are main factors leading to the quality changes of seafood (Kreyenschmidt et al., 2010; Mai et al., 2011). A simple method for evaluating the freshness of seafood in general, and tilapia fillets stored at low temperatures in particular is therefore important. QIM scheme for fresh Nile tilapia fillets was first developed by Cyprian et al. (2013) based on fish farmed in “warmed water” recirculation aquaculture system in Iceland. However, our pre-observations on the sensory changes of similar product farmed in Vietnam showed some differences from the description of certain attributes, thus the scheme needs to be modified for the product originated from other climatic regions such as Vietnam.

The aim of this work was to modify the original QIM scheme of Cyprian et al. (2013), and apply the modified one to evaluate the sensory/freshness changes of the product during low temperature storage.

MATERIALS AND METHODS

Materials and Storage Design

De-skinned farmed Nile tilapia (*Oreochromis niloticus*) fillets of size 120-170 g/fillet were bought in individual quick frozen form from a processing company in An Giang province, Vietnam. Frozen fish fillets on the day of processing was packed in 30-kg expanded

polystyrene (EPS) boxes with gel mats on top and cover with tight lids. Boxes were then transported by car to the laboratories in Nha Trang city within 16 h. On arrival at the laboratories, fillets were repacked into polyamide (PA) packs (2 fillets/pack) and stored at $-18 \pm 2^\circ\text{C}$ for further experiments.

Before each trial, fish in PA packs were thawed overnight (for about 8 hours) in a refrigerator at $6-8^\circ\text{C}$. Fillets were then put on EPS trays (2 fillets/tray), covered with thin polyethylene (PE) film, and stored in a refrigerator with controlled temperature for the study.

Three batches of tilapia fillets were used during modification of the QIM scheme. During the storage study, five stable storage temperature regimes were set at 1, 4, 9, 15 and $19 \pm 1^\circ\text{C}$, three batches of fish were assessed for every temperature. Day 0 was the first day of storage at certain temperature regime. The temperatures selected for this study were based on the temperatures being practiced as seafood and meat storage temperatures at retails ($1, 4 \pm 1^\circ\text{C}$) and at household refrigerators ($4, 9 \pm 1^\circ\text{C}$), or abused during cabinet opening for loading/unloading, during purchasing and transportation from supermarkets to home ($9, 15, 19 \pm 1^\circ\text{C}$); Also, these temperatures have been used for product shelf life modelling (Bruckner et al., 2013).

Loggers of EC850A type (MicroLogPRO II, Israel) were used to monitor the temperatures of the refrigerator. Loggers DS1922L-F5 iButton® (Maxim Integrated Products, Inc., CA) were put on tray surfaces (top and bottom), and inside the trays in direct contact with the fish recording temperature at 10-min intervals.

Sensory Evaluation by QIM

Sensory evaluation was carried out by 3 panellists familiar with QIM, selected from the staffs of the Faculty of Food Technology.

The original QIM scheme (Cyprian et al., 2013) included 6 attributes, namely Skin side Colour (lateral stripes at the middle of the loin), Flesh Colour-loin, Flesh Colour-flap, Flesh Mucus, Flesh Texture, and Flesh Odour. The quality index was within the range of 0-13.

During the modification step, panellists were asked to use the original QIM scheme to score the freshness of the fish fillets from 3 batches of different storage days at $1 \pm 1^\circ\text{C}$. The evaluation was conducted in 3 sessions, with fish of 0-15 days of storage, give comments on the scheme, and note down other/undescribed sensory attributes/changes of the fillets. QIM scheme was then modified by removing those attributes and describing words, which were destructive and difficult to evaluate and recorded minor changes over storage time (Odoli, 2008; Sveinsdottir et al., 2003). More suitable parameters and describing words were added to the new scheme to better illustrate the quality changes of fish fillets with time.

During the storage study at five stable temperatures regimes ($1, 4, 9, 15$ and $19 \pm 1^\circ\text{C}$), the modified QIM scheme was applied.

Two fillets of each batch were used at each evaluation. Fillets were coded with 3-digit random numbers.

Sensory Evaluation by QDA and Torry

Quantitative descriptive analysis (QDA) and Torry methods were used in parallel to assess the freshness of fish fillets stored at 1 and 4 ± 1°C for comparison.

Sensory vocabulary for cooked tilapia (QDA) developed by Cyprian et al. (2013) was modified. The new scheme consisted of 7 odour attributes (Boiled potatoes, Fishy upon cooling, Mud, Ammonia, Mouldy, Rancid, and Putrid), 2 appearance descriptors (Colour: Light-Dark, and Surface: Smooth-Rough), 6 texture attributes (Flake, Softness, Fibre, Mushy, Chewy, Juicy), and 5 flavour parameters (Sweet, Fatty, Sour, Rancid, and Rotten).

Torry scheme for medium fat fish, developed by Shewan et al. (1953) and modified by former Icelandic Fisheries Laboratories, was applied for testing cooked samples as well. Fish with Torry score under 5.5 was considered unfit for human consumption.

The panel included 7 assessors, selected and trained according to ISO 8586: 2012. During the storage study, at each session judges evaluated 4 samples of 2 different storage time. Samples were taken at 0, 72, 144, 192, 216, 240, and 264 h of storage at 1 ± 1°C; and at 0, 48, 96, 120, 144, 168, and 192 h of storage at 4 ± 1°C.

Fillets were trimmed from belly and tail parts, cut into pieces of about 2-2.5 cm long and 2-3 cm wide, placed in coded aluminium boxes (1 piece per box), covered with aluminium foil lids, and cooked by steam at 95-100 °C for 10 minutes, and finally served to the panel.

Statistical Analysis

Microsoft Excel 2010 was used to calculate means and standard deviations and to build charts. Analysis of variance (ANOVA) with Tukey's test were conducted in SPSS 17.0 software to compare means at a significance level of 0.05.

RESULTS AND DISCUSSION

Modification of QIM scheme

The modified QIM scheme consisted of 6 attributes, including Colour and Mucus of the skin side, Odour, Colour, Texture and Stickiness of the flesh (fillet side), with the total score or quality index (QI) of 13, as shown in Table 1.

During the QIM scheme modification, it was observed that the skin side colour of tilapia fillets were different from those described by Cyprian et al. (2013), e.g. fresh fillets had pink colour instead of dark red or red brown. Furthermore, in this study mucus on skin side changed remarkably with time, while the change of flesh mucus could not be clearly observed as indicated by Cyprian et al. (2013), which might be due to the fact that our

fillets were packed skin side down in direct contact with the tray surface. The two attributes Flesh Colour-loin and Flesh Colour-flap from the original scheme were combined into the parameter Flesh Colour. Besides, the stickiness of the flesh when touching also changed with time, thus the attribute Stickiness was added to the new scheme. Differences in sensory pattern changes of tilapia fillets between this study and Cyprian et al. (2013) might be due to fish origin (Vietnam versus Iceland) and farming conditions (non-recirculation versus recirculation aquaculture systems). It is a common practice to remove unchangeable or difficultly recordable attributes from a QIM scheme (Cyprian et al., 2013; Sveinsdottir et al., 2003) to improve its applicability.

Freshness Evaluation of Tilapia Fillets using the Modified QIM Scheme

Quality index progress of deskinning of tilapia fillets stored at 1, 4, 9, 15, and 19 ± 1°C was illustrated in Figure 1. All the QI at the five temperature regimes were in a well positive linear correlation with storage time ($R^2 = 0.83, 0.95, 0.98, 0.96,$ and 0.98 for the storage at 1, 4, 9, 15, and 19 ± 1°C, respectively). Furthermore, QI increased faster at

Table 1

Modified QIM scheme for chilled stored deskinning tilapia fillets

Quality parameter		Description	Score
Skin side	Colour	Pink, bright, lateral stripes reddish	0
		Pinkish, somewhat bright, sparse visible black thread, lateral stripes pale red with blue spots	1
		Bluish, greyish, or brownish, more visible black thread, lateral stripes brownish surrounded by yellow colour or covered by a thin opaque white film	2
	Mucus	Little or almost no mucus	0
		Thin opaque mucus	1
		Thick dry mucus	2
		Thick, dry, and clotted mucus	3
Fillet side/ Flesh	Odour	Fresh, light seaweed and/or grass smell	0
		Light marine, light alcohol	1
		Sour	2
		Acetic, putrid	3
	Colour	Pink, homogenous, bright/shiny	0
		Pinkish, not so homogenous, bluish around the longitudinal stripes at the middle of the loin	1
		Greyish, and/or yellowish, inhomogeneous, pale, sparse visible black thread, longitudinal stripes pale red to brownish, belly and tail parts turn yellow, blue-yellow, dark	2

Table 1 (Continued)

Quality Parameter	Description	Score
Texture	Firm	0
	Rather soft	1
	Soft	2
Stickiness	No flesh scraps attached to hands (after touching the fillet)	0
	Some or a lot of flesh scraps attached to hands (after touching the fillet)	1
Quality index (QI) (0-13)		

higher temperatures. This is in accordance with the QIM development procedure, which is to make the QI linearly correlated with storage time (Cyprian et al., 2008; Sykes et al., 2009; Sveinsdottir et al., 2003).

Significant growth ($p < 0.05$) of QI was observed after 192 h at $1 \pm 1^\circ\text{C}$, 144 h at $4 \pm 1^\circ\text{C}$, 48 h at $9 \pm 1^\circ\text{C}$, 63 h at $15 \pm 1^\circ\text{C}$, and 44 h at $19 \pm 1^\circ\text{C}$ (Figure 1). At the end of the shelf life, QI is normally around 75% of the maximal total QI (Sykes et al., 2009; Mai, 2014; Mai & Huynh, 2017). In this study, based on the time of fish rejection determined by the total viable count (TVC) level of 10^6 colony forming unit (CFU) per g (Decision 46-2007/QD-BYT, 2007), shelf life of tilapia fillets stored at $1, 4, 9, 15,$ and $19 \pm 1^\circ\text{C}$ were below 144, 48, 24, 24, and 20 h, respectively, when the TVC were $1.10 \times 10^7, 2.43 \times 10^6, 1.17 \times 10^6, 1.83 \times 10^7,$ and 1.28×10^8 CFU/g, accordingly. The QI after 144 h at $1 \pm 1^\circ\text{C}$ was as high as 4, accounting for only 30.8% of the maximal QI. The highest QI at $4 \pm 1^\circ\text{C}$ after 48 h, $9 \pm 1^\circ\text{C}$ after 24 h, $15 \pm 1^\circ\text{C}$ after 24 h, and $19 \pm 1^\circ\text{C}$ after 20 h were 5.9 (45.4%), 1.5 (11.5%), 1.8 (13.8%), and 5.2 (40.0%), respectively. The lower percentage of QI at the end of the product shelf life in this study compared to others, e.g. the case of *Pangasius* fillets at similar storage temperatures in a study of Mai and Huynh (2017), might be contributed by high initial TVC of tilapia fillets in this research ($5.29 \pm 3.87.10^5$ CFU/g (data not shown), closed to the acceptable limit of 10^6 CFU/g). This revealed the importance of good hygiene practices to keep microbial counts as low as possible, in order to maintain the quality and prolong the shelf life of aquatic products.

Freshness Evaluation of Tilapia Using QDA and Torry Scheme

Results of assessment of cooked samples prepared from tilapia fillets stored at 1 and $4 \pm 1^\circ\text{C}$ by QDA are shown in Table 2. At $1 \pm 1^\circ\text{C}$, only 3 out of 20 QDA attributes were detected with significant differences ($p < 0.05$) between storage hours, however, no correlation change with time was observed. At $4 \pm 1^\circ\text{C}$, only 1 descriptor (Flavour Sweet) decreased significantly ($p < 0.05$) after 194 h. In addition, there was no high

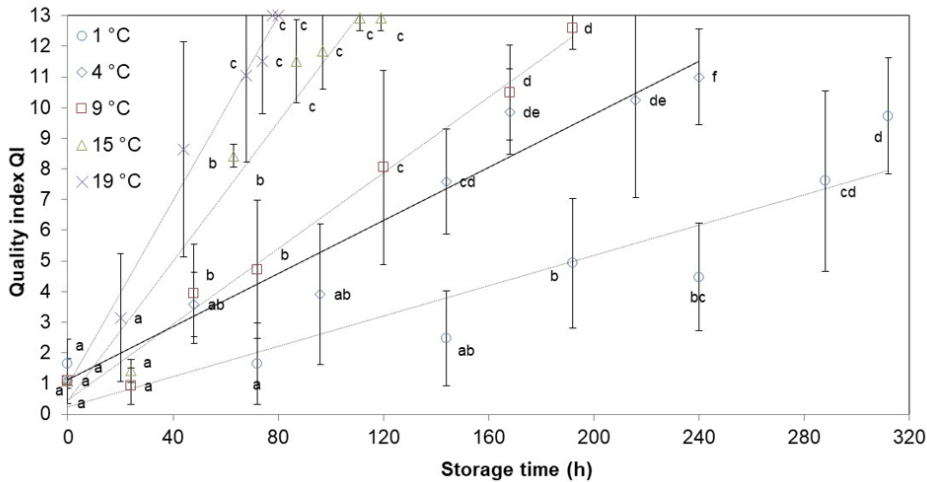


Figure 1. Changes of quality index (QI) of tilapia fillets stored at 1, 4, 9, 15, and 19 ± 1 °C over storage time. Different letters within the same storage temperature indicate significant differences ($p < 0.05$) in Torry scores between storage hours

enough score (≥ 20 on the scale 0-100) of bad attributes (e.g. Odour Mouldy, Rancid, or Putrid; Flavour Sour, Rancid or Rotten) to signal the rejection point of the product at both studied temperature regimes during the storage time. Rancid, putrid/rotten/spoilage and mouldy/musty odour and flavour are considered spoilage attributes of chilled-stored fish (Cyprian et al., 2008; Mai, 2013; Mai, 2014; Sveinsdóttir et al., 2002). The average score of above 20 for these negative parameters has been applied to determine the end of chilled seafood shelf life (Bonilla et al., 2007; Cyprian et al., 2008; Cyprian et al., 2013; Mai, 2013; Mai, 2014; Magnusson et al., 2006; Sveinsdóttir et al., 2002).

Linear correlation between Torry score and storage time was observed for both temperature regime 1 and 4 ± 1°C (Figure 2), which is in accordance with the characteristics of Torry score of other fresh fish products (Martinsdóttir et al., 2001). At storage temperature 1 ± 1°C, there was no difference ($p > 0.05$) in Torry scores during storage hours from 0 to 264 (Figure 2). The score after 264 h was 7 ± 1.2 , i.e. higher than the acceptable limit of 5.5 (Mai et al., 2011), while the TVC exceeded the allowable limit of 6 log CFU/g (Decision 46-2007/QD-BYT, 2007) after 144 h at 1 ± 1°C. At storage temperature 4 ± 1°C, significant drop ($p < 0.05$) of Torry score was observed after 144 h (Figure 2), when the score reached 6.6 ± 0.9 (> 5.5). Meanwhile TVC was higher than the allowable limit just after 48 h at 4 ± 1°C.

These above show that QIM was more sensitive than QDA and Torry methods in detecting the sensory changes of tilapia fillets stored at low temperatures. Similar findings were reported for cobia portion sensory evaluation (Mai, 2014), where QIM showed more advantageous compared to Torry method.

Results from this study also support those of Mai and Huynh (2017) that freshness and remaining shelf life of seafood should be judged based on the worst quality indicator, the one that exceed its acceptable limit the soonest/earliest during storage.

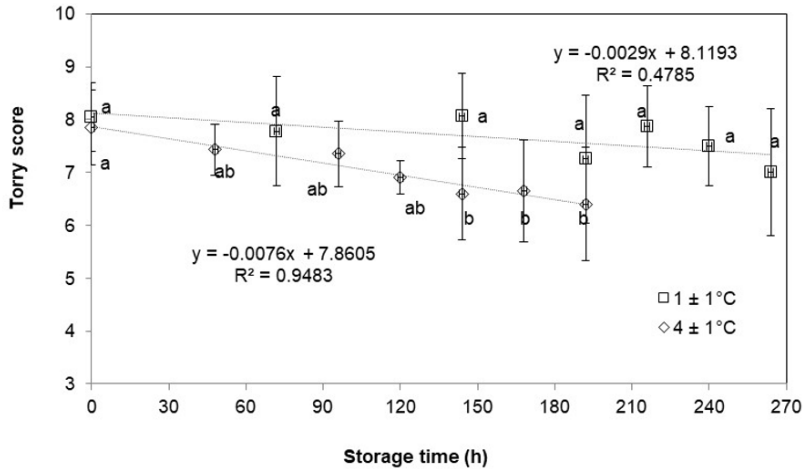


Figure 2. Changes of Torry scores of tilapia fillets stored at 1 and 4 ± 1°C over storage time. Different letters within the same storage temperature indicate significant differences (p < 0.05) in Torry scores between storage hours

Table 2

QDA attributes' scores of tilapia fillets stored at 1 and 4 ± 1°C

QDA attribute	Storage time (h) at 1°C						
	0	72	144	192	216	240	264
O_Boiled potatoes	45.73 ^a	44.60 ^a	51.07 ^a	56.40 ^a	54.07 ^a	45.07 ^a	59.67 ^a
O_Fishy	20.40 ^a	24.53 ^a	25.33 ^a	17.33 ^a	24.53 ^a	23.40 ^a	17.47 ^a
O_Mud	15.87 ^a	14.20 ^a	10.20 ^a	11.67 ^a	11.67 ^a	11.33 ^a	12.33 ^a
O_Ammonia	7.73 ^a	5.27 ^a	4.87 ^a	9.94 ^a	7.93 ^a	10.73 ^a	14.33 ^a
O_Mouldy	1.73 ^a	3.60 ^a	3.07 ^a	2.53 ^a	4.07 ^a	3.53 ^a	3.60 ^a
O_Rancid	0.60 ^a	1.27 ^a	0.73 ^a	1.20 ^a	1.73 ^a	1.33 ^a	2.07 ^a
O_Putrid	0.93 ^a	1.33 ^a	1.40 ^a	3.93 ^a	3.20 ^a	2.80 ^a	6.13 ^a

Table 2 (Continued)

QDA attribute	Storage time (h) at 1°C						
	0	72	144	192	216	240	264
A_Light-Dark	52.67 ^a	47.34 ^{ab}	25.60 ^b	50.47 ^{ab}	44.80 ^{ab}	39.47 ^{ab}	51.73 ^{ab}
A_Smooth-Rough	37.67 ^{ab}	47.93 ^a	20.93 ^b	43.27 ^{ab}	26.13 ^{ab}	33.47 ^{ab}	33.27 ^{ab}
T_Flake	35.40 ^a	38.33 ^a	30.20 ^a	37.20 ^a	37.40 ^a	33.67 ^a	37.33 ^a
T_Softness	48.00 ^a	51.60 ^a	38.00 ^a	52.13 ^a	44.47 ^a	48.27 ^a	50.13 ^a
T_Fibre	41.20 ^{ab}	45.33 ^{ab}	28.60 ^a	50.73 ^b	44.27 ^{ab}	42.13 ^{ab}	50.67 ^b
T_Mushy	29.07 ^a	32.47 ^a	27.53 ^a	35.27 ^a	38.20 ^a	33.00 ^a	33.93 ^a
T_Chewy	40.60 ^a	54.80 ^a	55.53 ^a	45.33 ^a	54.47 ^a	46.60 ^a	43.80 ^a
T_Juicy	31.13 ^a	33.00 ^a	44.67 ^a	36.60 ^a	38.07 ^a	42.20 ^a	34.67 ^a
F_Sweet	48.67 ^a	43.87 ^a	39.00 ^a	29.07 ^a	32.20 ^a	38.53 ^a	26.00 ^a
F_Fatty	9.27 ^a	10.27 ^a	13.27 ^a	4.60 ^a	12.87 ^a	9.07 ^a	4.73 ^a
F_Sour	3.07 ^a	1.20 ^a	2.53 ^a	7.93 ^a	4.47 ^a	3.80 ^a	4.34 ^a
F_Rancid	0.53 ^a	1.47 ^a	0.00 ^a	0.47 ^a	0.07 ^a	0.67 ^a	0.53 ^a
F_Rotten	0.07 ^a	0.07 ^a	0.00 ^a	5.47 ^a	0.00 ^a	0.33 ^a	0.40 ^a
	Storage time (h) at 4°C						
	0	48	96	120	144	168	192
O_Boiled potatoes	46.67 ^a	51.54 ^a	49.93 ^a	47.40 ^a	44.53 ^a	49.00 ^a	43.73 ^a
O_Fishy	19.53 ^a	18.27 ^a	19.53 ^a	15.87 ^a	15.93 ^a	22.40 ^a	14.53 ^a
O_Mud	7.73 ^a	11.20 ^a	9.67 ^a	8.27 ^a	10.20 ^a	6.13 ^a	12.33 ^a
O_Ammonia	11.67 ^a	14.60 ^a	13.93 ^a	11.40 ^a	15.07 ^a	8.93 ^a	11.73 ^a
O_Mouldy	3.53 ^a	3.40 ^a	8.00 ^a	5.20 ^a	5.80 ^a	2.93 ^a	4.87 ^a
O_Rancid	3.27 ^a	2.93 ^a	7.87 ^a	5.73 ^a	4.47 ^a	2.33 ^a	7.33 ^a
O_Putrid	6.00 ^a	4.73 ^a	5.27 ^a	5.93 ^a	5.27 ^a	6.87 ^a	4.73 ^a
A_Light-Dark	53.27 ^a	47.87 ^a	54.40 ^a	39.53 ^a	43.27 ^a	44.53 ^a	47.40 ^a
A_Smooth-Rough	32.07 ^a	39.73 ^a	42.00 ^a	36.93 ^a	42.40 ^a	35.87 ^a	36.93 ^a
T_Flake	41.20 ^a	44.20 ^a	45.27 ^a	38.54 ^a	50.33 ^a	50.53 ^a	56.13 ^a
T_Softness	32.93 ^a	41.13 ^a	40.80 ^a	41.27 ^a	47.80 ^a	51.67 ^a	46.20 ^a
T_Fibre	37.40 ^a	44.13 ^a	43.67 ^a	48.73 ^a	50.40 ^a	52.07 ^a	43.93 ^a
T_Mushy	35.53 ^a	38.07 ^a	33.40 ^a	37.60 ^a	44.00 ^a	45.13 ^a	41.33 ^a
T_Chewy	53.33 ^a	43.40 ^a	43.33 ^a	46.73 ^a	39.73 ^a	47.60 ^a	38.07 ^a
T_Juicy	47.20 ^a	39.20 ^a	40.07 ^a	29.67	35.53 ^a	30.33 ^a	30.47 ^a
F_Sweet	44.20 ^a	39.60 ^{ab}	37.94 ^{ab}	25.67 ^{ab}	35.87 ^{ab}	27.47 ^{ab}	15.33 ^b
F_Fatty	8.67 ^a	5.80 ^a	10.34 ^a	5.47 ^a	4.53 ^a	10.53 ^a	2.13 ^a
F_Sour	1.13 ^a	3.67 ^a	3.20 ^a	1.87 ^a	4.20 ^a	4.27 ^a	1.53 ^a
F_Rancid	0.00 ^a	0.33 ^a	3.27 ^a	0.60 ^a	0.53 ^a	2.40 ^a	1.73 ^a
F_Rotten	0.00 ^a	0.13 ^a	2.67 ^a	0.33 ^a	0.27 ^a	0.80 ^a	0.60 ^a

*Values followed by the different letters (a, b) within the same row are significantly different from each other ($p < 0.05$). Capitalized letter O denotes for Odour, A for Appearance, T for Texture, and F for Flavour.

CONCLUSIONS

All the QI at different stable temperatures were linearly correlated with storage time, and QI increased faster at higher temperatures. Quality index method showed to be more

sensitive than QDA and Torry in detecting the quality changes of fish over time, which supported the advantage of QIM compared to other methods and the application of QIM during cold chain management.

ACKNOWLEDGEMENTS

The authors would like to acknowledge VLIR Network Vietnam for partly sponsoring this work. The first author would like to thank NORHED Project: “Incorporating Climate Change into Ecosystem Approaches to Fisheries and Aquaculture Management in Sri-Lanka and Vietnam” (QZA-0485 SRV-13/0010) for the conference travel grant.

REFERENCES

- Bonilla, A. C., Sveinsdottir, K., & Martinsdottir, E. (2007). Development of Quality Index Method (QIM) scheme for fresh cod (*Gadus morhua*) fillets and application in shelf life study. *Food Control*, 18(4), 352–358.
- Bremner, A. (1985). A convenient easy to use system for estimating the quality of chilled seafood. In C. Scott, D., Summers, N., Nelson (Ed.), *Proceedings of the fish processing conference* (pp. 59–73). New Zealand: Fish Processing Bulletin.
- Bruckner, S., Albrecht, A., Petersen, B., & Kreyenschmidt, J. (2013). A predictive shelf life model as a tool for the improvement of quality management in pork and poultry chains. *Food Control*, 29(2), 451–460.
- Cai, J. (2017). Improving the technical and economic performance of tilapia farming under climate variation from a bio-economic modelling perspective. *FAO Aquaculture Newsletter*, 56, 40–41.
- Cyprian, O., Lauzon, H. L., Jóhannsson, R., Sveinsdóttir, K., Arason, S., & Martinsdóttir, E. (2013). Shelf life of air and modified atmosphere-packaged fresh tilapia (*Oreochromis niloticus*) fillets stored under chilled and superchilled conditions. *Food Science and Nutrition*, 1(2), 130–140.
- Cyprian, O. O., Sveinsdóttir, K., Magnússon, H., & Martinsdóttir, E. (2008). Quality Index Method (QIM) scheme and effects of short-time temperature abuse in shelf life study of fresh water arctic char (*Salvelinus alpinus*). *Journal of Aquatic Food Product Technology*, 17(3), 303–321.
- Decision 46/2007/QD-BYT. (2007). *Decision of the Minister of Health of Vietnam dated 19 December 2007 on the maximum acceptable limits of chemical and biological contamination in food*. Hanoi, Vietnam: Ministry of Health.
- FAO. (2017). *Fisheries and aquaculture statistics 2015*. Rome: Food and Agriculture Organization of the United Nations.
- FAO FishStat. (2017). *FishStatJ - software for fishery statistical time series*. Retrieved March 22, 2018 from <http://www.fao.org/fishery/statistics/software/fishstatj/en>
- Fitzsimmons, K. (2010 October 17-20). Potential to increase global tilapia production. In *Global Outlook for Aquaculture Leadership (GOAL) Conference* (p. 35). Kuala Lumpur, Malaysia.

- ISO. (2012). *ISO 8586:2012. Sensory analysis - General guidelines for the selection, training and monitoring of selected assessors and expert sensory assessors*. Geneva, Switzerland: The International Organization for Standardization.
- Kreyenschmidt, J., Christiansen, H., Hübner, A., Raab, V., & Petersen, B. (2010). A novel photochromic time-temperature indicator to support cold chain management. *International Journal of Food Science & Technology*, 45(2), 208–215.
- Magnússon, H., Sveinsdóttir, K., Lauzon, H. L., Thorkelsdóttir, Á., & Martinsdóttir, E. (2006). Keeping quality of desalted cod fillets in consumer packs. *Journal of food science*, 71(2), M69-M76.
- Mai, N., & Huynh, V. (2017). Kinetics of quality changes of pangasius fillets at stable and dynamic temperatures, simulating downstream cold chain conditions. *Journal of Food Quality*, 2017, 1-9.
- Mai, N. T. T., Gudjónsdóttir, M., Lauzon, H. L., Sveinsdóttir, K., Martinsdóttir, E., Audorff, H., Reichstein, W., Haarer, D., Bogason, S. G., & Arason, S. (2011). Continuous quality and shelf life monitoring of retail-packed fresh cod loins in comparison with conventional methods. *Food Control*, 22(6), 1000–1007.
- Mai, T. T. N. (2013). Development of sensory attributes for farmed cobia (*Rachycentron canadum*) used in quantitative descriptive analysis (QDA). *Journal of Fisheries Science and Technology (Vietnam)*, 3, 27–32.
- Mai, T. T. N. (2014). Application of quality index method for freshness evaluation of chilled-stored farmed cobia (*Rachycentron canadum*) portions. In *SPISE2014 Summer Program in Sensory Evaluation* (pp. 21–26). Ho Chi Minh, Vietnam: Ho Chi Minh City Publishing House.
- Martinsdóttir, E., Sveinsdóttir, K., Luten, J., Schelvis-Smit, R., & Hyldig, G. (2001). *Reference manual for the fish sector: sensory evaluation of fish freshness*. Denmark, Europe: QIM Eurofish.
- Odoli, C. O. (2009). *Optimal storage conditions for fresh farmed tilapia (Oreochromis niloticus) fillets*. (Unpublished Master thesis). Department of Food Science and Nutrition, University of Iceland, Iceland.
- Shewan, J. M., Macintosh, R. G., Tucker, C. G. & Ehrenberg, A. S. C. (1953). The development of a numerical scoring system for the sensory assessment of the spoilage of wet white fish stored in ice. *Journal of Science and Food Agriculture*, 4(6), 283–298.
- Sveinsdottir, K., Hyldig, G., Martinsdottir, E., Jorgensen, B. & Kristbergsson, K. (2003). Quality Index Method (QIM) scheme developed for farmed Atlantic salmon (*Salmo salar*). *Food Quality and Preference*, 14(3), 237–245.
- Sveinsdóttir, K., Martinsdóttir, E., Hyldig, G., Jørgensen, B., & Kristbergsson, K. (2002). Application of Quality Index Method (QIM) scheme in shelf-life study of farmed atlantic salmon (*Salmo salar*). *Journal of Food Science*, 67(4), 1570–1579.
- Sykes, A. V., Oliveira, A. R., Domingues, P. M., Cardoso, C. M., Andrade, J. P., & Nunes, M. L. (2009). Assessment of European cuttlefish (*Sepia officinalis* L.) nutritional value and freshness under ice storage using a developed Quality Index Method (QIM) and biochemical methods. *LWT - Food Science and Technology*, 42(1), 424–432.
- VASEP. (2017). Vietnam association of seafood exporters and producers. Retrieved March 24, 2018, from <http://hoinghecavietnam.org.vn/tinchitiet.aspx?newsid=5581&&cateid=>



Physical and Mechanical Properties of Unripe *Nipah* Banana Fruit (*Musa acuminata balbisiana*)

Farahana Nabilah Zainal A'bidin¹, Rosnah Shamsudin^{1,2*},
Mohd Salahuddin Mohd Basri¹ and Zanariah Mohd Dom¹

¹Department of Process and Food Engineering, Faculty of Engineering, Universiti Putra Malaysia, 43400, UPM Serdang, Selangor, Malaysia

²Halal Product Research Institute, Universiti Putra Malaysia, 43000 UPM, Serdang, Selangor, Malaysia

ABSTRACT

This paper describes the properties determined to acquire physical and mechanical properties of unripe *Nipah* banana. In Malaysia, most of the banana chips processing companies use a variety from *Nipah Banana*, also known as *Musa acuminata balbisiana* a triploid hybrid banana cultivar. The physical (diameter, weight and peel thickness on edge and side) and mechanical properties (penetration and compression test) of *Nipah Banana* variety were determined through five consecutive days to evaluate its behaviour throughout its ripening period. The average diameter is 38.78 ± 5.77 mm x 29.25 ± 4.92 mm. The average thickness of peel at the edge and side are 5.3 ± 0.93 mm and 3.65 ± 1.01 mm respectively. The average weight of the *Nipah* banana variety is 77.85 ± 28.61 g. Penetration force through 5 ripening days was found to decrease from 7.53N to 6.59 N (top position), 7.59N to 6.40N (middle position) and 8.31N to 6.43N (bottom position). The compressive force decreases

through 3 days from 1704 N to 1630 N with the sudden increase in day 4 to 1380 Using the following properties accumulated, the machine components specification can be obtained which are the blade force required to slit the banana peel, the thickness of the blade needed for the slitting of banana peel, the roller force to hold the banana in place and the peeler size.

Keywords: Banana, mechanical properties, peeling machine, physical properties

ARTICLE INFO

Article history:

Received: 24 October 2018

Accepted: 15 February 2019

Published: 21 June 2019

E-mail addresses:

fara_bila02@yahoo.com (Farahana Nabilah Zainal A'bidin)

rosnahs@upm.edu.my (Rosnah Shamsudin)

salahuddin@upm.edu.my (Mohd Salahuddin Mohd Basri)

nana@upm.edu.my (Zanariah Mohd Dom)

* Corresponding author

INTRODUCTION

Malaysia is famous for its tropical weather which results in massive agriculture activities. Agriculture activities contribute to at least a third of the country's population livelihood. Various types of fruits are available in the country such as watermelon, pineapple, orange and banana. However, it is found that banana is the most consumed fruit in Malaysia. Having banana as the second largest production area and the fifth in export revenue for Malaysia, with local consumption per capita of 9.4kg in 2014 (Department of Statistics Malaysia, 2011).

Apart from Malaysia, banana can also be found in many places across the wet tropics and subtropics such as in America, Africa, South Asia, Island South-east Asia and the Pacific. Countries such as India, China, Ecuador, Brazil, and Philippines are the top banana producing countries in the world. In 2001, the annual world consumption of banana reached 5.2kg/person as bananas have been the staple foods for many people around the world as it provides 10 to 27% of daily calorie intake (Ammawath et al., 2001). The fully ripe banana can be consumed raw by all and has a sweet taste. Besides, banana can also be cooked to become fried banana, banana cue, banana chips and maruya. Now, a lot of banana based products has been introduced widely which can contribute in increasing the world banana consumption.

In Malaysia, as banana is a highly consumed fruit, a lot of entrepreneurs are making variety of banana by-products. One of the famous by-products is banana chips. Banana chips are one of the products made for mass production. From the year 1996 until 2000, the industrial growth performance of banana chips shows a 70% increase within Malaysia. Based on the survey reported by Hamir and Ariff (2006), the average production of banana chips should be around 113.8 tonnes per month, however, the production rate is very low which is at 59% (Hamir & Ariff, 2006). Until now, in banana chips processing, the peeling process is still being done using manual hand peeling method which is by using their own hand and knife as a tool to separate the peel. This method is unhygienic and has low production rate. There is a need to develop a banana peeling machine to overcome the 41% of unutilised banana. Thus, a preliminary data gathering for machine components specification is conducted. The physical and mechanical properties of the banana are required to specify the size of the peeling mechanism and other parts of the machine.

Physical and mechanical properties of fruits are important data in food engineering as well as agricultural machine. Which is why, in designing an agricultural machine, most of the inventors examine their properties as a start. Many previous studies for fruit properties have been made with orange (Singh & Reddy, 2006), okro (Owolarafe & Shotonde, 2004), longan (Shi et al., 2016), apple (Ganai et al., 2016) and pomegranate (Radunić et al., 2015). Singh and Reddy (2006) measured the properties of orange peel through days to examine

its behaviour. Owolarafe and Shotonde (2004) examined the okro fruit properties for an okro slicer, chopper and grater machine development.

Banana fruits properties were also done by many researchers such as Soltani et al. (2011). Soltani et al. (2011) used the inner and outer length of the banana to measure the banana curvature. They also estimated the ellipsoid volume of banana fruit by weight. Besides that, there is also Kachru et al. (1995) who investigated two varieties of banana followed by their physical and mechanical properties. This paper aims to investigate some physical properties of *Nipah* banana fruit including weight, peel thickness at the plane and edge, diameter, penetration as well as compression force to identify the machine components specifications.

MATERIALS AND METHODS

Sample Preparation

Banana fruits of triploid hybrid banana cultivar which were fully matured but unripe with maturity index 1 were obtained from a small farm in Kampung Sungai Lang, Banting. Maturity index of bananas was referred based on standard grading by Federal Agricultural Marketing Authority (FAMA). The banana was stored at room temperature 25°C. The samples were randomly selected from the bunch and divided accordingly to different types of properties that are diameter (mm), peel thickness (mm), penetration (g) and compression force (N). 20 bananas were used for each property, only diameter and peel thickness used the same banana sample. After being studied, banana chips factories process bananas in the first three days of harvest only. Thus, the sample testing continued until the fifth day to evaluate its difference. For each day, four bananas were used to evaluate the mechanical properties. Experimental data obtained from penetration and compression force test were then plotted in a graph to determine their relationship with ripening period.

Diameter, Peel Thickness and Weight of Fruit

Banana (20 hands) were used to determine the diameter (mm), peel thickness (mm) and weight (kg). The diameter and peel thickness of the banana were recorded at three planes along the longitudinal axis of fruits, one plane in the middle and two in the middle of the banana that was cut in half as in Figure 1(a) similarly to the method by Kachru et al. (1995). It is labelled as top, middle and bottom. Since the banana shape is not circular and has an average of four planes, the diameter is measured as a rectangular shape which is described as height in mm and width in mm. The average height was measured on the upper part of the banana while the width was measured at the side of the banana. As for peel thickness, the thickness was measured at the side and edge of each plane. Diameter and thickness measurement are illustrated in Figure 1(b) for better understanding. Both

diameter and peel thickness of the banana were measured using Vernier calliper (Generic, China). The banana weight was measured using electronic weighing scale (Mettler Toledo, Model SB12001, Switzerland). All physical measurement on each plane were replicated three times and averaged out. An average of the banana physical properties measured was determined to get an overall representation of physical properties of banana fruit and reducing the chances of error.

Mechanical Properties of Fruit

Penetration Test. A penetration test is a test whereby a needle probe of 2mm diameter is passed through a sample with customized depth to obtain physical properties. It can be performed on a variety of food which is very useful for simulating the slitting mechanism of the banana peeler. This test is important to evaluate the force to penetrate the banana peel where the data obtained can be used to design agricultural machines. The sample was stored at room temperature of 25°C along 5 days of the test. A penetration test was done by puncturing each sample at the edge of the banana plane at three different spots which were at the top, middle and bottom (Hou et al., 2015) as shown in Figure 1(c) and Figure 2(a). The experiment was replicated four times and made at the same spot with different sides for each day. The test was conducted using texture analyser (Stable Micro Systems, TA.XTPlus, UK) equipped with a 5kg load cell and stainless-steel probe (PN-2) of 2mm diameter needle in compression mode. The operating settings of the instrument were: pre-test speed, 1mm/s, test speed, 2mm/s and post-test speed, 12mm/s. The force at an average thickness of banana with 16 readings of each ripening period was obtained. Penetration force is the force required to cut the edge of the banana in a longitudinal direction. It is used as the first step in peeling the banana.

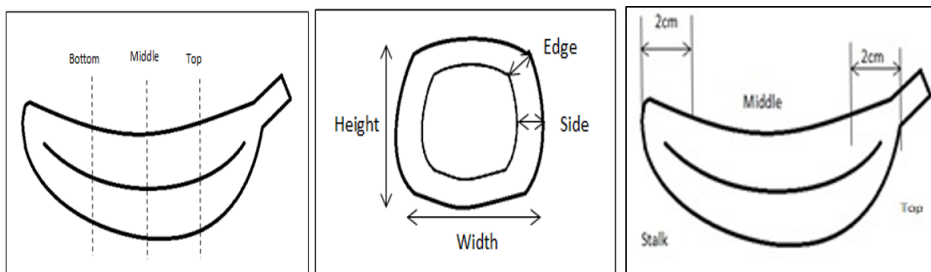


Figure 1(a). Banana section for physical measurement; (b) The banana diameter and thickness measurement; (c) Banana section for penetration force

Compression Test. A compression test is a test in which a sample is placed on a flat surface with an upper compression probe pushed down to the sample. Compression test is used for obtaining hardness, cohesiveness, springiness, and chewiness. With the test, textural attributes obtained can be used for machine designing. Compression test was

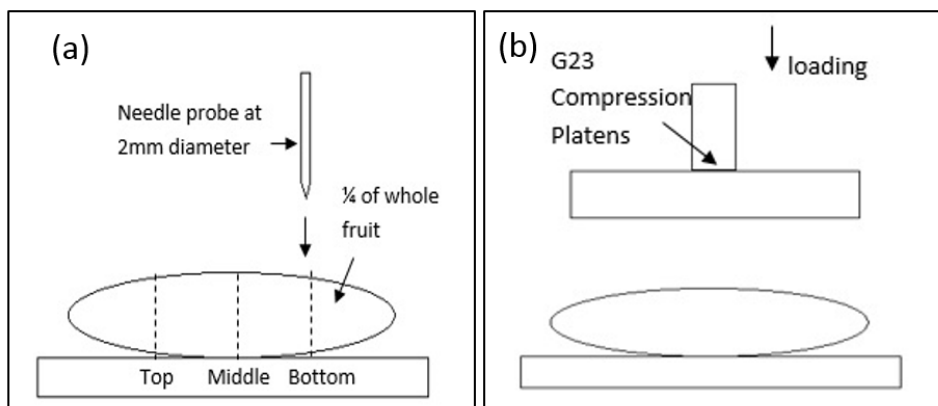


Figure 2(a). Penetration test; 2(b). Compression test

done by compressing each sample using a compression test fixture as shown in Figure 2(b). Four readings using four banana samples were obtained for each day. Banana fruits were stored at room temperature of 25°C for 5 days. The test was conducted using Instron Universal Testing Machine (Model 5566, USA) equipped with a 10kg load cell and a G23 Compression Platens. The operating settings of the instrument were: pre-test speed, 1.5cm/s. The test was stopped manually after a cracking sound was heard as it indicated the breakpoint. The load at break of banana was obtained and presented as maximum compressive force, C (N). Average of four readings of each ripening period was obtained.

RESULTS AND DISCUSSION

Diameter, Peel Thickness and Weight of Fruit

Physical properties of the banana which are the diameter, thickness of peel and weight are presented in Table 1. The weight of *Nipah* banana varies between 46.40 g and 150.90 g with an average value of 77.85 g while the diameter varies between 25.99 mm x 19.66 mm and 52.48 mm x 43.87 mm with an average value of 38.78 mm x 29.25 mm. Peel thickness at the edge varies between 3.54 mm and 7.37 mm with an average value of 5.3 mm while at the side is between 2.1 mm and 7.16 mm with an average of 3.65 mm. Previous research from Kachru et al. (1995) acquired some physical properties of Scavendish and Nendran banana variety. One of it was peel thickness. They obtained average peel thickness on the side for the two banana varieties with the value of 3.65 mm and 2.95 mm respectively. From the data obtained, both Scavendish and *Nipah* banana variety have similar peel thickness.

From Table 1, it can be concluded that the peel thickness of *Nipah* banana fruit at the edges of the plane is higher than the sides. Average edge peel thickness was measured at 5.30mm.while side peel thickness was 3.65 mm which was 44.18% different. This

difference is due to the rectangular shape of *Nipah* banana. Using the data obtained, some of the peeling machine component specifications can be determined. The thickness of the peel is used to determine the blade thickness for banana slitting mechanism. The minimum diameter will be used for entrance gap of the banana peeler. As for weight, it would be used later to calculate the force required on the slitting and peeling mechanism.

Table 1

Physical properties of unripe nipah banana fruit

	Weight of fruit (g)	Peel thickness, edge (mm)	Peel thickness, side (mm)	Diameter (mm)	
				Height	Width
Average	77.85	5.30	3.65	38.78	29.25
Min	46.40	3.54	2.10	25.99	19.66
Max	150.90	7.37	7.16	52.48	43.87
Standard Deviation	28.61	0.93	1.01	5.77	4.92

Mechanical Properties of Fruit

Penetration Test. Graphical output from texture analyser machine representing penetration force was presented in Figure 3. From the graph, the penetration force for all three points is decreasing throughout five days which are from 7.53N to 6.59 N (top position), 7.59N to 6.40N (middle position) and 8.31N to 6.43N (bottom position). The highest penetration force is needed at the bottom while the lowest was at the top for day 1 to 4. As for day 5, the textural behaviour changes as the top position needed higher penetration force compared to the bottom. A one-way ANOVA using SPSS ver. 20.0 and Duncan's multiple range test was used to analyse the significance difference of average penetration force as seen in Table 2. There is a significant difference ($P < 0.05$) in the bottom at day 3 to 4, as well as the top at day 4 to 5, while at the top position there is a significant difference between day 2, 3, 4 and 5. This represented the peel behaviour which softened through 5 days. As seen in the graph, the peel started to soften drastically on day 5. This trend follows similarly with results presented in Hou et al. (2015) for Cavendish banana. A study made by Kulkarni et al. (2011) concluded that when the banana started to ripen, moisture content in fruit pulp gradually increased while for peel it was gradually decreased. This softens the pulp and allows the force to penetrate the peel to decrease. As banana chip producers only use banana up to three days after harvest, the average of penetration force on the first three days was averaged out and was used to build the slitting mechanism of the banana peeling machine.

Compressive Test. Figure 4 shows the compressive force of *Nipah* banana variety throughout 5 ripening days. The compressive force decreased from 1704 N to 1336.14 N. The trend shows that when the banana started to ripen, the peel softened, allowing the force to press the banana decreases. A one-way ANOVA using SPSS ver. 20.0 and Duncan's multiple range test was used to analyse the significance difference of average compression force as seen in Table 2. It shows a significant difference ($P < 0.05$) on day 3 to 5. The rapid changes may be due to physicochemical changes during the banana ripening. A study was made by Kiyohide (1996) on pulp softening. Both physical and chemical component played their role in the banana pulp softening. Banana started to exhibit pulp softening after day 2 of ripening. The major components of pulp softening were found to be elasticity and viscosity of pulp, cell wall polysaccharides, pectin, and hemicellulose. Using the average force on the first three days, the force of roller to push the banana into the slitting and peeling mechanism can be obtained.

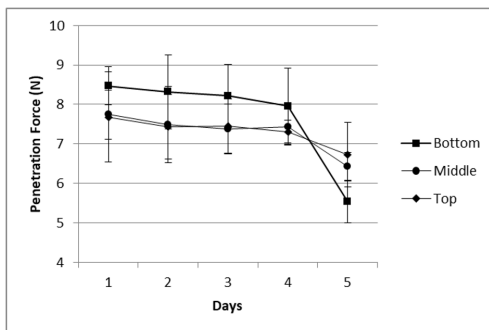


Figure 3. Effect of different positions of nipah banana on penetration force during maturity

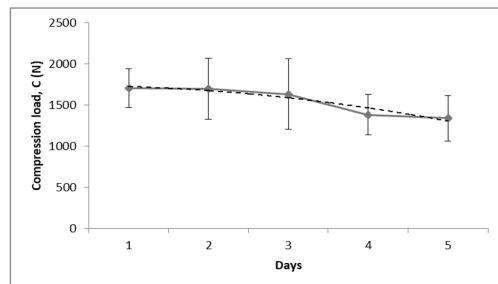


Figure 4. Effect of *Nipah* banana on compression force during maturity

Table 2

Mechanical properties of banana during ripening

Days	Average Penetration Force (N)			Average Compression Force (N)
	top	middle	bottom	
1	7.53 ^a	7.59 ^a	8.31 ^a	1704.00 ^a
2	7.29 ^a	7.35 ^a	8.16 ^a	1696.64 ^a
3	7.30 ^b	7.24 ^a	8.14 ^a	1630.70 ^{ab}
4	7.17 ^c	7.27 ^a	7.31 ^{ab}	1380.14 ^{bc}
5	6.59 ^d	6.40 ^b	6.43 ^b	1336.14 ^c

In each column, means followed by the same letter are not significantly different ($P < 0.05$) according to Duncan's multiple range test.

CONCLUSIONS

The physical properties of *Nipah* banana were measured. changes of mechanical properties of *Nipah* banana fruit as a function of ripeness stage were also conducted. A significant difference was found in both mechanical test. At different level of ripeness, there was a significant difference of penetration force at different positions (top, middle, and bottom) where there were rapid changes from day 3 to 5 at the top position. The compression force also shows a significant difference from day 3 to 5. Both mechanical properties show a significant difference starting from day 3 of ripening. This shows that the banana is unsuitable to be used for banana chip processing after day 3 as suggested by most banana chips factories. By using the average penetration and compression force for the first three days, it provides data to determine the suitable force required to slit the banana peel and maximum force for the roller of the banana peeler machine to transport from one point to another respectively. As for the physical properties, it is used to specify the size of each component. The results gathered are important for engineers working on machine development for bananas. It will be able to assist them to specify the physical dimension and requirements needed in their machine. Besides, it can also be used for postharvest handling and packaging of bananas.

ACKNOWLEDGEMENT

The authors acknowledge with thanks, the financial support (UPM/700-1/2/GPB/2017/9543400) and facility that Universiti Putra Malaysia has provided to carry out research activities.

REFERENCES

- Ammawath, W., Che Man, Y. B., Yusof, S., & Rahman, R. A. (2001). Effects of variety and stage of fruit ripeness on the physicochemical and sensory characteristics of deep-fat-fried banana chips. *Journal of the Science of Food and Agriculture*, 81(12), 1166-1171.
- Department of Statistics Malaysia. (2011). *Supply and utilization accounts selected agricultural commodities 2007-2011*. Putrajaya, Malaysia: Anon.
- Ganai, S. A., Ahsan, H., Tak, A., Mir, M. A., Rather, A. H., & Wani, S. M. (2018). Effect of maturity stages and postharvest treatments on physical properties of apple during storage. *Journal of the Saudi Society of Agricultural Sciences*, 17(3), 310-316.
- Hamir, N. A., & Ariff, M. K. M. (2006). Market potential of banana chips industry in Malaysia. *Economic and Technology Management Review*, 1(1), 83-90.
- Hou, J., Hu, Y., Huo, L., Guo, K., & Takaaki S. (2015). Classification of ripening stages of bananas based on support vector machine. *International Journal of Agricultural and Biological Engineering*, 8(6), 99-103.

- Kachru, R. P., Kotwaliwale N., & Balasubramanian, D. (1995). Physical and mechanical properties of green banana (*Musa paradisiaca*) fruit. *Journal of Food Engineering* 26(3), 369–78.
- Kiyohide, K. (1996). Softening of banana fruit: Relationship between firmness and chemical composition. *Japan Agricultural Research Quarterly* 30, 269-274.
- Kulkarni, S. G., Kudachikar, V. B., & Prakash, M. K. (2011). Studies on physico-chemical changes during artificial ripening of banana (*Musa sp*) variety 'Robusta'. *Journal of Food Science and Technology*, 48(6), 730–34.
- Owolarafe, O. K., & Shotonde, H. O. (2004). Some physical properties of fresh okro fruit. *Journal of Food Engineering*, 63(3), 299–302.
- Radunić, M., Špika, M. J., Ban, S. G., Gadže, J., Díaz-Pérez, J. C., & MacLean, D. (2015). Physical and chemical properties of pomegranate fruit accessions from Croatia. *Food Chemistry*, 177, 53-60.
- Shi, S., Wang, W., Liu, L., Shu, B., Wei, Y., Jue, D., Fu, J., Xie, J., & Lui, C. (2016). Physico-chemical properties of longan fruit during development and ripening. *Scientia Horticulturae*, 207, 160-167
- Singh, K. K., & Reddy, B. S. (2006). Post-harvest physico-mechanical properties of orange peel and fruit. *Journal of Food Engineering*, 73(2), 112-120.
- Soltani, M., Alimardani, R., Omid, M., & Karaj, I. (2011). Changes in physico-mechanical properties of banana fruit during ripening treatment. *Journal of American Science*, 7(5), 5-10.



The Effect of Packaging Materials on the Quality of Freshness of Longan Fumigated with Medium Concentration-ozone Gas

Saranyapak Chamnan¹, Jaturapatr Varith^{1*}, Somkiat Jaturonglumlert¹,
Pisuthi Klinkajorn¹ and Jakraphong Phimphimol²

¹Graduate Program in Food Engineering, Faculty of Engineering and Agro-industry, Maejo University, Chiang Mai 50290, Thailand.

²Program in Postharvest Technology, Faculty of Engineering and Agro-industry, Maejo University, Chiang Mai 50290, Thailand.

ABSTRACT

The objective of this research was to evaluate the performance of a medium concentration-ozone treatment in maintaining the quality of freshness of “Daw” longan packed in different types of packaging materials. For fumigation with ozone gas, a batch size of 3 kg of longan fruit was fumigated for 5 minutes at a concentration of 4,000 ppm. The longan was then packed in three different types of packaging- polyethylene (PE), polypropylene (PP) and wrap film (WF), and was then stored at 5°C for a shelf life of up to 36 days. Non-ozonated longan was kept as a control. The results showed that as storage time lengthened, the longan became more susceptible to disease incidences, pericarp browning, and weight loss under all treatments. During storage, the longan slightly changed in its firmness although there was

no significant difference ($p \geq 0.05$) among the three different types of packaging. The ozonated longan stored in PE, PP, WF, and those with no-packaging had more L^* and b^* values and a longer shelf life, than those of the control. Among the three different types of packaging, the ozone fumigated longan stored in PE yielded the longest storage time with a shelf life of up to 36 days; an extended 140% longer shelf life as compared to the control.

ARTICLE INFO

Article history:

Received: 24 October 2018

Accepted: 15 February 2019

Published: 21 June 2019

E-mail addresses:

saranyapak.cha@gmail.com (Saranyapak Chamnan)

varithj@maejo.mju.ac.th (Jaturapatr Varith)

yaidragon@mju.ac.th (Somkiat Jaturonglumlert)

psetton@hotmail.com (Pisuthi Klinkajorn)

jakrapho@mju.ac.th (Jakraphong Phimphimol)

* Corresponding author

Keywords: Fresh quality, longan, packaging materials, ozone fumigation, shelf life extension.

INTRODUCTION

One of the economically important fruits in the north of Thailand is longan (*Dimocarpus longan* Lour). China, Indonesia, Vietnam, Hong Kong and Malaysia are important trading countries of fresh longan fruit with Thailand (Department of International Trade Promotion, 2017). Unfortunately, longan rots easily in nature, rendering it susceptible to various postharvest pathogens intrusion which shortens the longan's shelf life at room temperature (Saengnil et al., 2014). This main problem results in restrictions on the export of longan to long distant markets due to rapid pericarp browning during storage (Sardsud et al., 1994).

Ozone is one of the powerful oxidants and has the strong capacity of disinfection and sterilization. It is a powerful germicide which destroys bacteria and fungi. Ozone gas has a longer half-life than in aqueous ozone solution (Gonçalves & Kechinski, 2011). Ozone has been confirmed as GRAS status, as a food processing aid and is compliant with the Environmental Protection Agency Disinfection by Products Rule (Ong et al., 2014). Ozone is an effective treatment for increasing shelf life and in decreasing fungal deterioration in the postharvest treatment of fresh vegetables and fruits such as tomatoes where its shelf life can be extended from 16 to 48 days (Zambre et al., 2010) as compared with control. Other fruits that yielded positive results after ozone treatment include stone fruit (Palou et al., 2002), strawberry (Thaer et al., 2013) and the papaya fruit (Ong et al., 2014), have been well documented.

Materials used for food packaging are essential to prevent physical damage to the product in order to obtain optimal shelf life. In addition, proper packaging has the proper characteristic of permeability, where a desirable equilibrium could modify the atmosphere when the rate of gas (oxygen and carbon dioxide) transmission permeating the packaging and thus balancing the respiration rate of the fruit (Kartal et al., 2012). Most packaging of fresh fruit uses polyethylene (PE) and polypropylene (PP) bags because of low water vapour permeability (Ščetar et al., 2010). Similarly, Sahoo et al. (2015) reported that the shelf life of pointed gourds packed in PP film and under refrigerated condition lasted for up to 16 days, while the shelf life of pointed gourds packed in LDPE film under ambient conditions could extend up to 4 days. The packaging of pointed gourds created a suitable headspace environment with low oxygen and high carbon dioxide concentrations. Chillies packed in microporous, PE-LD, polyolefin and anti-fog films had a shelf life of 16, 18, 22 and 28 days, respectively. In addition, control samples had shelf life of 15 days (Chitravathi et al., 2015).

Since ozone exhibits a high potential to extend shelf life of agricultural products, it can be used in combination with the proper packing material to prolong the shelf life of longan.

Thus, the objective of this study is to evaluate the effectiveness of fumigation with gaseous ozone, and the suitability in packaging, on the quality of freshness of longan during cold storage which could prevent desiccation, and which prolongs the shelf life of longan fruit.

MATERIALS AND METHODS

Longan Fruit Sample

Longan (*Dimocarpus longan* Lour.) cv. “Daw”, harvested in less than 3 days from the orchards in Chiang Mai, Thailand, was used in this study. The fruit was graded for uniformity of size (grade AA with a size of 30 mm. in diameter), color and non-disease appearance.

Ozone Fumigation System

The ozone fumigation system consisted of a corona discharge ozone generator from purified oxygen gas. The generator connected with the control system using a Labview™ program access through a wireless network. The system connected to a fumigation chamber of 0.4×0.4×1.2 m³. The system conveyed ozone gas by silicone tube. The optimum flow rate of ozone gas was 7.5 L/min and back pressure 12 kPa. The output of generating ozone gas was 5.5 g/h (Changchai et al., 2015). Ozone concentration was measured by an ozone gas sensor connected with a data logger. This data logger was calibrated by an ozone gas-sampling pump with a detector tube (Gastec Model GV-100, Japan).

Ozone Fumigation Treatment and Quality Evaluation

Longan fruit with a batch size of 3 kg was filled in a polycarbonate container. For fumigation process, the longan sample was fumigated with ozone gas at a concentration of 4,000ppm and held under pressure for 5 minutes. Longan fruit with and without fumigation were of packed size of 200g per pack. Accordingly, the longans were packed using 3 different types of packaging, namely, polyethylene (PE), polypropylene (PP) and foam tray wrap with film (WF), and stored at 5°C 95% RH until the end of shelf life. Treatments according to packaging type were defined by codenames as follows:

Untreated with gaseous ozone:

NC = control without packaging

NP = packed with PP

Treated with ozone gas:

OC = control without packaging

OP = packed with PP

NE = packed with PE

NF = packed with WF

OE = packed with PE

OF = packed with WF

The properties of these films used for packaging experiments are given in Table 1. The fruit was determined for its quality analysis immediately after fumigation and every

three days for disease incidence, pericarp browning, weight loss, firmness, color and shelf life evaluation.

Table 1

Permeability of gas through plastic films (Hernandez, 1997)

Permeability	PE	PP	WF
Water (g·µm/m ² ·d·kPa) at 37.8°C	66-99	16.5-26	330-2,000
Oxygen (cc(STP)·µm/m ² ·d·kPa) at 25°C	1,940	622	389-3,900
Carbon dioxide (cc(STP)·µm/m ² ·d·kPa) at 25°C	10,490	2,100	1,170-2,330

Determination of Disease Incidence

Disease incidence was assessed by measuring lesion area of fungal infection on each fruit's surface. Disease incidence was scored into levels as: Level 0 = no disease; Level 1 = 1-20%; Level 2 = 21-40%; Level 3 = 41-60%; Level 4 = 61-80%; and Level 5 = 81-100%. Longan fruit evaluated at a score > 0.20 were considered unacceptable for marketing.

Determination of Pericarp Browning

Pericarp browning was determined by estimating the browning area that appeared on each fruit's pericarp due to deterioration of the longan's shelf life during storage. The measurement was scored into 5 levels with respect to its browning area as Level 1 (0 - 20%), Level 2 (21 - 40%), Level 3 (41 - 60%), Level 4 (61- 80%) and Level 5 (81- 100%)

Determination of Weight Loss

Two batches of 200g treated samples were weighed for weight loss using 2 digits digital balance with ± 0.01g accuracy (model CP3202S, Sartorius, Germany). After weighing, the fruit was returned to storage cabinet at 5°C and 95%RH. The same batch of treated fruit was repeatedly weighed throughout storage time. Weight loss was expressed as Equation 1.

$$\text{Weight loss (\%)} = \frac{(\text{initial weight} - \text{final weight})}{\text{initial weight}} \times 100 \quad (1)$$

Determination of Firmness

Firmness analysis of 5 longan fruits from each treatment was selected at random where each fruit was penetrated on one side using a Texture Analyzer with ±0.1 g accuracy (model TA.XT-PLUS, Stable Micro Systems, UK). The firmness test applied a cylinder plunger SMS-P/2 probe (2 mm diameter), compressed by 20% strain using cross-head speed of pre-test, test, and post-test speed of 3 mm/s, 1 mm/s and 10 mm/s, respectively.

Determination of Color

The color of longan fruits was measured on the surface using a spectrophotometer with ± 5 nm accuracy (model Mini Scan XE PLUS 45/0-S, Hunter Lab, USA). The means of L^* (lightness) and b^* (yellowness and blueness) were reported according to the consumer preference on visual appearance of longan fruit with a yellow to light brown color (Jiang et al., 2002).

Determination of Shelf Life Evaluation

The shelf life of longan fruit was determined by disease incidence, immediately after fumigation and every 3 day-intervals during storage. The fruit was considered to be at the end of its shelf life when disease incidence of the fruit was evaluated with score > 0.20 .

Experimental Design and Statistical Analysis

The experiment was designed using factorial experimental design in a randomized complete block design (RCBD). Data were statistically analyzed by analysis of variance (ANOVA), and was carried out using SPSS 16.0. Duncan's Multiple Range Tests (DMRT) at a significance level of 0.05. Among the various treatments, the p-value less than 0.05 was considered as a significant difference.

RESULTS AND DISCUSSION

Effects on Disease Incidence

The first parameter related with the shelf life of the fruit can be defined as disease incidence. For Figure 1A, disease incidence of longan all treatments increased when storage time increased. The disease incidence of NC sample increased rapidly in 18 days. Longan treated with gaseous ozone exhibited less disease incidence than those of untreated samples when stored at 5°C. This corresponds with Ong et al. (2013) who found that ozone treatment reduced disease incidence up to 40% in papaya fruit. Other researchers also reported that ozone fumigation reduced the microorganism population in fruits such as longan fruit (Whangchai et al., 2006), date fruit (Habibi & Haddad, 2009), strawberry (Aday & Caner, 2014) and table grapes (Gabler et al., 2010) because it destroyed microorganisms by oxidizing the cellular components of cell fruit (Victorin, 1992). In our study, longan fruit packed in PE exhibited the least disease incidence when compared to PP, WF and without packaging. Since PE had more carbon dioxide (CO_2) permeability than other films (Table 1), it is possible that CO_2 might permeate to environment easier than those packed in other packaging. As a result, the ozonated longan packed in PE emerged less disease incidence than the others. The low percentages of diseases incidence in PE also slow down the rate of pathological disorder in PE films as well.

Effects on Pericarp Browning

The pericarp browning of longans under all treatments increased throughout shelf life (Figure 1B). At day 0, the longan fruit fumigated with gaseous ozone significantly exhibited less pericarp browning than that of non-fumigate longan fruit ($p < 0.05$). When stored for 15 days, the OE sample exhibited the least pericarp browning score of 1.80, whereas the NC sample exhibited the highest pericarp browning score of 4.40. Correspondingly, Whangchai et al. (2006) reported that with the increase of storage time, longan fruit treated with low concentration ozone showed an increase in pericarp browning because of the time limit in ozone efficiency to inhibit browning of longan fruit.

Effects on Weight Loss

Gaseous ozone treatments did not significantly affect ($p \geq 0.05$) the weight loss of longan fruit, however, type of packaging significantly did ($p < 0.05$). During 15 days in storage, longan fruits with no packaging gained more weight loss than those packed in WF, PE, and PP, respectively. The NC sample had the highest weight loss of 9.39% in 15 days. These results agreed with Mistriotis et al. (2016) who suggested that unwrapped samples (cherry tomatoes and peaches) had more weight loss than samples packed in PLA and OPP film. When storage time lengthened, longan fruit under all treatments was susceptible to weight loss. The OE sample had the highest weight loss of 13.42% in 36 days, as shown in Figure 1C. An increase in weight loss of longan is normally due to evaporation and respiration (water and heat production), but under different packaging types, it yielded different responses (Chitravathi et al., 2015).

Effects on Firmness

Firmness can be defined as the parameter which is related to cell wall strength and intercellular adhesion (Toivonen & Brummell, 2008). In Figure 1D, gaseous ozone treatments and packaging types did not significantly affect ($p \geq 0.05$) the firmness of the longan fruit. During storage at 5°C, the firmness of longan was within a range of 9.98 to 10.04 N. Longan fruit changed slightly in firmness but with no significant difference ($p \geq 0.05$). The firmness did not change. This may be due to lesser loss of moisture from the surface of longan fruit. In contrast to other fruits, Aday and Caner (2014) reported that significant difference in firmness values was observed between ozone treated and ozone untreated strawberries. All treated strawberries had higher firmness values than the control group. Pointed gourd in all packaging types had peak force decreased during storage under ambient and refrigerated storage condition (Sahoo et al., 2015).

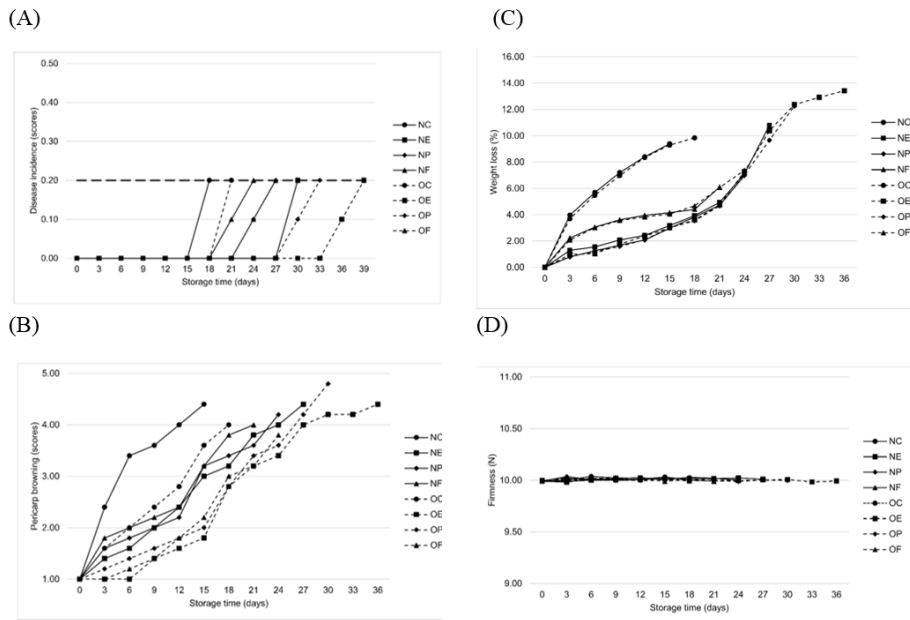


Figure 1. Effect of ozone fumigation and packaging materials on physicochemical properties of longan fruit during storage at 5°C: (A) disease incidence, (B) pericarp browning, (C) weight loss, and (D) firmness. Each data point represents a mean of three replicates (n=3)

Effects on Color

Color is the one factor in deciding visual attributes for buying and selling of longan fruit (Apai, 2010). At day 0, longan fruit without ozone fumigation possessed the L^* and b^* of 49.80 and 28.64. When fumigated with ozone gas, the longan had increased in L^* and b^* to 52.64 and 30.29, respectively. Ozone may cause an increase in L^* of longan due to the bleaching effect (Forney, 2003). During storage at 5°C, the ozonated longan stored in PE, PP, WF and without packaging had more L^* and b^* (light yellow-brown color) as well as a longer shelf life than those of the untreated longan (dark brown color), as shown in Figure 2A and 2B. Similar trend was also observed by Aday and Caner (2014) who suggested that strawberries with ozone treatments and storage times were significant factors affecting the L^* .

Effects on Shelf Life

The shelf life of longan fruit due to effects of ozone treatment and storage packaging type was determined by disease incidence, as shown in Figure 1A and Table 2. Longan fumigated with ozone gas had a longer shelf life than untreated samples. The ozonated longan packed in PE had a longer shelf life than that of PP, WF and those with no packaging when stored at 5°C. Among three different types of packaging, the ozone fumigated longan stored in PE

yielded the longest storage time up to 36 days, equivalent to 140% longer shelf life than that of the control. According to Zambre et al. (2010), tomatoes treated with ozone gas and stored at 15°C had a prolonged shelf life of tomato by 22 days. The longer shelf life of longan was possibly due to a reduction in the surface microbial count in combination with proper modified atmosphere effect inside the package. The modified gaseous composition in the different packaging created a suitable headspace with low oxygen and high carbon dioxide, which resulted in maintaining the quality and marketability of vegetables (Sahoo et al., 2015). Our results also agreed with that of Mangaraj et al. (2012) who found that the modified atmosphere packaging extended shelf life of the litchi fruit from 100 to 150% compared with unpackaged fruits.

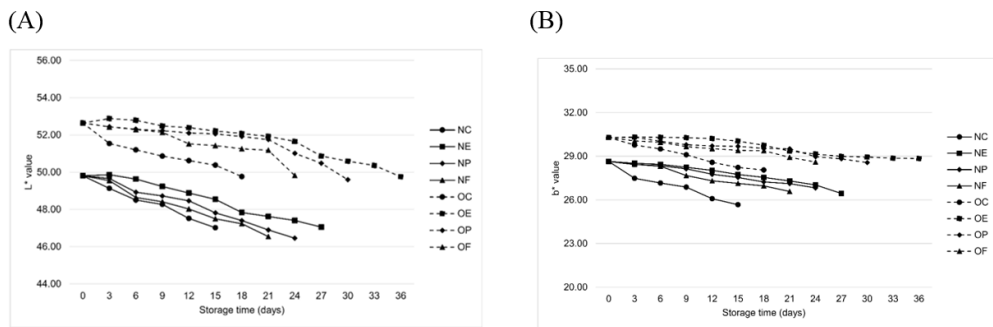


Figure 2. Effect of gaseous ozone and packaging type on color; (A) L* value and (B) b* value of longan fruit during storage at 5°C

Table 2

Shelf life at various treatment of longan fruit during storage at 5°C

Non-Ozone Treatment	Shelf life (days)	Ozone treatment	Shelf life (days)
NC	15	OC	18
NE	27	OE	36
NP	24	OP	30
NF	21	OF	24

CONCLUSION

Gaseous ozone treatment and the type of storage packaging materials are two important factors affecting the quality of freshness of the longan fruit. Without ozone fumigation, longan fruit had more incidences of disease, pericarp browning, and weight loss, with less L* and b* in storage for 15 days. With ozone fumigation, the disease incidences, weight

loss and shelf life of the longan fruit yielded positive effects, depending upon on the type of packaging materials. Using ozone fumigation combined with PE packaging was the optimum treatment that resulted in a storage shelf life up to 36 days. It is suggested that a combined treatment of a varied concentration of ozone fumigation, with more variety of packaging materials and storage conditions, can be further studied to improve the shelf life of fresh longan.

ACKNOWLEDGEMENTS

This research was supported by the Food Engineering Program, Faculty of Engineering and Agro-industry, Maejo University, Chiang Mai, Thailand. The authors gratefully acknowledge Assist. Prof. Dr. Kanda Whangchai at the Department of Biology, Faculty of Science, Chiang Mai University, Thailand, for providing the ozone calibration equipment.

REFERENCES

- Aday, M. S., & Caner, C. (2014). Individual and combined effects of ultrasound, ozone and chlorine dioxide on strawberry storage life. *LWT-Food Science and Technology*, 57(1), 344-351.
- Apai, W. (2010). Effects of fruit dipping in hydrochloric acid then rinsing in water on fruit decay and browning of longan fruit. *Crop Protection*, 29(10), 1184-1189.
- Changchai, S., Varith, J., & Jaturonglumlert, S. (2015). Effect of high concentration-ozone fumigation on chemical and physical changes in fresh chilli. In *7th International Conference on Sustainable Agriculture for Food, Energy and Industry in Regional and Global Context, ICSAFEI2015* (pp. 1-7). Kuala Lumpur, Malaysia.
- Chitravathi, K., Chauhan, O. P., & Raju, P. S. (2015). Influence of modified atmosphere packaging on shelf-life of green chillies (*Capsicum annum L.*). *Food Packaging and Shelf Life*, 4, 1-9.
- Department of International Trade Promotion, Ministry of Commerce, Thailand. (2017). *Thailand's top 15 export markets (Longan fruit)*. Retrieved May 28, 2018, from [http://www2.ops3.moc.go.th/Thailand's top 15 export markets](http://www2.ops3.moc.go.th/Thailand's%20top%2015%20export%20markets)
- Forney, C. F. (2003). Postharvest response of horticultural products to ozone. In D. M. Hodges (Eds.), *Postharvest oxidative stress in horticultural crops* (pp. 13-54). Binghamton, NY: Food Products Press.
- Gabler, F. M., Smilanick, J. L., Mansour, M. F., & Karaca, H. (2010). Influence of fumigation with high concentrations of ozone gas on postharvest gray mold and fungicide residues on table grapes. *Postharvest Biology and Technology*, 55(2), 85-90.
- Gonçalves, A. A., & Kechinski, C. P. (2011). *Ozone technology in the food industry*. Rio de Janeiro: Nova Science Publishers, Inc.
- Habibi, M. B. N., & Haddad M. H. K. (2009). Efficacy of ozone to reduce microbial populations in date fruits. *Food Control*, 20(1), 27-30.
- Hernandez, R. J. (1997). *Food packaging materials, barrier properties, and selection*. New York, USA: CRC Press.

- Jiang, Y., Zhang, Z., Joyce, D. C., & Ketsa, S. (2002). Postharvest biology and handling of longan fruit (*Dimocarpus longan* Lour.). *Postharvest Biology and Technology*, 26(3), 241-252.
- Kartal, S., Aday, M. S., & Caner, C. (2012). Use of microperforated films and oxygen scavengers to maintain storage stability of fresh strawberries. *Postharvest Biology and Technology*, 71, 32-40.
- Mangaraj, S., Goswami, T. K., Giri, S. K., & Tripathi, M. K. (2012). Permselective MA packaging of litchi (cv. Shahi) for preserving quality and extension of shelf-life. *Postharvest Biology and Technology*, 71, 1-12.
- Mistriotis, A., Briassoulis, D., Giannoulis, A., & D'Aquino, S. (2016). Design of biodegradable bio-based equilibrium modified atmosphere packaging (EMAP) for fresh fruits and vegetables by using microperforated poly-lactic acid (PLA) films. *Postharvest Biology and Technology*, 111, 380-389.
- Ong, M. K., Ali, A., Alderson, P. G., & Forney, C. F. (2014). Effect of different concentrations of ozone on physiological changes associated to gas exchange, fruit ripening, fruit surface quality and defence-related enzymes levels in papaya fruit during ambient storage. *Scientia Horticulturae*, 179, 163-169.
- Ong, M. K., Kazi, F. K., Forney, C. F., & Ali, A. (2013). Effect of gaseous ozone on papaya anthracnose. *Food and Bioprocess Technology*, 6(11), 2996-3005.
- Palou, I., Crisosto, C. H., Smilanick, J. I., Adaskaveg, J. E., & Zoffoli, J. P. (2002). Effects of continuous 0.3 ppm ozone exposure on decay development and physiological responses of peaches and table grapes in cold storage. *Postharvest Biological Technology*, 24(1), 39-48.
- Saengnil, K., Chumyarn, A., Faiyue, B., & Uthaibutra, J. (2014). Use of chlorine dioxide fumigation to alleviate enzymatic browning of harvested 'Daw' longan pericarp during storage under ambient conditions. *Postharvest Biology and Technology*, 91, 49-56.
- Sahoo, N. R., Bal, L. M., Pal, U.S., & Sahoo, D. (2015). Effect of packaging conditions on quality and shelf-life of fresh pointed gourd (*Trichosanthes dioica* Roxb.) during storage. *Food Packaging and Shelf Life*, 5, 56-62.
- Sardsud, U., Sittigul, C., & Chaiwangsri, T. (1994). Effect of plant extracts on the *in vitro* and *in vivo* development of fruit pathogens. In Johnson, G.I., Highley, E. (Eds.), *Development of Postharvest Handling Technology for Tropical Tree Fruits* (pp. 60-62). Canberra, Australia: ACIAR.
- Ščetar, M., Kurek, M., & Galić, K. (2010). Trends in fruit and vegetable packaging – a review. *Croatian Journal of Food Technology, Biotechnology and Nutrition*, 5(3-4), 69-86.
- Thaer, Y., D'Onghia, A. M., & Ricelli, A. (2013). The use of ozone in strawberry post-harvest conservation. *Biological Control of Fungal and Bacterial Plant Pathogens*, 86, 143-148.
- Toivonen, P. M. A., & Brummell, D. A. (2008). Biochemical bases of appearance and texture changes in fresh-cut fruit and vegetables. *Postharvest Biology and Technology*, 48(1), 1-14.
- Victorin, K. (1992). Review of genotoxicity of ozone. *Mutation Research*, 277(3), 221-238.
- Whangchai, K., Saengnil, K., & Uthaibutra, J. (2006). Effect of ozone in combination with some organic acids on the control of postharvest decay and pericarp browning of longan fruit. *Crop Protection*, 25(8), 821-825.
- Zambre, S. S., Venkatesh, K.V., & Shah, N.G. (2010). Tomato redness for assessing ozone treatment to extend the shelf life. *Journal of Food Engineering*, 96(3), 463-468.

Degradation Kinetics of Diazinon and Triazophos Pesticides in Dried Chili under Gaseous Ozone Fumigation

Panlop Sintuya^{1,2}, Kanjana Narkprasom¹, Jaturapatr Varith^{1*},
Somkiat Jaturonglumlert¹, Niwooti Whangchai³, Danuwat Peng-ont² and
Chanawat Nitatwichit¹

¹Graduate Program in Food Engineering, Faculty of Engineering and Agro-industry,
Maejo University, Chiang Mai, 50290, Thailand

²Institute of Product Quality and Standardization, Maejo University,
Chiang Mai, 50290, Thailand

³Faculty of Fisheries Technology and Aquatic Resources, Maejo University,
Chiang Mai, 50290, Thailand

ABSTRACT

Dried chili is normally contaminated with pesticide residue as a result from the excessive uses of pesticide in the field. The objective of this study was to determine the degradation kinetics of diazinon and triazophos pesticides in dried chili due to the oxidative potential of gaseous ozone fumigation. Both pesticides were spray-coated on dried chili and later fumigated with gaseous ozone at concentration rate of 5.5 g/hr for 30 min. Results showed that the degradation kinetic of diazinon and triazophos pesticides were presented on the first-order kinetic reaction. After 30 min of ozone fumigation, diazinon and triazophos residues were decreased by 69% and 47% with the half-life ($t_{1/2}$) of 17.9 and 32.1 min,

respectively. Scanning electron microscopy (SEM) images indicated that ozonated chili exhibited more rough surface morphology than unozoned chili. Ozone fumigation can be further developed as pesticide scrubber on agri-foods due to its high efficiency in terms of shortening of half-life period and rapid pesticide decay rate.

Keywords: Degradation kinetics, diazinon, dried chili, half-life period, ozone, triazophos

ARTICLE INFO

Article history:

Received: 24 October 2018

Accepted: 15 February 2019

Published: 21 June 2019

E-mail addresses:

panlop062@gmail.com (Panlop Sintuya)

varithj@maejo.mju.ac.th (Jaturapatr Varith)

aoihighso@hotmail.com (Kanjana Narkprasom)

yaidragon@mju.ac.th (Somkiat Jaturonglumlert)

niwooti@hotmail.co.th (Niwooti Whangchai)

danuwat_2493@hotmail.com (Danuwat Peng-ont)

n_chanawat@hotmail.com (Chanawat Nitatwichit)

* Corresponding author

INTRODUCTION

Dried chili is a popular spice product that is commonly used as ingredient for food flavoring and coloring (Jitbunjerdkul & Kijroongrojana, 2007; Toontom et al., 2012). Conventionally, dried chili is obtained by natural sun drying which takes about 7-20 days until moisture content decreased to 10-15% (Condorí et al., 2001; Öztekin et al., 1999; Toontom et al., 2012). The persistence problem remains as dried chili product in current market contains high level of pesticide residues (Pérez-Olvera et al., 2011). The pesticide contamination in chili product is due to the use of pesticide to increase crop production during agriculture of farmers (Ormad et al., 2010; Popp et al., 2013). Even if the drying process can help to degrade pesticide residue, it takes a long period (Özbey et al., 2017). A previous work reported that 59.3% of vegetables from farms and 13.2% of vegetables from markets contained organophosphorus pesticide residues at or above the maximum residue limits of the European Union (Sapbamrer & Hongsibsong, 2014). Despite the fact that organophosphates pesticides residue can be naturally degraded, Rasmussen et al. (2003) mentioned that organophosphates chlorpyrifos, diazinon and fenitrothion could be reduced only 25-69% during storage for 79 days. In order to create a safe dried chili product, pesticide residues degradation prior to export is a proper approach.

Gaseous ozone utilization is one of the most prominent technique to reduce pesticide efficiently. It is able to be applied by either ozonated water or gaseous ozone (Mezzanotte et al., 2005; Smilanick et al., 2002; Whangchai et al., 2011). However, a study indicated that gaseous ozone exhibited higher degradation activity than ozonated water (Whangchai et al., 2011). This study aimed to study the degradation kinetic of diazinon and triazophos pesticide residues using gaseous ozone fumigation treatment. The effect of ozone treatment to chili surface, total phenolic compounds and antioxidant properties were also conducted to ensure the product qualities after ozone treatment.

MATERIALS AND METHODS

Dried Chili Sample Preparation

Pesticide-free red dried chili samples used in this study were purchased from USDA Certified farm. Ten kg of dried chili samples were coated with 20 mL of pesticide solution containing 1,000 mg/L of diazinon and 1,000 mg/L of triazophos (Dr.ehrenstorfer GmbH., Germany). The pesticide coated chillies were then allowed to dry at room temperature for 10 h.

Ozone Fumigation Treatment

Red dried chili samples were treated with ozone by loading of 500 g of red dried chili samples into a fumigation chamber (Figure 1). The chamber was filled with gaseous ozone

with a flow rate of 5.5 g/hr. Corona discharger with O₂ flow rate of 7.5 L/min and back pressure of 12 kPa was used to generate ozone (Changchai et al., 2015). The pesticide coated dried chilies were treated with gaseous ozone for 0, 5, 10, 15, 20, 25 and 30 min. Pesticide coated chili without ozone treatment was used as a control. After the fumigation process, dried chili samples were kept in low density polyethylene (LDPE) bags at 25°C prior to evaluating the chemical, physical properties and kinetics degradation of pesticides.

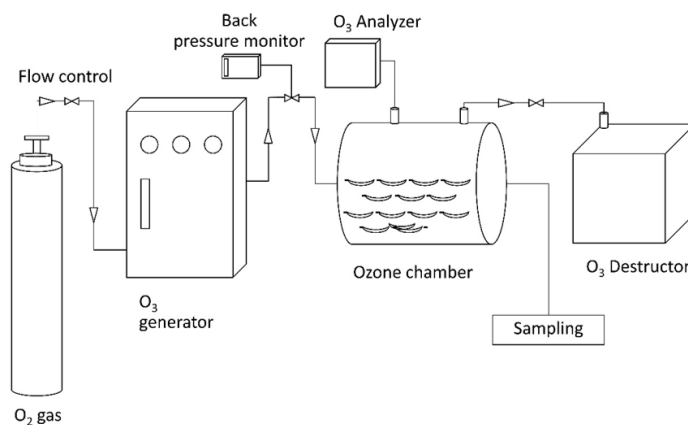


Figure 1. Gaseous ozone fumigation experimental setup

Diazinon and Triazophos Pesticide Residue Determination

The extraction of dried chili samples for the determination of diazinon and triazophos pesticide residue was achieved by QuEChERS technique using dispersive solid phase extraction (Grimalt & Dehouck, 2016). Pesticide residue determination was carried out using gas chromatograph equipped with flame photometric detector (GC/FPD, 6890N, Agilent Technologies Canada Inc.) using HP-5 capillary column (0.25 µm particle size, 30 m x 0.32 mm i.d., Agilent Technologies Canada Inc.). Helium gas with a flow rate of 1.5 mL.min⁻¹ was used as a carrier gas. The oven temperature was set up at 80°C for 2 min, then it was increased to 150°C at the rate of 25°C.min⁻¹ and was held for 5 min. After that it was increased to 190°C at the rate of 5°C.min⁻¹, held for 5 min, ramped up to 220°C at the rate of 10°C.min⁻¹, held for 5 min, and finally ramped up to 250°C at the rate of 10°C.min⁻¹, respectively.

Evaluation of Diazinon and Triazophos Pesticides Degradation Kinetic

The rate constant of diazinon and triazophos degradation and half-life period of pesticide degradation were evaluated using Equations 1 and 2, respectively.

$$\ln \frac{[C]}{[C_0]} = -kt \quad [1]$$

C_0 is initial concentration of pesticide at treatment time = 0 (mg/kg), C is concentration of pesticide at treatment time = t (mg/kg), k is rate constant of the pesticide degradation, t is treatment time (min). In order to obtain the half-life period ($t=t_{1/2}$) of each pesticide, a pesticide with concentration at half-life period is determined by $[C]=[C_0]/2$. Therefore, half-life period could be calculated as shown in Equation 2 (Alighourchi & Barzegar, 2009).

$$t_{1/2} = \frac{0.693}{k} \quad [2]$$

Determination of Total Phenolic Content (TPC)

The content of total phenolic compound (TPC) was studied using the Folin-Ciocalteu assay (Kovacova & MaliNoVá, 2007), with slight modification. Firstly, methanolic extract solution was prepared by mixing 5 g of sample with 20 ml of 70% methanol. The mixture was kept overnight at -20°C . Then the sample was adjusted final volume to 50 ml and was centrifuged at 2,500 rpm, 4°C for 10 min. The mixture of 0.5 ml of 50% Folin-Ciocalteu, 1 ml of 95% ethanol, 1 ml of methanolic extract, and 5 ml of reverse osmosis water was mixed and was kept at room temperature ($25 \pm 5^\circ\text{C}$) for 5 min. After that, 1ml of 5% (w/v) of sodium carbonate solution was added. The mixture was homogenized and was kept at room temperature for 60 min. TPC was analyzed using a NICOLET evolution 300 (Thermo Electron Corporation, USA) spectrophotometer at 725 nm. The standard calibration curve was plotted using gallic acid at the concentration of 10 – 200 mg/L. The TPC was presented as gallic acid equivalent (GAE) mg/100g.

Determination of Free Radical Scavenging Activity

The determination of scavenging activity of dried chili extract was carried out based on 2,2-diphenyl-1-picrylhydrazyl (DPPH) free radical scavenging assay (Milardović et al., 2006). The 2 ml of chili extract was mixed with 1 mL of 100 μM DPPH solution which was dissolved in 80% methanol. The mixture was then shaken vigorously and was kept in a dark room for 30 min at room temperature. The absorbance was evaluated using a spectrophotometer (Thermo Electron Corporation, NICOLET evolution 300, USA). The detection was determined at 515 nm of wavelength using methanol as a blank solution. Triplicate analysis was done and their activity was expressed as Trolox equivalent (TEAE) in mg/100g.

Scanning Electron Microscopy (SEM) Analysis

SEM technique was used to examine microstructure of chili surface without and with ozone fumigation for 30 min. Dried chili peel (5x5 mm) sample was cut into a small piece. The sample was coated with gold with 20 nm thickness in an ion sputter coater model JFC-1200 (JEOL, Japan). The microstructure of chili surface was observed by SEM JSM-5410LV (JEOL, Japan) at 10 kV.

Statistical Analysis

In this experiment, the obtained data were statistically examined using the Statistics Package for the Social Sciences (SPSS, IBM Corp., USA) by one-way analysis of variance (ANOVA). Duncan's test is commonly used in agricultural research. It has a great power for statistical analysis. The significant difference of responses was determined at $p < 0.05$ using Duncan's method.

RESULTS AND DISCUSSION

Diazinon and Triazophos Pesticide Residue Analysis

In this study, diazinon and triazophos pesticide residues of dried chili after ozone fumigation treatment were studied. They were compared with those of dried chili stored in a polyethylene bag without any fumigation. Figure 2 shows that after 30 min of ozone fumigation, diazinon and triazophos could be degraded 69 and 47%, respectively. For untreated dried chili sample, diazinon and triazophos could be degraded 40 and 42% after being stored in a polyethylene bag for 8 weeks. The reason behind this is that ozone is a strong oxidizing agent that can allow pesticide degradation (Ikehata & El-Din, 2006; Ikeura et al., 2011; Tiwari et al., 2010). Therefore, the degradation of pesticide with ozone fumigation exhibited higher efficiency than the degradation without ozone fumigation.

Determination of Diazinon and Triazopho Pesticides Degradation Kinetic

Kinetics parameters for degradation of diazinon and triazophos during storage at 25°C (without ozone fumigation) and with ozone fumigation were shown in Table 1. Degradation kinetics of diazinon and triazophos are considered to be the first-order reaction. The degradation rate constants (k) of diazinon and triazophos on ozone treated chili were 3.8×10^{-2} and 2.2×10^{-2} mg/kg/min, respectively. Meanwhile, the degradation rate constants (k) of diazinon and triazophos on untreated chili were 7.0×10^{-6} and 6.0×10^{-6} mg/kg/min, which were approximately 5,400 and 3,700 folds different in order of magnitude. The greater degradation rate constant revealed the shorter time for pesticide residue to decline. The results corresponded well with previous work by Bourgin et al. (2013) who reported that the degradation of pesticide by ozonation fumigation was the first-order reaction. For the

degradation half-life period ($t_{1/2}$), untreated chili revealed the $t_{1/2}$ for diazinon and triazophos of 68.8 and 80.2 days, respectively. However, chilies with ozone fumigation exhibited $t_{1/2}$ value for the degradation of diazinon and triazophos of 17.9 and 32.1 min.

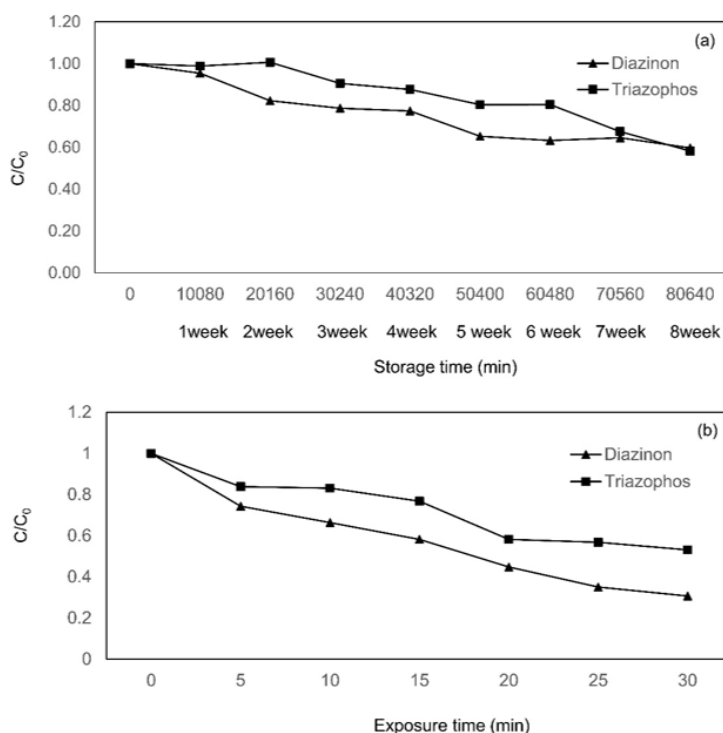


Figure 2. Diazinon and triazophos degradation by (a) self-degradation during storage at 25°C without ozone fumigation, and (b) accelerated degradation with ozone exposure.

Table 1

Kinetics study for degradation of the diazinon and triazophos during storage at 25°C (non-ozone fumigation) and with ozone fumigation

Pesticide	Non-ozone fumigation			Ozone fumigation			Half-life time difference (%)
	k (mg/kg/min)	R^2	$t_{1/2}$ (day)	k (mg/kg/min)	R^2	$t_{1/2}$ (min)	
Diazinon	7.0×10^{-6}	0.94	68.8	3.8×10^{-2}	0.99	17.9	99.9%
Triazophos	6.0×10^{-6}	0.88	80.2	2.2×10^{-2}	0.94	32.1	99.9%

Determination of Total Phenolic Content (TPC) and Free Radicals Scavenging Activity

The TPC and free radicals scavenging activity represent the quality of dried chili. The result of TPC in dried chili sample after fumigation for 30 min is shown in Table 2. The TPC tended to decrease due to fumigation time at 0, 5, 10, 15, 20 and 25 min but not significantly different ($p \geq 0.05$). However, after fumigation for 30 min, the TPC was significantly different ($p < 0.05$) from the others. This phenomenon occurred due to reaction of ozone and free radical (Misra et al., 2015; Sarangapani et al., 2017). For the free radical scavenging activity, there was not significantly different on fumigation 0 to 30 min as shown in Table 2. The results from this experiment corresponded to the previous reports (Alwi, 2017; Torres et al., 2011). It was found that total phenolic compound could be reduced by increasing of ozone concentration or time of fumigation.

Table 2

Total phenolic content and free radical scavenging activity in chili sample with ozone fumigation for 30 min.

Exposure time (min)	Total phenolic content (mgGAE/100g)	Free radical scavenging activity (mgTEAE/100g) ^{n.s.}
0	150.27 ^a ± 8.62	51.01 ± 5.57
5	145.28 ^a ± 2.98	43.94 ± 0.61
10	147.81 ^a ± 6.86	51.69 ± 3.68
15	150.93 ^a ± 6.28	44.30 ± 0.81
20	150.83 ^a ± 5.01	51.73 ± 0.85
25	145.53 ^a ± 9.77	44.33 ± 5.34
30	130.00 ^b ± 5.64	49.10 ± 1.22

*n.s. = not significantly different ($p \geq 0.05$).

*Values followed by the different letter within the same row are significantly different from each other ($p < 0.05$).

Scanning Electron Microscopy (SEM) Analysis

SEM image of chili surface without ozone fumigation was compared to chili surface with ozone fumigation for 30 min as shown in Figure 3. It was found that ozone affected surface of chili. The increasing of roughness structure of chili surface was observed after ozone treatment. This phenomenon cannot be clearly explained but it is possible that the ozone fumigation at high concentration may have oxidative reaction with some substance at surface causing the distort morphological changes as a rougher or corrosive surface of the chili (Alwi, 2017; O'Donnell et al., 2012).

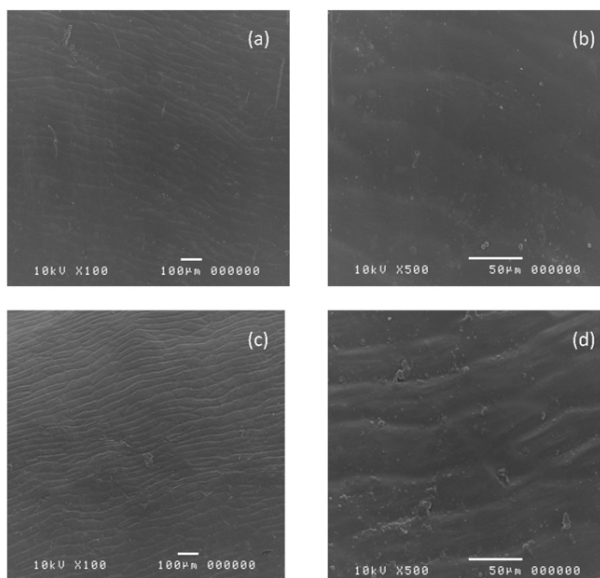


Figure 3. SEM image of chili surface (a, b) without ozone fumigation and (c, d) with ozone fumigation for 30 min.

CONCLUSIONS

Gaseous ozone treatment was successfully used to degrade diazinon and triazophos in dried chili. The kinetic study revealed that first-order reaction of diazinon and triazophos degradation on ozone treated chili showed rate constants (k) of 3.8×10^{-2} and 2.2×10^{-2} mg/kg/min, respectively, which were approximately 5,400 and 3,700 folds different in order of magnitude compared to untreated chili. For the degradation half-life period ($t_{1/2}$), the untreated chili revealed the $t_{1/2}$ for diazinon and triazophos of 68.8 and 80.2 days, respectively. However, chili with ozone fumigation exhibited $t_{1/2}$ value for the degradation of diazinon and triazophos of 17.9 and 32.1 min. TPC was significantly different ($p < 0.05$) after 30 min of ozone treatment. For the result of free radical scavenging activity, there was no significant difference on fumigation from 0 to 30 min. SEM image showed that roughness structure of chili surface was observed after ozone treatment, possibly due to the ozone corrosive effect. Since ozone fumigation shortens the $t_{1/2}$ diazinon and triazophos by 69 and 47%, it exhibits a promising potential to be applied for reducing the pesticide residues in dried chilli without significant changes in physical and chemical properties. Therefore, gaseous ozone fumigation can be an alternative to effectively reduce pesticide residue in chilli and other agricultural products in order to improve food qualities and safety.

ACKNOWLEDGEMENTS

The authors would like to acknowledge the financial support provided by Graduate Program

in Food Engineering at the Faculty of Engineering and Agro-Industry, Maejo University, Chiang Mai, Thailand. Grateful thanks to Assist. Prof. Dr. Kanda Whangchai, Department of Biology, Faculty of Science, Chiang Mai University, Thailand for the calibration reference of ozone.

REFERENCES

- Alighourchi, H., & Barzegar, M. (2009). Some physicochemical characteristics and degradation kinetic of anthocyanin of reconstituted pomegranate juice during storage. *Journal of Food Engineering*, 90(2), 179-185.
- Alwi, N. A. (2017). *Ozone fumigation effects on bacterial and anthracnose development on bell pepper (Capsicum annuum L.) and its effect on fruit quality*. (Unpublished Doctoral thesis), University of Nottingham, Malaysia.
- Bourgin, M., Albet, J., & Violleau, F. (2013). Study of the degradation of pesticides on loaded seeds by ozonation. *Journal of Environmental Chemical Engineering*, 1(4), 1004-1012.
- Changchai, S., Varith, J., & Jaturonglumlert, S. (2015). Effect of high concentration-ozone fumigation on chemical and physical changes in fresh chilli. In *7th International Conference on Sustainable Agriculture for Food, Energy and Industry in Regional and Global Context* (pp. 1-7). Kuala Lumpur, Malaysia.
- Condorí, M., Echazú, R., & Saravia, L. (2001). Solar drying of sweet pepper and garlic using the tunnel greenhouse drier. *Renewable Energy*, 22(4), 447-460.
- Grimalt, S., & Dehouck, P. (2016). Review of analytical methods for the determination of pesticide residues in grapes. *Journal of Chromatography A*, 1433, 1-23.
- Ikehata, K., & El-Din, M. G. (2006). Aqueous pesticide degradation by hydrogen peroxide/ultraviolet irradiation and Fenton-type advanced oxidation processes: A review. *Journal of Environmental Engineering and Science*, 5(2), 81-135.
- Ikeura, H., Kobayashi, F., & Tamaki, M. (2011). Removal of residual pesticides in vegetables using ozone microbubbles. *Journal of Hazardous Materials*, 186(1), 956-959.
- Jitbunjerdkul, S., & Kijroongrojana, K. (2007). Formulation of Thai herbal Nam prik. *Songklanakarin Journal of Science and Technology*, 29(3), 837-846.
- Kovacova, M., & MaliNoVá, E. (2007). Ferulic and coumaric acids, total phenolic compounds and their correlation in selected oat genotypes. *Czech Journal of Food Sciences*, 25(6), 325-332.
- Mezzanotte, V., Canziani, R., Sardi, E., & Spada, L. (2005). Removal of pesticides by a combined ozonation/ attached biomass process sequence. *Ozone: Science and Engineering*, 27(4), 327-331.
- Milardović, S., Iveković, D., & Grabarić, B. S. (2006). A novel amperometric method for antioxidant activity determination using DPPH free radical. *Bioelectrochemistry*, 68(2), 175-180.
- Misra, N. N., Pankaj, S. K., Frias, J. M., Keener, K. M., & Cullen, P. J. (2015). The effects of nonthermal plasma on chemical quality of strawberries. *Postharvest Biology and Technology*, 110, 197-202.

- Ormad, M. P., Miguel, N., Lanao, M., Mosteo, R., & Ovelheiro, J. L. (2010). Effect of application of ozone and ozone combined with hydrogen peroxide and titanium dioxide in the removal of pesticides from water. *Ozone: Science and Engineering*, 32(1), 25-32.
- Özbey, A., Karagöz, Ş., & Cingöz, A. (2017). Effect of drying process on pesticide residues in grapes. *GIDA/ The Journal of Food*, 42(2), 204-209.
- Öztekın, S., Başçetinçelik, A., & Soysal, Y. (1999). Crop drying programme in Turkey. *Renewable Energy*, 16(1), 789-794.
- O'Donnell, C., Tiwari, B. K., Cullen P. J., & Rice R. G. (Eds.) (2012). *Ozone in food processing*. New Jersey, USA: John Wiley & Sons.
- Pérez-Olvera, M. A., Navarro-Garza, H., & Miranda-Cruz, E. (2011). Use of pesticides for vegetable crops in Mexico. In Stoytcheva, M. (Ed.), *Pesticides in the Modern World-Pesticides Use and Management* (pp. 97-118). London, UK: IntechOpen.
- Popp, J., Pető, K., & Nagy, J. (2013). Pesticide productivity and food security. A review. *Agronomy for Sustainable Development*, 33(1), 243-255.
- Rasmussen, R. R., Poulsen, M. E., & Hansen, H. C. B. (2003). Distribution of multiple pesticide residues in apple segments after home processing. *Food Additives and Contaminants*, 20(11), 1044-1063.
- Sapbamrer, R., & Hongsibsong, S. (2014). Organophosphorus pesticide residues in vegetables from farms, markets, and a supermarket around Kwan Phayao Lake of Northern Thailand. *Archives of Environmental Contamination and Toxicology*, 67(1), 60-67.
- Sarangapani, C., O'Toole, G., Cullen, P. J., & Bourke, P. (2017). Atmospheric cold plasma dissipation efficiency of agrochemicals on blueberries. *Innovative Food Science and Emerging Technologies*, 44, 235-241.
- Smilanick, J. L., Margosan, D. M., & Mlikota Gabler, F. (2002). Impact of ozonated water on the quality and shelf-life of fresh citrus fruit, stone fruit, and table grapes. *Ozone: Science & Engineering*, 24(5), 343-356.
- Tiwari, B. K., Brennan, C. S., Curran, T., Gallagher, E., Cullen, P. J., & O'Donnell, C. P. (2010). Application of ozone in grain processing. *Journal of Cereal Science*, 51(3), 248-255.
- Toontom, N., Meenune, M., Posri, W., & Lertsiri, S. (2012). Effect of drying method on physical and chemical quality, hotness and volatile flavour characteristics of dried chilli. *International Food Research Journal*, 19(3), 1023-1031.
- Torres, B., Tiwari, B. K., Patras, A., Wijngaard, H. H., Brunton, N., Cullen, P. J., & O'Donnell, C. P. (2011). Effect of ozone processing on the colour, rheological properties and phenolic content of apple juice. *Food Chemistry*, 124(3), 721-726.
- Whangchai, K., Uthabutra, J., Phiyalaninmat, S., Pengphol, S., & Nomura, N. (2011). Effect of ozone treatment on the reduction of chlorpyrifos residues in fresh lychee fruits. *Ozone: Science and Engineering*, 33(3), 232-235.

Modeling River Flow using Artificial Neural Networks: A Case Study on Sumani Watershed

Nova Anika^{1*} and Tasuku Kato²

¹*Agricultural and Environmental Engineering, Tokyo University of Agriculture and Technology, Japan*

²*International Environmental and Agricultural Science, Tokyo University of Agriculture and Technology, Japan*

ABSTRACT

The Sumani River is an important water resource used for agriculture and domestic purposes. The river is also the main water supply for Lake Singkarak and used for a power plant. Proper water resource management is required for sustainable water availability for all water users. A hydrological model is a necessary tool to assess water management in the watershed. However, most models require several data sources not readily available in developing countries that describe the internal structure of the watershed. Artificial neural networks (ANN) are biologically inspired computer programs designed to simulate the way in which the human brain processes information and are capable of modeling a nonlinear system. River flow is an indicator of water availability in the watershed. It is greatly influenced by rain, so it has a pattern for its intensity. The objective of this study was to develop an artificial network model to predict river discharge in the Sumani River from rainfall and discharge patterns. Multiple Layer Perceptron with the backpropagation algorithm was applied to predict river flow. Data on rainfall and

discharge from the preceding day from 2008 to 2012 were used to train the model, and data from 2013 to 2014 were used to test the model. The Sumani River ANN scheme can be used to predict river flow with correlation coefficients of 0.95 and 0.92 in the training and testing stages.

ARTICLE INFO

Article history:

Received: 24 October 2018

Accepted: 15 February 2019

Published: 21 June 2019

E-mail addresses:

nv_anika@yahoo.com (Nova Anika)

taskkato@cc.tuat.ac.jp (Tasuku Kato)

* Corresponding author

Keywords: Artificial neural networks, Indonesia, river flow

INTRODUCTION

By the year 2050, the world population is projected to grow to nine billion people, with six billion of these people living in developing countries (Roson & van der Mensbrugge, 2010). This condition leads to an increased demand for food and water, with supply needing to increase around 60% (FAO, 2014). In addition, population growth decreases the available land, water, and labor resources, which threatens sustainability of rice production (Molden, 2007). The agricultural sector already draws around 70% of freshwater (Bates et al., 2008), but this will increase another 10% by 2050 (Dubois, 2011). This condition will threaten rice production, especially in the developing countries, such as Indonesia, which is the third largest producer of rice worldwide and one of the world's largest rice consumers (GRiSP, 2013).

Proper water resources management strategies are required for sustainable water availability. It is a prerequisite to have a clear understanding of the watershed hydrological processes, manageable water flows, interactions with land use, and opportunities to mitigate the negative effects and increased benefits of water depletion on society (Karimi et al., 2013). Such an assessment on water resources is required to address future concerns. Therefore, watershed models have important roles as tools to evaluate sustainable water resources.

Hydrological models are necessary to address water resource management in the watershed. They have been applied mainly to estimate water availability and to estimate the water regime of the watershed in a fast, economical, and safe (Pereira et al., 2016). However, most of hydrological model required several data that described the watershed condition where the limited data tend to be found in the developing country that affect the performance of model.

Artificial neural networks (ANN) are biologically inspired computer programs designed to simulate the way in which the human brain processes information (Agatonovic-Kustrin & Beresford, 2000). They are used increasingly in the analysis of hydrology and water resources, because ANN models do not require the internal structure of a watershed. ANNs are trained through experience with appropriate learning exemplars and gather their knowledge by detecting the patterns and relationships in data (Agatonovic-Kustrin & Beresford, 2000). The advantage of neural networks is their capability to model a nonlinear system (Aichouri et al., 2015).

River discharge, classified as blue water, is used typically as an indicator to analyze water availability in the watershed. It is influenced greatly by rain, which influences its intensity. Hence, the primary objective of this study is to develop an artificial network model to analyze hydrological conditions by predicting river discharge using rainfall and river discharge patterns.

MATERIALS AND METHODS

Study Area

The Sumani River (Figure 1) is an important water resource in the Solok Regency, West Sumatera, Indonesia that is used mainly for agriculture and domestic purposes. This river is also a main water supply for Lake Singkarak that is used for agriculture, domestic and power plant. The Sumani watershed has a humid tropical climate, with an annual average rainfall of 1896 mm that peaks between November and February (Indonesian Ministry of Public Work, 2015). The rainfall intensity ranges from 25.7 mm/month to 422.8 mm/month (Indonesian Ministry of Agriculture, 2015), and average monthly water flow ranges from 4.5 m³/s to 29.04 m³/s between 2008 and 2014 (Indonesian Ministry of Public Work, 2015).

Artificial Neural Networks

Artificial neural networks can be considered as an interconnected assembly of simple processing elements, and the processing ability of network is stored in the inter-unit connection strengths or weights obtained by a process of learning from a set of training patterns (Singh & Prajneshu, 2008). The objective of a neural network is to compute output values from input values by some internal calculations (Nasr et al., 2012). In general, an artificial neural network can be divided into three parts that are known as (1) an input layer, which is responsible for receiving information (data), signals, features, or measurements from the external environment; (2) a hidden layer that is composed of neurons that are

responsible for extracting patterns associated with the process or system being analyzed; and (3) an output layer that is responsible for producing and presenting the final network outputs, which result from the processing performed by the neurons in the previous layers (Da Silva, et al., 2017).

The information to the input nodes (i) forward this information to all nodes of the hidden layer. At any hidden node (h), the information received from all input nodes and the bias node of the input layer is summed up as Equation 1 (Ghumman, et al., 2011):

$$x_h = \sum_{j=1}^{j=n} w_{hj}i_j + w_{hb}b_i \quad [1]$$

where x_h is the input signal; w_{hj} is the synaptic weight between hidden and input

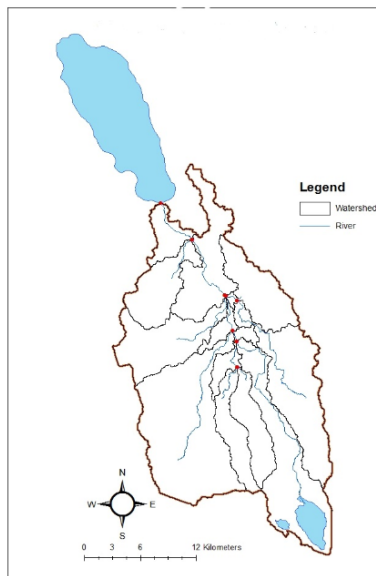


Figure 1. Sumani watershed

layers; w_{hb} is the synaptic weight between the hidden and bias node of the input layer; ‘ i ’ is the input node and ‘ b_i ’ is the bias node of the input layer.

The input signal is passed through a nonlinear activation function to produce the output signal of the node. The logistic sigmoid function is used for the networks, as it is continuously differentiable, monotonic, symmetric, and bounded between 0 and 1 (Equation 2) (Aichouri et al., 2015; Lee & Kang, 2016):

$$f(x_h) = \frac{1}{1 + e^{-x_h}} \quad [2]$$

where $f(x_h)$ is transfer function and x_h is the input signal.

Artificial Neural Networks (ANN) Schemes of the Study Area

In this study, the Multiple Layer Perceptron (MLP) algorithm was applied to predict river discharge. The input data is the preceding day’s rainfall (Pt-n) and discharge (Qt-n) data, including the rainfall data for the expected day (Pt). The output data was the discharge data for the expected day (Qt). Rainfall and discharge data from 2008 to 2012 were used to train the model, while the data from 2013 to 2014 was used for model testing. The ANN model was developed using the Stuttgart Neural Network Simulator (SNNS) written in the R programming code.

There are three schematics of the ANN model structure chosen for trial. In Model 1, the input variables are rainfall and discharge data for the preceding five days and rainfall data for the expected day (Figure 2). Model 2 includes the input variables of rainfall for the expected day and discharge for the preceding five days. In Model 3, the inputs are the discharge data for the preceding five days. The model simulation was stopped after 500 iterations, and the number of neurons in hidden layers was selected by trial and error.

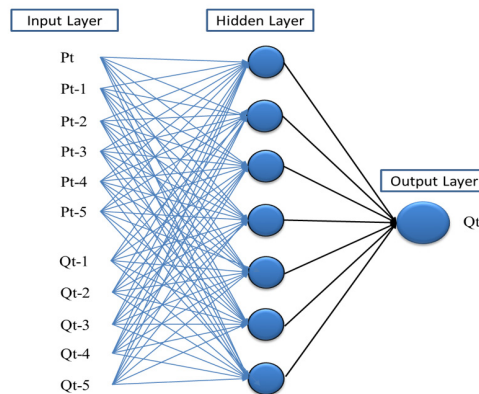


Figure 2. A schematic of the ANN Model in the study area

The performance of the ANN will be analyzed using statistical indicators, such as a root mean square error (Equation 3) and correlation coefficient (Equation 4) (Joorabchi et al., 2007);

$$RMSE = \sqrt{\frac{\sum_{t=1}^N (y_t - x_t)^2}{N}} \quad [3]$$

$$r = \frac{\sum_{t=1}^N (x_t - \bar{x})(y_t - \bar{y})}{\sqrt{\sum_{t=1}^N (x_t - \bar{x})^2 \sum_{t=1}^N (y_t - \bar{y})^2}} \quad [4]$$

where RMSE is root mean square error; r is correlation coefficient; x_t is the observed values at the respective time step, y_t is the simulated values at the respective time step, N is the number of time increments, and \bar{x} and \bar{y} are the mean values of observations and simulations, respectively. The r value ranges from 0 -1 and indicates: 0 is no correlation, 0–0.25 is a very weak correlation, 0.25–0.50 is a fair correlation, 0.50–0.75 is a strong correlation, 0.75–0.99 is a very strong correlation and 1 is a perfect correlation (Hadiani, 2015).

Hydrological Indicators

The Sumani watershed is evaluated based on hydrological indicators using a simulated discharge that has specific maximum discharge, specific minimum discharge, and a coefficient of surface runoff (Setyawan et al., 2016). The specific maximum (Equation 5) and minimum discharge (Equation 6) indicate the vulnerability to flooding and drought (Paimin et al., 2010). In addition, coefficient surface run off that indicate the run off rate is calculated using Rational Method Runoff Coefficients (Equation 7) (Hayes & Young, 2006).

$$Q_{maxs} = \frac{Q_{max}}{A} \quad [5]$$

$$Q_{mins} = \frac{Q_{min}}{A} \quad [6]$$

$$Q = C_u CIA \quad [7]$$

where Q_{maxs} is specific maximum discharge ($m^3/s/km^2$); Q_{max} is maximum discharge (m^3/s); A is watershed area (km^2); Q_{mins} is specific minimum discharge ($m^3/s/km^2$); Q_{min} is minimum discharge (m^3/s); Q is the peak discharge (m^3/s); C_u is units conversion coefficient; C is runoff coefficient; I is rainfall intensity (mm/day).

Data Collection

The daily rainfall data were collected from rainfall stations of the Indonesian Ministry of Agriculture located in the downstream region of the Sumani watershed. The discharge data were collected from the gauge station of the Indonesian Ministry of Public Work located near the outlet of the watershed. The data records were from July 2008 to December 2014.

RESULTS AND DISCUSSION

Model Performance

The ANN schematic of Model 1 and Model 2 have good performance in describing the relationship between rainfall and discharge. Both models show a strong correlation between rainfall and discharge. In addition, to check the reliability of the discharge data, Model 3 showed the best performance in predicting discharge of the expected day using discharge data of the preceding five days. Even though the error in the compatibility of the rainfall and discharge data decreased model performance, all model schemes can be used to predict discharge in the study area.

Based on statistical indicators (Table 1), the best ANN schematic to describe rainfall and discharge relationship is Model 2, with the input data of rainfall of the expected day and discharge data of the preceding five days. Model reliability in the training stage is slightly higher than in the testing stage, as shown by the r values that are higher in the training stage and RMSE values that are lower in the training stage compared to the testing stage.

Table 1.

Statistical indicators of AAN model performance

Schemes	Nodes		Training (2008-2012)		Testing (2013-2014)	
	Inputs	Neurons	r	RMSE	r	RMSE
Model 1	11	7	0.86	2.63	0.82	3.01
Model 2	6	4	0.95	2.04	0.92	2.51
Model 3	5	3	0.96	1.95	0.94	2.39

Training Stage and Testing Stage

Figure 3 shows that the discharge simulation pattern explained a rainfall pattern with significant information for discharge prediction. The simulated discharge fluctuation was smaller than the observed discharge, and the pick of simulated discharge was lower than observed discharge. The average observed discharge from 2008 to 2012 was $10.9 \text{ m}^3/\text{s}$, or approximately 31% of the average annual rainfall of 1904 mm. The wet season was from October to April, and the dry season occurred between May and September. The daily discharge fluctuated from $2.2 \text{ m}^3/\text{s}$ in the dry season to $71.1 \text{ m}^3/\text{s}$ in the wet season. The average discharge of the model simulation was $10.9 \text{ m}^3/\text{s}$. The discharge fluctuation of Model 2 and Model 3 ranged from $2.5 \text{ m}^3/\text{s}$ to $39.7 \text{ m}^3/\text{s}$ and from 2.7 to $39.5 \text{ m}^3/\text{s}$, respectively. In addition, the simulated discharge of Model 1 fluctuated from $2.4 \text{ m}^3/\text{s}$ to $43.8 \text{ m}^3/\text{s}$.

In the testing stage (2013-2014), the average discharge was approximately 28% of the annual 2035 mm of rainfall. The wet season lasted from October to May and the dry

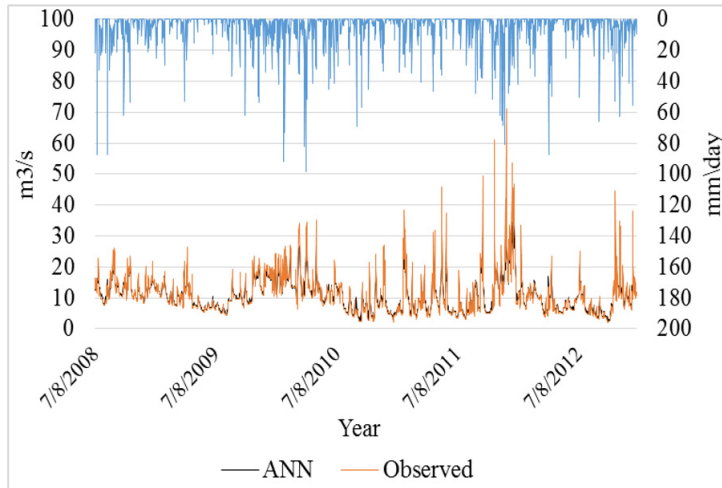


Figure 3. The observed and simulated discharge of Model 2 in the training stage

season lasted between June and September. The average observed discharge was $10.5 \text{ m}^3/\text{s}$, with a minimum discharge of $3.9 \text{ m}^3/\text{s}$ and a maximum discharge of $80.9 \text{ m}^3/\text{s}$. Model 2 fluctuated from $4.5 \text{ m}^3/\text{s}$ to $45.1 \text{ m}^3/\text{s}$. The fluctuation of Model 3 was less than Model 2, with a minimum discharge of $4.5 \text{ m}^3/\text{s}$ to a maximum discharge of $42.3 \text{ m}^3/\text{s}$. Model 1 had the greatest fluctuation range from $4.2 \text{ m}^3/\text{s}$ to $50.2 \text{ m}^3/\text{s}$. The observed and simulated discharge in the testing stage is shown in Figure 4.

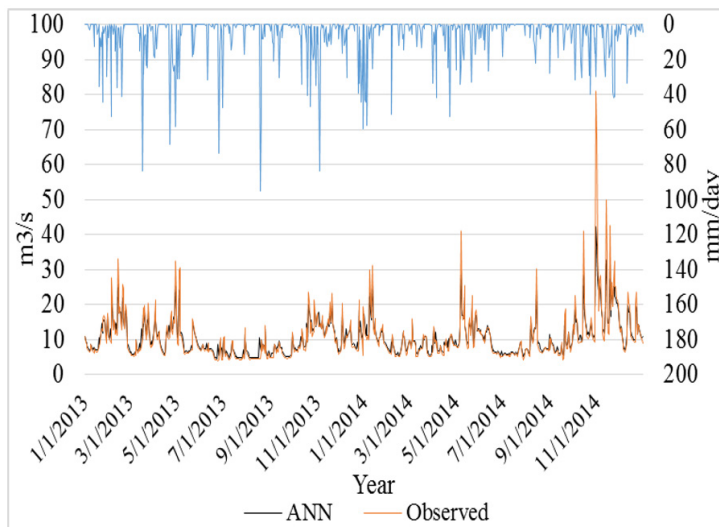


Figure 4. The observed and simulated discharge of Model 2 in the testing stage

Watershed Evaluation

The specific maximum discharges are divided into three categories according to (Paimin et al., 2010) and (Setyawan et al., 2016): “good” (<0.58), “moderate (between 0.58 and 1.5), and “bad” (>1.5). The specific minimum discharge also is divided into three categories: “good” (>0.03), “moderate” (0.01-0.03), and “bad” (<0.01) (Paimin et al., 2010). For coefficient surface runoff, it is considered as “good” if the value is <0.1 , “moderate” if the value is between 0.1 and 0.3, and “poor” if the value is >0.3 (State Water Resources Control Board, 2011).

The specific maximum discharge of the Sumani watershed is $0.07 \text{ m}^3/\text{s}/\text{km}^2$. This value indicates that the Sumani watershed has a low potential for flooding. However, the Sumani watershed has a moderate potential for drought, with a specific minimum discharge of $0.01 \text{ m}^3/\text{s}/\text{km}^2$. In addition, the coefficient surface runoff of the Sumani watershed is 0.2. The coefficient run off shows that this watershed has a moderate probability of surface runoff.

CONCLUSIONS

An ANN model scheme with four neurons and inputs of rainfall for the expected day and discharge for the preceding five days is the best model to describe the relationship between rainfall and discharge in the study area. This model was trained with data from 2008-2012 and validated using data from 2013 to 2014 and accurately predicts the discharge for the expected day. The average observed and simulated discharge are similar. The fluctuation in the simulated discharge is smaller than the observed discharge, with the peak simulated discharge at only half of the peak observed discharge. However, based on statistical indicators, all ANN model schemes in this study can be used to predict daily discharge in the Sumani watershed. Based on hydrological indicators using simulated discharge, the Sumani watershed has a low potential for flooding, moderate potential for drought, and a moderate probability for surface runoff.

ACKNOWLEDGEMENTS

The authors gratefully acknowledge Indonesian Ministry of Agriculture and Indonesian Ministry of Public Work for providing relevant information and valuable data. The authors also acknowledge the financial support of Ministry of Research, Technology and Higher Education of Indonesia.

REFERENCES

- Agatonovic-Kustrin, S., & Beresford, R. (2000). Basic concepts of artificial neural network (ANN) modeling and its application in pharmaceutical research. *Journal of Pharmaceutical and Biomedical Analysis*, 22(5), 717–727.

- Aichouri, I., Hani, A., Bougherira, N., Djabri, L., Chaffai, H., & Lallahem, S. (2015). River flow model using Artificial Neural Networks. *Energy Procedia*, 74, 1007–1014.
- Bates, B., Kundzewicz, Z. W., Wu, S., & Palutikof, J. (Eds.). (2008). *Climate change and water*. Geneva, Switzerland: Intergovernmental Panel on Climate Change.
- Da Silva, I. N., Spatti, D. H., Flauzino, R. A., Liboni, L. H. B., & dos Reis Alves, S. F. (2017). *Artificial Neural Networks : A practical course*. Springer International Publishing. Retrieved May 24, 2018, from [//www.springer.com/la/book/9783319431611](http://www.springer.com/la/book/9783319431611)
- Dubois, O. (2011). *The state of the world's land and water resources for food and agriculture: Managing systems at risk*. New York, USA: The Food and Agriculture Organization of the United Nations.
- FAO. (2014). *The water-energy-food nexus: A new approach in support of food security and sustainable agriculture*. Food and Agriculture Organization of the United Nations. Retrieved May 24, 2018, from <http://www.fao.org/3/a-bl496e.pdf>
- Ghumman, A. R., Ghazaw, Y. M., Sohail, A. R., & Watanabe, K. (2011). Runoff forecasting by artificial neural network and conventional model. *Alexandria Engineering Journal*, 50(4), 345–350.
- GRiSP. (2013). *Rice almanac* (4th Ed.). Global Rice Science Partnership. Retrieved May 24, 2018, from http://books.irri.org/9789712203008_content.pdf.
- Hayes, D. C., & Young, R. L. (2006). *Comparison of peak discharge and runoff characteristic estimates from the rational method to field observations for small basins in central Virginia* (USGS Numbered Series No. 2005–5254). Retrieved May, 24 2018, from <http://pubs.er.usgs.gov/publication/sir20055254>
- Indonesian Ministry of Agriculture. (2015). *Rainfall data of Saniang Baka climatological station 2008-2014* (pp. 1-84). West Sumatra, Indonesia: Ministry of Public Work.
- Indonesian Ministry of Public Work. (2015). *Discharge data of Sumani river gauge station 2008-2014* (pp. 1-84). West Sumatra, Indonesia: Ministry of Public Work.
- Joorabchi, A., Zhang, H., & Blumenstein, M. (2007). Application of artificial neural networks in flow discharge prediction for the Fitzroy River, Australia. *Journal of Coastal Research*, 50, 287-291.
- Karimi, P., Bastiaanssen, W. G. M., & Molden, D. (2013). Water Accounting Plus (WA+); a water accounting procedure for complex river basins based on satellite measurements. *Hydrology and Earth System Sciences*, 17(7), 2459–2472.
- Lee, D. H., & Kang, D. S. (2016). The application of the artificial neural network ensemble model for simulating streamflow. *Procedia Engineering*, 154, 1217–1224.
- Molden, D. (Ed.). (2007). *Water for food, water for life: A comprehensive assessment of water management in agriculture*. London, UK: Earthscan.
- Nasr, M. S., Moustafa, M. A. E., Seif, H. A. E., & El Kobrosy, G. (2012). Application of Artificial Neural Network (ANN) for the prediction of EL-AGAMY wastewater treatment plant performance-EGYPT. *Alexandria Engineering Journal*, 51(1), 37–43.
- Paimin, Sukresno, & Purwanto. (2010). *Prompt investigation on sub-watershed degradation*. Retrieved May 28, 2018, from http://www.forda-mof.org/files/Sidik_Cepat_Degradasi_SubDAS.pdf

- Pereira, D. D. R., Martinez, M. A., Pruski, F. F., & da Silva, D. D. (2016). Hydrological simulation in a basin of typical tropical climate and soil using the SWAT model part I: Calibration and validation tests. *Journal of Hydrology: Regional Studies*, 7, 14–37.
- Roson, R., & van der Mensbrugge, D. (2010). *Climate change and economic growth: Impacts and interactions*. Retrieved May 24, 2018, from file:///C:/Users/SuiriNEC/Favorites/Downloads/SSRN-id1594708.pdf
- Setyawan, C., Lee, C. Y., & Prawitasari, M. (2016). Hydrologic modeling for tropical watershed monitoring and evaluation. *American Journal of Engineering Research (AJER)*, 5(11), 36-42.
- Singh, R. K., & Prajneshu. (2008). Artificial Neural Network methodology for modelling and forecasting Maize crop yield. *Agriculture Economics Research Review*, 21, 5-10.
- State Water Resources Control Board. (2011). *The clean water team guidance compendium for watershed monitoring*. Retrieved May 28, 2018, from <https://www.coursehero.com/file/p6c13pd/The-Clean-Water-Team-Guidance-Compendium-for-Watershed-Monitoring-and/>

The Potential of Fluorescence Technology for Quality Monitoring of Miyauchi Iyokan (*C. iyo* Hort. Ex Tanaka) during Post-harvest Treatment

Muharfiza^{1,2*}, Dimas Firmanda Al Riza^{1,3}, Nie Sen¹, Yasushi Kohno⁴, Tetsuhito Suzuki¹, Makoto Kuramoto⁵ and Naoshi Kondo¹

¹Division of Environmental Science and Technology, Graduate School of Agriculture, Kyoto University, Kyoto 606-8502, Japan

²Indonesia Agency for Agricultural Research and Development, Ministry of Agriculture, Jakarta 12540, Indonesia

³Departement of Agricultural Engineering, Faculty of Agricultural Technology, University of Brawijaya, Malang 65145, Indonesia

⁴Department of Planning and Environment, Ehime Research Institute of Agriculture, Forestry and Fisheries, Matsuyama 700-2405, Ehime, Japan

⁵Advanced Research Support Center, Ehime University, Matsuyama 790-8577, Ehime, Japan

ABSTRACT

The potential of fluorescence technology for monitoring Miyauchi Iyokan citrus during post-harvest treatment was investigated in this research. Citrus fruits were harvested when still a greenish-yellow color with a low soluble solids (SS)/acid ratio. Dark storage of fruits at 80-90% of RH and 6-10⁰C for sixty days is expected to increase the quality of the fruits (becoming reddish orange in color and having a high SS/acid ratio). However, monitoring the quality during the treatment is substantial. In general, farmers monitored

the quality by seeing the appearance, however, this way is subjective. Thus, the fluorescence technique was proposed since it was objective, relatively cheap and easy to apply. Two main fluorescence compounds from peel, polymethoxylated flavones (PMFs) (Ex. 370 nm/Em. 540 nm) and tryptophan-like (Ex. 260 nm/Em. 330 nm) compounds were found, and PMFs were used in this research since it is an essential constituent for the fruit quality. This work demonstrated that during treatment bright

ARTICLE INFO

Article history:

Received: 24 October 2018

Accepted: 15 February 2019

Published: 21 June 2019

E-mail addresses:

muharfiza@gmail.com (Muharfiza)

dimasfirmanda@yahoo.com (Dimas Firmanda Al Riza)

nisbetter@gmail.com (Nie Sen)

kohno-yasusi@pref.ehime.lg.jp (Yasushi Kohno)

ts@kais.kyoto-u.ac.jp (Tetsuhito Suzuki)

kuramoto.makoto.mx@ehime-u.ac.jp (Makoto Kuramoto)

kondonao@kais.kyoto-u.ac.jp (Naoshi Kondo)

* Corresponding author

yellow color (suspected PMF compounds) had appeared when excited under 365 nm with UV-light from the beginning of storage period until day eighty, however, day fifty and sixty showed stronger intensity. Furthermore, SS/acid ratio reached the highest peak in day sixty. In addition, on day sixty an unpleasant odor appeared, which might be related to the off-flavor condition of metabolic excess. These results demonstrate the potential of fluorescence to monitor citrus fruit quality changes during postharvest treatment

Keywords: Acidity, iyokan, post-harvest treatment, polymethoxylated flavones, soluble solid content, tryptophan-like

INTRODUCTION

Miyauchi Iyokan (*C. iyo* Hort. Ex Tanaka) is usually harvested in December in Japan when it is still greenish-yellow in color. Collection is done preventing low-temperature injury to the fruit during the winter. However, at this stage the fruit still has a low Soluble Solid (SS)/acid ratio; thus an improvement in this ratio is required before fruit quality becomes acceptable for sales. To achieve this increased ratio, the Iyokan are stored for two months at 5-15^oC until they reach the desired criteria, such as color (reddish orange), a sweet and aromatic flavor, and a glossy surface (Kondo et al., 2000; Uchida et al., 1983). This storage period is referred to as the “post-harvest treatment” process.

In general, during the post-harvest storage period, fruit quality monitoring is not conducted by the farmer. Moreover, the main quality attribute which changes during this post-harvest period is the internal fruit quality characteristic of SS/acid ratio (Marcilla et al., 2006). Techniques to determine the SS/acid ratio and color of fruit have been successfully applied to postharvest fruit sorting operations. In the case of citrus, many on a farm, as well as off-farm techniques, such as Brix and acid meters, Near Infrared Spectroscopy (NIR), and machine vision system have been utilized.

In the citrus industry brix and acid refractometers are widely used to measure SS and acidity (Olmo et al., 2000). While these methods are accurate, cheap, and fast, they are, unfortunately, destructive. On the other hand, near-infrared spectroscopy (NIR), which has also been widely used in the citrus grading industry for many years, is a robust and non-destructive method for quantifying SS content of citrus fruit (Ruslan et al., 2012; Zude et al., 2008). Its drawback is, however, the technology is relatively expensive and beyond the reach of many individual farmers. Another technique, a machine vision based system, quantifies citrus quality based on color (color component ratios, such as R/G (red/green), or the R/G value of the reddish fruit and the correlation of this to sweetness) (Iqbal et al., 2016; Kondo et al., 2000). The disadvantage of the methods based on this technology is the requirement for specific artificial lighting conditions in strictly controlled dark room situations.

Although it has not been applied to citrus, fluorescence spectroscopy is another possible technique without the above disadvantages, which has been widely used for assessing the maturity of mango by utilizing chlorophyll fluorescence (Lechaudel et al., 2010); the ripening of apples by utilizing anthocyanin, flavonol, and chlorophyll concentration (Betemps et al., 2012); the maturity of grapes by monitoring the anthocyanin accumulation (Agati et al., 2013; Ghozlen et al., 2010), and for the maturity classification for oil palm bunches using multiple spectral bands (Saeed et al., 2012). Fortunately, Iyokan is a fruit that is categorized as containing medium levels of fluorescence compounds that are relatively easy to detect. Thus, this study aims to explore the potential of fluorescence techniques to monitor citrus fruit quality during the post-harvest treatment process. To do this, fluorescence characteristics of the fruit were observed during the post-harvest period under 365 nm UV-light and compared to standard fruit quality measurements of SS/acid ratio.

MATERIALS AND METHODS

Tested Materials

In this experiment, 240 Miyauchi Iyokan (*C. iyo* Hort. Ex Tanaka) fruit were harvested in December 2016 (210 days after anthesis) from 20-year-old trees growing in the Ehime Research orchard, Ehime Prefecture, Japan.

Methods

Sample Preparation. After harvest, the fruit was then sorted manually based on peel appearance, with only the whole fruit being selected as potential samples. Color images of the fruit were then captured using a color camera equipped with a polarized filter and illuminated by four halogen lamps. Subsequently, based on the color component ratio red/green (R/G) (using Python™ Version 2.7.12 with OpenCV Version 2.4.13 library algorithm, Delaware, USA), the potential samples were reduced to 135. Finally, 27 fruits which had the closest color component values were selected from this 135 fruit.

The 27 selected fruits were kept at ambient temperature and 80-90% RH. All fruits were kept in fruit baskets, covered with paper, and stored in a storage room for 80 days. Measurements were made at ten-day intervals for a total of nine times, with measurements replicated three times and data averaged (data reported in this article is the average value). At each measurement time, three fruit was extracted and measurements made. Time-lapse color and UV-images were taken under halogen lamps and a 365 nm UV-light. A cross-sectional peel image for observing the cuticle layer was also captured using a microscope (Keyence VH-Z250R microscope) coupled with image acquisition software.

Standard Soluble Solid Content and Acidity Measurement. Soluble solids content (SSC) and acidity were measured using a hand-held digital refractometer (Atago PAL-BX | ACID F5, Atago Co., Ltd., Tokyo, Japan). The flesh sample was squeezed manually to

collect the juice and then filtered (Whatman No. 41 filter paper). A 0.2 mL clear liquid aliquot of the juice was directly pipetted (Pipetman P1000, Gilson Inc, USA) onto the refractometer and SSC content (% Brix) measured. Once the Brix value was recorded, the aliquot was diluted by adding distilled water up to 10 mL on the refractometer, and the acidity measured and recorded as a percentage of citric acid. Also in this paper, SSC/acid ratio was calculated as a fruit flavor determination.

RESULT AND DISCUSSION

Soluble Solids, Acidity during Storage

Citrus is considered to be a non-climacteric fruit, which means after harvesting the maturing process stops and the fruit enters a senescent period. Farmers generally perform postharvest treatment for sixty days without monitoring the process at all. Results show that during the experimental postharvest treatment, the SS/acid ratio of the Iyokan fruit juice remained relatively constant from day one to thirty, then significantly increased after that until day sixty (Figure 1) remaining stable until day eighty. The increasing SS/acid ratio from day thirty to sixty is thought to be due to the decreasing in acidity in citrus fruit, which is, at least in part, due to the breakdown of the organic acid for energy production and alcoholic fermentation (Echeverria & Valich, 1989; El-Otmani & Coggins, 1991).

Valencia oranges have been reported to develop a distinct flavor and high ethanol concentration after long storage (Marcilla et al., 2006; Shi et al., 2007). The main reason for these changes is caused by low concentrations of metabolic compounds in the juice and of off-flavour volatiles, such as ethanol and acetaldehyde (Shi et al., 2005). In our experiment, we observed from day fifty to eighty that the acid content declined to its lowest level and remained stable until the fruit began to decay. Besides, on day sixty we observed an unpleasant odor. This perceived odor give an ethanol-like aroma.

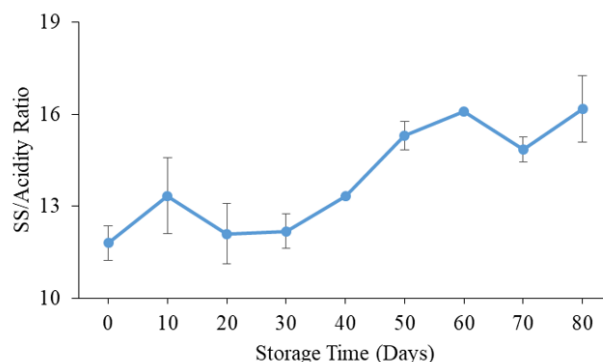


Figure 1. Soluble solids (SS) and acidity (as a % of citric acid) ratio during the post-harvest period under 80-90% RH.

Fruit Condition during Postharvest Treatment

The appearance of Iyokan fruits under UV-light (UV-images) progressed as shown in Figure 2. Fruit observed under the halogen lamps showed little change in color (images are not shown). However, under UV-light, the differences can be easily found among the fruit. On the day sixty an intense bright yellow color could be observed, which we suspected to be related to the presence of polymethoxylated flavones (PMFs) (Dugo et al., 2005; Muharfiza et al., 2017). Since PMFs have a strong fluorescence when excited at 365 nm, this yellow color also has the potential to mark the deterioration of the fruit. Muharfiza et al. (2017) also found the main compounds in citrus Unshiu were suspected as tryptophan-like (Ex. 260 nm/Em. 330 nm) and polymethoxylated flavones (PMFs) (Ex. 370 nm/Em. 540 nm), based on their report PMFs has the strong fluorescence intensity. And machine vision based on PMFs fluorescence excitation wavelength was constructed as shown in Figure 3.

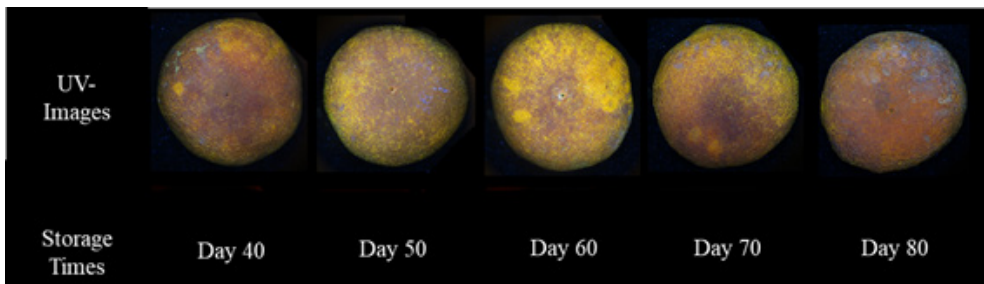


Figure 2. Iyokan appearance during postharvest treatment under 365 nm UV-light.

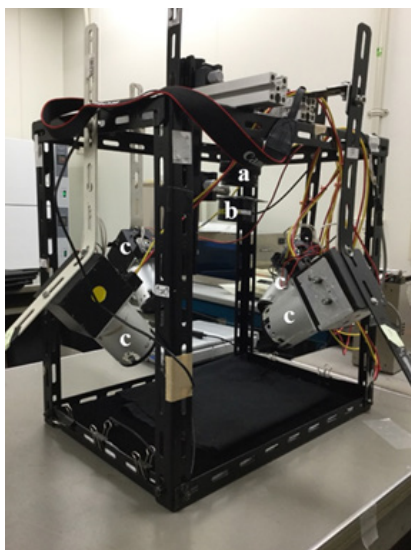


Figure 3. Machine vision system: (a) camera; (b) 365 nm UV-light; (c) halogen lamps

The bright yellow color became conspicuous from day fifty to sixty, this bright color might be a critical signal during the treatment period, and here, the internal fruit changes related to the quality are occurring. Figure 1 demonstrates that the peak ratio was reached on day sixty and remaining stable flavor afterward. Also, the abnormal odor perceived on day sixty reinforced the suspicion that during this period the metabolism of the organic acid for energy and the production of off-aromas from alcoholic fermentation marked the transition to over-maturity (Echeverria & Valich, 1989; Shi et al., 2005).

In fact, PMFs are suspected to be responsible for the bright yellow fluorescence that is visible on the peel surface because of the oil glands rupture and allowing oil diffusing until the peel surface (Slaughter et al., 2008). The literature would suggest that this bright yellow color is due to the breakdown of oil glands during postharvest treatment and the gradual movement of this oil to the peel surface, which is visible when illuminated under ultraviolet (Obenland et al., 2009). In addition, the degradation of the citrus cuticle layer at this time would enhance movement of the oil to the surface. This cuticle condition could play an important role as a sensing or an interaction with the surrounding environment (Domínguez et al., 2011; Lara et al., 2015).

The fresh peel has a thicker and smoother cuticle, and the epidermal cell beneath the cuticle was uniform (Figure 4). Several weeks after storage the cuticle became thinner, rougher and the epidermal cell became more difficult to observe, this phenomena caused by the climatic condition and might be affected the degradation of oil glands (Lara et al., 2014). This degradation (break-up) of the oil glands would enable the spread of the oil to the surface, making it visible under the UV-light. Thus, this signal could be an important signal for optimum storage time.

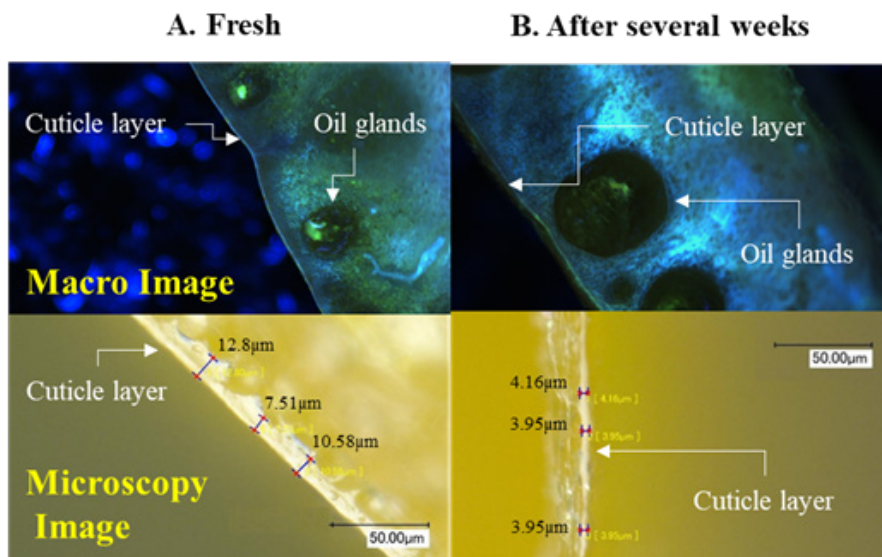


Figure 4. The cross-section macro and microscopy images of Iyokan peel: (A) fresh citrus; (B) stored after several weeks. Macro images were illuminated under 365 nm UV-light.

CONCLUSION

Fluorescence measurements of Iyokan fruit made during the postharvest period identified PMFs as the main compounds observed. The presence of the compounds provides an opportunity to determine optimum storage time for high-quality fruit. Over the examined

storage treatment period, from day fifty to sixty, a critical period was observed, where a bright yellow background color on the peel surface was apparent and was indicative of the beginning of fruit deterioration.

RECOMMENDATION AND FUTURE WORKS

In this paper, fluorescence measurements were shown to have the potential to classify Miyauchi Iyokan quality in a sorting line application. This study provides basic research details on fluorescent spectroscopy of Miyauchi Iyokan using right angle measurement (extraction method), however, in industrial applications, a front-face measurement (solid method) is probably more applicable.

ACKNOWLEDGEMENTS

I would like to thank the Ministry of Agriculture of the Republic of Indonesia for granting the scholarship during this study. Thanks to Supporting Program for InteRaction-Based Initiative Team Studies (SPIRITS) for funding this research, and my honor to say thanks to Prof. Garry Piller for proof-reading this article.

REFERENCES

- Agati, G., D'Onofrio, C., Ducci, E., Cuzzola, A., Remorini, D., Tuccio, L., Iazzinis, F., & Mattii, G. (2013). Potential of a multiparametric optical sensor for determining *in situ* the maturity components of red and white *Vitis vinifera* wine grapes. *Journal of Agricultural and Food Chemistry*, *61*(50), 12211–12218.
- Betemps, D. L., Fachinello, J. C., Galarça, S. P., Portela, N. M., Remorini, D., Massai, R., & Agati, G. (2012). Non-destructive evaluation of ripening and quality traits in apples using a multiparametric fluorescence sensor. *Journal of the Science of Food and Agriculture*, *92*(9), 1855–1864.
- Domínguez, E., Cuartero, J., & Heredia, A. (2011). An overview on plant cuticle biomechanics. *Plant Science*, *181*(2), 77–84.
- Dugo, P., Mondello, L., Favoino, O., Cicero, L., Zenteno, N. A. R., & Dugo, G. (2005). Characterization of cold-pressed Mexican dancy tangerine oils. *Flavour and Fragrance Journal*, *20*(1), 60–66.
- Echeverria, E., & Valich, J. (1989). Enzymes of sugar and acid metabolism in stored “Valencia” oranges. *Journal of the American Society for Horticultural Science (USA)*, *114*, 445–449, Retrieved May 12, 2018, from <http://agris.fao.org/agris-search/search.do?recordID=US8924848>
- El-Otmani, M., & Coggins, C. W. (1991). Growth regulator effects on retention of quality of stored citrus fruits. *Scientia Horticulturae*, *45*(3), 261–272.
- Ghozlen, N. B., Cerovic, Z. G., Germain, C., Toutain, S., & Latouche, G. (2010). Non-destructive optical monitoring of grape maturation by proximal sensing. *Sensors*, *10*(11), 10040–10068.
- Iqbal, S. M., Gopal, A., Sankaranarayanan, P. E., & Nair, A. B. (2016). Classification of selected citrus fruits based on color using machine vision system. *International Journal of Food Properties*, *19*(2), 272–288.

- Kondo, N., Ahmad, U., Monta, M., & Murase, H. (2000). Machine vision based quality evaluation of Iyokan orange fruit using neural networks. *Computers and Electronics in Agriculture*, 29(1–2), 135–147.
- Lara, I., Belge, B., & Goulao, L. F. (2014). The fruit cuticle as a modulator of postharvest quality. *Postharvest Biology and Technology*, 87(Supplement C), 103–112.
- Lara, I., Belge, B., & Goulao, L. F. (2015). A focus on the biosynthesis and composition of cuticle in fruits. *Journal of Agricultural and Food Chemistry*, 63(16), 4005–4019.
- Lechaudel, M., Urban, L., & Joas, J. (2010). Chlorophyll fluorescence, a nondestructive method to assess maturity of mango fruits (Cv. ‘Cogshall’) without growth conditions bias. *Journal of Agricultural and Food Chemistry*, 58(13), 7532–7538.
- Marcilla, A., Zarzo, M., & Río, M. A. D. (2006). Effect of storage temperature on the flavour of citrus fruit. *Spanish Journal of Agricultural Research*, 4(4), 336–344.
- Muharfiza, Al Riza, D. F., Saito, Y., Itakura, K., Kohno, Y., Suzuki, T., Kuramoto, M., & Kondo, N. (2017). Monitoring of fluorescence characteristics of satsuma mandarin (*Citrus unshiu* Marc.) during the maturation period. *Horticulturae*, 3(4), 51–61.
- Obenland, D., Margosan, D., Collin, S., Sievert, J., Fjeld, K., Arpaia, M. L., Thompson, J., & Slaughter, D. (2009). Peel fluorescence as a means to identify freeze-damaged navel oranges. *HortTechnology*, 19(2), 379–384.
- Olmo, M., Nadas, A., & García, J. M. (2000). Nondestructive methods to evaluate maturity level of oranges. *Journal of Food Science*, 65(2), 365–369.
- Ruslan, R., Ehsani, R., & Lee, W. S. (2012). Quantification of total soluble solids and titratable acidity for citrus maturity using portable VIS-NIR spectroradiometer. *Applied Engineering in Agriculture*, 28(5), 735–743.
- Saeed, O. M. B., Sankaran, S., Shariff, A. R. M., Shafri, H. Z. M., Ehsani, R., Alfatni, M. S., & Hazir, M. H. M. (2012). Classification of oil palm fresh fruit bunches based on their maturity using portable four-band sensor system. *Computers and Electronics in Agriculture*, 82, 55–60.
- Shi, J. X., Goldschmidt, E. E., Goren, R., & Porat, R. (2007). Molecular, biochemical and anatomical factors governing ethanol fermentation metabolism and accumulation of off-flavors in mandarins and grapefruit. *Postharvest Biology and Technology*, 46(3), 242–251.
- Shi, J. X., Porat, R., Goren, R., & Goldschmidt, E. E. (2005). Physiological responses of ‘Murcott’ mandarins and ‘Star Ruby’ grapefruit to anaerobic stress conditions and their relation to fruit taste, quality and emission of off-flavor volatiles. *Postharvest Biology and Technology*, 38(2), 99–105.
- Slaughter, D. C., Obenland, D. M., Thompson, J. F., Arpaia, M. L., & Margosan, D. A. (2008). Non-destructive freeze damage detection in oranges using machine vision and ultraviolet fluorescence. *Postharvest Biology and Technology*, 48(3), 341–346.
- Uchida, K., Matsumoto, M., Kobayashi, A., & Yamanishi, T. (1983). Composition of oxygenated compounds in peel oil from citrus iyo and its variation during storage. *Agricultural and Biological Chemistry*, 47(8), 1841–1845.
- Zude, M., Pflanz, M., Kaprielian, C., & Aivazian, B. L. (2008). NIRS as a tool for precision horticulture in the citrus industry. *Biosystems Engineering*, 99(3), 455–459.

Mechanical Analysis of a Wedge Device in Sawing Technology

Mohd Salahuddin Mohd Basri*, Mohd Zuhair Mohd Nor and
Rosnah Shamsudin

Department of Process and Food Engineering, Faculty of Engineering, Universiti Putra Malaysia,
43400 Serdang, Selangor, Malaysia

ABSTRACT

The oil palm trunk (OPT) currently represents a massive volume of agricultural waste with great potential to be rapidly developed in the wood composite industry. An improvement in sawing technology has potential to improve the yield of the commercially hard outer core of the OPT by about 27 % thus replacing the present sub-optimal square sawing pattern with a more efficient and higher-yielding polygon sawing pattern. To achieve this, a 'wedge' device was designed to be mounted on the existing sawing carriage. The proper methodology was followed including extraction of the design layout of the machine, development of the schematic drawing and wireframe model, modification of the design in computer-aided design (CAD) environment, the performance of stress, total deformation, and fatigue analysis, and production of a complete drawing for fabrication purpose. Results from the analysis showed that the designed part was safe to be fabricated with a small maximum equivalent stress of 2.546 MPa, maximum total deformation of 0.007935 mm and total life cycle of one million cycles. These evaluation results indicate that the material

used for the wedge device (including the base part) satisfies the design requirements of static strength and is safe within its designed fatigue life.

Keywords: Deformation, fatigue analysis, oil palm stems, polygon sawing pattern, sawmill carriage, stress, wedge

ARTICLE INFO

Article history:

Received: 24 October 2018

Accepted: 15 February 2019

Published: 21 June 2019

E-mail addresses:

salahuddin@upm.edu.my (Mohd Salahuddin Mohd Basri)

rosnahs@upm.edu.my (Rosnah Shamsudin)

zuhair@upm.edu.my (Mohd Zuhair Mohd Nor)

* Corresponding author

INTRODUCTION

The main issue faced by most wood manufacturers all over the world is the shortage of wood. The gap between supply and demand is big where the supplies of wood material are significantly lower as compared to the demand. This gap is becoming bigger due to the aggressive depletion of forest that leads to a reduced wood supply. On the other hand, the wood demand increases due to the fast population growth (Antwi-Boasiako & Boadu, 2016). Wood which is a raw material is classified into solid wood and composite wood. Between these two categories, solid woods have a more severe supply problem than the composites wood. As a result, many efforts have been made to increase the application of composites wood such as plywood, laminated veneer lumber (LVL), parallel strand lumber (PSL), particleboard, oriented strand board (OSB) and medium density fiberboard (MDF) as an alternative to the use of solid wood, and is becoming increasingly important (Kampman, et al., 2008). However, certain properties of solid wood cannot be compared with that of composites wood. This is the main reason why composites wood cannot be the substitution and at the same time, the demand for solid woods have never been on the decline, although their price becomes more expensive.

One of the agriculture wastes that can be used as an alternative material for solid wood is oil palm trunk (OPT). In Malaysia, it is estimated that about 120,000 hectares of oil palm were planted annually between 2006 and 2010 totaling about 4.3 million trees in 2007 (Wahid, 2008). Compared to fronds and empty fruit bunches, the OPT offers the best properties of wood. Tens of million cubic meters of OPT were yielded from the replanting of the old oil palm trees annually. The study also reported that oil palm wood from the outer parts of matured oil palm stems, which is more than 25 years old, have considerable good properties. Thus, these parts of the stem could be used as solid wood after being properly treated (Haslett, 1990). The production of solid wood requires the conversion of logs into sawn timber through the sawing process. There are three main sawing patterns used which are life or plain sawing, round sawing and quartered or rift sawing. All three patterns are suitable for hardwood and softwood logs which have central heartwood cores and peripheral sapwoods characteristic of dicotyledon species (Bakar et al., 1998). Saw logs from heartwood core are preferred due to their high quality. However, the round or polygon sawing pattern for OPT would be the most suitable sawing pattern. The polygon pattern should potentially produce the maximum volume of quality outer lumber as compared with life and quartered sawing patterns.

To date, no literature or patent on the wedge device used as an integrated part in sawmill carriage has been published. However, several patents on devices to facilitate the rotation of lumber for life sawing are available. Invention introduced by Yoder (1999) is a device mounted on a sawmill carriage that enables an operator to turn a log carried by the sawmill carriage. The device is such a time-saving convenience in the operation of sawmill and

it is widely used in sawmills throughout the country. Bonneau (1992) invented a timber device for positioning on the carriage log-door of a sawing plant. The device gives the angular direction that allows to obtain an optimal sawing for an irregular shape of lumber. However, there are some disadvantages to be fixed and many sensors of operation cause the sawmill turned into a dusty environment.

The literature on the advantages of polygon sawing on the OPT has been discussed by Bakar et al. (2006). The objective in OPT sawing is to maximally produce high-quality outer lumber. Unlike conventional hardwoods and softwoods, the outer lumber of OPT does not contain defects such as knots, sapwood and split and the quality is basically determined by their width. For example, the wider the sawn lumber slab the higher is the quality. Sawing accuracy for the polygon pattern is hence important in controlling slab width which in turn determines pricing structure. This is clearly shown in Figure 1 where polygon sawing (PS) yielded the largest quantity of broad slabs compared with life sawing (LS) and cobweb sawing (CS). This is contradictory to ordinary softwood and hardwood logs sawing where life sawing normally yielded the wider lumber.

The study showed that life and cobweb sawing produced a larger amount of smaller lumber (less than 10cm) which is 77% and 88%, respectively. In comparison, polygon sawing only produced 47% of such lumber. Cobweb sawing, in fact, did not produce any lumber less than 15cm width. By comparison, polygon sawing produced three slabs of 20cm width and two slabs of 16 to 20 cm width. Polygon sawing is clearly the most suitable pattern for sawing OPT in terms of the width of outer lumber (Bakar et al., 2006). The polygon sawing, however, has disadvantages. Firstly, the log or cant on the carriage needs to be rotated quite frequent at a certain angle during the sawing process. Secondly, the angle for log rotation is not a simple perpendicular (90°) angle that can easily be controlled by the conventional carriage. A specific non-perpendicular angle is more difficult to achieve with the present carriage facility.

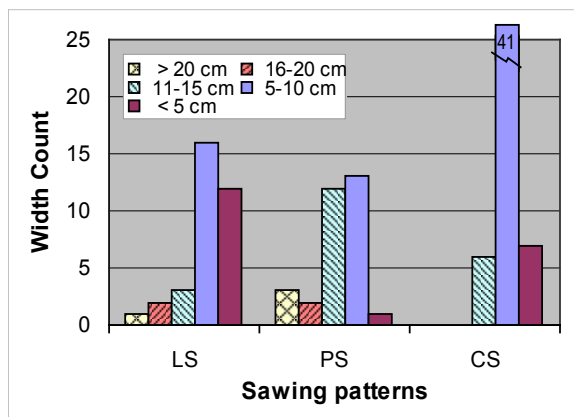


Figure 1. Width count against sawing patterns

For greater accuracy, hence productivity, polygon sawing requires adjustment to the log carriage. Without this, sawing time is longer, and the lumber produced more wedged or tapered. A better controlled and more accurate polygon sawing will improve on the overall productivity of OPT milling. Under conventional polygon sawing only the highly skilled operator can achieve such high productivity

(Bakar et al., 2005). A modified carriage attachment system is necessary to make a polygon sawing process better controlled and more accurate. The attachment system will facilitate the log rotation and hold it firmly at a required angle against the cutting line of band saw. However, to date, neither concept design nor device has been suggested for this innovation. The innovation of the modified carriage system is now quite timely since the number of sawmill processing OPT is still limited. However, the number of such sawmills is set to increase rapidly in the near future. The introduction of a new device prototype for the attachment system should greatly improve on the productivity of OPT milling and the overall lumber yield for the industry.

In this study, stress, total deformation and fatigue analysis of the base part of the wedge device when the base part receives maximum force is discussed. The analysis was done using SolidWorks simulation software. The base part that created using SolidWorks software and analyzed using SolidWorks simulation software allows finite element method analysis for this study. Analysis of stress, total deformation and fatigue were simulated under the restriction of materials mechanical characteristic, base part dimension and force to determine the point of maximum stress, deformation and total lifecycle experienced by the base part.

MATERIALS AND METHODS

Materials

The material used for the wedge device in the finite element method stress analysis is aluminum alloy (201.0-T7 Insulated Mold casting (SS)). This material was selected based on the previous research conducted by Ssomad et al. (2015). Among three materials tested for stress distribution on a hand tool harvester which are aluminium alloy (201.0-T7 Insulated Mold casting (SS)), cast carbon steel and plain carbon steel, the aluminium alloy was found to be the most suitable material for fabrication due to lightweight and the stress distribution was the lowest as compared to other two materials (Ssomad et al., 2013). Table 1 shows the material properties of the aluminum alloy (201.0-T7 Insulated Mold Casting (SS)).

Table 1

Material properties of aluminum alloy (201.0-T7 Insulated Mold Casting (SS))

Property	Value	Units
Elastic modulus	7.099999739e+010	N/m ²
Shear modulus	2.300000022e+010	N/m ²
Mass density	2800	kg/m ³
Tensile strength	344999997.1	N/m ²
Yield strength	344000003.3	N/m ²

Methods

In developing a new conceptual design, problems faced by the oil palm lumber producer were identified. Therefore, a visit to Forest Research Institute of Malaysia (FRIM) was conducted to have a close look at the existing sawmill machine. The design specification is determined and ensures the objectives of the innovation is encountered. The following stages were conducted in accordance to the journal written by Ssomad et al. (2015). The design layout of the machine was extracted, the schematic drawing and wireframe model was developed, design in computer-aided design (CAD) environment was modified, the mechanical simulation was conducted and complete drawing for fabrication purpose was produced. Figure 2 shows the engineering drawing of the wedge device at scale 1:3 with complete dimensions in millimeter.

Every detailed dimension of the drawing must be shown for the determining of the machine size. SolidWorks 2014 and SolidWorks Simulation software was used to construct all the drawings and perform the analysis, respectively. Stress analysis is an engineering methodology to determine the maximum or minimum stress in structures or components subjected to static forces, dynamic forces or given loads (Molaghab et al., 2017). The analysis is usually performed to determine the safety factor or whether the elements or materials can safely withstand the specific forces. The material is safe from any failure when the calculated stress is less than the maximum allowable tensile stress, maximum compression strength, fatigue strength or maximum deformation (Goswami, 2004). Thus, every material has its own safety factor before it can be used.

The safety factor depends on many aspects such as load or force that act on the component, type of material, temperature or other surrounding influences. The safety factor of any component is equal to the fraction of ultimate tensile strength and maximum

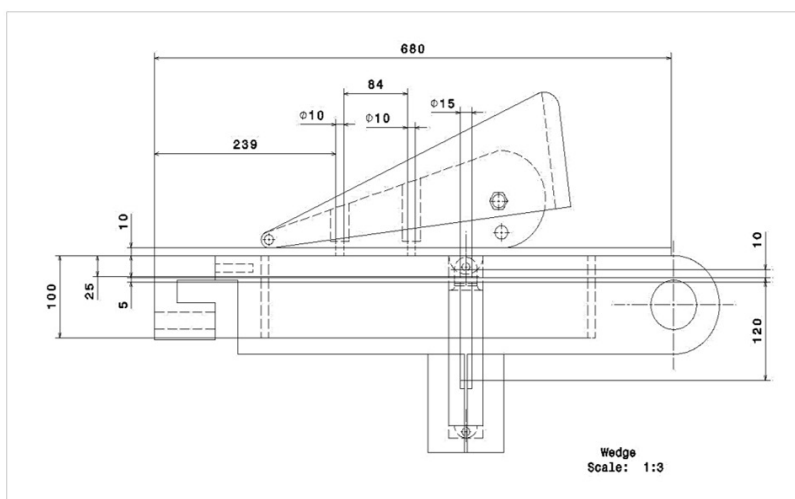


Figure 2. Engineering drawing of the wedge device

allowable stress. The main part of this analysis involves determining the type of loads acting on the component including tension, compression, shear, torsion, bending or combination of such loads. The information regarding the applied load, distribution of forces between components, stress distribution and the deformation of the components can be obtained from SolidWorks Simulation software.

Calculation of Wedge and Inner Angle of the OPT

The five-angled polygon (pentagon) pattern is used to saw OPT. The diameter range of oil palm stems between 40cm and 50cm was been taken into consideration. In the pentagon shape, the total angle, ω and each corner angle, α can be calculated as in Equation 1. This angle is the same for all corners, regardless of stem diameter as shown in Figure 3.

$$\begin{aligned} \omega &= (n - 2) \times 180^\circ \\ \alpha &= \omega/n \\ \omega &= 3 \times 180^\circ = 570^\circ \\ \alpha &= 570^\circ/5 = 108^\circ \end{aligned} \quad [1]$$

On a band sawmill, the log is laid down in a series of the L-shaped knee on the carriage and the saw cut the log vertically. After the first cutting is made, the log is rotated clockwise to position it for the second cutting in which the angle ' α ' (angle between the two lines) is 108° . At that position, the angle α can be easily set by putting a "wedge" with an angle ' β ' to support the log that makes it perpendicular to the first cut as shown in Figure 3. The wedge angle β can be then calculated as in Equation 2.

$$\begin{aligned} \beta &= \alpha - 90^\circ \\ \beta &= 108^\circ - 90^\circ = 18^\circ \end{aligned} \quad [2]$$

Since the pentagon shape is symmetrical, the angle of the "wedge" for all cutting must be at the same angle of β equal to 18° . The position of the knee on the base is adjustable, depending on the diameter of log or cant being sawn. In some carriage system, the knee is also equipped with a hydraulic mechanism to rotate the log or cant above the knee base. The wedge can be moved 'up' and 'down' at each set of the knee on the carriage. At the

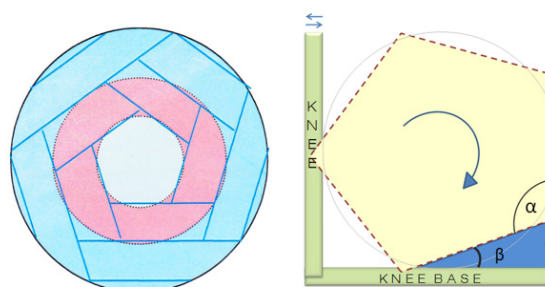


Figure 3. Polygon sawing pattern (left) and polygon sawing process using a wedge (right)

'up' position, the wedge will serve as a slanted base and accurately support the log/cant to allow the new cutting line to form an α angle to the previous cutting line. At 'down' position, the knee base is at the free horizontal condition to allow the log to be easily moved or rotated on the base. Since the OPT is long and heavy, the attachment system must be securely and strongly positioned for each set of knees, and all moving components (log and wedge) can be moved simultaneously with one button.

Components of the Wedge Device

The wedge is basically made of five components as shown in Figure 4. These are the rod, wedge support, movable table, hydraulic cylinder, adjustable wedge, and base. The rod secures the adjustable wedge which holds the log at a specific angle; 108° with the wedge support and 120° with the adjustable wedge. The movable table supports the log which is moved in the vertical plane by the attached hydraulic cylinder. The base supports the movable table. Figure 5(a) shows the position next to the carriage base where the innovative wedge device was assembled. The top dog is a conventional device that assists in holding securely the OPT during the sawing process. It is mounted on the vertical knee.

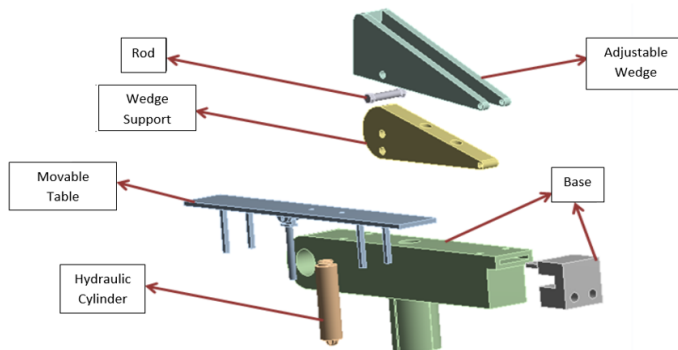


Figure 4. Components of the wedge device

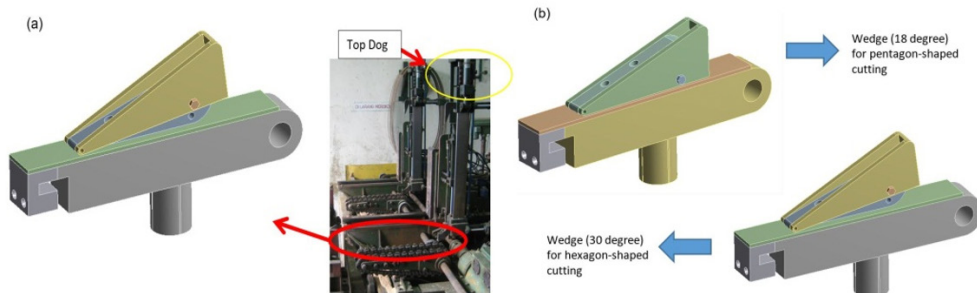


Figure 5(a). Wedge mounted on the existing sawmill carriage (b). and adjustable wedge for pentagon-and hexagon-cutting

RESULTS AND DISCUSSION

Stress and Total Deformation Analysis

Figure 6(a) and (b) show the static components which act on the base and the mesh generation, respectively. The base is used as a support for the wedge. It is soldered at the bottom to the hydraulic cylinder which lifts the wedge at a maximum force of 2598N. Therefore, the bottom part of the inner tube where the cylinder placed will experience a maximum force of 2598N. Green arrows at the left and right side of the base are where the part is fixed to the existing sawmill carriage. Mesh is one of the critical aspects of engineering simulation. Too many cells may result in long solver runs and too few may result in inaccurate results. Type of mesh either tetrahedral, hexahedral or mixed elements are important as well in determining the quality of results displayed. The tetrahedral mesh was used in this analysis as compared to hexahedral mesh since it gave a good quality for the domain interior and near the boundary. Similar results were obtained by Duggleby et al. (2011).

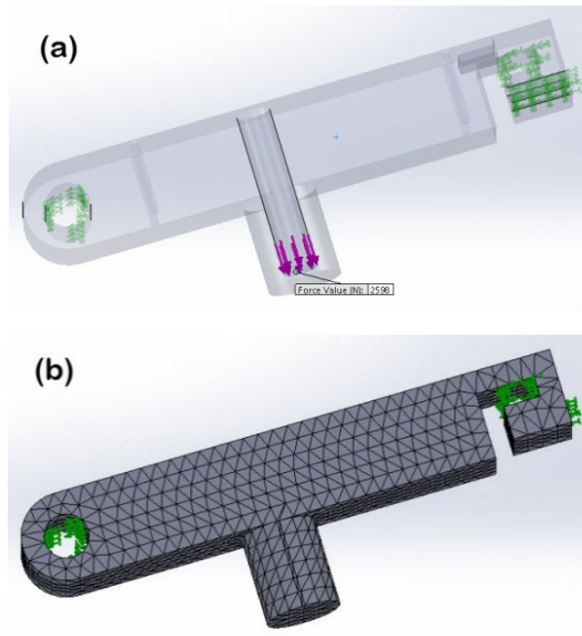


Figure 6(a). Force component on wedge base (b). mesh on wedge base

Further analysis was performed using SolidWorks Simulation and the results are illustrated in Figure 7(a) and (b). The analysis showed that the maximum equivalent stress exerted on the wedge base was 2.546 MPa and the maximum total deformation was about 0.007935 mm. According to Sukumar and Ramachandran (2016), for a manufacturer to approve any mechanical design, the value of maximum equivalent stress (von Mises stress) in a system during a worst-case situation should be lower than that of the yield strength of the material used. Since the yield strength is 344 MPa, which is much higher than the value of maximum equivalent stress of 2.546 MPa, the design is safe under designated stress or force. The total deformation is also very small and will not affect the accuracy of the cutting process. The result shows that the maximum equivalent stress is around the holes and the minimum point is on the left- and right-hand sides.

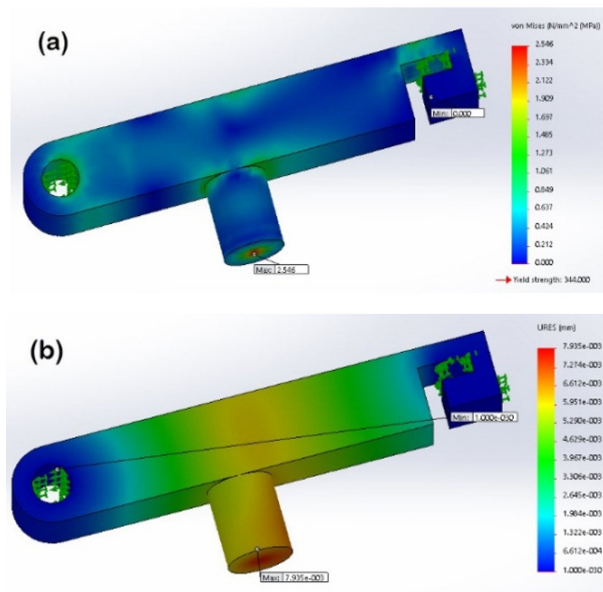


Figure 7(a). Total deformation (b). equivalent stress

Calculation of Static Component Strength against Crack

The static component strength is calculated to identify whether the wedge base can withstand deformation or otherwise. The component strength is determined and compared with the analysis results from SolidWorks Simulation. Following equations were available in Roloff/Matek Maschinenelemente (Muhs, 2003).

The calculation for the static component strength against crack is defined in Equation 3 where f_c is the factor to calculate the material strength value which equal to 1, R_m is the tensile strength of the material, and K_B is the static construction factor. The static component strength against crack is proportional to the tensile strength of the material.

$$\text{Crack, } \sigma_B = \frac{f_\sigma \cdot R_m}{K_B} \quad [3]$$

For components deviating from the standard dimensions, the strength value of R_{mN} must be converted with the factor of K_t . Tensile strength can be calculated using Equation 4 where k_t is the technological size factor for tensile strength and yield strength which equal to 1, R_{mN} is the tensile component which is 355 N/mm².

$$\text{Tensile strength, } R_m = K_t \cdot R_{mN} \quad [4]$$

The static construction factor, K_B can be determined from the plastic support, n_{pl} as shown in Equation 5 where n_{pl} is the notch sensitivity (factor). The plastic support number should consider that stress peaks in components made of tough materials, as they occur in bending and torsion and notch effect, may locally exceed the yield point without destruction of the component (local plastic deformation).

$$\text{Static construction factor, } K_B = \frac{1}{n_{pl}} \quad [5]$$

Equation 6 applies to the calculation of local stresses where R_{pmax} is the maximum yield strength which is 320 N/mm² for aluminum alloy, R_p is the yield strength, and α_p is the plastic stress concentration factor for a component without groove. With the *Neuber* approach, the plastic stress concentration factor can be calculated as the ratio of the transient stress to the yield stress. With an assumed tolerable elongation for a notched component, the plastic stress concentration factor or the notch sensitivity for the verification with nominal stresses can be determined.

$$\text{Notch sensitivity, } n_{pl} = \sqrt{\frac{R_{pmax}}{R_p}} \leq \alpha_p \quad [6]$$

For components deviating from the standard dimensions, the yield value of R_{pN} must be converted with the factor of K_t . Yield strength can be calculated using Equation 7 where K_t is the technological size factor for tensile strength and yield strength which equal to 1 and R_{pN} is the yield component (355 N/mm²).

$$\text{Yield strength, } R_p = K_t \cdot R_{pN} \quad [7]$$

Based on Equation 6 and the value of α_p is equal to 1.5, the notch sensitivity, n_{pl} is equal to 0.96 which is lower than 1.5. Therefore, value of notch sensitivity of 0.96 is used in Equation 5 to find the value for the static construction factor, K_B .

$$K_B = \frac{1}{0.96} = 1.04$$

Once the value for the tensile strength of the material, R_m , factor to calculate the material strength value, f_σ , and the static construction factor, K_B has been determined, the maximum stress against crack for the base can be calculated using Equation 3 and shown below.

$$\text{Crack, } \sigma_B = \frac{1 \cdot 345 \text{ N/mm}^2}{1.04} = 331.731 \text{ N/mm}^2$$

In comparison with the maximum equivalent stress calculated from the SolidWorks Simulation which is 2.546 MPa, the maximum tensile stress at the crack for the aluminum alloy is much higher which is 331.731 MPa. It can be concluded that using the aluminum alloy for the base is very reliable and safe against deformation and crack. The result is similar to that of Ssomad et al. (2013) based on the factor of safety analysis. They found that under safety factor of 5, the critical value of stress was removed for only aluminum alloy as compared to cast carbon steel and plain carbon steel. The aluminum alloy base would only crack or break if the equivalent stress is higher than 331.731 N/mm² (MPa).

Besides stress and total deformation analyze, fatigue analysis was performed in determining the durability of the aluminum alloy material under prolong compression and tension. Figure 8(a) and (b) show the damage percentage and total life cycle of the base part made of aluminum alloy. After 500,000 cycles, the damage experienced by the base part is 50 percent. The total life cycle is one million cycles. It means that, after one million cycles, the base part will be fully damaged and requires a replacement.

Based on the analyses conducted on the wedge device, it proved that the aluminium alloy was significantly appropriate to be used in manufacturing the base part of the wedge device. The analyses contribute a cheap yet accurate results for a manufacture to approve the mechanical design of this wedge device for manufacturing purpose. In addition, the theory behind the calculation of maximum stress against crack can be applied in any stress analyses and be practiced in various field of applications including machinery design. The theory is unduly important to ensure that the maximum equivalent stress obtained from the analysis is safe for the subsequent manufacturing process of the wedge device. The developed wedge device is expected to be integrated in various type of sawmill machines due to its ability to be adjusted based on the shape of the existing sawmill machine. However, performance evaluation of this wedge device is required to prove the efficiency of the conceptual design.

CONCLUSION

This work has focused on stress and fatigue behaviors of a base part of a wedge device based on finite element analysis which experiences the highest force during the working process. The analysis has been carried out using SolidWorks Simulation software. The stress analysis results show that aluminum alloy used as the manufacturing material for the base part of the wedge device is suitable since it able to withstand a maximum force of 2598N without a crack. The fatigue analysis results also show that the base part will fail due to fatigue after one million cycles. These evaluation results indicate that the material used for the wedge device (including the base part) satisfies the design requirements of

static strength and is safe within its designed fatigue life. This has essentially laid the foundation for future work in terms of shape optimization and performance evaluation after prototype fabrication.

ACKNOWLEDGEMENTS

The authors acknowledge with thanks all laboratory assistances and the facilities provided by Universiti Putra Malaysia to carry out research activities.

REFERENCES

- Antwi-Boasiako, C., & Boadu, K. B. (2016). The level of utilization of secondary timber species among furniture producers. *South-East European Forestry*, 7(1), 39-47.
- Bakar, E. S., Rahman, O., Wayan, D., & Rusdiana, N. (1998). Utilization of oil palm stems as building and furniture material: Basic properties of oil-palm wood. *Journal of Forest Production Technology*, 11, 1-12.
- Bakar, E. S., Febrianto, F., & Ashaari, Z. (2005). The optimum sawing pattern for oil palm wood. *Proceeding of International Advanced Technology Congress (IATC)*(p. 8). Kuala Lumpur, Malaysia.
- Bakar, E. S., Febrianto, F., Wahyudi, I., & Ashaari, Z. (2006). Polygon sawing: An optimum sawing pattern for oil palm stems. *Journal of Biological Sciences*, 6(4), 744-749.
- Bonneau, J. C. (1994). *French Patent No. FR2694516A1*. Paris, ACT: IP France.
- Duggleby, A., Camp, J. L., Doron, Y., & Fischer, P. F. (2011). Massively parallel computational fluid dynamics with large eddy simulation in complex geometries. In *ASME 2011 International Mechanical Engineering Congress and Exposition* (pp. 817-824). Colorado, USA.
- Goswami, D. Y. (Eds.) (2004). *The CRC handbook of mechanical engineering*. Florida, USA: CRC press.
- Haslett, A. N. (1990). Suitability of oil palm trunk for timber uses. *Journal of Tropical Forest Science*, 2(3), 243-251.
- Kampman, B., Brouwer, F., & Schepers, B. (2008). *Agricultural land availability and demand in 2020: A global analysis of drivers and demand for feedstock, and agricultural land availability*. Delft, Netherlands: AEA Technology.
- Molaghab, A., Taherynia, M. H., Aghda, S. M. F., & Fahimifar, A. (2017). Determination of minimum and maximum stress profiles using wellbore failure evidences: A case study—a deep oil well in the southwest of Iran. *Journal of Petroleum Exploration and Production Technology*, 7(3), 707-715.
- Muhs, D., Wittel, H., Becker, M., Jannasch, D., & Vossiek, J. (2003). *Roloff/Matek Maschinenelemente*. Berlin, Germany: SpringerVieweg.
- Ssomad, M. A. H. A., Hudzari, R. M., Syazili, R., Noordin, M. N. A., & Abdullah, S. J. (2015). Agricultural mechanization practise and simulation analysis of hand tool harvester. *Australian Journal of Basic and Applied Sciences*, 9(32), 10-14.
- Ssomad, M. A. H. A., Hudzari, R. M., Noordin, M. N. A., Sapuan, S. M., Norhayati, N., & Soran, A. J. (2013). Finite element analysis for stress distribution of hand tool harvester. *Procedia Engineering*, 68, 219-224.

Sukumar, C., & Ramachandran, K. I. (2016). Three dimensional design, simulation and optimization of a novel, universal diabetic foot offloading orthosis. In *IOP Conference Series: Materials Science and Engineering* (pp. 1-9). Bangalore, India: IOP Publishing.

Wahid, M. B. (2008). *Malaysian oil palm statistics 2007*. Selangor, Malaysia: Malaysian Palm Oil Board.



Simulation Study for the Compressed BMC Materials of Kenaf/Coir Reinforced Unsaturated Polyester: Flow Behaviour and the Effects of Charges Shapes Studies

Sameer Adnan Ibraheem^{1*}, Khalina Abdan¹ and Lee Ching Hao²

¹*Department of Biological and Agricultural Engineering, Faculty of Engineering, Universiti Putra Malaysia, 43400 Serdang, Selangor, Malaysia*

²*Laboratory of Biocomposite Technology, Institute of Tropical Forestry and Forest Products (INTROP), Universiti Putra Malaysia, 43400 UPM Serdang, Selangor, Malaysia*

ABSTRACT

This study provides predictable flow behavior of a hybrid biocomposites made from kenaf/coir reinforced unsaturated polyester using the Moldflow software. A medium size electrical part has been chosen as a mold having multi-wall thicknesses and complex surfaces. Three different shapes of charges of the bulk molding materials were used and compressed into the mold part. The shapes of charges would be rectangular, cubic and cylindrical shapes. The results showed that rectangular charge took 0.2 seconds to fill up the part while the cubic and the cylindrical charges took 1.911 and 2.898 seconds respectively. After 70 seconds the conversion at nodes was more than 98% for all charges. On the other hand, the final densities were $1.88 \pm 0.08 \text{ g/cm}^3$ for all charges. The cubic charges

showed a better temperatures distribution at flow front followed by rectangular, the last being the cylindrical charge, and the average shrinkage was 5-7% for the charges. The cubic shape showed good fibers orientation to the flow direction of the bulk materials followed by cylindrical charge while the rectangular charge showed poor orientation of fibers affected on the deflections, weld lines and air traps in the internal part. For the rectangular, the charge showed more critical weld lines and more air traps especially on the surface of the molded part and more

ARTICLE INFO

Article history:

Received: 24 October 2018

Accepted: 15 February 2019

Published: 21 June 2019

E-mail addresses:

sameer_eng81@yahoo.com (Sameer Adnan Ibraheem)

khalina@upm.edu.my (Khalina Abdan)

leechinghao@upm.edu.my (Lee Ching Hao)

* Corresponding author

deflections on the corner edges. But, the cubic charge showed the lowest deflections rate, air traps and weld lines defects.

Keywords: Coir, compression molding, hybrid biocomposites, kenaf, moldflow simulation

INTRODUCTION

Favourable mechanical and thermal properties can be obtained from hybridizing the natural fibers to reinforce thermoset polymers, however designing hybrid composite for compression molding parts offers some challenges such as fiber orientation, mold shape, position and shape of charges which may leads to reduction in the mechanical and thermal properties and presents increase in the costs of manufacturing these parts. To overcome these challenges several simulation softwares and finite element models have been developed to reduce both time and cost of the design (Davis et al., 1997; Osswald et al., 1996; Rios et al., 2018).

The final structural performance of the part can be affected directly by molding process, and the location of gates and charges (Rosato & Rosato, 2000). In the molding process the flow pattern is considered complex due to the three dimensional flow of the molded materials and the effects of gravity on that materials (Mitani & Hamada, 2005).

Few reports in the literature employed simulation analysis to study hybrid composites curing behavior and temperature distribution of natural fiber composites during molding. Mitani et al. (2005) presented only a one-dimensional model using finite difference (FD) method to predict the temperature distribution and cure behavior of natural fiber composites in the RTM process. While A non-linear heat transfer analysis combined with a cure kinetic model based on finite element procedures was developed by Behzad (2007), using hemp fiber/thermoset composite, three-dimensional mode was developed for a simple block of the composite and compared with experimental results. Experimental data shows that the simulation procedure is numerically valid and stable (Behzad & Sain, 2007).

Practical observation was done by Sridhar and Kumar (2013) for the power box component with single gate and two gates and analyzed for mold flow using Pro/Engineer and Mould flow analysis Software. Original component die has single gate and two gates and by changing processing conditions in seven tests each. Surface temperature of 40°C, Melt temperature of 240°C, and Maximum machine injection pressure of 180 MPa were the optimum parameters for better quality products for both single and two gates designs.

MATERIALS AND METHODS

Part Selection and Drawings for Compression Molding

In this step the molded part was selected regarding to the availability of compression mold of this part in local company. For bulk molding compounds, the part were produced

previously using BMC technique and the composites materials were glass fibers reinforced unsaturated polyester as shown in Figure 1. The part was considered as a medium size part and contains precise details with multi wall thickness which can give a good indicator of developed hybrid compounds ability to produce a complex small parts with precise details not only a simple products shapes.

The mold part and the materials charge were created using SOLIDWORK drawing software due to the good capability of this software in drawing of 3D objects. However, three shapes of charge materials were used to indicate the effect of the charge shape on the materials flow, temperature profile of the materials during the molding process, the defects that might occur such as (porosities, shrinkage and weldlines), and the pressure. The charge shapes were (rectangular, cubic and cylindrical), knowing that these three shapes were the easiest and fastest to be produced by the operator.

Figure 2 and 3 show 3D drawing of the part and the charges shapes respectively. From Figures 2 and 3 it can be seen that all the details of the part are reflected from the real part to the 3D drawing to give significance reliability for the simulation results.

Optimum charge weight was calculated by the simulation software after the first run. Charge weight optimization step is very important to avoid overloading materials into mold which might reduce the mold life time and mold efficiency. However, insufficient materials will give an incomplete shape and defected products. Knowing the required weight and the materials bulk density, the volume of the three charges shapes can be easily calculated from the density equation (density = mass / volume).



Figure 1. Shape of molded part

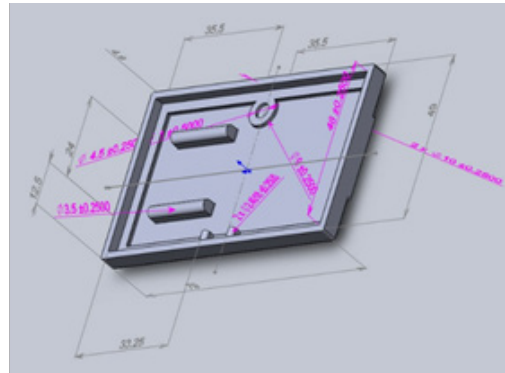


Figure 2. 3D drawing of molded part (measurements in mm)

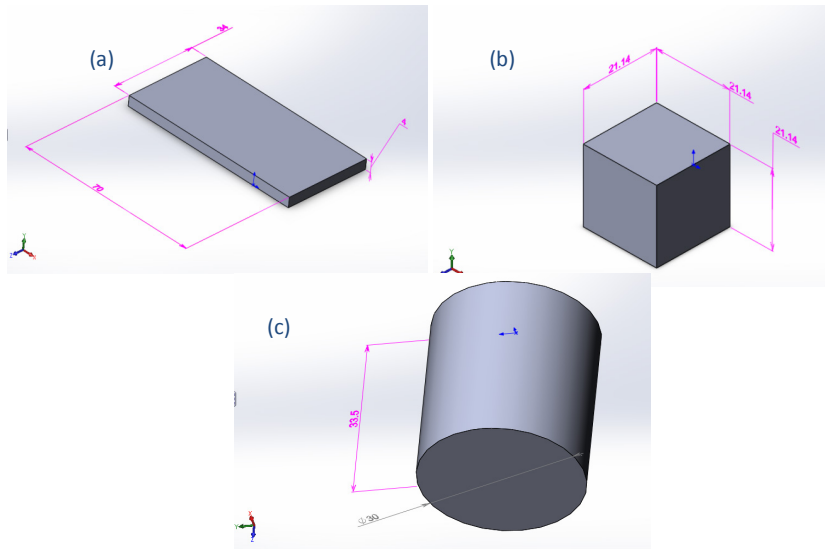


Figure 3. 3D Drawing of charges (Measurements in mm): (a) rectangular charge, (b) cubic charge (c) cylindrical charge

Simulation of Materials Flow

Autodesk® Simulation Moldflow® plastic injection molding simulation software was used to validate and optimise the design of plastic parts in compression molds by providing an actual prediction for the plastic compression molding process. Simulating the molding process reduces the need for costly physical prototypes, avoids manufacturing defects and assists delivering innovative products to market faster.

In order to run the software simulations, several procedures need to be set up to run the analysis of the simulation software.

Setting Up the Project Name and Importing the Drawing

After creating the new project 3D drawing for the mold part and the charge can be imported from the SOLIDWORK drawing software files with .SLDPRT extension and should import as Solid 3D as shown in Figure 4.

Selection the Molding Process

Several molding processes are available to be select such as (thermoplastics Overmolding, thermoplastics injection molding, Gas-assisted injection molding Reactive molding, Microchip Encapsulation, underfill Encapsulation, Reactive compression molding, etc). Reactive compression molding was selected for the bulk molding compounds materials.

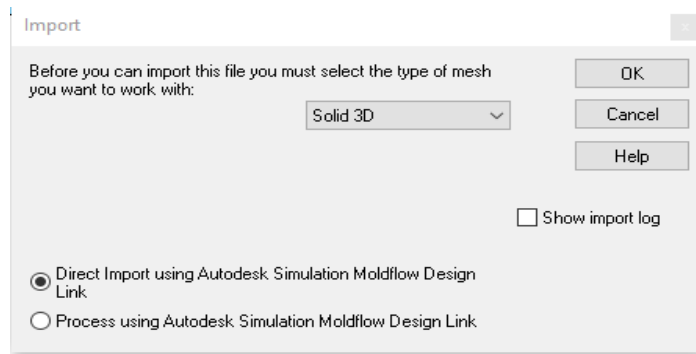


Figure 4. Import of 3D drawing to autodesk simulation moldflow

Generate Mesh and Selecting the Analysis Sequence

In this procedure the mesh type was set as 3D Tetrahedra elements with global edge length of 0.5 mm and merge tolerance of 0.1 mm for both mold part and materials charge. After generating the meshed part and charge, the property of both of them should be identified as “compression element 3D” for the mold part, and as “initial charge” for the charge in order to be recognized by the software which one is 3D mold part and which one is the charge.

As analysis sequence, Fill + Pack + Warp was selected to present the sequence of analysis for the compression molding process, it has other available sequences which include the mold cooling analysis option which is not applicable to this study hence the real mold used was small and did not have a cooling system .

Materials Selections

UPM BMC-KF12-20 trade name material had been selected from the materials library of the software, this reactive material consists of kenaf fibers with 12 mm length reinforced unsaturated polyester. Figure 5 shows material description and recommended processing. To modify the material properties and include the optimized hybrid premixed bulk compounds properties and reinforcements (Kenaf and Coir) properties in each single run this selected material (UPM BMC-KF12-20) was edited and some of the thermal and mechanical properties were changed to present the real hybrid premixed bulk compounds.

Process Settings

In this procedure several parameters were edited regarding to the process parameters, machine parameters, temperatures control and curing parameters, which can be illustrated as:

Machine parameters:

Maximum machine clamp force = 7.0002E+003 tonne

Reaction Kinetics Properties	pvT Properties	Mechanical Properties	Filler Properties
Description	Recommended Processing	Rheological Properties	Thermal Properties
Family name	THERMOSET POLYESTER		
Trade name	UPM BMC-KF12-20		
Manufacturer	University Putra Malaysia		
Link			
Family abbreviation	BMC		
Data source	University Putra Malaysia		
Date last modified	04-SEP-15		
Date tested	04-SEP-15		
Data status	Non-Confidential		
Material ID			
Fibers/fillers	Unfilled		

Reaction Kinetics Properties	pvT Properties	Mechanical Properties	Filler Properties
Description	Recommended Processing	Rheological Properties	Thermal Properties
Melt temperature	50		C
Melt temperature range (recommended)			
Minimum	40		C
Maximum	60		C
Mold surface temperature	140		C
Mold temperature range (recommended)			
Minimum	120		C
Maximum	160		C
Ejection conversion	0.9		

Figure 5. UPM BMC-KF12-20

Machine hydraulic response time = 1.0000E-002 s

Temperature control:

Melt temperature = 50.00 C

Mold temperature = 180.00 C

Mold-melt heat transfer coefficients

Filling = 5000.0000 W/m²-C

Packing = 2500.0000 W/m²-C

Detached = 1250.0000 W/m²-C

Atmospheric temperature = 25.00 C

Curing parameters:

Curing time = 60.00 s

Inlet melt conversion = 0.0000

Perform preconditioning analysis = No

Press compression direction = -Z

Pure compression press open distance option = Automatic

Press compression time = 10.0000 s

Compression speed cap = 1000.00000 mm/s

Press compression force = 150.0000 tonne

Press compression speed at incremental distances :

0.1000 mm 10.0000 mm/s

10.0000 mm 10.0000 mm/s

Switch to force control by % node volume filled = 99.00000 %

Final procedure was running the analysis to obtain the simulation results. The obtained simulation results includes the materials flow, temperature profile of the materials during the molding process, the defects that might occur such as porosities, shrinkage and weldlines, and the pressures. These results helped us to analysis and to compare the effects of the three charges shapes on the final products.

RESULTS AND DISCUSSION

Meshing Results for the Mold

Figure 6 shows mold after meshing process had been done, while Table 1 provides the information for the numbers of nodes and elements with acceptable aspect ratio, the element size was 2.11044 mm with 0.1055 mm of tolerance.

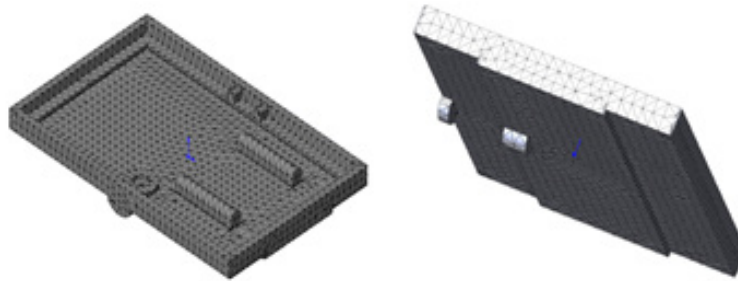


Figure 6. Mold after meshing process

Table 1

Meshing process results

Meshing Process	Results
Total Nodes	17967
Total Elements	9251
Maximum Aspect Ratio	18.053
% of elements with aspect ratio < 3	84.8
% of elements with aspect ratio > 10	0.389
% of distorted elements (Jacobian)	0

Materials Flow Results

Table 2 represent the comparison between the bulk molding materials flow results such as fill time, cavities volume, clamp forces and densities for the different charges shapes.

Table 2

Molding flow results for different charges types

Charge Shape	Fill Time (s)	Cavities Volume (cm ³)	Clamp Forces (tonne)	Densities (g/cm ³)
Rectangular	0.28	11.5	0.253	1.88 + - 0.08
Cubic	1.91	77.5	0.85	1.88 + - 0.08
Cylindrical	2.89	117.5	0.175	1.88 + - 0.08

The rectangular shape charge had the lowest cavities volume and took the shortest time to make the materials flow through the mold cavities, due to the distribution of the materials represented by rectangular shape and covered the large surface area of the mold. On the other hand the cylindrical shape charge covered a small surface area of the mold and left a much higher cavities volume at the beginning of the fill which took longer time to be filled.

Pressure at End of Fill

Figure 7 shows the pressure distribution at the end of fill for the three charges. It was obvious that the cylindrical and rectangular shapes needed less pressure and the distribution of the pressure was much uniform at the three dimensions than the cubic shapes. Thus, due to the higher compactness of the materials in the cubic shapes and much pressure was needed to fill up the edges of the mold.

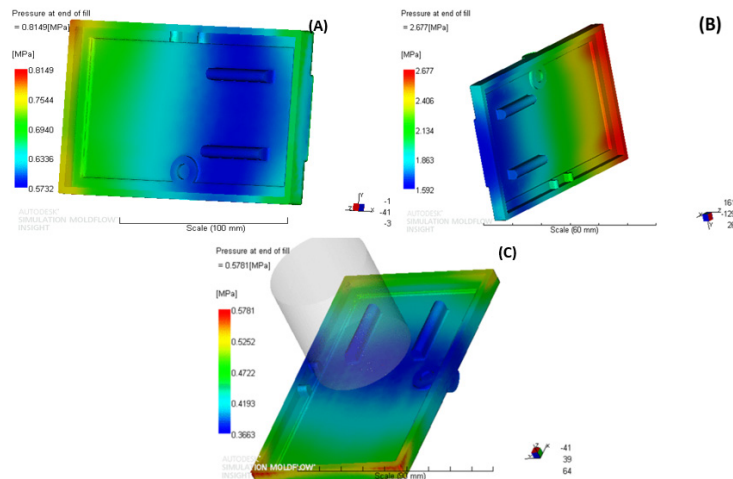


Figure 7. Pressures at end of fill (A) rectangular charge, (B) cubic charge, (C) cylindrical charge

Temperatures at Flow Front

As shown in Figure 8, temperature at flow front can be increased by increasing the filling time for the total cavities of the mold and also by reducing the thickness (the contact distance between the two parts of the mold and the surfaces of the charge). Thus, the cylindrical and the rectangular shape charge had more temperature at flow front than the cubic charge shape.

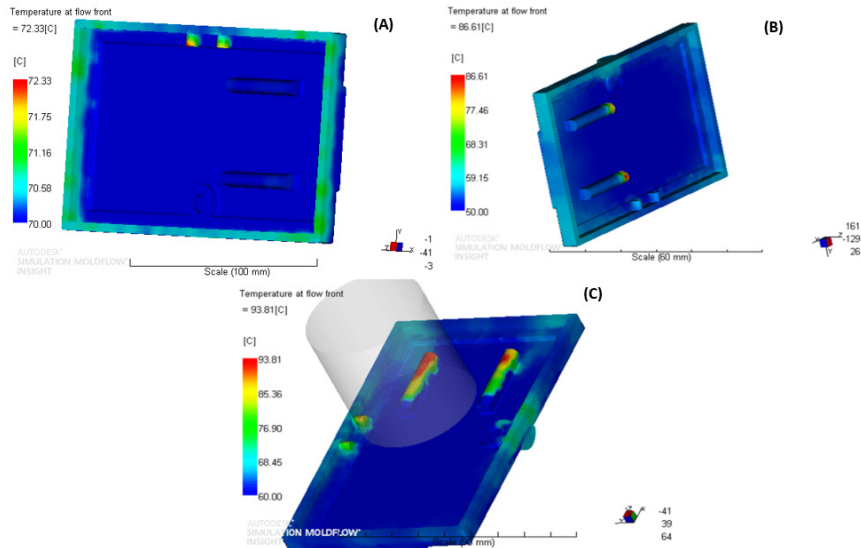


Figure 8. Temperatures at flow front (A) rectangular charge, (B) cubic charge, (C) cylindrical charge.

Average Volumetric Shrinkage

The cubic charge shape shows the lowest average volumetric shrinkage differences throughout the molded part of 5% as minimum and 7% as maximum with 2% differences approximately. This reflects the good temperature distribution in all direction for the materials while been pressed into the cavities of the mold. On the other hand, the cylindrical and the rectangular shape charges show more than 3.5% of differences in average volumetric shrinkage, as shown in Figure 9.

Fiber Orientation Tensor

The Fiber orientation tensor result shows the probability of fiber alignment in the specified principal direction. A high probability of fiber alignment in the specified principal direction is indicated by a value of close to 1 on the result scale, whereas a low probability is indicated by a value close to 0. The fiber orientation tensor in the first principal direction is the most useful result to view. Knowing that the first principal direction is close to the material flow direction in most cases, may not always coincide with the flow direction.

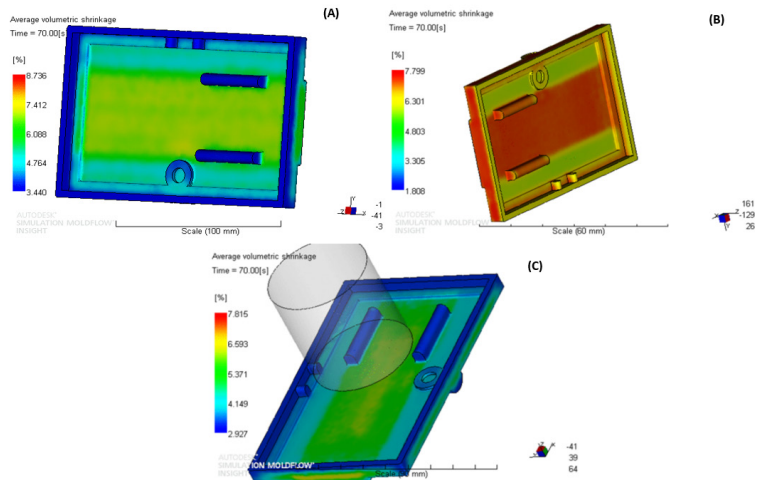


Figure 9. Average volumetric shrinkage (A) rectangular charge, (B) cubic charge, (C) cylindrical charge

Figure 10 shows fiber orientation tensor to the flow of the materials and the pressure applied on the charges. The cubic charge shape presents a good fiber orientation with range (0.66 – 0.99) over the mold cavities compared to the other two types of charges followed by cylindrical shape. This can be as result of the optimum time to fill to the volume of the cavities to the pressure applied which it can give the fibers to follow the flow of the matrix without any blockages from other fibers.

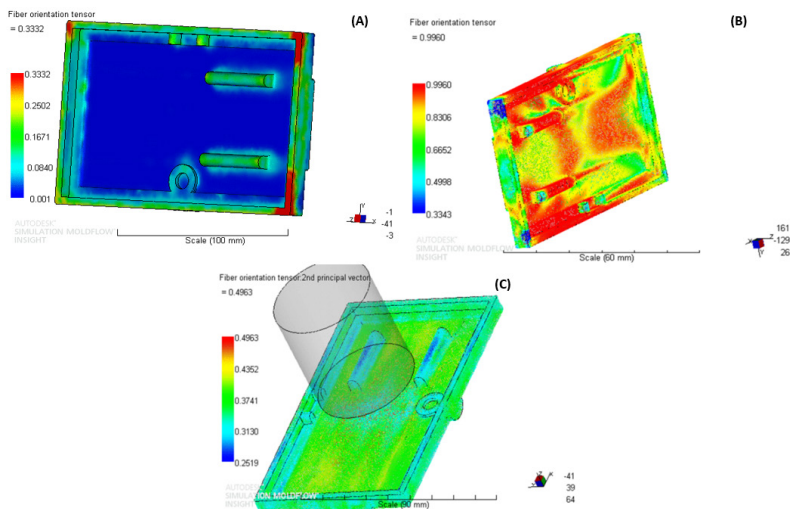


Figure 10. Fiber orientation tensor (A) rectangular charge, (B) cubic charge, (C) cylindrical charge

Predicted Defects Results

Figures 11, 12 and 13 show the predicted defects (weld lines, air traps and deflections) respectively, for the weld lines the cubic shape charge shows less critical weld lines compared to the other two types and the higher critical weld lines presented by the rectangular charge shape. However, these critical weld lines were concentrated on the edges of the mold where the heat transfer was higher and the curing was faster.

The air traps formed by the rectangular shape charge were higher and concentrated in the middle of the molded part. This was due to the rectangular large surface area covered by this shape which trapped more air between the mold surface area and the charge.

Generally the deflections were concentrated on the edges of the part for all charges type, and the cubic charge shape had the lowest values for these deflections.

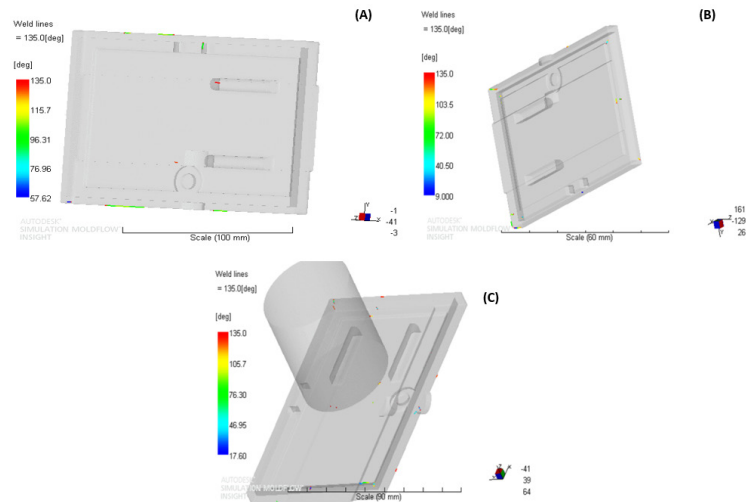


Figure 11. Weld lines (A) rectangular charge, (B) cubic charge, (C) cylindrical charge

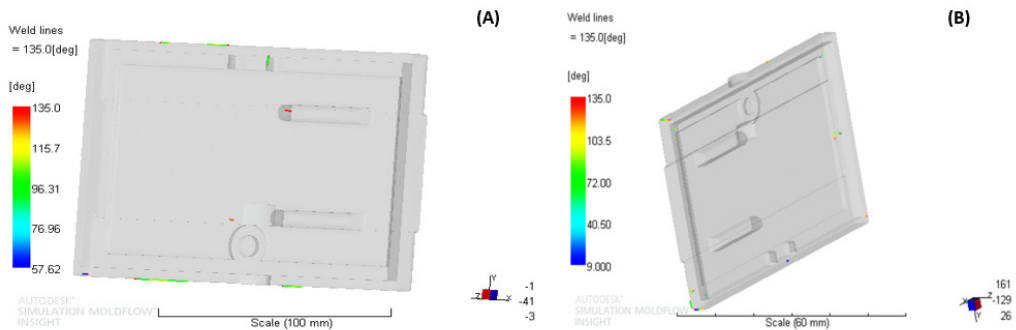


Figure 12. Air Traps (A) rectangular charge, (B) cubic charge

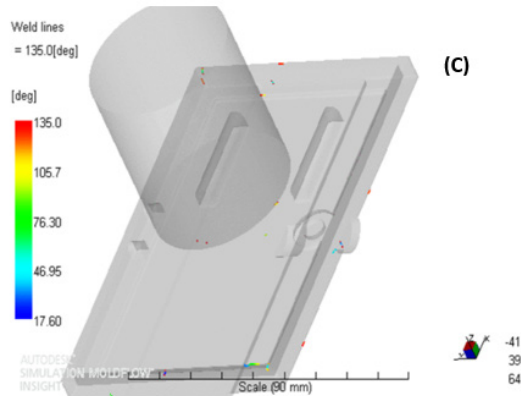


Figure 12. Air traps (C) cylindrical charge

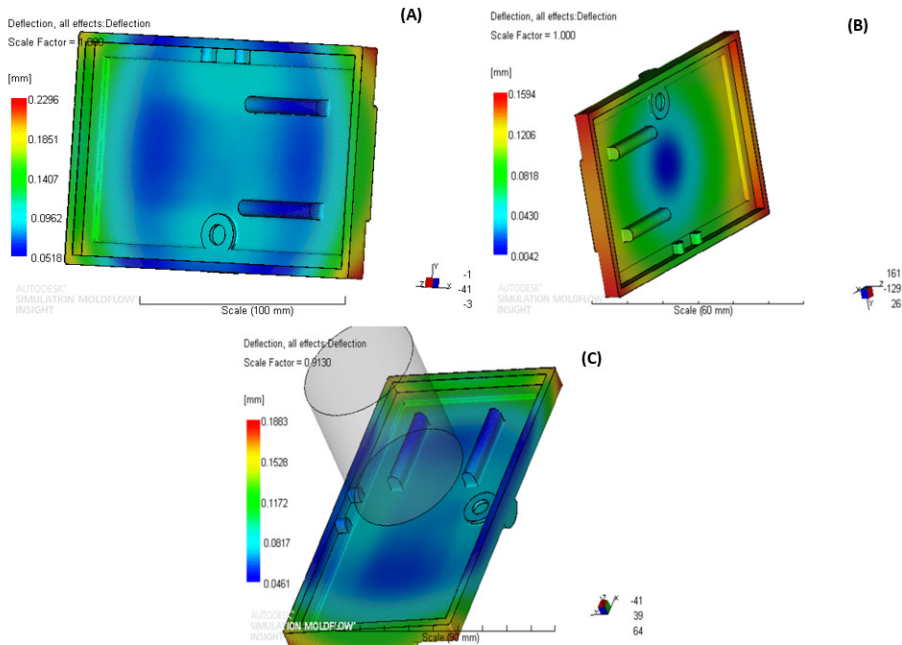


Figure 13. Deflection for (A) rectangular charge, (B) cubic charge, (C) cylindrical charge

CONCLUSIONS

It can be concluded that the shape of the charge had an effective effect on the molding parameters process and the final shape of the molded materials, and the developed materials approved that it can be implemented in complex shape parts and can flow smoothly to fill up all the cavities of the mold. The cubic charges showed lowest average shrinkage differences and a better temperatures distribution at flow front followed by rectangular

while the last was the cylindrical charge. Due to the good fiber orientation for the cubic charge shape, the defects that accrued with this shape was the lowest compared to the other charges shapes, while the rectangular charge shape showed a critical air traps in the middle of the surface of molded part.

ACKNOWLEDGEMENT

The authors thank the Universiti Putra Malaysia (UPM), supporting the project to be completed. Not to forget, the authors would also like to acknowledge MOSTI Escience fund entitles “Developing Hybrid Biocomposites Reinforced Thermoset Moulding Compounds” to provide fund for research conduction.

REFERENCES

- Behzad, T., & Sain, M. (2007). Finite element modeling of polymer curing in natural fiber reinforced composites. *Composites Science and Technology*, 67(7), 1666-1673.
- Davis, B. A., Theriault, R. P., & Osswald, T. (1997, September 30-October 2). Optimization of the compression (injection/compression) molding process using numerical simulation. In *ASME Conference* (pp. 1-14). Singapore.
- Mitani, T., & Hamada, H. (2005). A flow simulation for the epoxy casting process using a 3D finite-element method. *Polymer Engineering & Science*, 45(3), 364-374.
- Osswald, T. A., Sun, E. M., & Tseng, S. C. (1996). Orientation and warpage prediction. In J. F. Stevenson (Ed.), *Innovation in Polymer Processing: Molding* (p. 60). Ohio, USA: Hanser.
- Rios, A., Davis, B., & Gramann, P. (2001, October 3-6). Computer aided engineering in compression molding. In *CFA Technical Conference*. (pp. 1-12). Florida, USA.
- Rosato, D. V., & Rosato, M. G. (2000). *Injection Molding Handbook* (3rd Ed.). Boston, USA: Springer.
- Sridhar, A. V., & Kumar, T. J. (2013). Effects of moulding parameters on the performance of plastic materials. *International Journal of Mechanical Engineering and Computer Applications* 1(7), 163-168.



Evaluations of Soil Resistivity in Relation to Basal Stem Rot Incidences Using Soil Moisture Sensor

Mohd Hamim Abdul Aziz¹, Siti Khairunniza Bejo^{1,2,3*}, Fazirulhisyam Hashim⁴, Nur Hidayah Ramli⁵ and Desa Ahmad^{1,2}

¹Department of Biological and Agricultural Engineering, Faculty of Engineering, Universiti Putra Malaysia, 43400 Serdang, Selangor, Malaysia

²Smart Farming Technology Research Centre, Universiti Putra Malaysia, 43400 Serdang, Selangor, Malaysia

³Institute of Plantation Studies, Universiti Putra Malaysia, 43400 Serdang, Selangor, Malaysia

⁴Department of Computer Systems and Communication, Faculty of Engineering, Universiti Putra Malaysia, 43400 Serdang, Selangor, Malaysia

⁵Department of Electronic Engineering Technology, Faculty of Engineering Technology, Universiti Malaysia Perlis, Unicity Alam Campus, 02100 Padang Besar, Perlis, Malaysia

ABSTRACT

Basal stem rot (BSR) caused by *Ganoderma boninense* is a major disease attacking the oil palm plantation in Malaysia, and incur big losses in palm oil industries. The disease is spread mostly by root either through spore availability in soil or roots contacts. Soil properties were reported to have significant influence on the growth of fungi. Meanwhile, the value of soil resistivity is influenced by soil properties. This paper presents a new approach of BSR detection by using soil moisture sensor which measures resistivity of soil in unit ohm (Ω) at 15 cm surrounding the basal stem of oil palm trees. The study was

conducted on 39 oil palm trees at different healthiness levels. The sensor was embedded approximately 4.7 cm deep in the soil at eight different points for each palm. The results showed that healthy oil palm trees significantly have higher mean ($ER_{MEAN} \geq 400$) of electrical resistance (ER) readings compared to infected trees ($ER_{MEAN} < 400$). More specifically, ER readings at points without symptoms (i.e. fruiting bodies and/or hollow) were significantly higher compared with ER readings at points where

ARTICLE INFO

Article history:

Received: 24 October 2018

Accepted: 15 February 2019

Published: 21 June 2019

E-mail addresses:

m_hamim@upm.edu.my (Mohd Hamim Abdul Aziz)

skbejo@upm.edu.my (Siti Khairunniza Bejo)

fazirul@upm.edu.my (Fazirulhisyam Hashim)

hidayahramli@unimap.edu.my (Nur Hidayah Ramli)

desa@upm.edu.my (Desa Ahmad)

* Corresponding author

symptoms appeared even though the points of measurements were on the same palm. This finding has brought to the introduction of a new index to detect *Ganoderma* infection, named as K-index. Combination of ER_{MEAN} taken from eight points of measurement and its K-index gave better results of detection and a new model was developed based on these two parameters (i.e. ER_{MEAN} and K-index). The developed model has accuracy rates of 82% and gained 100% successful rate during validation. This research showed that soil resistivity can contribute to *Ganoderma*-infected detection in oil palms with a high degree of accuracy.

Keywords: Basal stem rot, electrical resistance, ganoderma boninense, soil moisture sensor, soil resistivity

INTRODUCTION

The oil palm production in Malaysia is threatened by basal stem rot (BSR) disease caused by the wood-rotting fungus named *Ganoderma boninense*, which reduces the oil palm production (Liaghat et al., 2014). Primary route of infection appears to be through root contact with inoculum sources in the soil (Rees et al., 2009). Previous studies indicated that occurrence of BSR was higher in coastal areas and in areas previously planted with coconuts (Turner, 1965). High incidence was recorded in locales where an old stand of oil palm had been felled and the stumps left in the ground. This gives advantages to fungi to grow as there is a wounded host in the soil. Subsequently, the disease spreads from plant to plant by roots or by spores (Paterson, 2007).

Available techniques of *Ganoderma* detection can be classified into three main approaches i.e. human inspection, lab-based and remote sensing. The difficulty of detecting this disease at early stage of infections is due to its less external symptoms appearance (Su'ud et al., 2007). *Ganoderma* detection based on remote sensing approach can be classified into three scopes i.e. ground-based, space borne and airborne (Khosrokhani et al., 2016). The use of space borne images is limited where the images are not always available when needed or sometimes the resolutions of available images are too coarse to be used. Meanwhile, a manned airborne platform has disadvantages on operational complexity, high costs and lengthy product delivery.

The advanced technologies in electronics and computation have widely been used to resolve present day challenges. Microcontroller is leading the electronics revolution. Various sensors had been used together with microcontroller to measure and control physical quantities such as heat, light, humidity and temperature (Abbasi et al., 2014). For instance, electrical resistance-based sensor is a common sensor used in agriculture as a means of soil moisture content measurement. The electrical resistance of a medium is a measure of the difficulty to pass an electric current through that medium. Larsson et al. (2004) proposed point resistivity measurements to detect decay in living trees. The results

of their study showed that healthy trees gave a higher voltage difference than those with decay. The electrical properties of the trees changes with the decay (Larsson et al., 2004). Accordingly, trees having decay showed a lower resistivity than sound trees. According to Shigo and Shigo (1974), when wood decays, cations will increase, and resistance will decrease. There are more free ions in the decayed wood than in non-decayed wood, thus causing a drop of resistivity (Moore, 1999). As the fungi consume the cell structure, metallic ions, in particular potassium are released (Jartti, 1978). These ions are mobile in the humid trunk of the decay. Nurnadiah et al. (2014) studied the potential use of electrical resistance to detect the infection of *Ganoderma boninense* in oil palm tree. Land Mapper ERM-2 (Landviser, LLC, USA) was used to detect the diseases by collecting ER data at eight positions surrounding the trunk at three different levels of height for each tree. The infected trees gave low ER readings. Paglis (2013) studied the potential use of electrical resistance tomography (ERT) in order to detect the root biomass in coffee trees. The results showed that soil resistivity was quantitatively related to root biomass. Borges et al. (2012) studied the possibilities of using Electrical Impedance Spectroscopy (EIS) to detect plant disease by recording changes in amplitude and phase of the current as it passed through the sample. In the study, a young pine specimen revealed some discrimination between healthy specimens and those infected with nematode diseases. The preliminary tests demonstrated that the EIS system was a promising technique to diagnose plant diseases.

Based on the literature, the use of electrical sensors to detect disease is promising. However most of the detections were done at the tree trunk. Since the spread of the BSR disease was reported through root (Paterson, 2007; Rees et al., 2009), an observation of root growth or health is crucial. Roots play an important role in plants and are responsible for several functions; nutrient and water absorption (Fitter, 2002). Soil properties including moisture content (Chang, 2003), pH (Nawawi & Ho, 1990) and nutrient content of soil (Bivi et al, 2016) were reported to have significant influence on the growth of *Ganoderma boninense* and the tendency of the tree to be infected with the BSR disease. The value of soil resistivity is influenced by soil properties such as moisture content, chemical content and temperature. Thus, the same concept has been used in our study by manipulating soil moisture sensor in the soil as an electric conductor allowing the current to flow through the soil medium. This paper suggests the use of Arduino soil moisture sensor to investigate soil resistivity related to BSR incidence.

MATERIALS AND METHODS

Arduino Soil Moisture Sensor

The properties of healthy and infected oil palm trees were evaluated based on the output given by the Arduino soil moisture sensor. The sensor measures the soil moisture by measuring its soil resistivity in unit ohm (Ω). The measuring systems consist of YL-69

soil moisture sensor (Shenzhen JiexingWeiye Electronic Co. Ltd, China), Arduino Uno microcontroller (Adafruit Industries, USA) and a Windows 8 platform laptop (Asus, Taiwan). There are two sensor probes, set in the soil to pass current through the soil and then record the resistance value to get the moisture level. At higher water content in the soil, the sensor detected less resistance due to the soil conducting electricity easier. The dry soil conducted electricity poorly due to more resistance. The Arduino Uno is a microcontroller board based on the ATmega328. It contains everything needed to support the microcontroller. In this research, the Arduino Uno board would received an analogue data converted from the electronic signal recorded by the soil moisture sensor. The analogue data interpreted by the processor and the value of ER appeared at the LCD display of the computer in real time.

Data Collection

The study was conducted in the oil palm plantation located at Teluk Intan, Perak, Malaysia (4.112169°, 100.890208°) from 16th to 20th of January 2017. Soil type of the plantation area is coastal compacted peat soil. The oil palm trees (10 years old palms) were categorized into four healthiness levels i.e. T0: healthy, T1: mild (with fruiting body but no foliar symptom), T2: moderate (with fruiting body and less 50% foliar symptom) and T3: severe (with fruiting body and more than 50% foliar symptom). The identification of the healthiness condition of the palm was done by expert from Malaysian Palm Oil Board (MPOB). The data were collected during day time period, i.e. between 8 am to 5 pm. In this preliminary study, environmental factors such as temperature, humidity and sunlight were not discussed. A total of 39 palms were randomly selected with 8 palms were taken from T0, 11 palms from T1, 12 palms from T2 and 8 palms from T3. The measurement was conducted on eight points around the tree trunk with distance (d) 15 cm from the tree.

RESULTS AND DISCUSSION

ER Readings at Each Point

Figure 1 shows example of eight points of ER readings for T0, T1, T2 and T3. The ER values of the eight points varied especially at infected oil palm trees. For healthy oil palm tree, the ER values of T0 for the eight points were above 400 Ω ranging from 414 Ω to 534 Ω . Meanwhile, for infected palms, the ER values of T1, T2 and T3 ranged from 231 Ω to 558 Ω , 296 Ω to 474 Ω and 195 Ω to 484 Ω , respectively. There were five points with ER values less than 400 Ω and three points with ER values above 400 Ω for T1 and T2, respectively. Most of the ER values of T3 were less than 400 Ω , where only one point with ER value greater than 400 Ω .

A low variation of ER value was obtained on healthy palm with standard deviation of 38.97 Ω . Standard deviation of infected palms varies between 69.75 Ω to 125.04 Ω .

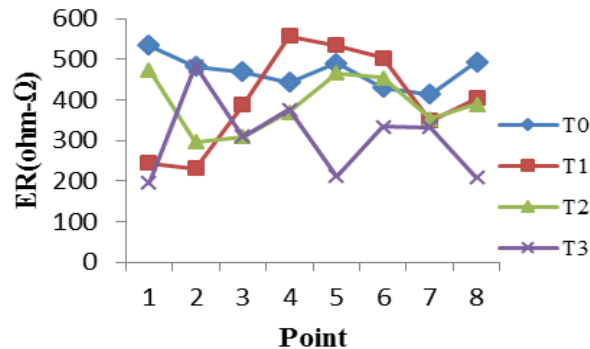


Figure 1. Eight points of ER readings for T0, T1, T2 and T3

Based on detail investigation, the fluctuation value of ER at infected palms depended on the existence of fruiting body or hollow around the palm. For instance, the values of ER at the same palm were higher ($\geq 400 \Omega$) at points which had no hollow and fruiting body. The values of ER were lower ($\leq 200 \Omega$) when there were hollow and fruiting body at the point. Previous work conducted by Nurnadiah et al. (2014) showed that ER values of oil palm tree infected with *Ganoderma* at base positions with appearance of fruiting bodies were lower than healthy palms. The data was collected using Land Mapper ERM-2 (Landviser, USA).

Based on the ER readings taken at eight point positions, it has clearly shown that a single point cannot be used to indicate the healthiness condition of the palm. Results from all eight points gave clear indicator where the higher the severity level, the higher number of points with less ER values. Thus, the detection of healthiness condition should consider the eight points measurement instead of using only a single point measurement.

Model Development

Average value of ER (ER_{MEAN}) for each palm has been calculated by averaging ER readings taken from eight points. The distribution of the results is presented in Figure 2. It can be seen that all healthy palms have ER_{MEAN} above 400Ω . While for unhealthy palms, the ER_{MEAN} ranged from 232Ω to 581Ω . Therefore, a value of 400Ω was set as ER_{MEAN} threshold value (t-value) to roughly differentiate between healthy and unhealthy palms based on ER_{MEAN} value. Some of the infected palms recorded ER_{MEAN} higher than 400Ω . This is due to the influence of point with very much larger ER values than most of the values. This has already been proven as explained in previous section where the standard deviation for infected palm is larger than healthy palm. Thus, based on this trend, a new index (K-index) for each palm has been developed based on the value of ER_{MEAN} and ER standard deviation (ER_{STDEV}) of ER taken from eight points at each palm calculated as in equation [3]. The healthy palm is expected to have K-index value of nearly one due to low value of ER_{STDEV} .

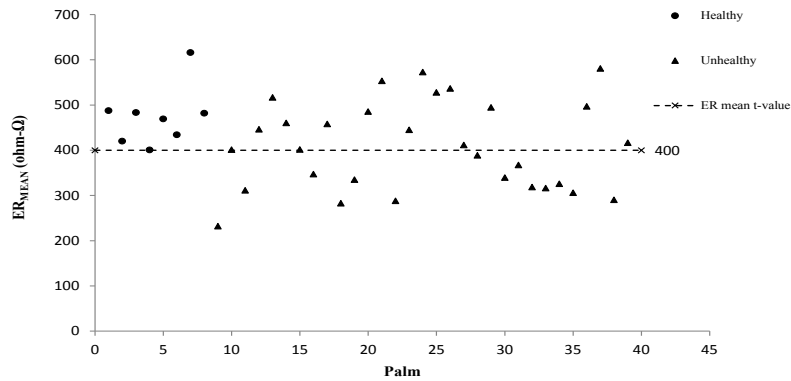


Figure 2. ER_{MEAN} for each palm

$$ER_{MEAN} = \frac{\sum_{i=1}^n x_i}{n} \quad [1]$$

$$ER_{STDEV} = \sqrt{\frac{\sum (x - \bar{x})^2}{n}} \quad [2]$$

$$K - index = \frac{(ER_{MEAN} - ER_{STDEV})}{ER_{MEAN}} \quad [3]$$

n = number of sample points for each palm

Figure 3 shows K-index of 39 palms. For healthy palms, values of K-index ranged from 0.706 to 0.918 with mean value of 0.847. While for unhealthy palms, values of K-index ranged from 0.280 to 0.888 with mean value of 0.727. As expected, the values of K-index for healthy palms were higher than the infected palm. A t-value to differentiate between healthy and unhealthy palms was determined based on following consideration; (mean of K-index of healthy palms + mean of K-index of unhealthy palms)/2 i.e. $(0.847+0.727)/2 = 0.787$.

Two ANOVA test were carried out to see possibility of ER_{MEAN} and K-index to differentiate between healthy and infected palms. For ER_{MEAN} analysis, there is no significant difference between healthy and infected palms as F value (3.232) is smaller than F critical (4.105). However, analysis for K-index showed significant difference between healthy and infected palms as F value (5.861) is larger than F critical (4.105). A graph of K-index versus ER_{MEAN} (Figure 4) was plotted to best describe the relationship between these two parameters. An x-axis intersection line and y-axis intersection line with value of 400 and 0.787 respectively, act as separator line between healthy and unhealthy palms. Thus, four different regions were formed represented as A, B, C and D. Region A, B and C represent unhealthy regions, where plotted dots for unhealthy palms should fall, while region D

Soil Resistivity in Relation to BSR Incidences

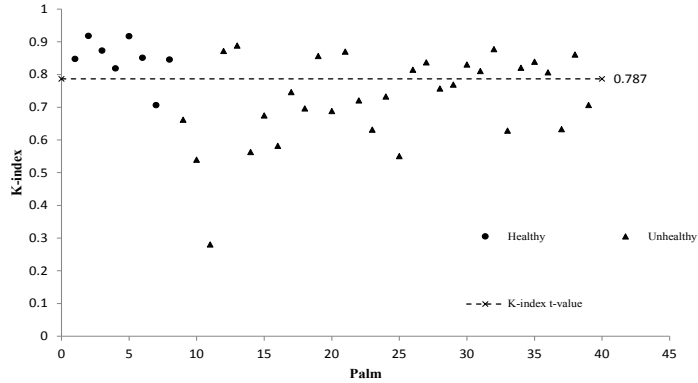


Figure 3. K-index for each palm

is for healthy palms. Based on Figure 5, one unhealthy palm was in region C. While, six infected palms were in region D. This indicates that a total of seven palms were not correctly categorized according to its actual healthiness condition. Other than moisture, soil compaction rate also affects sensor readings. This contributed to the error of the actual value which should measure the value of the soil ER. In summary, this model successfully categorizes the healthy and unhealthy palms with accuracy rate of 82 %.

Model Validation

Ten palms with a total of 80 points were taken to validate the developed model which consists of four T0 palms, two T1 palms, two T2 palms and two T3 palms. The graph of

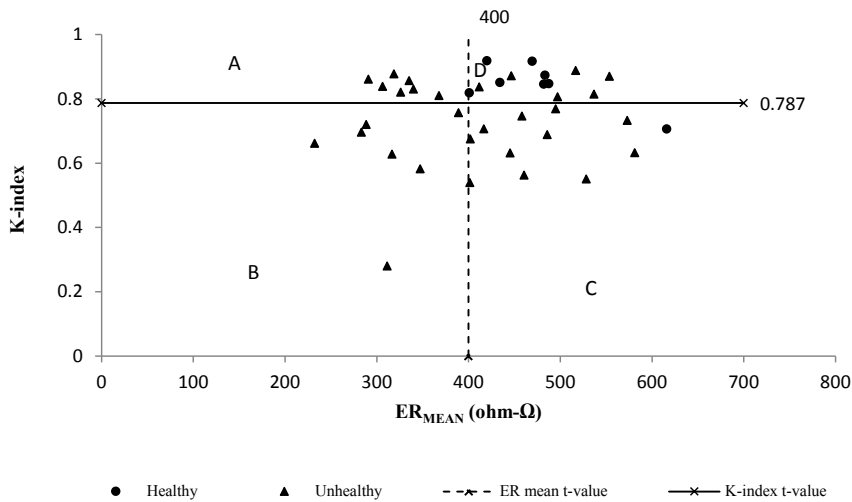


Figure 4. K-index versus ER_{MEAN} of 39 palms for development of the model

K-index versus ER_{MEAN} was plotted and the result is shown in Figure 5. It can be seen that all palms were correctly categorized to healthy (D) and unhealthy (B) regions. All T0 palms plotted dots are in D region categorized as healthy palms while another six palms (two palms for each T1, T2 and T3) are in B region categorized as unhealthy palms. The successful rate of the validation process was 100 %. Lelong et al (2009) also successfully obtained 100% accurate result when detecting *Ganoderma* using hyperspectral remote sensing data by applying partial least square regression (PLS) and discriminant analysis (DA). Shafri and Hamdan (2009) had shown that Lagrangian interpolation red edge technique gave better results than vegetation indices (Khairunniza-Bejo et al., 2015) to identify *Ganoderma*-infected oil palm, however it only gave 84% accuracy.

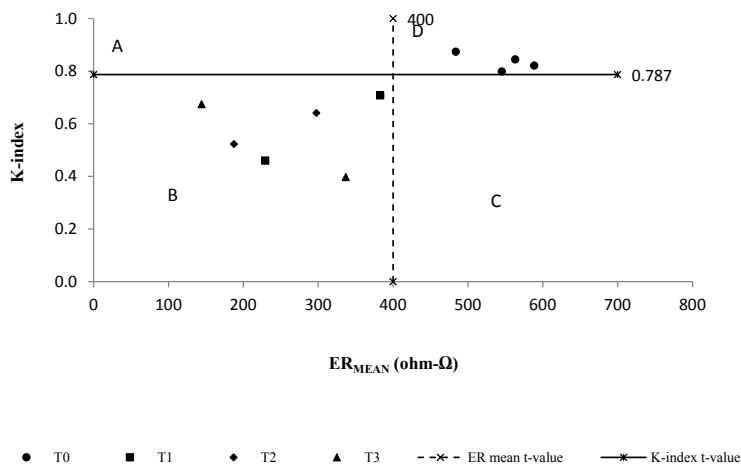


Figure 5. K-index versus ER_{MEAN} of 10 palms for validation of the model

CONCLUSIONS

The ER readings obtained from soil using soil moisture sensor were feasible to identify healthy and infected oil palm trees. Healthy oil palm tree gave higher ER reading ($\geq 400 \Omega$) compared to infected tree ($< 400 \Omega$) especially at the position with the existence of fruiting bodies and/or hollow. However, a single point ER reading could not be used to indicate the healthiness condition of the palm. Result had shown that the higher the severity level, the higher the number of points with less ER values. Combination of average value of ER taken from all eight points and its standard deviation led to the introduction of a new parameter to detect *Ganoderma* infection, named as K-index. A new model was later developed using K-index and ER_{MEAN} . The model gave accurate results of detection, with 82% accuracy during testing and 100% accuracy during validation. Although the proposed

method showed promising results, however, there is still room for improvement. Currently the model is only applicable to differentiate between healthy and infected palms, not to the level of basal stem rot severities (i.e. T1, T2 and T3). Therefore, further investigation needs to be done in the future to improve the method especially on the severity level of detection. This process needs detailed analysis and might require other parameters and different type of sensors. Besides that, environmental factors such as temperature, humidity and sunlight are also recommended for further investigation.

ACKNOWLEDGEMENTS

The authors would like to acknowledge the Ministry of Higher Education Malaysia and Universiti Putra Malaysia for sponsoring this research under Long Term Research Grant Scheme (LRGS)-Nanomite, research number UPM/700-2/1/LRGS-NANOMITE/5526305.

REFERENCES

- Abbasi, A. Z., Islam, N., & Shaikh, Z. A. (2014). A review of wireless sensors and networks' applications in agriculture. *Computer Standards & Interfaces*, 36(2), 263-270.
- Bivi, M. S. H. R., Paiko, A. S., Khairulmazmi, A., Akhtar, M. S., & Idris, A. S. (2016). Control of basal stem rot disease in oil palm by supplementation of calcium, copper, and salicylic acid. *The Plant Pathology Journal*, 32(5), 396-406.
- Borges, E., Matos, A. P., Cardoso, J. M., Correia, C., Vasconcelos, T., & Gomes, N. (2012). Early detection and monitoring of plant diseases by Bioelectric Impedance Spectroscopy. In *2012 IEEE 2nd Portuguese Meeting in Bioengineering (ENBENG)* (pp. 1-4). New Jersey, USA.
- Chang, T. (2003). Effect of soil moisture content on the survival of Ganoderma species and other wood-inhabiting fungi. *Plant Disease*, 87(10), 1201-1204.
- Fitter, A. (2002). Characteristics and functions of root systems. *Plant roots* (pp. 49-78). Florida, USA: CRC Press.
- Jartti, P. (1978). On the measurement of internal decay in living trees. *Silva Fennica (Finland)*, 12(2), 140-148.
- Khairunniza-Bejo, S., Yusoff, Y., Yusoff, N. S. N., Seman, I. A., & Anuar, M. I. (2015). Identification of healthy and BSR-infected oil palm trees using color indices. *International Journal of Agricultural and Biosystems Engineering*, 9(8), 786-789.
- Khosrokhani, M., Khairunniza-Bejo, S., & Pradhan, B. (2016). Geospatial technologies for detection and monitoring of Ganoderma basal stem rot infection in oil palm plantations: A review on sensors and techniques. *Geocarto International*, 33(3), 260-276.
- Larsson, B., Bengtsson, B., & Gustafsson, M. (2004). Nondestructive detection of decay in living trees. *Tree Physiology*, 24(7), 853-858.

- Lelong, C. C. D., Roger, J. M., Bregand, S., Dubertret, F., Lanore, M., Sitorus, N. A., Raharjo, D. A., & Caliman, J. P. (2009). Discrimination of fungal disease infestation in oil-palm canopy hyperspectral reflectance data. In *2009 First Workshop on Hyperspectral Image and Signal Processing: Evolution in Remote Sensing* (pp. 1-4). New Jersey, USA.
- Liaghat, S., Mansor, S., Ehsani, R., Shafri, H. Z. M., Meon, S., & Sankaran, S. (2014). Mid-infrared spectroscopy for early detection of basal stem rot disease in oil palm. *Computers and Electronics in Agriculture*, *101*, 48-54.
- Moore, W. (1999). The combined use of the resistograph and the shigometer for the accurate mapping and diagnosis of the internal condition of woody support organs of trees. *Arboricultural Journal*, *23*(3), 273-287.
- Nawawi, A., & Ho, Y. W. (1990). Effect of temperature and pH on growth pattern of *Ganoderma boninense* from oil palm in Peninsular Malaysia. *Pertanika*, *13*(3), 303-307.
- Nurnadiah, E., Aimrun, W., Amin, M. S. M., & Idris, A. S. (2014). Preliminary study on detection of basal stem rot (BSR) disease at oil palm tree using electrical resistance. *Agriculture and Agricultural Science Procedia*, *2*, 90-94.
- Paglis, C. M. (2013). Application of electrical resistivity tomography for detecting root biomass in coffee trees. *International Journal of Geophysics*, *2013*, 1-6.
- Paterson, R. R. M. (2007). Ganoderma disease of oil palm-A white rot perspective necessary for integrated control. *Crop Protection*, *26*(9), 1369-1376.
- Rees, R. W., Flood, J., Hasan, Y., Potter, U., & Cooper, R. M. (2009). Basal stem rot of oil palm (*Elaeis guineensis*); mode of root infection and lower stem invasion by *Ganoderma boninense*. *Plant Pathology*, *58*(5), 982-989.
- Shafri, H. Z., & Hamdan, N. (2009). Hyperspectral imagery for mapping disease infection in oil palm plantation using vegetation indices and red edge techniques. *American Journal of Applied Sciences*, *6*(6), 1031.
- Shigo, A. L., & Shigo, A. (1974). *Detection of discoloration and decay in living trees and utility poles*. Pennsylvania, USA: Forest Service, US Department of Agriculture.
- Su'ud, M. M., Loonis, P., & Seman, I. A. (2007). Towards automatic recognition and grading of Ganoderma infection pattern using fuzzy systems. *International Journal of Medical and Health Science*, *1*(1), 1-6.
- Turner, P. D. (1965). The incidence of Ganoderma disease of oil palms in Malaya and its relation to previous crop. *Annals of Applied Biology*, *55*(3), 417-423.

**REFEREES FOR THE PERTANIKA
JOURNAL OF SCIENCE AND TECHNOLOGY**

VOL. 27 (S1) 2019

The Editorial Board of the Journal of Science and Technology wishes to thank the following:

Ahmad Suhaizi Mat Su
(UPM, Malaysia)

Aida Isma Mohd Idris
(SEGI, Malaysia)

Akmal Hadi Ma'radzi
(UNIMAP, Malaysia)

Chua Yan Piaw
(UM, Malaysia)

Amir Izzwan Zamri
(UMT, Malaysia)

Anas Mohd Mustafah
(UPM, Malaysia)

Chua Gek Kee
(UMP, Malaysia)

Daniel I. Onwude
(UNIUYO, Nigeria)

Darius El Pebrian
(UiTM, Malaysia)

Diana Jamaludin
(UPM, Malaysia)

Diyana Jamaludin
(UPM, Malaysia)

Farhan Bt Mohd Said
(UMP, Malaysia)

Habibu Ismail
(Ahmadu Bello University, Nigeria)

Hadai Hama Aziz Muhammed
(Darbandikhan Education, Iraq)

Hadi Galavi
(University of Zabol, Iran)

Hayati Samsudin
(USM, Malaysia)

Huzairy Hassan
(UNIMAP, Malaysia)

Lim Ying Pei
(UiTM, Malaysia)

M Rashid
(UTM, Malaysia)

Mahirah Jahari
(UPM, Malaysia)

Mazhar Iqbal
(University Of Agriculture Faisalabad, Pakistan)

Md Rowshon Kamal
(UPM, Malaysia)

Mohd Afandi P Mohammed
(UPM, Malaysia)

Mohd Hudzari Haji Razali
(UiTM, Malaysia)

Mohd Zuhri Mohamed Yusoff
(UPM, Malaysia)

Muhammad Firdaus Abdul Muttalib
(UNIMAP, Malaysia)

Muhammad Hazwan Hamzah
(UPM, Malaysia)

Noor Akhmazillah Mohd Fauzi
(UTHM, Malaysia)

Noor Shazliana Aizee Abidi
(UNIMAP, Malaysia)

Noor Zafira Noor Hasnan
(UPM, Malaysia)

Nor Amaiza Mohd Amin
(UPM, Malaysia)

Norashikin Mat Zain
(UMP, Malaysia)

Norawanis Abdul Razak
(UNIMAP, Malaysia)

Shanti Chandran Sandaran
(UTM, Malaysia)

Norazatul Hanim Mohd Rozalli
(USM, Malaysia)

Norhayu Asib
(UPM, Malaysia)

Norkhairunnisa Mazlan
(UPM, Malaysia)

Norlelawati Arifin
(USIM, Malaysia)

Nur Hamizah Abdul Ghani @ Hashim
(UPM, Malaysia)

Nur Hanani Zainal Abidin
(UPM, Malaysia)

Nur Lailina Makhtar
(UNIMAP, Malaysia)

Nurul Ain Maidin
(UTEM, Malaysia)

Nurul Aini Mohd Azman
(UMP, Malaysia)

Ras Izzati Ismail
(UNIMAP, Malaysia)

Segun Emmanuel Adebayo
(FUTMINNA, Nigeria)

Siti Norasmah Surip
(UiTM, Malaysia)

Siti Raihanah Shafie
(UPM, Malaysia)

Suleiman Samaila
(UNIUYO, Nigeria)

Yasmin Binti Che Ani
(LINCOLN, Malaysia)

FUTMINNA	Federal University of Technology Minna
UiTM	Universiti Teknologi Mara
UMP	Universiti Malaysia Pahang
UMT	Universiti Malaysia Terengganu
UNIMAP	Universiti Malaysia Perlis
UNIUYO	Universiti of Uyo

UPM	Universiti Putra Malaysia
USIM	Universiti Sains Islam Malaysia
USM	Universiti Sains Malaysia
UTEM	Universiti Teknikal Malaysia Melaka
UTHM	Universiti Tun Hussein Onn Malaysia
UTM	Universiti Teknologi Malaysia

While every effort has been made to include a complete list of referees for the period stated above, however if any name(s) have been omitted unintentionally or spelt incorrectly, please notify the Chief Executive Editor, *Pertanika* Journals at executive_editor.pertanika@upm.my

Any inclusion or exclusion of name(s) on this page does not commit the *Pertanika* Editorial Office, nor the UPM Press or the University to provide any liability for whatsoever reason.

Pertanika Journals

Our goal is to bring high quality research to the widest possible audience

INSTRUCTIONS TO AUTHORS (Manuscript Preparation & Submission Guide)

Revised: May 2019

Please read the Pertanika guidelines and follow these instructions carefully. Manuscripts not adhering to the instructions will be returned for revision without review. The Chief Executive Editor reserves the right to return manuscripts that are not prepared in accordance with these guidelines.

MANUSCRIPT PREPARATION

Manuscript Types

Pertanika accepts submission of mainly **four** types of manuscripts for peer-review.

1. REGULAR ARTICLE

Regular articles are full-length original empirical investigations, consisting of introduction, materials and methods, results and discussion, conclusions. Original work must provide references and an explanation on research findings that contain new and significant findings.

Size: Generally, these are expected to be between 6 and 12 journal pages or not exceeding 6000 words (excluding the abstract, references, tables and/or figures), a maximum of 80 references, and an abstract of 100–200 words.

2. REVIEW ARTICLE

These report critical evaluation of materials about current research that has already been published by organizing, integrating, and evaluating previously published materials. It summarizes the status of knowledge and outline future directions of research within the journal scope. Review articles should aim to provide systemic overviews, evaluations and interpretations of research in a given field. Re-analyses as meta-analysis and systemic reviews are encouraged. The manuscript title must start with "Review Article:".

Size: Generally, these are expected to be between 8 and 12 journal pages or not exceeding 6000 words (excluding the abstract, references, tables and/or figures), a maximum of 80 references, and an abstract of 100–200 words.

3. SHORT COMMUNICATIONS

They are timely, peer-reviewed and brief. These are suitable for the publication of significant technical advances and may be used to:

- (a) report new developments, significant advances and novel aspects of experimental and theoretical methods and techniques which are relevant for scientific investigations within the journal scope;
- (b) report/discuss on significant matters of policy and perspective related to the science of the journal, including 'personal' commentary;
- (c) disseminate information and data on topical events of significant scientific and/or social interest within the scope of the journal.

Size: These are usually between 2 and 4 journal pages and have a maximum of three figures and/or tables, from 8 to 20 references, and an abstract length not exceeding 100 words. Information must be in short but complete form and it is not intended to publish preliminary results or to be a reduced version of Regular or Rapid Papers.

4. OTHERS

Brief reports, case studies, comments, concept papers, Letters to the Editor, and replies on previously published articles may be considered.

Language Accuracy

Pertanika **emphasizes** on the linguistic accuracy of every manuscript published. Articles must be in **English** and they must be competently written and argued in clear and concise grammatical English. Contributors are strongly advised to have the manuscript checked by a colleague with ample experience in writing English manuscripts or a competent English language editor.

Author(s) **may be required to provide a certificate** confirming that their manuscripts have been adequately edited. **All editing costs must be borne by the author(s)**. This step, taken by authors before submission, will greatly facilitate reviewing, and thus publication if the content is acceptable.

Linguistically hopeless manuscripts will be rejected straightaway (e.g., when the language is so poor that one cannot be sure of what the authors really mean). This process, taken by authors before submission, will greatly facilitate reviewing, and thus publication if the content is acceptable.

MANUSCRIPT FORMAT

The paper should be submitted in one column format with at least 4cm margins and 1.5 line spacing throughout. Authors are advised to use Times New Roman 12-point font and *MS Word* format.

1. Manuscript Structure

Manuscripts in general should be organised in the following order:

Page 1: Running title

This page should **only** contain the running title of your paper. The running title is an abbreviated title used as the running head on every page of the manuscript. The running title should not exceed 60 characters, counting letters and spaces.

Page 2: Author(s) and Corresponding author information.

This page should contain the **full title** of your paper not exceeding 25 words, with name(s) of all the authors, institutions and corresponding author's name, institution and full address (Street address, telephone number (including extension), hand phone number, and e-mail address) for editorial correspondence. First and corresponding authors must be clearly indicated.

The names of the authors may be abbreviated following the international naming convention. e.g. Salleh, A. B.¹, Tan, S. G.^{2*}, and Sapuan, S. M.³

Authors' addresses. Multiple authors with different addresses must indicate their respective addresses separately by superscript numbers:

Abu Bakar Salleh¹ and Mohd Adzir Mahdi²

¹Faculty of Biotechnology and Biomolecular Sciences, Universiti Putra Malaysia, 43400 Serdang, Selangor, Malaysia

²Faculty of Engineering, Universiti Putra Malaysia, 43400 Serdang, Selangor Malaysia

A **list** of number of **black and white / colour figures and tables** should also be indicated on this page. Figures submitted in color will be printed (upon request) in colour. See "5. *Figures & Photographs*" for details.

Page 3: Abstract

This page should **repeat** the **full title** of your paper with only the **Abstract** (the abstract should be less than 250 words for a Regular Paper and up to 100 words for a Short Communication), and **Keywords**.

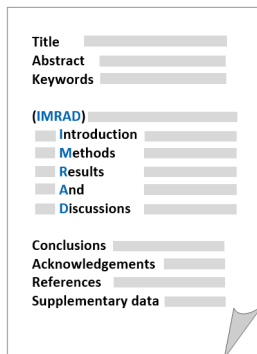
Keywords: Not more than eight keywords in alphabetical order must be provided to describe the contents of the manuscript.

Page 4: Introduction

This page should begin with the **Introduction** of your article and followed by the rest of your paper.

2. Text

Regular Papers should be prepared with the headings *Introduction, Materials and Methods, Results and Discussion, Conclusions, Acknowledgements, References, and Supplementary data* (if available) in this order.



Title _____

Abstract _____

Keywords _____

(IMRAD)

Introduction _____

Methods _____

Results _____

And _____

Discussions _____

Conclusions _____

Acknowledgements _____

References _____

Supplementary data _____

MAKE YOUR ARTICLES AS CONCISE AS POSSIBLE

Most scientific papers are prepared according to a format called IMRAD. The term represents the first letters of the words Introduction, Materials and Methods, Results, And, Discussion. It indicates a pattern or format rather than a complete list of headings or components of research papers; the missing parts of a paper are: Title, Authors, Keywords, Abstract, Conclusions, and References. Additionally, some papers include Acknowledgments and Appendices.

The Introduction explains the scope and objective of the study in the light of current knowledge on the subject; the Materials and Methods describes how the study was conducted; the Results section reports what was found in the study; and the Discussion section explains meaning and significance of the results and provides suggestions for future directions of research. The manuscript must be prepared according to the Journal's instructions to authors.

3. Equations and Formulae

These must be set up clearly and should be typed double spaced. Numbers identifying equations should be in square brackets and placed on the right margin of the text.

4. Tables

All tables should be prepared in a form consistent with recent issues of Pertanika and should be numbered consecutively with Roman numerals. Explanatory material should be given in the table legends and footnotes. Each table should be prepared on a new page, embedded in the manuscript.

When a manuscript is submitted for publication, tables must also be submitted separately as data - .doc, .rtf, Excel or PowerPoint files- because tables submitted as image data cannot be edited for publication and are usually in low-resolution.

5. Figures & Photographs

Submit an **original** figure or photograph. Line drawings must be clear, with high black and white contrast. Each figure or photograph should be prepared on a new page, embedded in the manuscript for reviewing to keep the file of the manuscript under 5 MB. These should be numbered consecutively with Roman numerals.

Figures or photographs must also be submitted separately as TIFF, JPEG, or Excel files- because figures or photographs submitted in low-resolution embedded in the manuscript cannot be accepted for publication. For electronic figures, create your figures using applications that are capable of preparing high resolution TIFF files.

6. References

References begin on their own page and are listed in alphabetical order by the first author's last name. Only references cited within the text should be included. All references should be in 12-point font and double-spaced.

NOTE: When formatting your references, please follow the **APA reference style** (6th Edition). Ensure that the references are strictly in the journal's prescribed style, failing which your article will **not be accepted for peer-review**. You may refer to the *Publication Manual of the American Psychological Association* for further details (<http://www.apastyle.org/>).

7. General Guidelines

Abbreviations: Define alphabetically, other than abbreviations that can be used without definition. Words or phrases that are abbreviated in the introduction and following text should be written out in full the first time that they appear in the text, with each abbreviated form in parenthesis. Include the common name or scientific name, or both, of animal and plant materials.

Acknowledgements: Any individuals and entities who have contributed should be acknowledged appropriately.

Authors' Affiliation: The primary affiliation for each author should be the institution where the majority of their work was done. If an author has subsequently moved to another institution, the current address may also be stated in the footer.

Co-Authors: The commonly accepted guideline for authorship is that one must have substantially contributed to the development of the paper and share accountability for the results. Researchers should decide who will be an author and what order they will be listed depending upon their order of importance to the study. Other contributions should be cited in the manuscript's Acknowledgements.

Copyright Permissions: Authors should seek necessary permissions for quotations, artwork, boxes or tables taken from other publications or from other freely available sources on the Internet before submission to Pertanika. Acknowledgement must be given to the original source in the illustration legend, in a table footnote, or at the end of the quotation.

Footnotes: Current addresses of authors if different from heading may be inserted here.

Page Numbering: Every page of the manuscript, including the title page, references, tables, etc. should be numbered.

Spelling: The journal uses American or British spelling and authors may follow the latest edition of the Oxford Advanced Learner's Dictionary for British spellings.

SUBMISSION OF MANUSCRIPTS

All submissions must be made electronically using the **online submission system ScholarOne™**, a web-based portal by Clarivate Analytics. For more information, go to our web page and [click "Online Submission"](#).

Submission Checklist

1. **MANUSCRIPT:** Ensure your MS has followed the Pertanika style particularly the first four pages as explained earlier. The article should be written in a good academic style and provide an accurate and succinct description of the contents ensuring that grammar and spelling errors have been corrected before submission. It should also not exceed the suggested length.
2. **COPYRIGHT FORM:** Authors publishing the Journal will be asked to sign a copyright form. In signing the form, it is assumed that authors have obtained permission to use any copyrighted or previously published material. All authors must read and agree to the conditions outlined in the form, and must sign the form or agree that the corresponding author can sign on their behalf. Articles cannot be published until a signed form (*original pen-to-paper signature*) has been received.

Visit our Journal's website for more details at <http://www.pertanika.upm.edu.my/home.php>.

ACCESS TO PUBLISHED MATERIALS

Under the Journal's open access initiative, authors can choose to download free material (via PDF link) from any of the journal issues from Pertanika's website. Under "**Browse Journals**" you will see a link, "*Current Issues*" or "*Archives*". Here you will get access to all current and back-issues from 1978 onwards. No hard copy of journals or off prints are printed.

PUBLICATION CHARGE

Upon acceptance of manuscript, a processing fee of RM 750 / USD 250 will be imposed on authors; RM 750 for corresponding author affiliated to institution in Malaysia; USD 250 for corresponding author affiliated to institution outside Malaysia. Payment must be made online at http://pertanika.upm.edu.my/publishing_charge.php.

Any queries may be directed to the **Chief Executive Editor's** office via email to executive_editor.pertanika@upm.my.



The Potential of Fluorescence Technology for Quality Monitoring of Miyauchi Iyokan (<i>C. iyo</i> Hort. Ex Tanaka) during Post-harvest Treatment <i>Muharfiza, Dimas Firmanda Al Riza, Nie Sen, Yasushi Kohno, Tetsuhito Suzuki, Makoto Kuramoto and Naoshi Kondo</i>	189
Mechanical Analysis of a Wedge Device in Sawing Technology <i>Mohd Salahuddin Mohd Basri, Mohd Zuhair Mohd Nor and Rosnah Shamsudin</i>	197
Simulation Study for the Compressed BMC Materials of Kenaf/ Coir Reinforced Unsaturated Polyester: Flow Behaviour and the Effects of Charges Shapes Studies <i>Sameer Adnan Ibraheem, Khalina Abdan and Lee Ching Hao</i>	211
Evaluations of Soil Resistivity in Relation to Basal Stem Rot Incidences Using Soil Moisture Sensor <i>Mohd Hamim Abdul Aziz, Siti Khairunniza Bejo, Fazirulhisyam Hashim, Nur Hidayah Ramli and Desa Ahmad</i>	225

Stochastic Models for Greenhouse Whitefly Flight Behavior based on Wireless Image Monitoring System Measurements <i>Dan Jeric Arcega Rustia and Ta-Te Lin</i>	81
Mechanical Properties of Tapioca Starch-Based Film Incorporated With Bulk Chitosan and Chitosan Nanoparticle: A Comparative Study <i>Ruzana Ahmad Shapi'i, Siti Hajar Othman, Mohd Nazli Naim and Roseliza Kadir Basha</i>	95
Optimization of Hydrothermal Conditioning Conditions for <i>Pennisetum purpureum x Pennisetum americanum</i> (Napier PakChong1 grass) to Produce the Press Fluid for Biogas Production <i>Pitchaya Suaisom, Patiroop Pholchan, Hasfalina Che Man and Pruk Aggarangsi</i>	109
Mapping the Distribution of Oil Palm using Landsat 8 Data by Comparing Machine Learning and Non-Machine Learning Algorithms <i>Nur Shafira Nisa Shaharum, Helmi Zulhaidi Mohd Shafri, Wan Azlina Wan Ab Karim Ghani, Sheila Samsatli and Badronnisa Yusuf</i>	123
Modification of Quality Index Method Scheme for Nile Tilapia Fillets and Application in Quality Assessment of the Product Stored at Low Temperatures <i>Mai Thi Tuyet Nga and Nguyen Thi Kieu Diem</i>	137
Physical and Mechanical Properties of Unripe <i>Nipah</i> Banana Fruit (<i>Musa Acuminata Balbisiana</i>) <i>Farahana Nabilah Zainal A'bidin, Rosnah Shamsudin, Mohd Salahuddin Mohd Basri and Zanariah Mohd Dom</i>	149
The Effect of Packaging Materials on the Quality of Freshness of Longan Fumigated with Medium Concentration-ozone Gas <i>Saranyapak Chamnan, Jaturapatr Varith, Somkiat Jaturonglumlert, Pisuthi Klinkajorn and Jakraphong Phimphimol</i>	159
Degradation Kinetics of Diazinon and Triazophos Pesticides in Dried Chili under Gaseous Ozone Fumigation <i>Panlop Sintuya, Kanjana Narkprasom, Jaturapatr Varith, Somkiat Jaturonglumlert, Niwooti Whangchai, Danuwat Peng-ont and Chanawat Nitatwichit</i>	169
Modeling River Flow using Artificial Neural Networks: A Case Study on Sumani Watershed <i>Nova Anika and Tasuku Kato</i>	179

Contents

Adapting to Challenges

- Preface** i
Rosnah Shamsudin
- Characterization of Jackfruit Straw-based Films: Effect of Starch and Plasticizer Contents 1
Muslimah Solehah Mohd Nazri, Intan Syafinaz Mohamed Amin Tawakkal, Nozieana Khairuddin, Rosnita A Talib and Siti Hajar Othman
- Phytochemical Compositions and Antioxidant Activities of Malaysian Stingless Bee Honey 15
Bernard Maringgal, Norhashila Hashim, Intan Syafinaz Mohamed Amin Tawakkal, Mahmud Tengku Muda Mohamed and Nur Indah Abdul Shukor
- Impact of Gamma Irradiation on Physical Parameters, Microbial Safety and the Total Polyphenolic Content of Commercially Available Ceylon Black Tea (*Camellia sinensis* L.) 29
Arosha Rashmi De Silva, Rathnayake Mudiyanseelage Nalaka Priyanga Rathnayake, Rampati Devage Roshani Ranasinghe and Chamila Vinodanee Liyanage Jayasinghe
- Optimization of Enzymatic Hydrolysis for the Production of Antioxidative Peptide from *Nannochloropsis gaditana* using Response Surface Methodology 41
Nur Izzati Md Saleh, Wan Azlina Wan Ab Karim Ghani, Mohd Razif Harun and Siti Mazlina Mustapa Kamal
- Effect of Drying Temperature on Malaysia Pomelo (*Citrus grandis* (L.) Osbeck) Pomace Residue under Vacuum Condition 57
Nur Farhana Abd Rahman, Amin Ismail, Nor Nadiah Abdul Karim Shah, Jaturapatr Varith and Rosnah Shamsudin
- Assessment on Flux Reduction and Protein Rejection Behavior in Fractionating Tilapia By-Product Protein Hydrolysate by Ultrafiltration Membrane 67
Jumardi Roslan, Siti Mazlina Mustapa Kamal, Khairul Faezah Md Yunos and Norhafizah Abdullah



Pertanika Editorial Office, Journal Division
Office of the Deputy Vice Chancellor (R&I),
1st Floor, IDEA Tower II,
UPM-MTDC Technology Centre
Universiti Putra Malaysia
43400 UPM Serdang
Selangor Darul Ehsan
Malaysia

<http://www.pertanika.upm.edu.my/>
E-mail: executive_editor.pertanika@upm.my
Tel: +603 8947 1622/1616

PENERBIT
UPM
UNIVERSITI PUTRA MALAYSIA
PRESS

<http://penerbit.upm.edu.my>
E-mail : penerbit@upm.edu.my
Tel : +603 8946 8855/8854

